

POLITECNICO DI MILANO
Dipartimento di Elettronica, Informazione e Bioingegneria
DOTTORATO DI RICERCA IN INGEGNERIA DELL'INFORMAZIONE

Continuous-time model identification with applications to rotorcraft dynamics

Doctoral Dissertation of:
Marco Bergamasco

Advisors:

Prof. Marco Lovera

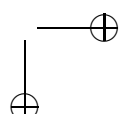
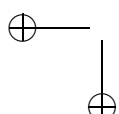
Tutor:

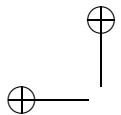
Prof. Patrizio Colaneri

Supervisor of the Doctoral Program:

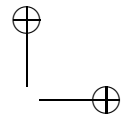
Prof. Carlo Fiorini

2012 - XXV edition





|

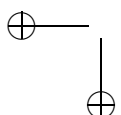


—

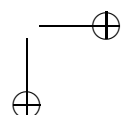
—

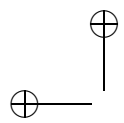
Marco Bergamasco

Dipartimento di Elettronica, Informazione e Bioingegneria
Politecnico di Milano
e-mail: marco.bergamasco@mail.polimi.it

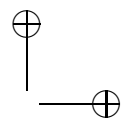


|





|



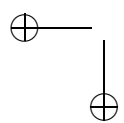
42

DEEP THOUGHT

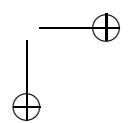
—

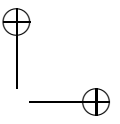
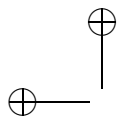
two by two... hands of blue...

RIVER TAM



|

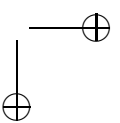
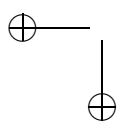




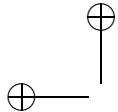
—

|

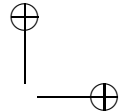
—



|



|



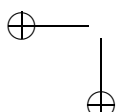
ACKNOWLEDGMENTS

I would like to thank you for reading my unreadable thesis.

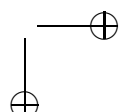
Honestly, thank you.

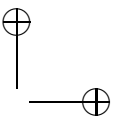
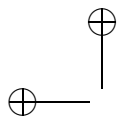
Marco

Since you are still here, I would like to suggest you some better readings: *A Song of Ice and Fire* written by George R. R. Martin and *The Hitchhiker's Guide to the Galaxy* written by Douglas Adams. If you are lazy you can find the TV series of the former while I suggest to avoid the movie based on the latter. It is even worst than this thesis.



|

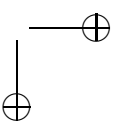
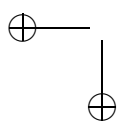




—

|

—



|



ACKNOWLEDGMENTS & RINGRAZIAMENTI

I would like to thank Professor Yoshito Ohta whose work has been a source of inspiration during my PhD, particularly during the (too) short period at the Kyoto University.

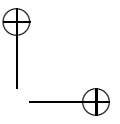
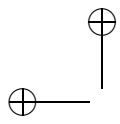
I would also like to thank Professor Guillaume Mercère who kindly accepted to review this work. His comments have been very helpful in improving my thesis.

In modo quasi scontato, da quanto sentito, ringrazio il Professore Marco Lovera per il lungo viaggio in cui mi ha accompagnato, insegnandomi più di quanto sia contenuto in questa tesi.

Ringrazio i Professori Luigi Piroddi e Danilo Ardagna per avermi concesso di lavorare su argomenti certamente lontani da quelli contenuti in questa tesi, ma ugualmente interessanti.

Ringrazio i dottorandi che hanno condiviso con me questo percorso. Non ne elencherò i nomi per non dimenticarmi ingiustamente di qualcuno. Ringrazio in particolar modo i miei compagni di ufficio, passati e presenti, per le discussioni ed i confronti costruttivi, pressoché quotidiani, che tanto mi hanno permesso di imparare.

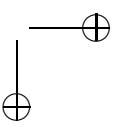
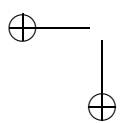




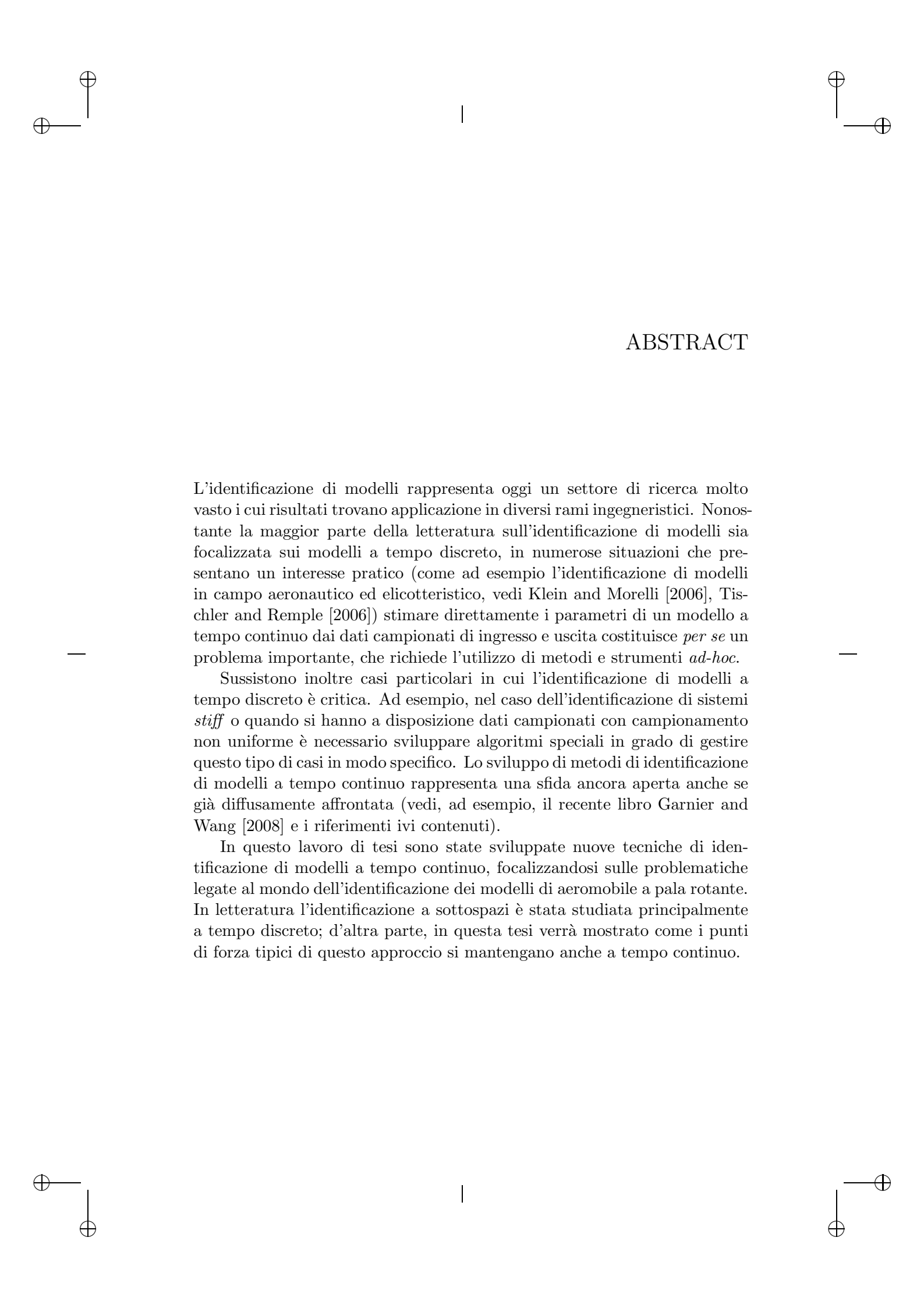
—

|

—



|

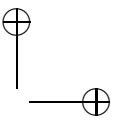
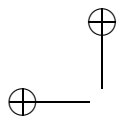


ABSTRACT

L’identificazione di modelli rappresenta oggi un settore di ricerca molto vasto i cui risultati trovano applicazione in diversi rami ingegneristici. Nonostante la maggior parte della letteratura sull’identificazione di modelli sia focalizzata sui modelli a tempo discreto, in numerose situazioni che presentano un interesse pratico (come ad esempio l’identificazione di modelli in campo aeronautico ed elicotteristico, vedi Klein and Morelli [2006], Tischler and Remple [2006]) stimare direttamente i parametri di un modello a tempo continuo dai dati campionati di ingresso e uscita costituisce *per se* un problema importante, che richiede l’utilizzo di metodi e strumenti *ad-hoc*.

Sussistono inoltre casi particolari in cui l’identificazione di modelli a tempo discreto è critica. Ad esempio, nel caso dell’identificazione di sistemi *stiff* o quando si hanno a disposizione dati campionati con campionamento non uniforme è necessario sviluppare algoritmi speciali in grado di gestire questo tipo di casi in modo specifico. Lo sviluppo di metodi di identificazione di modelli a tempo continuo rappresenta una sfida ancora aperta anche se già diffusamente affrontata (vedi, ad esempio, il recente libro Garnier and Wang [2008] e i riferimenti ivi contenuti).

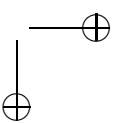
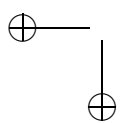
In questo lavoro di tesi sono state sviluppate nuove tecniche di identificazione di modelli a tempo continuo, focalizzandosi sulle problematiche legate al mondo dell’identificazione dei modelli di aeromobile a pala rotante. In letteratura l’identificazione a sottospazi è stata studiata principalmente a tempo discreto; d’altra parte, in questa tesi verrà mostrato come i punti di forza tipici di questo approccio si mantengano anche a tempo continuo.



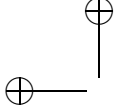
—

|

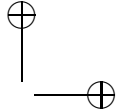
—



|



|



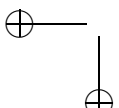
INTRODUCTION

System identification is today a very wide research area, the results of which find application in a very diverse range of fields. While most of the literature on system identification focuses on discrete-time models, in many situations of practical interest (such, as, *e.g.*, aircraft and rotorcraft identification, see for example Klein and Morelli [2006], Tischler and Remple [2006]) the direct estimation of the parameters of a continuous-time model from sampled input-output data is an important problem *per se*, for which dedicated methods and tools have to be employed. Moreover, the problem of identifying models under special circumstances which turn out to be critical in discrete-time, such as the identification of stiff systems or the use of non-equidistantly sampled data make it necessary to develop special algorithms that can deal with these cases. The development of identification methods for continuous-time models is a challenge its own, and has been studied extensively (see, *e.g.*, the recent book Garnier and Wang [2008] and the references therein).

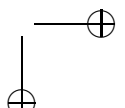
In this thesis continuous-time model identification methods are developed with a special focus on the issues of rotorcraft system identification. Subspace approaches have been mainly studied in the discrete-time domain but in this thesis it will be shown that their charming properties are still valid in the continuous-time domain.

Subspace model identification

As recounted in Gevers [2006], by the late 70s the theory of MIMO linear systems had been completely understood, and yet from a practical point of view black-box identification of MIMO systems remained an issue until the late 80s. The cause for this was the estimation of the structural indices that characterize the parameterizations of MIMO systems, which is tricky and often leads to ill-conditioned numerical problems (see *e.g.*, Guidorzi



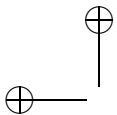
|



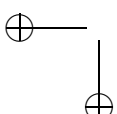
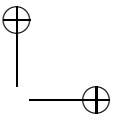
[1975]). Therefore, there was a strongly felt need for simple, possibly sub-optimal, procedures bypassing the need for estimating structural indices. Subspace model identification (SMI) methods offered exactly the potential to overcome this difficulty.

In the last twenty years or so, SMI algorithms have been developed, which have proven extremely successful in dealing with the estimation of discrete-time state space models for MIMO systems. Classical SMI methods, developed in the early 90s for the estimation of discrete-time models, are the MIMO Output-Error State sPace (MOESP, see Verhaegen [1994] and the references therein) class of algorithms, based on the idea of estimating a basis of the observability subspace directly from data, and the N4SID algorithm (see Van Overschee and De Moor [1994]), which relies on the estimation of the state sequence for the system as an intermediate step for the estimation of the state space model. A tutorial, detailed account of such methods can be found in the textbooks Van Overschee and De Moor [1996], Verhaegen and Verdult [2007]. Besides the possibility of dealing with MIMO problems in a simple and natural way, one of the keys to the success of SMI methods in applications is that all the operations performed by subspace algorithms can be implemented with numerically stable and efficient tools from numerical linear algebra, based on the numerically robust QR factorisation and on the singular value decomposition (see, *e.g.*, Sima and Van Huffel [2000]).

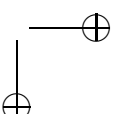
Not surprisingly, the problem of extending SMI methods to the identification of continuous-time systems has been studied in a number of contributions. In Van Overschee and De Moor [1996] a frequency-domain approach to subspace identification of continuous-time models was proposed, while a time-domain SMI algorithm able to identify a continuous-time model from sampled input-output data was first proposed in Haverkamp [2001], building on the framework introduced in Johansson et al. [1999a]. More precisely, in the cited thesis the class of SMI algorithms was extended to the identification of continuous-time models through the use of Laguerre filters: this allowed the development of a method that deals with noise in a similar way as its discrete-time counterparts. More recently, in Ohsumi et al. [2002] the version of the MOESP algorithm presented in Verhaegen and Dewilde [1992a,b] was adopted and a discrete-time algebraic equation was derived starting from sampled input-output data by describing derivatives of stochastic processes in the distribution sense, while in Bastogne et al. [2001], Mercère et al. [2008b] the combination of the MOESP algorithm with filtering methods to avoid the need to compute numerical derivatives of input-output signals was proposed. In Ohta and Kawai [2004] a novel approach to the problem of continuous-time SMI has been presented, based on



|



|



the adoption of orthonormal basis functions to arrive, again, at a MOESP-like data equation for a continuous-time system.

All the above mentioned contributions, however, assume that the system under study is operating in open-loop. This assumption is frequently restrictive in practice and is typically violated, for example, in aerospace applications, in which partial loop closures must be retained during identification experiments, primarily for safety issues (see, *e.g.*, Jategaonkar [2006], Klein and Morelli [2006], Tischler and Remple [2006]). The problem of closed-loop SMI has been studied extensively in recent years due to its high relevance for practical applications (see, *e.g.*, Ljung and McKelvey [1996], Chou and Verhaegen [1997], Chiuso and Picci [2005], Chiuso [2007], Huang et al. [2005] and the references therein). The present state-of-the-art is represented by the so-called Predictor-Based Subspace IDentification (PBSID) algorithm (see, again, Chiuso and Picci [2005], Chiuso [2007]) which, under suitable assumptions, can provide consistent estimates of the state space matrices for a discrete-time, linear time-invariant system operating under feedback. The problem of closed-loop subspace identification in continuous-time has been first considered in the literature in Mohd-Moktar and Wang [2008], where the application of the errors-in-variables approach of Chou and Verhaegen [1997] is proposed to deal with correlation in a continuous-time setting.

In the light of the above discussion, the aim of this thesis is to propose novel continuous-time SMI schemes, based on the derivation of PBSID-like algorithms within the all-pass domains proposed in Haverkamp [2001] and Ohta and Kawai [2004], Ohta [2011] and relying, respectively, on Laguerre filtering and Laguerre projections of the sampled input-output data.

More in details, the first results of this thesis are the continuous-time predictor based subspace model identification algorithms that consistently estimate continuous-time linear time invariant system operating in open- or closed-loop.

Recursive subspace model identification (RSMI) in discrete-time has been extensively studied in recent years (see, *e.g.*, Verhaegen and Deprettere [1991], Cho et al. [1994], Gustafsson [1998], Lovera et al. [2000], Oku and Kimura [2002], Mercère et al. [2004], Houtzager et al. [2009], Chiuso et al. [2010], Houtzager et al. [2012]), while methods for RSMI in continuous-time have received less attention. In this regard, the recursive implementation of the continuous-time version of PO-MOESP first proposed in Ohta and Kawai [2004], Ohta [2011] has been presented in Kinoshita and Ohta [2010]. In this thesis a recursive continuous-time counterpart of the PBSID method, able to provide estimates of models for system operating in closed-loop, is devised.

Another relevant and common problem in the engineering field is to

design a single control system that guarantees stability and performance requirements for a given plant in many different operating conditions. The gain scheduling technique solves this problem (see, *e.g.*, Shamma and Athans [1990], Kaminer et al. [1995], Apkarian and Adams [1998]), provided that a suitable model in parameter-dependent form has been derived. This modelling problem can be solved using methods based entirely on identification, *i.e.*, aiming at deriving linear parameter varying (LPV) models for the plant directly from input/output data. A number of algorithms has been proposed in the literature aiming at the estimation of the parameters for both input/output and state-space models, the latter either in affine or Linear Fractional Transformation (LFT) form (see, *e.g.*, Nemanic et al. [1995], Lovera et al. [1998], Lee and Poolla [1999], Bamieh and Giarré [2002], Verdult [2002], Previdi and Lovera [2003], van Wingerden and Verhaegen [2009], Toth [2010]). The continuous-time LPV model identification has been mostly studied using *a-priori* knowledge of the system (see, *e.g.*, Mercère et al. [2011]) or input/output models (see, *e.g.*, Laurain et al. [2011], Chouaba et al. [2011]). In this thesis the problem of the estimation of continuous-time state space LPV models, without *a-priori* knowledge of the system, will be carried out using a local approach. The identification of the local models will be performed using the continuous-time SMI schemes derived in the first part of the thesis.

The only, well known, downside of the subspace model identification approach to state space model identification is the impossibility to impose a parameterisation to the state space matrices and therefore it is tricky to recover physically-motivated models. The problem has been originally considered in Xie and Ljung [2002], Parrilo and Ljung [2003], Lyzell et al. [2009]. More recently, the problem has been addressed in Prot and Mercère [2011], Prot et al. [2012], where it is assumed that the structured and unstructured models, of the same order, are related to each other via a similarity transformation. The bilinear equations resulting from the definition of the transformation are then converted into a null-space problem, the solution of which leads to a non-convex optimization problem. In this thesis the problem is addressed in a different perspective, *i.e.*, it is formulated as an input-output model matching problem, in terms of the \mathcal{H}_∞ norm of the difference between the structured and the unstructured state space representations. The solution of the problem is subsequently computing using recent results in non-smooth optimisation techniques, see Apkarian and Noll [2006], Gahinet and Apkarian [2011].

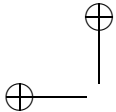
Rotorcraft model identification

Rotorcraft dynamics is described by the interaction of inertial and aerodynamic forces as well as control forces acting on the rotor and the airframe. The resulting physical-based model contains a number of uncertain or unknown parameters which are very difficult to determine; for example, fluid dynamics is necessary to describe helicopter motion but the associated mathematical modelling is very complex and is affected by a number of unmeasurable physical parameters, *e.g.*, wake interferences with the empennage and tail rotor. System identification in time and frequency domain has emerged as a viable approach for the estimation of the physical parameters.

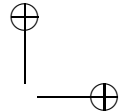
In helicopter engineering, in the last two decades, frequency-domain system identification has been widely developed, as suggested by the number of contributions in the literature describing the relevant approaches (see Lawler et al. [2006], Tischler and Remple [2006] and the references therein) and case studies, *e.g.*, Bell XV-15 Tischler and Kaletka [1987], Sikorsky UH-60 Blackhawk Fletcher [1995], BO-105 Tischler and Cauffman [1992], Hamel and Kaletka [1997], R-MAX Cheng et al. [2006], SH2G Tischler and Tomashoski [2002], Fire Scout MQ-8B, S-76, and ARH-70A Ivler and Tischler [2008], MH-47G Link et al. [2011], and Unmanned K-MAX Mansur et al. [2011]. In the frequency-domain approach, flight test data is used for the reconstruction of a nonparametric model, *i.e.*, the frequency response data curve that characterizes the input-to-output process at a large number of discrete frequencies. Then, a parametric frequency response curve is matched with the nonparametric model to find the estimates.

Starting from another point of view, time domain system identification has been taken into account for rotorcraft system identification by German Aerospace Center DLR (Hamel and Kaletka [1997]). In the time domain the model is considered in state space form and it is directly matched with the flight test data using least squares and/or maximum likelihood methods.

The methods in the time or frequency domain have shown to be suitable for rotorcraft identification in a comparative study conducted under U.S./German memorandum of understanding using flight test data from the XV-15 tilt-rotor aircraft Tischler and Kaletka [1987] and the BO-105 helicopter Hamel and Kaletka [1997]. Both classes of methods provide results of similar quality though they are characterized by different issues. One of the common problems of these methods is the selection of the model structure, indeed the helicopter can be regarded as a single rigid body with 6-DOF as well as a coupled multibody dynamic system with 13-DOF, or even more, depending of the considered frequency range. The time or frequency domain



|



identification methods commonly used in rotorcraft field set out above have some drawbacks that will be exposed in the following.

First of all, the identification problem is intrinsically multivariable, that is the natural condition for a subspace algorithm. The classical least squares or maximum likelihood time-domain methods have some drawbacks that are avoided by a subspace approach, *e.g.*, they need estimates of the initial state vector which is a numerical ill-conditioned problem for unstable system, like a helicopter in most of the flight conditions. Then, the model structure selection can be tricky, indeed the physical model can include from six to thirteen degree of freedoms, and so a method that suggests the model order during the estimation directly from the data is preferable. The subspace approach certainly avoids over-parametrization that is a major problem in the classical time or frequency domain identification approaches, usually solved using iterative methods. As already said, in most of the flight conditions rotorcraft vehicles are open-loop unstable, therefore the identification algorithm must be able to treat data acquired in closed-loop.

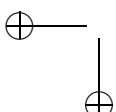
All the above mentioned problems are well solved by a continuous-time closed-loop subspace model identification algorithm. Another characteristic useful in the rotorcraft system identification is that it can merge in a very simple way information from separate data sets into a single state space model. In this thesis a particular attention is given to another common requirement in the rotorcraft model identification, *i.e.*, the model must be physically interpretable or, using the terminology of control theory, a structured one. A solution to this problem will be given thanks to a developed method that allows to transform an unstructured model, for example identified using a subspace algorithm, in a structured one.

Structure and contributions

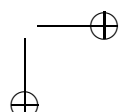
The thesis is divided in two parts:

Methods The continuous-time subspace model identification approach is derived herein. A recursive version of the algorithm is obtained. The method is also extended to identify linear parameter varying systems using a local approach and to compute estimates of model uncertainty. Moreover an approach to transform the identified unstructured model to a structured one is developed.

Applications In this part rotorcraft system identification is first introduced and the practical problems of this field are summarized. Then a methodology useful to ensure the data consistency, *i.e.*, to guarantee that the dataset is cleaned from all measurements errors, is explained.



|



After the pre-processing of the data, the methods exposed in the first part are used in a simulation and in an experimental examples.

More in details, the mentioned topics are covered in this thesis as follows.

In Chapter 1 the problem of continuous-time model identification is introduced. The algorithms are developed by reformulating the identification problem from the continuous-time model to equivalent ones to which discrete-time subspace identification techniques can be applied. The continuous-time to discrete-time transformation is faced using two different methods, the former leading to the so-called all-pass domain by using a bank of Laguerre filters applied to the input-output data and the latter corresponding to the projection of the input-output data onto an orthonormal basis, again defined in terms of Laguerre filters. In both frameworks, the PBSID subspace identification algorithm, originally developed in the case of discrete-time systems, can be reformulated for the continuous-time case. As result two novel subspace-based algorithms, capable of dealing with data generated by systems operating in closed-loop, are presented and simulation results are used to illustrate the achievable performance of the proposed approaches with respect to existing methods available in the literature.

Chapter 2 deals with the problem of recursive model identification in continuous-time using subspace techniques. Recursive implementation is particularly important in connection to continuous-time subspace methods in view of the significant computational burden associated with their implementation. More precisely, the algorithm presented in Chapter 1 which relies on a system transformation using the Laguerre basis is considered, together with a novel set of orthonormal Laguerre-like basis function with the specific feature of being compactly supported, and the recursive counterparts are developed.

In Chapter 3 an approach, formulated in the subspace model identification framework, is proposed for deriving continuous-time Linear Parameter Varying (LPV) models in state-space form starting from sampled measurements of input, output and scheduling variables, using a local approach.

For the purpose of control design it is desirable to have information about the reliability of the identified model. In Chapter 4 an approach to evaluate the uncertainty of the identified models is presented. A procedure, based on the statistical tool bootstrap, for the evaluation of the uncertainty associated with the frequency response of the estimated models is proposed.

Chapter 5 deals with the problem of recovering the numerical values of the physical parameters of a structured representation of a linear system starting from a fully parameterised identified model as obtained by means of a subspace model identification method. As shown this can be achieved without explicitly constructing the similarity transformation relating the

unstructured model to the structured one, for linear time-invariant systems, linear time-periodic systems, and linear parameter-varying systems identified either from a periodic scheduling sequence or a generic one.

The rotorcraft community has exploited extensively model identification, precisely in order to overcome the difficulties associated with the accurate description of the interaction between dynamics and aerodynamics. In Chapter 6 a concise overview of the relevant literature of rotorcraft model identification is provided and the potential of the continuous-time subspace model identification methods in this area is analyzed.

All the possible error sources introduced by the rotorcraft sensors have to be at least reduced, otherwise the identification procedure may introduce significant modelling errors. Chapter 7 introduces the data compatibility analysis, *i.e.*, a methodology that aims at cleaning up the measured data by the systematic measurement errors introduced by different sensors. Such a method can be reformulated as the parametric estimation of a nonlinear system, and so different nonlinear identification techniques are taken into account: Output Error (OE), Unscented Kalman Filter (UKF), and Particle Filter (PF). For comparison they have been applied to DCA analysis of measured data for a small scale quadrotor Unmanned Aerial Vehicle (UAV).

Chapter 8 has the objective to illustrate the achievable model accuracy, using the continuous-time subspace algorithm, by means of simulation results for the full-scale helicopter BO-105. Moreover it is shown that the parameters of the gray-box model of the BO-105 can be successfully estimated using the novel \mathcal{H}_∞ approach that allows to obtain a parametrised state-space model starting from the unstructured model.

In Chapter 9 the problem of deriving continuous-time models for the dynamics of a real small-scale quadrotor helicopter is considered. More precisely, the continuous-time predictor-based subspace identification approach exposed and the model uncertainty estimation method are adopted and the results obtained in the experimental study are presented and discussed.

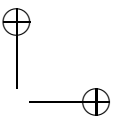
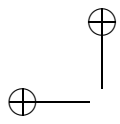
CONTENTS

| | |
|--|-----------|
| I Methods | 1 |
| 1 Continuous-time predictor based subspace identification | 3 |
| 1.1 Introduction | 3 |
| 1.2 Problem statement | 6 |
| 1.3 Continuous-time to discrete-time transformation | 7 |
| 1.3.1 Laguerre filters | 8 |
| 1.3.2 Laguerre projections | 15 |
| 1.4 CT-PBSID using Laguerre filters (CT-PBSID _w) | 24 |
| 1.5 CT-PBSID using Laguerre projections (CT-PBSID _o) | 30 |
| 1.6 Simulation examples | 36 |
| 1.6.1 Open-loop case | 37 |
| 1.6.2 Closed-loop case | 43 |
| 1.6.3 Tuning parameters | 49 |
| 1.7 Concluding remarks | 54 |
| 2 Recursive continuous-time subspace identification | 57 |
| 2.1 Introduction | 57 |
| 2.2 Problem statement | 58 |
| 2.3 Recursive implementations of Laguerre projections | 59 |
| 2.3.1 Infinity integral truncation | 59 |
| 2.3.2 Finitely-supported filter kernels generated from La- guerre basis functions | 60 |
| 2.4 Recursive subspace model identification | 64 |
| 2.5 Simulation examples | 70 |
| 2.5.1 Open-loop case | 70 |
| 2.5.2 Closed-loop case | 72 |
| 2.6 Concluding remarks | 73 |

| | |
|--|------------|
| 3 Continuous-time Linear Parameter Varying model identification | 75 |
| 3.1 Introduction | 75 |
| 3.2 Problem statement | 78 |
| 3.3 A balanced subspace approach to identification for gain scheduling | 79 |
| 3.3.1 Balancing of the identified models | 79 |
| 3.3.2 Model interpolation | 81 |
| 3.3.3 Implementation issues | 85 |
| 3.4 Simulation examples | 85 |
| 3.5 Concluding remarks | 97 |
| 4 Model uncertainty estimation: bootstrap approach | 99 |
| 4.1 Introduction | 99 |
| 4.2 Quantifying model uncertainty: a bootstrap-based approach . | 100 |
| 4.2.1 The bootstrap | 100 |
| 4.2.2 Bootstrapping dynamic models: the residuals method | 102 |
| 4.2.3 Bootstrap based estimates of uncertainty in SMI . | 103 |
| 4.3 Simulation example | 104 |
| 4.4 Conclusions | 108 |
| 5 From unstructured to structured models with an \mathcal{H}_∞ approach | 109 |
| 5.1 Introduction | 109 |
| 5.2 Problem statement | 110 |
| 5.3 Approach | 111 |
| 5.3.1 Linear time-invariant systems | 111 |
| 5.3.2 Linear time-periodic systems | 112 |
| 5.3.3 Linear parameter-varying systems | 114 |
| 5.4 Simulation examples | 115 |
| 5.4.1 A linear time-invariant system | 115 |
| 5.4.2 A linear time-periodic system | 117 |
| 5.4.3 A linear parameter varying system | 120 |
| 5.5 Concluding remarks | 122 |
| II Applications | 125 |
| 6 Rotorcraft system identification | 127 |
| 6.1 Introduction | 127 |
| 6.2 Challenges of rotorcraft system identification | 129 |
| 6.2.1 Models of rotary-wing aircraft dynamics | 129 |
| 6.2.2 Flight test procedure | 130 |
| 6.2.3 Data consistency | 131 |

| | | |
|----------|---|------------|
| 6.3 | Classical rotorcraft identification methods | 132 |
| 6.3.1 | Time domain system identification | 132 |
| 6.3.2 | Frequency domain system identification | 133 |
| 6.3.3 | Comparison between frequency and time domain identification techniques | 135 |
| 6.4 | An underrated rotorcraft model identification method: the subspace approach | 138 |
| 7 | Data consistency analysis for rotorcraft model identification | 141 |
| 7.1 | Introduction | 141 |
| 7.2 | Problem Statement | 143 |
| 7.3 | Data compatibility analysis methods | 146 |
| 7.3.1 | Output Error | 147 |
| 7.3.2 | Unscented Kalman Filter | 148 |
| 7.3.3 | Expectation Maximisation with Particle Filter | 149 |
| 7.4 | Experimental results | 150 |
| 7.4.1 | System description | 151 |
| 7.4.2 | Case study: rotational kinematics | 151 |
| 7.4.3 | Results | 152 |
| 7.5 | Conclusions | 157 |
| 8 | Helicopter dynamics identification: black-box and gray-box modelling | 159 |
| 8.1 | Introduction | 159 |
| 8.2 | Black-box and gray-box modelling of the helicopter dynamics | 160 |
| 8.3 | BO-105 simulation model | 161 |
| 8.4 | Model identification results | 163 |
| 8.5 | Concluding remarks | 166 |
| 9 | Identification of linear models for the dynamics of a hovering quadrotor | 175 |
| 9.1 | Introduction | 175 |
| 9.2 | Identification-oriented quadrotor flight testing | 176 |
| 9.2.1 | Input-output variables selection | 176 |
| 9.2.2 | Identification experiments | 177 |
| 9.3 | Experimental results | 179 |
| 9.3.1 | Time-domain data | 179 |
| 9.3.2 | Identification of uncoupled models for the individual DOFs | 180 |
| 9.3.3 | Time-domain validation | 182 |
| 9.3.4 | Uncertainty analysis: frequency responses | 184 |

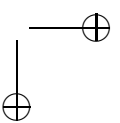
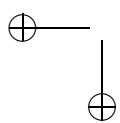
| | |
|--|------------|
| 9.3.5 Uncertainty analysis: poles and zeros | 188 |
| 9.4 Concluding remarks | 191 |
| A Signals and systems theory: some preliminaries | 199 |
| A.1 Signals | 199 |
| A.1.1 Time-domain norms of signals | 200 |
| A.1.2 Signals in the frequency-domain | 201 |
| A.2 Systems | 203 |
| A.2.1 Linear systems | 204 |
| A.2.2 The space $\mathcal{L}_\infty(j\mathbb{R})$ | 206 |
| A.2.3 The space \mathcal{H}_∞ | 207 |
| A.2.4 Adjoint systems | 208 |
| A.2.5 All-pass/Inner systems | 208 |
| A.3 Basis of $\mathcal{L}_2(j\mathbb{R})/\mathcal{L}_2(-\infty, \infty)$ | 209 |
| A.3.1 Continuous-time generalized orthonormal basis function (CT-GOBF) | 211 |
| A.3.2 The Laguerre basis | 212 |
| Bibliography | 215 |



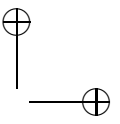
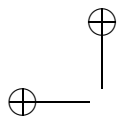
—

|

—



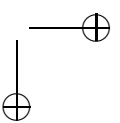
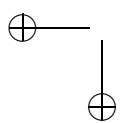
|



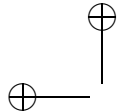
—

|

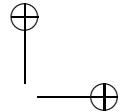
—



|



|

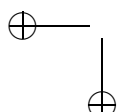


Part I

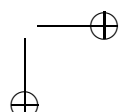
Methods

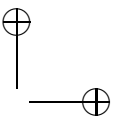
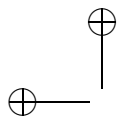
—

—



|

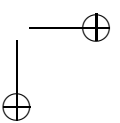
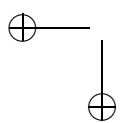




—

|

—



|

CHAPTER ONE

CONTINUOUS-TIME PREDICTOR BASED SUBSPACE IDENTIFICATION

In this Chapter the problem of continuous-time model identification is introduced and two novel subspace-based algorithms capable of dealing with data generated by systems operating in closed-loop are presented. The algorithms are developed by reformulating the identification problem from the continuous-time model to equivalent ones to which discrete-time subspace identification techniques can be applied. More precisely, two approaches are considered, the former leading to the so-called all-pass domain by using a bank of Laguerre filters applied to the input-output data and the latter corresponding to the projection of the input-output data onto an orthonormal basis, again defined in terms of Laguerre filters. In both frameworks, the PBSID subspace identification algorithm, originally developed in the case of discrete-time systems, can be reformulated for the continuous-time case. Simulation results are used to illustrate the achievable performance of the proposed approaches with respect to existing methods available in the literature.

1.1 Introduction

In the engineering field most physical phenomena are usually described using continuous-time mathematical model. Discrete-time models can be obviously used to describe a physical system but this kind of choice is usually preferable only to design a digital controller. In a number of real situations the continuous-time models are favored merely because the physical systems evolve continuously with respect to time.

As example consider a model filled with parameters with a physical

meaning such as time constants, reaction time, elasticity, mass, etc. The continuous-time model contains directly the physical parameters. Consider the following second order continuous-time transfer function (Garnier and Wang [2008])

$$\frac{1}{ms^2 + bs + k} \quad (1.1)$$

where the parameters can represent mass, elasticity and friction. Discrete-time models, on the other hand, do not have the same physical interpretability as do the continuous-time representations. Considering the continuous-to-discrete time transformation (1.2), the parameters in the discrete time model of the process described by (1.1), *i.e.*,

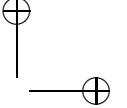
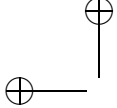
$$\frac{b_0 z + b_1}{a_0 z^2 + a_1 z + a_2}$$

do not have a physical meaning.

The continuous-time system identification techniques have several advantages respect to their discrete-time counterparts, as underlined in Garnier and Wang [2008]. First of all, in some cases the sampled input/output data are possibly associated with a non equidistant sequence of sampling instants. This problem arises in areas where the instant of a measurement is not under control of the experimenter, *e.g.*, medicine, transport and traffic systems, astrophysics. In all these cases a discrete-time model can not be used since it is inherently based on a constant sampling period. On the other hand, the continuous-time model, which is independent of the sampling period, is more flexible, indeed it is able to capture the system behavior at every time instance. The measurements are basically just points on a continuous line, which do not need to be equidistantly spaced.

Another advantage of the continuous-time model identification methods is their capability to deal with the identification of stiff systems. A stiff system is characterized by time constants that are of different order of magnitude, *i.e.*, a stiff system contains both slow and fast dynamics. In order to capture the fast dynamics the sampling must be in turn very fast, at the same time to capture the slow dynamics a long recording is required. As result, a large amount of data is necessary to identify a stiff system leading to long calculation times and numerical ill-conditioning (see Haverkamp [2001], where data from an experimental example is taken into account).

As will be shown in this Chapter, the proposed continuous-time identification algorithms allow to use different sample time in the same experiment so that stiff system can be identified properly without the use of large amount of samples. In other words, the sampling can be adapted according



to the dynamics of the system, *i.e.*, taking every time constant or group of time constants into account separately, in order to identify consistently fast and slow dynamics. This approach reduces the size of dataset and so the computation load and numerical instability.

The common way to identify a continuous-time model from equidistantly sampled data is to estimate a discrete-time model and then to transform it using the well-known relation between the continuous time Laplace operator s and the discrete time z operator, *i.e.*,

$$s = \frac{\ln z}{T_s} \quad (1.2)$$

where T_s is the sampling period. This relation has several well-known drawbacks because of the involved logarithm, *e.g.*, poles with a negative real part in the discrete-time model yield continuous-time model with complex coefficients without physical meaning. The choice of the sampling time T_s is tricky since a large sampling time leads to loss of information but, on the other hand, small sampling time groups the poles of the discrete time model near $z = 1$ leading to numerical ill-conditioning as shown in Sinha and Rao [1991]. The function between s and z defined in (1.2) is not bijective, *i.e.*, considering its inverse

$$z = e^{sT_s}, \quad (1.3)$$

it is clear that the transformation from s -domain to z -domain is not injective, indeed (1.3) maps the points $s = (x+iy)+i\left(k\frac{2\pi}{T_s}\right)$, $k = -\infty, \dots, 0, \dots, \infty$ to the same point in the z -plane. As shown in Figure 1.1, every horizontal band in the s -domain of height $\frac{2\pi}{T_s}$, *i.e.*, S_k , $k = -\infty, \dots, 0, \dots, \infty$, maps to the entire z -domain.

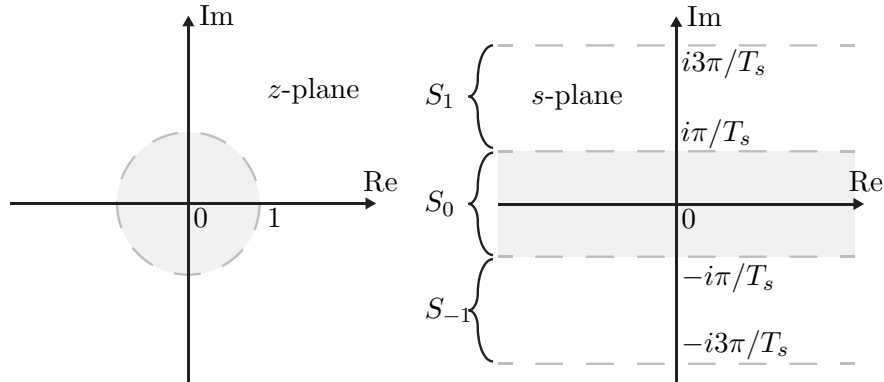
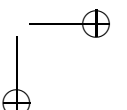
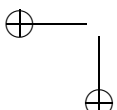


Figure 1.1: Relation among z -plane and s -plane.



In this thesis two different discrete-time domains are introduced to overcome all the problems of the relation $s-z$, indeed the new domains are characterized by a bijective relation with the s -domain. The discrete-time models defined in these new domains can be estimated directly from data, using a filtered or a projected version of the original signals. Due to the bijective nature of the new relations the parameters of the discrete-time models can be transformed to their corresponding of the continuous-time model using simple algebraic relations.

Finally, in this Chapter a continuous-time version of the so-called Predictor-Based Subspace IDentification (PBSID) algorithm (see Chiuso [2007]) is provided, based on the adoption of Laguerre filtering, as proposed in Haverkamp [2001], and orthonormal basis functions, as originally proposed in Ohta and Kawai [2004], Ohta [2011].

The Chapter is organised as follows: Section 1.2 provides a concise statement of the continuous-time SMI problem. The continuous-time to discrete-time transformation is faced in 1.3 where two different methods are analyzed. The proposed approaches are presented in detail in Sections 1.4 and 1.5. Issues related with the actual discrete-time implementation of the algorithms are highlighted in Sections 1.4 and 1.5, while simulation results are presented and discussed in Section 1.6. Some concluding remarks are done in Section 1.7.

1.2 Problem statement

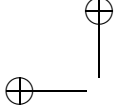
In this Section the problem statement is introduced. Some preliminaries necessary to understand this Section can be found in Appendix A.

Definition 1.2.1. Consider the linear, time-invariant stochastic continuous-time system

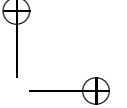
$$\begin{aligned} dx(t) &= Ax(t)dt + Bu(t)dt + dw(t), \quad x(0) = x_0 \\ dz(t) &= Cx(t)dt + Du(t)dt + dv(t) \\ y(t)dt &= dz(t) \end{aligned} \tag{1.4}$$

where $x \in \mathbb{R}^n$, $u \in \mathbb{R}^{n_u}$ and $y \in \mathbb{R}^{n_y}$ are, respectively, the state, input and output vectors and $w \in \mathbb{R}^n$ and $v \in \mathbb{R}^{n_y}$ are the process and the measurement noises modelled as Wiener processes with incremental covariance given by

$$E \left\{ \begin{bmatrix} dw(t) \\ dv(t) \end{bmatrix} \begin{bmatrix} dw(t) \\ dv(t) \end{bmatrix}^T \right\} = \begin{bmatrix} Q & S \\ S^T & R \end{bmatrix} dt. \tag{1.5}$$



|



A definition of a Wiener process is given in Stark and Woods [2002].

Assumption 1. *The system matrices A , B , C and D , of appropriate dimensions, are such that (A, C) is observable, and $(A, [B \ Q^{\frac{1}{2}}])$ is controllable.*

The unmeasurable disturbance signals $w(t)$ and $v(t)$, respectively, represent the uncertainty in the system model and the measurement noise. Assume that a dataset $\{u(t_i), y(t_i)\}$, $i \in [1, N]$ of sampled input/output data (possibly associated with a non equidistant sequence of sampling instants) obtained from system (1.4) is available. Then, the problem is to provide a consistent estimate of the state space matrices A , B , C and D (up to a similarity transformation) on the basis of the available data.

Definition 1.2.2. *Under the Assumption 1, the innovation form of the continuous-time system (1.4) is*

$$\begin{aligned} d\hat{x}(t) &= A\hat{x}(t)dt + Bu(t)dt + Kde(t), \quad x(0) = x_0 \\ d\hat{z}(t) &= C\hat{x}(t)dt + Du(t)dt \\ y(t)dt &= dz(t) + de(t), \end{aligned} \tag{1.6}$$

— where $e \in \mathbb{R}^{n_y}$ is a Wiener process and it is called innovation. If the system matrices and the noises covariance matrices are known, the Kalman gain K and the error covariance P are given by —

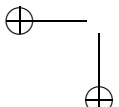
$$\begin{aligned} K &= (PC^T + S)R^{-1} \\ 0 &= AP + PA^T + Q - PC^TR^{-1}CP. \end{aligned}$$

The main issue in the application of SMI methods to continuous-time model identification is the need of computing the high order derivatives of input-output measurements arising from the continuous-time data equation. This problem has been faced in the literature using a number of different approaches, of which two will be considered in the present study (see Garnier and Wang [2008] and the references therein for further details).

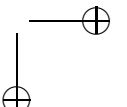
1.3 Continuous-time to discrete-time transformation

In this Section two methods to transform a continuous-time system and signals to their discrete-time representations are shown.

The former approach is based on the idea first introduced in Johansson et al. [1999a], where a filtered version of the signals is used instead of computing high-order derivatives of the input/output signals. An evolution of



|



this idea is presented in Haverkamp [2001], where the Laguerre filters are used providing a number of suitable properties.

The latter approach is based on the idea first introduced in Ohta [1999] where a general framework for the signal and system transformation is shown. This transformation can be specialized in order to identify LTI systems, as shown in Ohta and Kawai [2004], where a continuous-time version of the PO-MOESP algorithm is derived. The transformation theory explores the relation between the first order inner function and the Laguerre basis to transform both signals and system model. The advantage of using the Laguerre basis instead of other bases, *e.g.*, the Kautz basis as in Wahlberg [1994], is matter of discussion, but it is not addressed in this thesis since there is no evidence of better performance taking more complex basis. The transformation theories presented in this Chapter introduce operators applied to the input and output signals of a system, so that a discrete-time model can be derived directly from the continuous-time model.

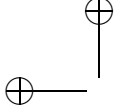
Many other choices of operators have been considered in literature, for instance low-pass filtering Johansson et al. [1999b] or Poisson moment functional (PMF) Saha and Rao [1982], leading to a wide family of similar identification methods. A problem one encounters with more complex operators is the increase in the number of parameters the user has to specify. The optimal choice of the tuning parameters of the operators presented herein is investigated in Section 1.6.3. As will be shown this problem can be solved only numerically even if the number of parameters is low.

1.3.1 Laguerre filters

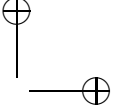
The first approach relies on the idea, first proposed in Johansson et al. [1999a] and further developed in Haverkamp [2001], of resorting to the bilinear transformation associated with a first order all-pass filter in order to convert the derivative operation to low-pass filtering based on the class of Laguerre orthogonal filters. It can be shown that an input-output data equation similar to the one for discrete-time state space models can be derived, to which SMI techniques can be applied.

The Laguerre filter

In this Section the Laguerre filter is introduced. The Laguerre filters are widely used in system identification as basis-functions; indeed they are an orthonormal basis for the function space $\mathcal{L}_2(i\mathbb{R})$ as discussed in Appendix A. Some of their properties will be demonstrated in this Section. The Laguerre filter has a close relation to the first order all-pass filter, see also Section



|



1.3.2. A bank of Laguerre filters can be viewed as a single low-pass filter in combination with a bank of all-pass filters.

The transfer function of the i -th (order $i+1$) continuous-time Laguerre filter is given by

$$\mathcal{L}_i(s) = \sqrt{2a} \frac{(s-a)^i}{(s+a)^{i+1}}. \quad (1.7)$$

For $a > 0$ this filter is stable, while for $a < 0$ the filter is unstable. As is shown in Green and Limebeer [1994], an unstable filter (system) can be regarded as an anti-causal filter (system) which is used backwards in time. The filter is assumed to be always stable.

In this thesis $\ell_i(t)$ denotes the impulse response of the i -th Laguerre filter. $[\ell_i u](t)$ denotes the convolution of the signal $u(t)$ with the impulse response $\ell_i(t)$, i.e., $[\ell_i u](t) = \int_0^t \ell_i(t-\tau)u(\tau)d\tau$.

Then, the following results hold.

Lemma 1.3.1. ([Haverkamp, 2001, Lemma 3.2]) Let $\ell_q(t)$ and $\ell_r(t)$ be the Impulse Response Functions (IRF)s of the q -th and r -th Laguerre filter respectively then

$$\int_0^\infty \ell_q(\tau)\ell_r(\tau)d\tau = \delta_{qr},$$

with δ_{qr} the Kronecker delta.

Lemma 1.3.2. (Makila [1990]) Every function $h(t) \in \mathcal{L}_2(0, \infty)$ can be written as a weighted sum of Laguerre filters

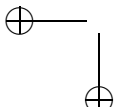
$$h(t) = \sum_{i=0}^{\infty} \alpha_i \ell_i(t),$$

where $\alpha_i = \int_0^\infty h(\tau)\ell_i(\tau)d\tau$.

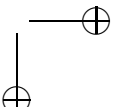
Theorem 1.3.3. ([Haverkamp, 2001, Theorem 3.3]) Let $\mathcal{L}_q(s)$ and $\mathcal{L}_r(s)$ be the q -th and r -th Laguerre filter defined by equation (1.7) and $\ell_q(t)$ and $\ell_r(t)$ the IRFs belonging to these filters. Let $v(t)$ and $w(t)$ be two Wiener processes with incremental cross-covariance Sdt . Let $[\ell_q v](t)$ denote the filtering of $v(t)$ with $\ell_q(t)$ and $[\ell_r w](t)$ the filtering of $w(t)$ with $\ell_r(t)$. Then

$$E \{ [\ell_q v](t) [\ell_r w]^T(t) \} = S \delta_{qr}. \quad (1.8)$$

This theorem shows a similarity between the Laguerre filters and the discrete time shift operator. Let $v(k)$ and $w(k)$ be two discrete time white



|





noise sequences with cross-covariance $S\delta(k)$. Let z denote the forward shift operator with the property $[z^i v](k) = v(k+i)$, then

$$E \{ [z^q v](k) [z^r w]^T(k) \} = S\delta(q-r).$$

This relation is very similar to equation (1.8). The Laguerre filter can be seen as a replacement of the z operator in the continuous-time domain.

In order to understand the behavior of the stable Laguerre filters in the time domain, the IRFs of the first 5 Laguerre filters are shown in Figure 1.2.

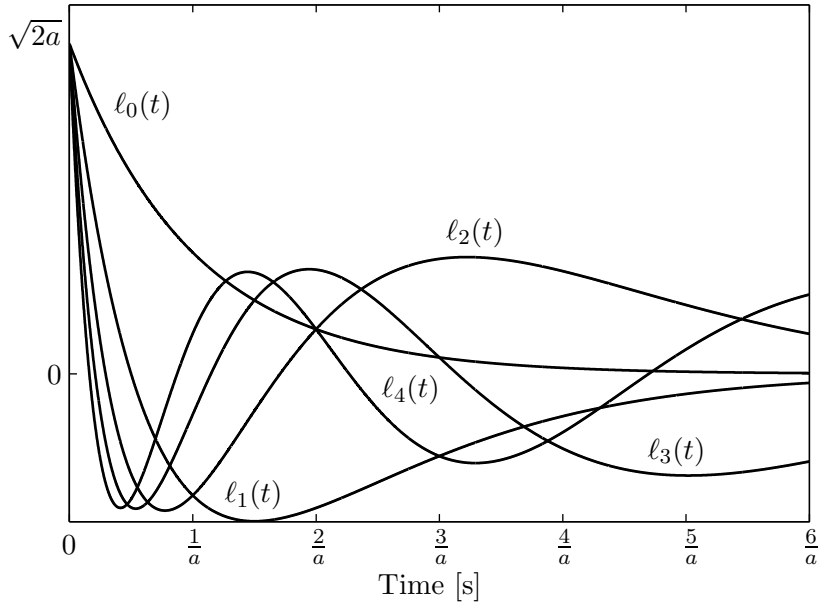


Figure 1.2: IRFs of the Laguerre filters $\mathcal{L}_0(s)$ up to $\mathcal{L}_4(s)$.

In the next Section the first order all-pass filter is introduced. The relation between the all-pass filter and the Laguerre filters will be shown. Both filters will be used in the derivation of the continuous-time predictor based subspace identification algorithm presented in Section 1.3.1.

The all-pass filter

The first order all-pass filter is given by the following equation:

$$w(s) = \frac{s-a}{s+a}. \quad (1.9)$$





On the imaginary axis, the magnitude of $w(s)$ is constant, in other words $|w(j\omega)| = 1$ or $w^\sim(j\omega)w(j\omega) = 1$ almost everywhere on the imaginary axis, where $w^\sim(j\omega) = w^T(-j\omega)$ is the para-conjugate. This means that the filter has a constant, unit amplitude amplification.

The all-pass filter is used as an operator. The argument s of $w(s)$ can be omitted for brevity. The notation $w_i(t)$ denotes the time domain representation (impulse response) of a concatenation of i first order all-pass filters, i.e., $w_i(t) = \mathcal{F}^{-1}[w^i(s)]$, where $\mathcal{F}^{-1}[\cdot]$ is the inverse Fourier transform. $[w_i u](t)$ denotes the convolution of $u(t)$ with $w_i(t)$, i.e., $[w_i u](t) = \int_0^t w_i(t-\tau)u(\tau)d\tau$. According to Haverkamp [2001], a bank of Laguerre filters can be defined using the all-pass filter in the following way,

$$\mathcal{L}_0(s) = \frac{\sqrt{2a}}{s+a} = \frac{(1-w(s))}{\sqrt{2a}}.$$

It is trivial to show that the first Laguerre filter $\mathcal{L}_1(s)$ can be obtained multiplying the zero-th Laguerre filter with $w(s)$. The multiplication can be iterated in order to obtain high-order Laguerre filters. This procedure can be packed in a bank of Laguerre filters which structure is shown in Figure 1.3.

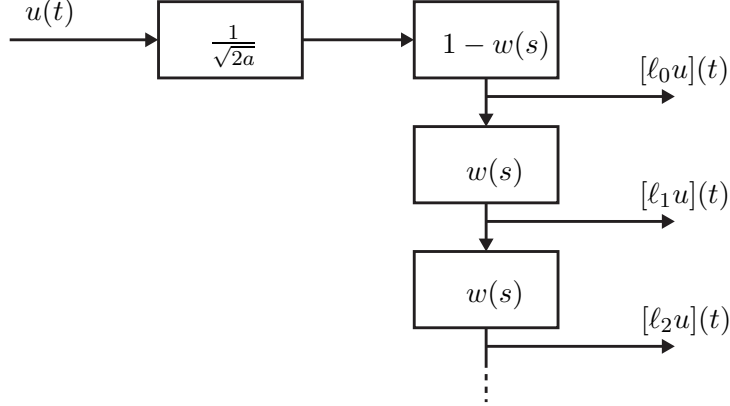


Figure 1.3: Block diagram of a Laguerre filter bank, constructed from all-pass filters.

In order to simplify the notation, a modified version of Laguerre filters is introduced in Haverkamp [2001], so

$$L_i(s) = 2a \frac{(s-a)^i}{(s+a)^{i+1}}. \quad (1.10)$$

This filter equals the Laguerre filter $\mathcal{L}_i(s)$ up to the constant factor $\sqrt{2a}$. Since the orthogonality property of the Laguerre filters is unchanged the





name Laguerre filter for this filter is kept, even if the normality property is lost. Using this definition, it holds the relation

$$L_i(s) = (1 - w(s))w(s)^i \quad (1.11)$$

that will be used frequently in the next Sections.

Like previous filters, the notation $l_i(t)$ denotes the time domain representation (impulse response) of the $L_i(s)$ filter. $[l_i u](t)$ denotes the convolution of the signal $u(t)$ with the impulse response $l_i(t)$, *i.e.*, $[l_i u](t) = \int_0^t l_i(t - \tau)u(\tau)d\tau$.

The choice of the all-pass operator is guided by its simplicity and the orthogonality properties in the Laguerre filters that result from it. These properties make it a very suitable choice for system identification, indeed in Section 1.3.2 another kind of relation between the first order all-pass filter and the Laguerre filters will be exploited.

All-pass domain state-space description

On the basis of the definitions given in the previous Sections, according to [Haverkamp, 2001, Lemma 3.4] and considering the Laguerre-like filters defined in (1.10), the state space model (1.4) can be equivalently written as

$$\begin{aligned} [wx](t) &= A_w x(t) + B_w [l_0 u](t) + [l_0 w_w](t) + F_1 x_0 l_0(t) \\ [l_0 y](t) &= C_w x(t) + D_w [l_0 u](t) + [l_0 v_w](t) + F_2 x_0 l_0(t), \end{aligned} \quad (1.12)$$

where the state space matrices are given by

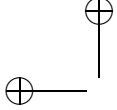
$$\begin{aligned} A_w &= (A + aI)^{-1}(A - aI) \\ B_w &= (A + aI)^{-1}B \\ C_w &= 2aC(A + aI)^{-1} \\ D_w &= D - C(A + aI)^{-1}B \\ F_1 &= (A + aI)^{-1} \\ F_2 &= C(A + aI)^{-1}. \end{aligned} \quad (1.13)$$

The new noise processes w_w and v_w are defined as

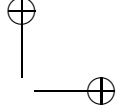
$$\begin{aligned} w_w(t)dt &= (A + aI)^{-1}dw(t) \\ v_w(t)dt &= dv(t) - C(A + aI)^{-1}dw(t), \end{aligned} \quad (1.14)$$

and x_0 is the initial state of the original continuous-time system.





|



Given two Wiener processes $w(t)$ and $v(t)$ with incremental cross-covariance Sdt , according to equation (1.8) the cross-covariance of the signals $[l_q w](t)$ and $[l_r v](t)$ is

$$E \{ [l_q w](t) [l_r v]^T(t) \} = 2aS\delta_{qr}. \quad (1.15)$$

Therefore the covariance matrix of the signals $[l_q w_w](t)$ and $[l_r v_w](t)$, as defined in (1.14), is given by

$$E \left\{ \begin{bmatrix} [l_q w_w](t) \\ [l_r v_w](t) \end{bmatrix} \begin{bmatrix} [l_q w_w]^T(t) & [l_r v_w]^T(t) \end{bmatrix} \right\} = \begin{bmatrix} Q_w & S_w \\ S_w^T & R_w \end{bmatrix} \delta_{qr},$$

where

$$E \{ [l_0 w_w](t) [l_0 w_w]^T(t) \} = Q_w \delta_{qr} = 2a(A + aI)^{-1}Q(A^T + aI)^{-1}\delta_{qr}$$

$$\begin{aligned} E \{ [l_0 w_w](t) [l_0 v_w]^T(t) \} &= S_w \delta_{qr} \\ &= 2a [(A + aI)^{-1}S + \\ &\quad -(A + aI)^{-1}Q(A^T + aI)^{-1}C^T] \delta_{qr} \end{aligned}$$

$$\begin{aligned} E \{ [l_0 v_w](t) [l_0 v_w]^T(t) \} &= R_w \delta_{qr} \\ &= 2a [R - S^T(A^T + aI)^{-1}C^T - C(A + aI)^{-1}S + \\ &\quad + C(A + aI)^{-1}Q(A^T + aI)^{-1}C^T] \delta_{qr}. \end{aligned}$$

System (1.12) can be equivalently written in innovation form

$$\begin{aligned} [w\hat{x}](t) &= A_w\hat{x}(t) + B_w[l_0 u](t) + F_1 x_0 l_0(t) + K_w[l_0 e](t) \\ [l_0 \hat{y}](t) &= C_w\hat{x}(t) + D_w[l_0 u](t) + F_2 x_0 l_0(t) \\ [l_0 y](t) &= [l_0 \hat{y}](t) + [l_0 e](t), \end{aligned} \quad (1.16)$$

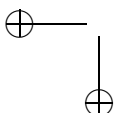
where the Kalman gain K_w is given by

$$\begin{aligned} P_w &= A_w P_w A_w^T + Q_w + \\ &\quad - (A_w P_w C_w^T + S_w^T)(C_w P_w C_w^T + R_w)^{-1}(C_w P_w A_w^T + S_w) \\ K_w &= (A_w P_w C_w^T + S_w^T)(C_w P_w C_w^T + R_w)^{-1}. \end{aligned} \quad (1.17)$$

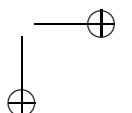
K_w is also related to the steady state continuous-time Kalman gain K of (1.6) by

$$K = 2a(I - A_w + K_w C_w)^{-1} K_w.$$

The innovation form of the discrete-time system (1.16) will be used to derive the continuous-time predictor based identification method as explained in the Section 1.4.



|



Lemma 1.3.4. Let the continuous-time system matrix A related to the matrix A_w according to the transformation (1.13). Then the eigenvalues of A located in the open left half plane are mapped in eigenvalues of A_w located outside the open unit disk, and the eigenvalues of A located in the open right half plane are mapped in eigenvalues of A_w located inside the open unit disk.

Proof. The Schur decomposition of matrix A is taken into account, i.e., $A = UTU^H$. U is a unitary matrix and T is called Schur form of A and it is an upper triangular matrix. The eigenvalues of A , i.e., $\sigma(A) = \{\lambda_1, \lambda_2, \dots, \lambda_n\}$, are the diagonal entries of T . Then

$$\begin{aligned} A_w &= (A + aI)^{-1}(A - aI) \\ &= (UTU^{-1} + aI)^{-1}(UTU^{-1} - aI) \\ &= U(T + aI)^{-1}(T - aI)U^{-1} \end{aligned}$$

and the eigenvalues of A_w are

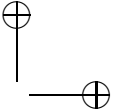
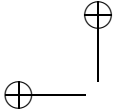
$$\begin{aligned} \sigma(A_w) &= \sigma(U(T + aI)^{-1}(T - aI)U^{-1}) \\ &= \sigma((T + aI)^{-1}(T - aI)) \\ &= \sigma((T + aI)^{-1}(T - aI)) \\ &= \sigma\left(\begin{bmatrix} \lambda_1 + a & * & * \\ * & \ddots & * \\ 0 & 0 & \lambda_n + a \end{bmatrix}^{-1} \begin{bmatrix} \lambda_1 - a & * & * \\ * & \ddots & * \\ 0 & 0 & \lambda_n - a \end{bmatrix}\right) \\ &= \sigma\left(\begin{bmatrix} \frac{1}{\lambda_1+a} & * & * \\ * & \ddots & * \\ 0 & 0 & \frac{1}{\lambda_n+a} \end{bmatrix}^{-1} \begin{bmatrix} \lambda_1 - a & * & * \\ * & \ddots & * \\ 0 & 0 & \lambda_n - a \end{bmatrix}\right) \\ &= \left\{ \frac{\lambda_1 - a}{\lambda_1 + a}, \frac{\lambda_2 - a}{\lambda_2 + a}, \dots, \frac{\lambda_n - a}{\lambda_n + a} \right\}. \end{aligned}$$

Given λ_i eigenvalue of A with $\operatorname{Re}(\lambda_i) < 0$ and $a > 0$, i.e., stable Laguerre filter, then

$$\left| \frac{\lambda_i - a}{\lambda_i + a} \right| > 1 \quad \forall i.$$

□

Assumption 2. Considering Lemma 1.3.4 the Laguerre basis pole a is assumed different from the eigenvalues of A , i.e., $a \notin \sigma(A)$.



Remark. It is interesting to point out that in view of the choice of using stable Laguerre filters to operate on the input-output data, the bilinear transformation relating the continuous-time state space matrices to the equivalent discrete-time ones is not the classical mapping from the open left half plane to the open unit disk. Indeed it is shown in Lemma 1.3.4 that the transformation (1.13) maps eigenvalues of A located in the open left half plane into eigenvalues of A_w located outside the open unit disk.

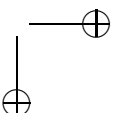
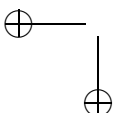
1.3.2 Laguerre projections

The second approach, based on the results presented in Ohta and Kawai [2004], Ohta [1999, 2005, 2007], allows to obtain a discrete-time equivalent model starting from the continuous-time system (1.4). Some preliminaries exposed in Appendix A.3 are necessary in order to fully understand this Section.

In Yamamoto [1994] the lifting technique was originally introduced in the framework of sampled-data control systems. The lifting technique is based on the idea to represent a continuous-time system by an equivalent discrete-time system whose input and output spaces are functional spaces. In Yamamoto's paper the space decomposition for the input and output signals is based on the irrational inner function $\phi(s) = e^{-sh}$. As explained in Appendix A.3 the delay function can be used in order to obtain a basis of $\mathcal{L}_2[0, \infty)$. In Ohta [1999, 2005] the lifting technique is extended. In Ohta [1999] it has been shown that any inner function can be used in order to decompose the input and output signals spaces, while in Ohta [2005] the rational inner functions are taken into account. Indeed, when the inner function is rational the orthogonal complement S , introduced in Appendix A.3, is finite-dimensional and the *lifted system* is called *transformed system*. Notice that the system transformation is induced by the signals transformation. This transformation is related to the Hambo system transformation, presented in detail in Heuberger et al. [1995], de Hoog et al. [2002], and Heuberger et al. [2003].

Lifting technique

In Yamamoto [1994] the lifting technique is used for hybrid sampled-data control systems. Instead of considering the state only at sampling instants, a function piece is introduced during the sampling period as the state and gives an infinite-dimensional model with such a state space.





Consider a continuous-time LTI system

$$\begin{aligned}\dot{x}(t) &= Ax(t) + Bu(t) \\ y(t) &= Cx(t) + Du(t).\end{aligned}\tag{1.18}$$

For simplicity, assume that the system is stable. System (1.18) defines an input-output map $\mathcal{L}_2[0, \infty) \mapsto \mathcal{L}_2[0, \infty) : u \mapsto y$. By the Fourier transform, system (1.18) also defines a map $\mathcal{H}_2 \mapsto \mathcal{H}_2 : \hat{u} \mapsto \hat{y}$. Let $G(s) = C(sI - A)^{-1} + D$ be the transfer function of the system, then $\hat{y} = G(s)\hat{u}$.

Given the inner function $\phi(s) = e^{-sh}$, a basis of $\mathcal{L}_2[0, \infty)$ can be defined as explained in Appendix A.3. Basically the idea is to regard a trajectory $x(t) \in \mathcal{L}_2[0, \infty)$ as a sequence of projections onto the basis of $\mathcal{L}_2[0, \infty)$, as shown in Figure 1.4.

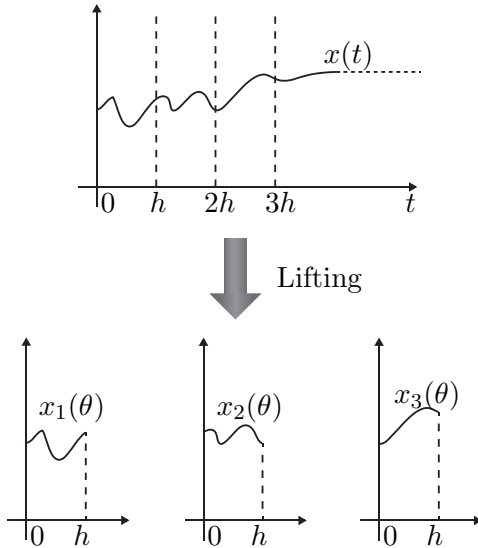


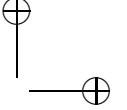
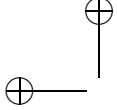
Figure 1.4: Projections of $x(t)$ onto basis of $\mathcal{L}_2[0, \infty)$ induced by the inner function $\phi(s) = e^{-sh}$.

The sequence of functions $\{x_k(\theta)\}_{k=1}^{\infty}$, projections of $x(t)$ on the basis of $\mathcal{L}_2[0, \infty)$, is defined as

$$x_k(\theta) = x((k-1)h + \theta), \quad \theta \in (0, h],\tag{1.19}$$

and gives a discrete-time state transition rule x_k . According to the Lagrange





formula (see Astrom and Murray [2008]), the evolution of the state is

$$\begin{aligned} x(t + \theta) &= e^{A(t+\theta)}x(0) + \int_0^{t+\theta} e^{A(t+\theta-\nu)}Bu(\nu)d\nu \\ &= e^{A\theta}x(t) + \int_t^{t+\theta} e^{A(t+\theta-\nu)}Bu(\nu)d\nu. \end{aligned}$$

Defining $\tau = \nu - t$ it holds

$$x(t + \theta) = e^{A\theta}x(t) + \int_0^\theta e^{A(\theta-\tau)}Bu(\tau+t)d\tau.$$

Considering (1.19), the state trajectory $x_{k+1}(\theta)$ follows the transition rules

$$x_{k+1}(\theta) = e^{A\theta}x_k(h) + \int_0^\theta e^{A(\theta-\tau)}Bu_{k+1}(\tau)d\tau$$

and the output trajectory is

$$y_k(\theta) = Cx_k(\theta) + Du_k(\theta), \quad 0 < \theta \leq h.$$

Introducing the operators

$$\begin{aligned} F : x(\theta) &\mapsto e^{A\theta}x(h), \\ G : u(\theta) &\mapsto \int_0^\theta e^{A(\theta-\tau)}Bu(\tau)d\tau, \\ H : x(\theta) &\mapsto Cx(\theta), \\ M : u(\theta) &\mapsto Du(\theta), \end{aligned}$$

the system can be written as

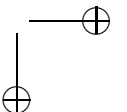
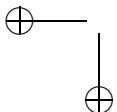
$$\begin{aligned} x_{k+1} &= Fx_k + Gu_{k+1} \\ y_k &= Hx_k + Mu_k. \end{aligned} \tag{1.20}$$

It is clear that (1.18) and (1.20) give exactly the same input-output correspondence. On the right-hand side of (1.20), the input term is u_{k+1} , not u_k . Introducing a new state variable

$$\xi_k = x_k - Gu_k,$$

the state trajectory becomes

$$\begin{aligned} x_{k+1} &= Fx_k + Gu_{k+1} \\ \xi_{k+1} + Gu_{k+1} &= F\xi_k + FGGu_k + Gu_{k+1} \\ \xi_{k+1} &= F\xi_k + FGGu_k, \end{aligned}$$



and the output trajectory is

$$\begin{aligned} y_k &= Hx_k + Mu_k \\ &= H\xi_k + HGu_k + Mu_k \\ &= H\xi_k + (HG + M)u_k. \end{aligned}$$

Summarizing, (1.20) becomes

$$\begin{aligned} \xi_{k+1} &= A_d\xi_k + B_d u_k \\ y_k &= C_d\xi_k + D_d u_k, \end{aligned} \tag{1.21}$$

where

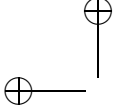
$$\begin{aligned} A_d : \xi &\mapsto e^{Ah}\xi, \\ B_d : u_k &\mapsto \int_{-h}^0 e^{-A\tau}Bu_k(h+\tau)d\tau, \\ C_d : \xi &\mapsto Ce^{A\theta}\xi, \quad \theta \in [0, h), \\ D_d : u_k &\mapsto Du_k(\theta) + C \int_0^t e^{A(\theta-\tau)}Bu_k(\tau)d\tau. \end{aligned}$$

The system (1.21) is the lifted system considered in Yamamoto [1994] to solve the sampled-data control problem. In the next Section will be shown that this idea can be extended to any inner function.

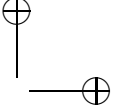
Deterministic system transformation

In Ohta [1999] the problem of deriving an exact formula for singular values and vectors of Hankel operators which arise from the \mathcal{H}_∞ control problem is faced. In order to solve this problem it was shown that a finite-dimensional continuous-time system has an equivalent input-output map (*lifted system*), characterized by an arbitrary single-input single-output inner function. In other words, the result in Yamamoto [1994] was extended to any SISO inner function, with a special attention to the functions that have a state-space representation.

In Ohta [2005] the input-output equivalent transformation (or Hambo transformation, see Heuberger et al. [2003]) of linear time-invariant systems induced by generalized orthonormal basis functions is studied. The transformation formulas presented therein are an extension of the work presented in Ohta [1999], since allow the use of any rational inner functions (even MIMO) (see Appendix A for any details).



|



Let ϕ be an inner function. The subspace $S = \mathcal{H}_2 \ominus \phi\mathcal{H}_2$ is the orthogonal complement of the subspace $\phi\mathcal{H}_2$. As shown in Appendix A the space of square integrable functions on the imaginary axis $\mathcal{L}_2(j\mathbb{R})$ can be written as

$$\mathcal{L}_2(j\mathbb{R}) = \bigoplus_{k=-\infty}^{\infty} \phi^k S, \quad (1.22)$$

where $\phi^{-1} = \phi^\sim$. From (1.22), any $u \in \mathcal{L}_2(j\mathbb{R})$ has the expression

$$u = \sum_{k=-\infty}^{\infty} \phi^k \tilde{u}(k), \quad \tilde{u}(k) \in S. \quad (1.23)$$

Furthermore, $\|u\|_2^2 = \sum_{k=-\infty}^{\infty} \|\tilde{u}(k)\|_2^2$. If the signal u is vector-valued, the transformation can be applied component-wise. Thus (1.22) and (1.23) are valid if $\tilde{u}(k)$ is interpreted as an S -valued vector function. Using the Fourier transform, this signal transformation is also applicable to the signal space $\mathcal{L}_2(-\infty, \infty)$. The transformation in (1.23) can be interpreted from a geometrical point of view as a *projection* of the signal u on the basis of $\mathcal{L}_2(j\mathbb{R})$ defined via the space S and the inner function ϕ .

As in the lifted technique, the signal transformation induce a system transformation. Consider a linear time-invariant continuous-time system

$$\begin{aligned} \dot{x}(t) &= Ax(t) + Bu(t) \\ y(t) &= Cx(t) + Du(t), \end{aligned} \quad (1.24)$$

where A , B , C , and D are matrices of compatible dimensions. It is assumed that A does not have eigenvalues on the imaginary axis. Then the transfer function

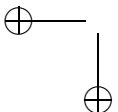
$$G(s) = C(sI - A)^{-1}B + D \quad (1.25)$$

defines an operator on $\mathcal{L}_\infty(j\mathbb{R})$, i.e., $(u \in \mathcal{L}_2(j\mathbb{R})) \mapsto y = Gu \in \mathcal{L}_2(j\mathbb{R})$. Because u and y are in $\mathcal{L}_2(j\mathbb{R})$, the signal transformation (1.23) induces a bounded map G_d , as shown in Ohta [1999]. It is also proved that the map G_d has the state space realisation

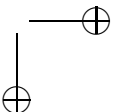
$$\begin{aligned} \xi(k+1) &= A_d\xi(k) + B_d\tilde{u}(k) \\ \tilde{y}(k) &= C_d\xi(k) + D_d\tilde{u}(k), \end{aligned} \quad (1.26)$$

with the operators

$$\begin{aligned} A_d : \xi &\mapsto \phi^\sim(A)\xi, \\ B_d : \tilde{u} &\mapsto \frac{1}{2\pi} \int_{-\infty}^{\infty} \overline{(-\phi^\sim(-A)(i\omega I - A)^{-1}B + \phi(i\omega)(i\omega I - A)^{-1}B)} u(i\omega) d\omega, \\ C_d : \xi &\mapsto (C(sI - A)^{-1} - \phi(s)C(sI - A)^{-1}\phi^\sim(A))\xi, \\ D_d : \tilde{u} &\mapsto h(s)u(s) - \phi(s)C(sI - A)^{-1}B_d u. \end{aligned} \quad (1.27)$$



|





This general result may not seem easily applicable to the continuous-time to discrete-time transformation problem arising in continuous-time system identification. As will be shown, the operators (1.27) assume a very simple formulation when the all-pass filter (1.9) is considered as inner function.

Indeed, taking the special case $\phi(s) = w(s) = \frac{s-a}{s+a}$ the *projection* of the signals on the basis is given by

$$\begin{aligned}\tilde{u}(k) &= \int_0^\infty \Lambda_w^k \ell_0(t) u(t) dt \\ \tilde{y}(k) &= \int_0^\infty \Lambda_w^k \ell_0(t) y(t) dt,\end{aligned}\quad (1.28)$$

where $\Lambda_w^k v(t) = \mathcal{F}^{-1}[w^k \mathcal{F}[v(t)]]$ is the multiplication operator as defined in (A.30). Note that $\Lambda_w^k \ell_0(t)$ is the impulse response function of the k -th Laguerre filter, *i.e.*, $\ell_k(t) = \Lambda_w^k \ell_0(t)$. In this special case the operators of the map G_d are constant and are given by

$$\begin{aligned}A_d &= (A - aI)^{-1}(A + aI) \\ B_d &= \sqrt{2a}(A - aI)^{-1}B \\ C_d &= -\sqrt{2a}C(A - aI)^{-1} \\ D_d &= D - C(A - aI)^{-1}B.\end{aligned}$$

Summarizing the results, the continuous-time system (1.24) has the equivalent representation (1.26) under the signal-based transformation (*projection*) (1.28).

Stochastic system transformation

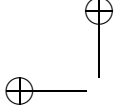
The results previously presented for the transformation of a deterministic continuous-time system are extended to the transformation of a stochastic system in Ohta [2007]. Consider a continuous-time linear stochastic system

$$\begin{aligned}dx(t) &= Ax(t)dt + Bdw(t) \\ dy(t) &= Cx(t)dt + Ddw(t),\end{aligned}\quad (1.29)$$

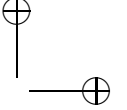
where A, B, C and D are of appropriate dimensions, w is a Wiener process with incremental covariance given by $E[dw(t)dw(t)^T] = Idt$. Considering the signal transformation

$$\begin{aligned}\tilde{w}(k) &= \int_0^\infty \Lambda_w^k \ell_0(t) dw(t) \\ \tilde{y}(k) &= \int_0^\infty \Lambda_w^k \ell_0(t) dy(t),\end{aligned}$$





|



the system (1.29) can be transformed in a discrete-time linear stochastic system given by

$$\begin{aligned}\xi(k+1) &= A_d\xi(k) + B_d\tilde{w}(k) \\ \tilde{y}(k) &= C_d\xi(k) + D_d\tilde{w}(k),\end{aligned}\quad (1.30)$$

where $\tilde{w}(k)$ is a discrete-time white Gaussian process defined as

$$\begin{aligned}E[\tilde{w}(k)] &= 0 \\ E[\tilde{w}(k)\tilde{w}(l)^T] &= I\delta_{kl},\end{aligned}$$

and the matrices are given by

$$\begin{aligned}A_d &= (A - aI)^{-1}(A + aI) \\ B_d &= \sqrt{2a}(A - aI)^{-1}B \\ C_d &= -\sqrt{2a}C(A - aI)^{-1} \\ D_d &= D - C(A - aI)^{-1}B.\end{aligned}$$

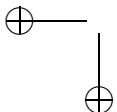
As can be seen, the deterministic and the stochastic signals and system transformations are exactly the same. This property is useful in order to consider the deterministic and the stochastic signals in the same setting.

Laguerre domain state-space description

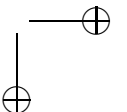
Consider the linear time-invariant continuous-time system in (1.4). It is possible to apply the results previously exposed to derive a discrete-time equivalent model, as follows.

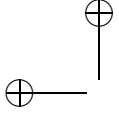
Theorem 1.3.5. (Ohta and Kawai [2004], Ohta [2007]) Consider the first order inner function $w(s)$ and apply to the input u , the output y , the process and the output noises w , and v of (1.4) the transformations

$$\begin{aligned}\tilde{u}(k) &= \int_0^\infty \Lambda_w^k \ell_0(t) u(t) dt \\ \tilde{w}(k) &= \int_0^\infty \Lambda_w^k \ell_0(t) dw(t) \\ \tilde{v}(k) &= \int_0^\infty \Lambda_w^k \ell_0(t) dv(t) \\ \tilde{y}(k) &= \int_0^\infty \Lambda_w^k \ell_0(t) y(t) dt,\end{aligned}\quad (1.31)$$

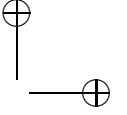


|





|



where $\tilde{u}(k) \in \mathbb{R}^m$, $\tilde{w}(k) \in \mathbb{R}^m$, $\tilde{v}(k) \in \mathbb{R}^p$, and $\tilde{y}(k) \in \mathbb{R}^p$. Then the transformed system has the state space representation

$$\begin{aligned}\xi(k+1) &= A_o\xi(k) + B_o\tilde{u}(k) + B_{ow}\tilde{w}(k), \quad \xi(0) = 0 \\ \tilde{y}(k) &= C_o\xi(k) + D_o\tilde{u}(k) + D_{ow}\tilde{w}(k) + \tilde{v}(k),\end{aligned}\quad (1.32)$$

where the state space matrices are given by

$$\begin{aligned}A_o &= (A - aI)^{-1}(A + aI) \\ B_o &= \sqrt{2a}(A - aI)^{-1}B \\ C_o &= -\sqrt{2a}C(A - aI)^{-1} \\ D_o &= D - C(A - aI)^{-1}B \\ B_{ow} &= \sqrt{2a}(A - aI)^{-1} \\ D_{ow} &= -C(A - aI)^{-1},\end{aligned}\quad (1.33)$$

and the signals $\tilde{w}(k)$ and $\tilde{v}(k)$ are zero-mean white Gaussian noises with covariance

$$E \left\{ \begin{bmatrix} \tilde{w}(k) \\ \tilde{v}(k) \end{bmatrix} \begin{bmatrix} \tilde{w}(l) \\ \tilde{v}(l) \end{bmatrix}^T \right\} = \begin{bmatrix} Q & S \\ S^T & R \end{bmatrix} \delta_{kl}. \quad (1.34)$$

Note that the subscript of the matrices o is used instead of d as in the previous Sections in order to emphasize the final results with respect to the intermediate ones. The system (1.32) can be written as follows

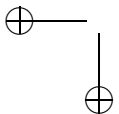
$$\begin{aligned}\xi(k+1) &= A_o\xi(k) + B_o\tilde{u}(k) + \tilde{w}_v(k), \quad \xi(0) = 0 \\ \tilde{y}(k) &= C_o\xi(k) + D_o\tilde{u}(k) + \tilde{v}_v(k),\end{aligned}\quad (1.35)$$

where $\tilde{v}_v(k)$ and $\tilde{w}_v(k)$ are zero-mean white Gaussian noises by construction and are given by

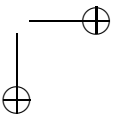
$$\begin{aligned}\tilde{w}_v(k) &= B_{ow}\tilde{w}(k) \\ \tilde{v}_v(k) &= D_{ow}\tilde{w}(k) + \tilde{v}(k),\end{aligned}$$

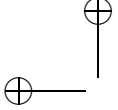
with

$$E \left\{ \begin{bmatrix} \tilde{w}_v(k) \\ \tilde{v}_v(k) \end{bmatrix} \begin{bmatrix} \tilde{w}_v^T(l) & \tilde{v}_v^T(l) \end{bmatrix} \right\} = \begin{bmatrix} Q_v & S_v \\ S_v^T & R_v \end{bmatrix} \delta_{kl},$$

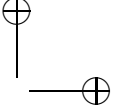


|





|



where

$$\begin{aligned}
 E\{\tilde{w}_v(k)\tilde{w}_v^T(l)\} &= Q_v\delta_{kl} = B_{ow}QB_{ow}^T\delta_{kl} \\
 &= 2a(A-aI)^{-1}Q(A^T-aI)^{-1}\delta_{kl} \\
 E\{\tilde{w}_v(k)\tilde{v}_v^T(l)\} &= S_v\delta_{kl} = B_{ow}(QD_{ow}^T+S)\delta_{kl} \\
 &= \sqrt{2a}(A-aI)^{-1}(S-Q(A^T-aI)^{-1}C^T)\delta_{kl} \\
 E\{\tilde{v}_v(k)\tilde{v}_v^T(l)\} &= R_v\delta_{kl} = (D_{ow}QD_{ow}^T+D_{ow}S+S^TB_{ow}^T+R)\delta_{kl} \\
 &= \left(C(A-aI)^{-1}Q(A^T-aI)^{-1}C^T-C(A-aI)^{-1}S\right. \\
 &\quad \left.+\sqrt{2a}S^T(A^T-aI)^{-1}+R\right)\delta_{kl}.
 \end{aligned}$$

System (1.35) can be equivalently written in innovation form

$$\begin{aligned}
 \xi(k+1) &= A_o\xi(k) + B_o\tilde{u}(k) + K_o\tilde{e}(k), \quad \xi(0) = 0 \\
 \tilde{y}(k) &= C_o\xi(k) + D_o\tilde{u}(k) + \tilde{e}(k),
 \end{aligned} \tag{1.36}$$

where the Kalman gain K_o is given by

$$\begin{aligned}
 P_v &= A_oP_vA_o^T + Q_v - (A_oP_vC_o^T + S_v^T)(C_oP_vC_o^T + R_v)^{-1}(C_oP_vA_o^T + S_v) \\
 K_o &= (A_oP_vC_o^T + S_v^T)(C_oP_vC_o^T + R_v)^{-1}.
 \end{aligned} \tag{1.37}$$

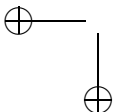
K_o is also related to the steady state continuous-time Kalman gain K of (1.6) by

$$K_o = \sqrt{2a}(I - C(A-aI)^{-1}K)^{-1}(A-aI)^{-1}K. \tag{1.38}$$

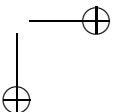
Lemma 1.3.6. *Let the continuous-time system matrix A related to matrix A_o according the transformation (1.33). Then the eigenvalues of A located in the open left half plane are mapped in eigenvalues of A_o located inside the open unit disk, and the eigenvalues of A located in the open right half plane are mapped in eigenvalues of A_o located outside the open unit disk.*

Proof. The Schur decomposition of matrix A is taken into account, i.e., $A = UTU^H$. U is a unitary matrix and T is called Schur form of A and it is an upper triangular matrix. The spectrum of A , i.e., $\sigma(A) = \{\lambda_1, \lambda_2, \dots, \lambda_n\}$, are the diagonal entries of T .

$$\begin{aligned}
 A_o &= (A-aI)^{-1}(A+aI) \\
 &= (UTU^{-1}-aI)^{-1}(UTU^{-1}+aI) \\
 &= U(T-aI)^{-1}(T+aI)U^{-1}.
 \end{aligned}$$



|



The eigenvalues of A_o are

$$\begin{aligned}
 \sigma(A_o) &= \sigma(U(T - aI)^{-1}(T + aI)U^{-1}) \\
 &= \sigma((T - aI)^{-1}(T + aI)) \\
 &= \sigma((T - aI)^{-1}(T + aI)) \\
 &= \sigma\left(\begin{bmatrix} \lambda_1 - a & * & * \\ \vdots & \ddots & \vdots \\ 0 & 0 & \lambda_n - a \end{bmatrix}^{-1} \begin{bmatrix} \lambda_1 + a & * & * \\ \vdots & \ddots & \vdots \\ 0 & 0 & \lambda_n + a \end{bmatrix}\right) \\
 &= \sigma\left(\begin{bmatrix} \frac{1}{\lambda_1 - a} & * & * \\ \vdots & \ddots & \vdots \\ 0 & 0 & \frac{1}{\lambda_n - a} \end{bmatrix}^{-1} \begin{bmatrix} \lambda_1 + a & * & * \\ \vdots & \ddots & \vdots \\ 0 & 0 & \lambda_n + a \end{bmatrix}\right) \\
 &= \left\{ \frac{\lambda_1 + a}{\lambda_1 - a}, \frac{\lambda_2 + a}{\lambda_2 - a}, \dots, \frac{\lambda_n + a}{\lambda_n - a} \right\}.
 \end{aligned}$$

Given λ_i eigenvalue of A with $\text{Re}(\lambda_i) < 0$ and $a > 0$, i.e., stable Laguerre filter, then

$$\left| \frac{\lambda_i + a}{\lambda_i - a} \right| < 1 \quad \forall i.$$

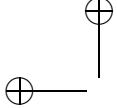
□

Assumption 3. Considering Lemma 1.3.6 the Laguerre basis pole a is assumed different from the eigenvalues of A , i.e., $a \notin \sigma(A)$.

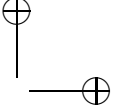
Remark. As in the case of the Laguerre filtering approach, it is interesting to focus on the bilinear transformation relating matrix A of the continuous-time system (1.4) with the corresponding matrix A_o of the discrete-time equivalent. It is apparent that in this case the conventional bilinear transformation (i.e., the one mapping the open left half plane into the open unit disk) is used, so the stability of A is preserved in the process.

1.4 CT-PBSID using Laguerre filters (CT-PBSID_w)

In this Section a subspace algorithm based on the well-known PBSID method (see Chiuso [2007] for further details) is derived along the lines exposed in Bergamasco and Lovera [2010a, 2011a]. Considering system (1.16) in the all-pass domain, a PBSID-like approach to the estimation of the state space matrices A_w , B_w , C_w , D_w , K_w , F_1 and F_2 can be derived. To this purpose, note that the system (1.16) in the all-pass domain can be written in



|



prediction form as

$$\begin{aligned}[w\hat{x}](t) &= \bar{A}_w\hat{x}(t) + \bar{B}_w[l_0u](t) + K_w[l_0y](t) + \bar{F}_wx_0l_0(t) \\ &= \bar{A}_w\hat{x}(t) + \tilde{B}_w[l_0z](t),\end{aligned}\quad (1.39)$$

where

$$\begin{aligned}\bar{A}_w &= A_w - K_wC_w \\ \bar{B}_w &= B_w - K_wD_w \\ \bar{F}_w &= F_1 - K_wF_2 \\ \tilde{B}_w &= [\bar{B}_w \quad K_w \quad \bar{F}_wx_0],\end{aligned}$$

and

$$[l_0z](t) = \begin{bmatrix} [l_0u](t) \\ [l_0y](t) \\ l_0(t) \end{bmatrix}. \quad (1.40)$$

Iterating $p - 1$ times the filtering operation in the all-pass domain (where p is the so-called past window length) one gets

$$\begin{aligned}[w^2\hat{x}](t) &= \bar{A}_w^2\hat{x}(t) + [\bar{A}_w\tilde{B}_w \quad \tilde{B}_w] \begin{bmatrix} [l_0z](t) \\ [l_1z](t) \end{bmatrix} \\ &\vdots \\ [w^p\hat{x}](t) &= \bar{A}_w^p\hat{x}(t) + \mathcal{K}^p Z_0^{p-1}(t),\end{aligned}\quad (1.41)$$

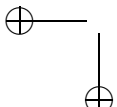
where

$$\mathcal{K}^p = \begin{bmatrix} \bar{A}_w^{p-1}\tilde{B}_w & \dots & \tilde{B}_w \end{bmatrix} \quad (1.42)$$

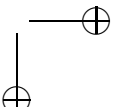
is the extended controllability matrix of the system in the all-pass domain and

$$Z_0^{p-1}(t) = \begin{bmatrix} [l_0z](t) \\ \vdots \\ [l_{p-1}z](t) \end{bmatrix}.$$

Under the Assumptions 1 and 2, \bar{A}_w has all the eigenvalues inside the open unit circle, so the term $\bar{A}_w^p x(t)$ is negligible for sufficiently large values of p and it holds that $[w^p\hat{x}](t) \simeq \mathcal{K}^p Z_0^{p-1}(t)$. As a consequence, denoting with



|





f the future window length, the input-output behaviour of the system is approximately given by

$$\begin{aligned} [l_p y](t) &\simeq C_w \mathcal{K}^p Z_0^{p-1}(t) + D_w [l_p u](t) + F_2 x_0 l_p(t) + [l_p e](t) \\ &\vdots \\ [l_{p+f} y](t) &\simeq C_w \mathcal{K}^p Z_f^{p+f-1}(t) + D_w [l_{p+f} u](t) + F_2 x_0 l_{p+f}(t) + [l_{p+f} e](t), \end{aligned} \quad (1.43)$$

so that introducing the vector notation

$$\begin{aligned} Y^{p,f}(t) &= [[l_p y](t) \quad [l_{p+1} y](t) \quad \dots \quad [l_{p+f} y](t)] \\ U^{p,f}(t) &= [[l_p u](t) \quad [l_{p+1} u](t) \quad \dots \quad [l_{p+f} u](t)] \\ E^{p,f}(t) &= [[l_p e](t) \quad [l_{p+1} e](t) \quad \dots \quad [l_{p+f} e](t)] \\ \Psi^{p,f}(t) &= [l_p(t) \quad l_{p+1}(t) \quad \dots \quad l_{p+f}(t)] \\ X^{p,f}(t) &= [[w^p x](t) \quad [w^{p+1} x](t) \quad \dots \quad [w^{p+f} x](t)] \\ \bar{Z}^{p,f}(t) &= [Z_0^{p-1}(t) \quad Z_1^p(t) \quad \dots \quad Z_f^{p+f-1}(t)], \end{aligned}$$

equations (1.41) and (1.43) can be rewritten as

$$\begin{aligned} X^{p,f}(t) &\simeq \mathcal{K}^p \bar{Z}^{p,f}(t) \\ Y^{p,f}(t) &\simeq C_w \mathcal{K}^p \bar{Z}^{p,f}(t) + D_w U^{p,f}(t) + F_2 x_0 \Psi^{p,f}(t) + E^{p,f}(t). \end{aligned} \quad (1.44)$$

Considering now the sampled input-output data instead of the continuous-time evolution of the relevant signals, the data matrices become

$$Y_N^{p,f} = [[l_p y](t_1) \quad \dots \quad [l_p y](t_N) \quad \dots \quad [l_{p+f} y](t_1) \quad \dots \quad [l_{p+f} y](t_N)], \quad (1.45)$$

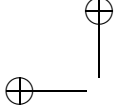
and similarly for $U^{p,f}(t)$, $E^{p,f}(t)$, $\Psi^{p,f}(t)$, $X^{p,f}(t)$ and $\bar{Z}^{p,f}(t)$. The data equations (1.44), in turn, are given by

$$\begin{aligned} X_N^{p,f} &\simeq \mathcal{K}^p \bar{Z}_N^{p,f} \\ Y_N^{p,f} &\simeq C_w \mathcal{K}^p \bar{Z}_N^{p,f} + D_w U_N^{p,f} + F_2 x_0 \Psi_N^{p,f} + E_N^{p,f}. \end{aligned}$$

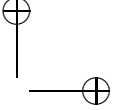
From this point on, the algorithm can be developed along the lines of the discrete-time PBSID_{opt} method, *i.e.*, by carrying out the following steps in which the past and future window lengths are considered equal (*i.e.*, $f = p$). Estimates of the matrices $C_w \mathcal{K}^p$, D_w and $F_2 x_0$ are first computed by solving the least-squares problem

$$\min_{C_w \mathcal{K}^p, D_w, F_2 x_0} \|Y_N^{p,p} - C_w \mathcal{K}^p \bar{Z}_N^{p,p} - D_w U_N^{p,p} - F_2 x_0 \Psi_N^{p,p}\|_F. \quad (1.46)$$





|



The estimates of F_2x_0 and of D_w provide information, respectively, on the effect of the initial state of the system on the future outputs and on the direct feedthrough term. The estimate of $C_w\mathcal{K}^p$, on the other hand, is useful in computing an estimate of the state sequence for the system, as described in the following. First note that defining the extended observability matrix Γ^p as

$$\Gamma^p = \begin{bmatrix} C_w \\ C_w\bar{A}_w \\ \vdots \\ C_w\bar{A}_w^{p-1} \end{bmatrix}, \quad (1.47)$$

the product of Γ^p and \mathcal{K}^p can be written as

$$\begin{aligned} \Gamma^p\mathcal{K}^p &= \begin{bmatrix} C_w\bar{A}_w^{p-1}\tilde{B}_w & \dots & C_w\tilde{B}_w \\ C_w\bar{A}_w^p\tilde{B}_w & \dots & C_w\bar{A}_w\tilde{B}_w \\ \vdots & & \\ C_w\bar{A}_w^{2p-2}\tilde{B}_w & \dots & C_w\bar{A}_w^{p-1}\tilde{B}_w \end{bmatrix} \\ &\approx \begin{bmatrix} C_w\bar{A}_w^{p-1}\tilde{B}_w & \dots & C_w\tilde{B}_w \\ 0 & \dots & C_w\bar{A}_w\tilde{B}_w \\ \vdots & & \\ 0 & \dots & C_w\bar{A}_w^{p-1}\tilde{B}_w \end{bmatrix}, \end{aligned} \quad (1.48)$$

where the approximation holds provided that p is sufficiently large to have $\bar{A}_w^k \simeq 0$ for $k \geq p$. In view of the definition of \mathcal{K}^p in (1.42), one can see that the first block row in the product $\Gamma^p\mathcal{K}^p$ can be computed using the estimate $\widehat{C}_w\mathcal{K}^p$ of $C_w\mathcal{K}^p$ obtained by solving the least squares problem (1.46), while the subsequent block rows can be obtained by exploiting the shift structure apparent from the right-hand side of (1.48).

Recalling now that

$$X_N^{p,p} \simeq \mathcal{K}^p \bar{Z}_N^{p,p} \quad (1.49)$$

it also holds that

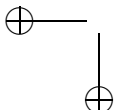
$$\Gamma^p X_N^{p,p} \simeq \Gamma^p \mathcal{K}^p \bar{Z}_N^{p,p}. \quad (1.50)$$

Therefore, computing the singular value decomposition

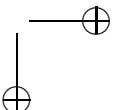
$$\Gamma^p \mathcal{K}^p \bar{Z}_N^{p,p} = U \Sigma V^T \quad (1.51)$$

an estimate of the state sequence can be obtained as

$$\widehat{X}_N^{p,p} = \Sigma_n^{\frac{1}{2}} V_n^T = \Sigma_n^{-\frac{1}{2}} U_n^T \Gamma^p \mathcal{K}^p \bar{Z}_N^{p,p}, \quad (1.52)$$



|



from which, in turn, an estimate of C_w can be computed by solving the least squares problem

$$\min_{C_w} \|Y_N^{p,p} - \widehat{D}_w U_N^{p,p} - \widehat{F}_2 x_0 \Psi_N^{p,p} - C_w \widehat{X}_N^{p,p}\|_F. \quad (1.53)$$

The final steps consist of the estimation of the innovation data matrix $E_N^{p,p}$

$$E_N^{p,p} = Y_N^{p,p} - \widehat{C}_w \widehat{X}_N^{p,p} - \widehat{D}_w U_N^{p,p} - \widehat{F}_2 x_0 \Psi_N^{p,p}, \quad (1.54)$$

and of the entire set of the state space matrices for the system in the all-pass domain, which can be obtained by solving the least squares problem

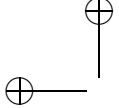
$$\min_{A_w, B_w, K_w, F_1 x_0} \|\widehat{X}_N^{p+1,p} - A_w \widehat{X}_N^{p,p-1} - B_w U_N^{p,p-1} - K_w E_N^{p,p-1} - F_1 x_0 \Psi_N^{p,p-1}\|_F. \quad (1.55)$$

Finally, the state space form for the original continuous-time system can be recovered by means of equations (1.13).

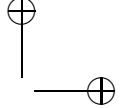
In Table 1.1 a summary of the algorithm proposed in this Section is provided.

Implementation issues

Some additional comments related to the implementation and the choice of the main parameters are in order. First of all, the identification algorithm outlined in this Section assumes that continuous-time filtering of the input-output variables can actually be performed. This is obviously not the case, so suitable discretisation schemes for the considered Laguerre filters must be devised. A detailed analysis of the impact of filter discretisation on the performance of continuous-time SMI algorithms has been carried out in Haverkamp [2001]. In particular, it has been shown that a bias term in the estimation of the state space matrices appears. More precisely, the discrete-time implementation of the filters leads to a perturbation of the estimated column space of the observability matrix of the system, which in turn leads to bias in the estimated state space matrices. The perturbation is related to the choice of sampling interval (faster sampling implies smaller bias) and with the conditioning of the system under study (the computed upper bound in the perturbation is inversely proportional to the smallest "system" singular value in the decomposition leading to the estimate of the observability subspace). For the purpose of the present study, the Laguerre filters used in the implementation of the algorithm have been implemented in discrete-time by means of a conventional bilinear (Tustin) transformation.

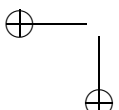


|

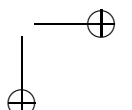


Algorithm CT-PBSID_w

1. Compute $[l_i u](t)$, $[l_i y](t)$ for $i = 0, \dots, p + f$.
 2. Build the matrices $Y_N^{p,p}$, $U_N^{p,p}$ and $\bar{Z}_N^{p,p}$ according to (1.45).
 3. Solve the least-squares problem (1.46) obtaining $C_w \mathcal{K}^p$, D_w , $F_2 x_0$.
 4. According to (1.48) an estimate of $\Gamma^p \mathcal{K}^p$ is obtained using $C_w \mathcal{K}^p$.
 5. Compute the SVD of the matrix $\Gamma^p \mathcal{K}^p \bar{Z}_N^{p,p} = U_n \Sigma_n V_n^T$, choose model order by inspecting the singular values.
 6. Obtain an estimate of the state sequence using (1.52).
 7. Solve the least-squares problem (1.53) obtaining C_w .
 8. Compute $E_N^{p,p}$ with (1.54).
 9. Solve the least-squares problem (1.55) obtaining A_w , B_w , K_w and $F_1 x_0$.
 10. Use the matrix relations (1.13) to obtain A , B , C , D , F_1 , F_2 .
-

Table 1.1: Summary of the CT-PBSID_w algorithm.

|



1.5 CT-PBSID using Laguerre projections (CT-PBSID_o)

Starting from system (1.4), in this Section the derivation of a PBSID-like approach to the estimation of the state space matrices A_o, B_o, C_o, D_o, K_o is presented, as exposed in Bergamasco and Lovera [2010b, 2011a], based on the Laguerre projections introduced in Section 1.3.2.

Considering the sequence of sampling instants $t_i, i = 1, \dots, N$, the input u , the output y , the state and the output noises w and v of (1.4) are subjected to the transformations

$$\begin{aligned}\tilde{u}_i(k) &= \int_0^\infty (\Lambda_w^k \ell_0(\tau)) u(t_i + \tau) d\tau \\ \tilde{w}_i(k) &= \int_0^\infty (\Lambda_w^k \ell_0(\tau)) dw(t_i + \tau) \\ \tilde{v}_i(k) &= \int_0^\infty (\Lambda_w^k \ell_0(\tau)) dv(t_i + \tau) \\ \tilde{y}_i(k) &= \int_0^\infty (\Lambda_w^k \ell_0(\tau)) y(t_i + \tau) d\tau,\end{aligned}\tag{1.56}$$

where $\tilde{u}_i(k) \in \mathbb{R}^m$, $\tilde{w}_i(k) \in \mathbb{R}^n$, $\tilde{v}_i(k) \in \mathbb{R}^p$, and $\tilde{y}_i(k) \in \mathbb{R}^p$. Then, as shown in Section 1.3.2, the transformed system has the state space representation in innovation form

$$\begin{aligned}\xi_i(k+1) &= A_o \xi_i(k) + B_o \tilde{u}_i(k) + K_o \tilde{e}_i(k), \quad \xi_i(0) = x(t_i) \\ \tilde{y}_i(k) &= C_o \xi_i(k) + D_o \tilde{u}_i(k) + \tilde{e}_i(k),\end{aligned}\tag{1.57}$$

where the state space matrices are given by (1.33) and (1.37).

Letting now

$$\begin{aligned}\tilde{z}_i(k) &= \begin{bmatrix} \tilde{u}_i(k) \\ \tilde{y}_i(k) \end{bmatrix} \\ \bar{A}_o &= A_o - K_o C_o \\ \bar{B}_o &= B_o - K_o D_o\end{aligned}$$

and

$$\tilde{B}_o = [\bar{B}_o \quad K_o],$$

system (1.57) can be written in prediction form as follows

$$\begin{aligned}\xi_i(k+1) &= \bar{A}_o \xi_i(k) + \tilde{B}_o \tilde{z}_i(k), \quad \xi_i(0) = x(t_i) \\ \tilde{y}_i(k) &= C_o \xi_i(k) + D_o \tilde{u}_i(k) + \tilde{e}_i(k),\end{aligned}\tag{1.58}$$



to which the PBSID_{opt} algorithm can be applied to compute estimates of the state space matrices A_o, B_o, C_o, D_o, K_o .

More precisely, iterating $p - 1$ times the state equation in (1.58) one gets

$$\begin{aligned}\xi_i(k+2) &= \bar{A}_o^2 \xi_i(k) + [\bar{A}_o \tilde{B}_o \quad \tilde{B}_o] \begin{bmatrix} \tilde{z}_i(k) \\ \tilde{z}_i(k+1) \end{bmatrix} \\ &\vdots \\ \xi_i(k+p) &= \bar{A}_o^p \xi_i(k) + \mathcal{K}^p Z_i^{0,p-1},\end{aligned}\tag{1.59}$$

where

$$\mathcal{K}^p = \begin{bmatrix} \bar{A}_o^{p-1} \tilde{B}_0 & \dots & \tilde{B}_o \end{bmatrix}\tag{1.60}$$

is the extended controllability matrix of the system in the transformed domain and

$$Z_i^{0,p-1} = \begin{bmatrix} \tilde{z}_i(k) \\ \vdots \\ \tilde{z}_i(k+p-1) \end{bmatrix}.$$

Under the Assumptions 1 and 3, \bar{A}_o has all the eigenvalues inside the open unit circle, so the term $\bar{A}_o^p \xi_i(k)$ is negligible for sufficiently large values of p and it holds have that

$$\xi_i(k+p) \simeq \mathcal{K}^p Z_i^{0,p-1}.$$

As a consequence, the input-output behaviour of the system is approximately given by

$$\begin{aligned}\tilde{y}_i(k+p) &\simeq C_o \mathcal{K}^p Z_i^{0,p-1} + D_o \tilde{u}_i(k+p) + \tilde{e}_i(k+p) \\ &\vdots \\ \tilde{y}_i(k+p+f) &\simeq C_o \mathcal{K}^p Z_i^{f,p+f-1} + D_o \tilde{u}_i(k+p+f) + \tilde{e}_i(k+p+f),\end{aligned}\tag{1.61}$$

so that introducing the vector notation

$$\begin{aligned}Y_i^{p,f} &= [\tilde{y}_i(k+p) \quad \tilde{y}_i(k+p+1) \quad \dots \quad \tilde{y}_i(k+p+f)] \\ U_i^{p,f} &= [\tilde{u}_i(k+p) \quad \tilde{u}_i(k+p+1) \quad \dots \quad \tilde{u}_i(k+p+f)] \\ E_i^{p,f} &= [\tilde{e}_i(k+p) \quad \tilde{e}_i(k+p+1) \quad \dots \quad \tilde{e}_i(k+p+f)] \\ \Xi_i^{p,f} &= [\xi_i(k+p) \quad \xi_i(k+p+1) \quad \dots \quad \xi_i(k+p+f)] \\ \bar{Z}_i^{p,f} &= [Z_i^{0,p-1} \quad Z_i^{1,p} \quad \dots \quad Z_i^{f,p+f-1}],\end{aligned}$$



equations (1.59) and (1.61) can be rewritten as

$$\begin{aligned}\Xi_i^{p,f} &\simeq \mathcal{K}^p \bar{Z}_i^{p,f} \\ Y_i^{p,f} &\simeq C_o \mathcal{K}^p \bar{Z}_i^{p,f} + D_o U_i^{p,f} + E_i^{p,f}.\end{aligned}\quad (1.62)$$

Considering now the entire dataset for $i = 1, \dots, N$, the data matrices become

$$Y^{p,f} = [\tilde{y}_1(k+p) \ \dots \ \tilde{y}_N(k+p) \ \dots \ \tilde{y}_1(k+p+f) \ \dots \ \tilde{y}_N(k+p+f)], \quad (1.63)$$

and similarly for $U_i^{p,f}$, $E_i^{p,f}$, $\Xi_i^{p,f}$ and $\bar{Z}_i^{p,f}$. The data equations (1.62), in turn, are given by

$$\begin{aligned}\Xi^{p,f} &\simeq \mathcal{K}^p \bar{Z}^{p,f} \\ Y^{p,f} &\simeq C_o \mathcal{K}^p \bar{Z}^{p,f} + D_o U^{p,f} + E^{p,f}.\end{aligned}$$

From this point on, the algorithm can be developed along the lines of the discrete-time PBSID_{opt} method, *i.e.*, by carrying out the following steps. Considering $p = f$, estimates for the matrices $C_o \mathcal{K}^p$ and D_o are first computed by solving the least-squares problem

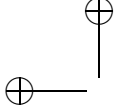
$$\min_{C_o \mathcal{K}^p, D_o} \|Y^{p,p} - C_o \mathcal{K}^p \bar{Z}^{p,p} - D_o U^{p,p}\|_F. \quad (1.64)$$

Defining now the extended observability matrix Γ^p as

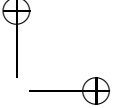
$$\Gamma^p = \begin{bmatrix} C_o \\ C_o \bar{A}_o \\ \vdots \\ C_o \bar{A}_o^{p-1} \end{bmatrix} \quad (1.65)$$

and noting that the product of Γ^p and \mathcal{K}^p can be written as

$$\begin{aligned}\Gamma^p \mathcal{K}^p &= \begin{bmatrix} C_o \bar{A}_o^{p-1} \tilde{B}_o & \dots & C_o \tilde{B}_o \\ C_o \bar{A}_o^p \tilde{B}_o & \dots & C_o \bar{A}_o \tilde{B}_o \\ \vdots & & \\ C_o \bar{A}_o^{2p-2} \tilde{B}_o & \dots & C_o \bar{A}_o^{p-1} \tilde{B}_o \end{bmatrix} \\ &\simeq \begin{bmatrix} C_o \bar{A}_o^{p-1} \tilde{B}_o & \dots & C_o \tilde{B}_o \\ 0 & \dots & C_o \bar{A}_o \tilde{B}_o \\ \vdots & & \\ 0 & \dots & C_o \bar{A}_o^{p-1} \tilde{B}_o \end{bmatrix},\end{aligned}\quad (1.66)$$



|



such product can be computed using the estimate $\widehat{C_o \mathcal{K}^p}$ of $C_o \mathcal{K}^p$ obtained by solving the least squares problem (1.64).

Recalling now that

$$\Xi^{p,p} \simeq \mathcal{K}^p \bar{Z}^{p,p}, \quad (1.67)$$

it also holds that

$$\Gamma^p \Xi^{p,p} \simeq \Gamma^p \mathcal{K}^p \bar{Z}^{p,p}. \quad (1.68)$$

Therefore, computing the singular value decomposition,

$$\Gamma^p \mathcal{K}^p \bar{Z}^{p,p} = U \Sigma V^T, \quad (1.69)$$

an estimate of the state sequence can be obtained as

$$\widehat{\Xi}^{p,p} = \Sigma_n^{\frac{1}{2}} V_n^T = \Sigma_n^{-\frac{1}{2}} U_n^T \Gamma^p \mathcal{K}^p \bar{Z}^{p,p}, \quad (1.70)$$

from which, in turn, an estimate of C_o can be computed by solving the least squares problem

$$\min_{C_o} \|Y^{p,p} - \widehat{D}_o U^{p,p} - C_o \widehat{\Xi}^{p,p}\|_F. \quad (1.71)$$

The final steps consist of the estimation of the innovation data matrix $E^{p,p}$, *i.e.*,

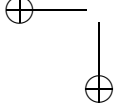
$$E^{p,p} = Y^{p,p} - \widehat{C}_o \widehat{\Xi}^{p,p} - \widehat{D}_o U^{p,p} \quad (1.72)$$

and of the entire set of the state space matrices for the system in the transformed domain, which can be obtained by solving the least squares problem

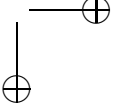
$$\min_{A_o, B_o, K_o} \|\widehat{\Xi}^{p+1,p} - A_o \widehat{\Xi}^{p,p-1} - B_o U^{p,p-1} - K_o E^{p,p-1}\|_F. \quad (1.73)$$

Finally, the state space form for the original continuous-time system can be recovered by means of equations (1.33).

In Table 1.2 a summary of the algorithm proposed in this Section is provided.



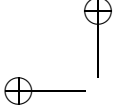
|



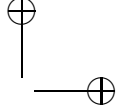
Algorithm CT-PBSID_o

1. Compute $\tilde{u}_i(k)$ and $\tilde{u}_i(k)$ for $k = 0, \dots, p+f$ and $i = 0, \dots, \frac{N}{2}$ using (1.56) (or its approximation (1.74)).
 2. Build the matrices $Y^{p,p}$, $U^{p,p}$ and $\bar{Z}^{p,p}$ according to (1.63).
 3. Solve the least-squares problem (1.64) obtaining $C_o \mathcal{K}^p$ and D_o .
 4. According to (1.66) an estimate of $\Gamma^p \mathcal{K}^p$ is obtained using $C_o \mathcal{K}^p$.
 5. Compute the SVD of the matrix $\Gamma^p \mathcal{K}^p \bar{Z}_N^{p,p} = U_n \Sigma_n V_n^T$, choose model order by inspecting the singular values.
 6. Obtain an estimate of the state sequence using (1.70).
 7. Solve the least-squares problem (1.71) obtaining C_o .
 8. Compute $E^{p,p}$ with (1.72).
 9. Solve the least-squares problem (1.73) obtaining A_o , B_o and K_o .
 10. Use the matrix relations (1.33), (1.38) to obtain A , B , C , D , and K .
-

 Table 1.2: Summary of the CT-PBSID_o algorithm.



|



Implementation issues

The algorithm proposed in this Section is expected to suffer from similar implementation issues as the algorithm proposed in Section 1.3.1, however a detailed analysis of the effect of filter discretisation on the bias of the computed estimates of the state space matrices is left as future work.

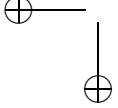
The computation of the continuous-time projections of the input-output data on the Laguerre basis can not be performed exactly, and so a suitable discretisation method for the projection operations must be considered. In the case of the numerical implementation of such operators no detailed study in terms of perturbation analysis is available in the literature. In this work, the approximate implementation

$$\begin{aligned}\tilde{u}_i(k) &= \int_0^\infty \Lambda_w^k \ell_0(\tau) u(t_i + \tau) d\tau = \int_{t_i}^\infty \Lambda_w^k \ell_0(\tau - t_i) u(\tau) d\tau = \\ &\simeq \int_{t_i}^{t_{N/2} + t_i} \Lambda_w^k \ell_0(\tau - t_i) u(\tau) d\tau,\end{aligned}\quad (1.74)$$

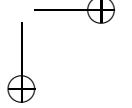
and similarly for $\tilde{y}_i(k)$, has been adopted, in which the infinity integral is computed over a sliding window of length equal to half of the duration of the available dataset. The sliding window approximation introduces an error that is function of the impulse response of the Laguerre basis and the length of the dataset. Indeed the approximation error tends to zero increasing the Laguerre pole position, decreasing the considered maximum Laguerre basis order, and increasing the length of the dataset.

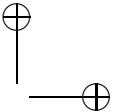
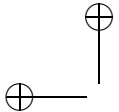
In order to obtain an efficient implementation of (1.74) the integral (1.56) can be written as follows

$$\begin{aligned}\tilde{u}_i(k) &= \int_0^\infty \Lambda_w^k \ell_0(\tau) u(t_i + \tau) d\tau = \int_{t_i}^\infty \Lambda_w^k \ell_0(\tau - t_i) u(\tau) d\tau \\ &= - \int_{-t_i}^{-\infty} \Lambda_w^k \ell_0(-\nu - t_i) u(-\nu) d\nu, \quad \nu = -\tau, \quad d\nu = -d\tau \\ &= \int_{-\infty}^{-t_i} \Lambda_w^k \ell_0(-\nu - t_i) v(\nu) d\nu, \quad v(t) = u(-t) \quad \forall t \\ &= \int_{-t_N}^{-t_i} \Lambda_w^k \ell_0(-\nu - t_i) v(\nu) d\nu, \quad v(t) = 0 \quad \forall t < -t_N \\ &= \int_0^{t_N - t_i} \Lambda_w^k \ell_0((t_N - t_i) - \eta) v(\eta - t_N) d\eta, \quad \eta = \nu + t_N, \quad d\eta = d\nu \\ &= \int_0^{t_N - t_i} \Lambda_w^k \ell_0((t_N - t_i) - \eta) m(\eta) d\eta, \quad m(t) = v(t - t_N) = u(t_N - t)\end{aligned}\quad (1.75)$$



|





which is the convolution between the k -th Laguerre filter and the signal $u(t)$ properly translated in time as shown in Figure 1.5. As in (1.74) only data computed using at least half data window are retained, *i.e.*, with $i = 1, \dots, \frac{N}{2}$. This formulation can use very efficient implementation of the convolution, *e.g.*, *lsim* in Matlab, but it is based on several approximations. Insight in the significance of such effect can be obtained by inspecting the

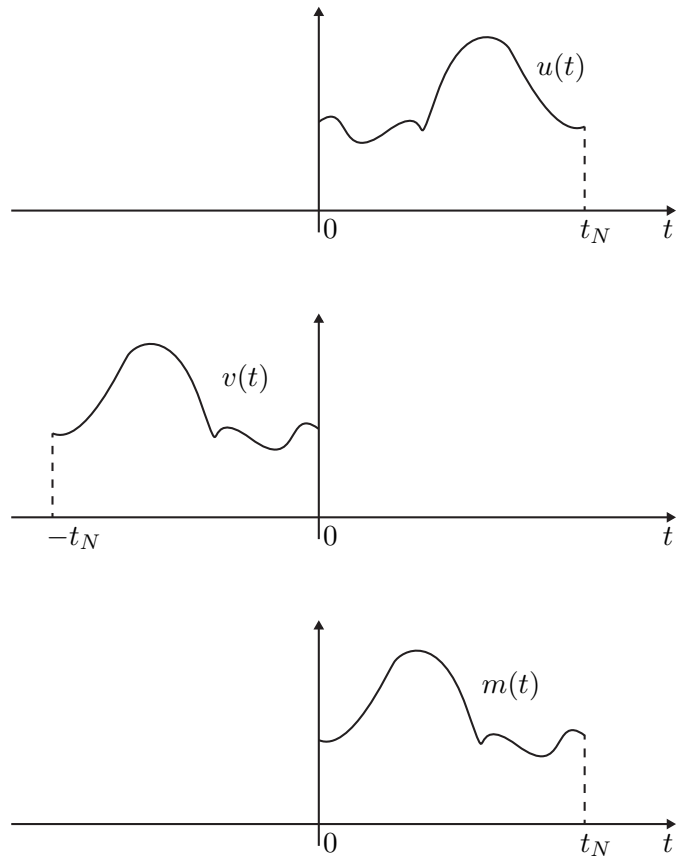
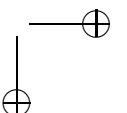
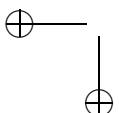


Figure 1.5: Signal shifting.

identification results provided in Section 1.6 for the noise-free case, in which errors are only due to approximations in the discrete-time implementation of the filtering/projection operations.

1.6 Simulation examples

The performance of the continuous-time SMI algorithms proposed in Sections 1.4 and 1.5 has been evaluated and compared with the one achieved



by the continuous-time PO-MOESP algorithms presented, respectively, in Haverkamp [2001] (and denoted in the following as PO-MOESP_w) and Ohta and Kawai [2004] (denoted in the following as PO-MOESP_o) in a simulation study in which input-output data have been collected from a stable MIMO system operating first in open-loop and then in closed-loop.

1.6.1 Open-loop case

The considered open-loop system is given by the state space matrices

$$S : \begin{cases} A = \begin{bmatrix} -2 & 1 \\ 0 & -4 \end{bmatrix} & B = \begin{bmatrix} 1 & 0.5 \\ 0 & 1 \end{bmatrix} \\ C = \begin{bmatrix} 1 & 0 \\ 4 & 1 \end{bmatrix} & D = \begin{bmatrix} 0 & 0 \\ 0 & 0 \end{bmatrix}. \end{cases} \quad (1.76)$$

The simulated data has been collected by applying to each input channel of the system a piece-wise constant input with base period $T_p = 0.01$ s, for a duration of 10s. The input level is chosen randomly according to a Gaussian distribution with zero mean and unit variance. White Gaussian noise of increasing variance has been added to the output in order to assess the influence of decreasing signal-to-noise ratio on the quality of the computed estimates. For the measured variables the sampling intervals $\Delta t = 0.0005$ s, $\Delta t = 0.001$ s, and $\Delta t = 0.002$ s have been considered. Similar choices for the p and f parameters have been made in the four algorithms, namely $p = f = 10$.

The first issue to be investigated is the role of the choice of the parameter of the Laguerre filter bank a , which is known to be a critical issue for the continuous-time PO-MOESP_w algorithm of Haverkamp [2001]. The results obtained repeating the identification exercise for values of a ranging between 10 and 60 with $\sigma_v^2/\sigma_y^2 = 0.01$ are depicted in Figure 1.6, where the sampling interval is fixed to $\Delta t = 0.001$ s. As can be seen from the Figure, the algorithms provide very different results as a function of a : the bias on the estimates of the eigenvalues increases faster for the PO-MOESP_o algorithm than for the other algorithms but only for very large values of a .

On the other hand, over the, closest to the system dynamics, range between 10 and 30, the CT-PBSID_o algorithm leads to a consistently lower bias and also to a more regular behaviour of the estimation error with respect to the tuning of the Laguerre filters.

Similar comments apply to the variance of the estimated eigenvalues. First of all, the results confirm findings already present in the literature about the somewhat unfavorable behaviour of the estimates of PO-MOESP_w

as functions of a . As for the other algorithms, the estimates of the eigenvalues have a similar variance, with CT-PBSID_w consistently providing the best performance.

In Section 1.6.3 an extension of this analysis is performed in which the Laguerre pole position a is varying together with the windows length p and f .

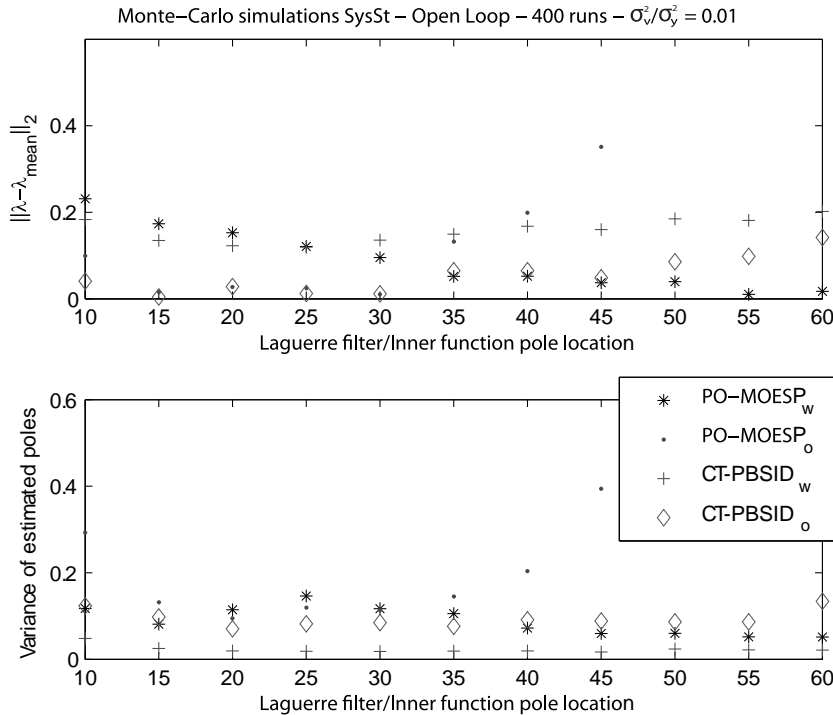


Figure 1.6: Bias and variance of the estimated eigenvalues - open loop experiments.

A more detailed comparison between the performance of the algorithms can be carried out by looking at Tables 1.3-1.8 and at Figures 1.7-1.12, where the results obtained in a Monte Carlo study (averaging over 400 runs, with $a = 20$) are presented. More precisely, the estimation error for the eigenvalues of the system under study has been analysed for decreasing signal-to-noise ratio, as measured on the output. Note that in each table, the first row provides a measure of the estimation error in the noise-free case, which is useful to assess the effect of the implementation aspects discussed in Sections 1.4 and 1.5.

The Tables confirm in a more quantitative way the conclusions which were already drawn from the analysis of Figure 1.6. Note, in passing, that

1.6 Simulation examples

| σ_v^2/σ_y^2 | PO-MOESP _w | CT-PBSID _w |
|-------------------------|---|---|
| 0 | 0.0000 0.0000 | 0.0000 0.0000 |
| 0.01 | -0.0759 ± (0.2462) 0.0059 ± (0.0185) | -0.0612 ± (0.0899) 0.0050 ± (0.0116) |
| 0.05 | -0.4981 + 0.0179 <i>i</i> ± (0.5849 + 0.0769 <i>i</i>) 0.0605 - 0.0179 <i>i</i> ± (0.0892 + 0.0769 <i>i</i>) | -0.3159 ± (0.2039) 0.0310 ± (0.0318) |
| 0.10 | -0.9837 + 0.1146 <i>i</i> ± (0.7785 + 0.1832 <i>i</i>) 0.0633 - 0.1146 <i>i</i> ± (0.2492 + 0.1832 <i>i</i>) | -0.6727 + 0.0093 <i>i</i> ± (0.3461 + 0.0565 <i>i</i>) 0.0880 - 0.0093 <i>i</i> ± (0.0927 + 0.0565 <i>i</i>) |

Table 1.3: Mean and standard deviation of the eigenvalue estimation error - open-loop experiments with $\Delta t = 0.0005$ s.

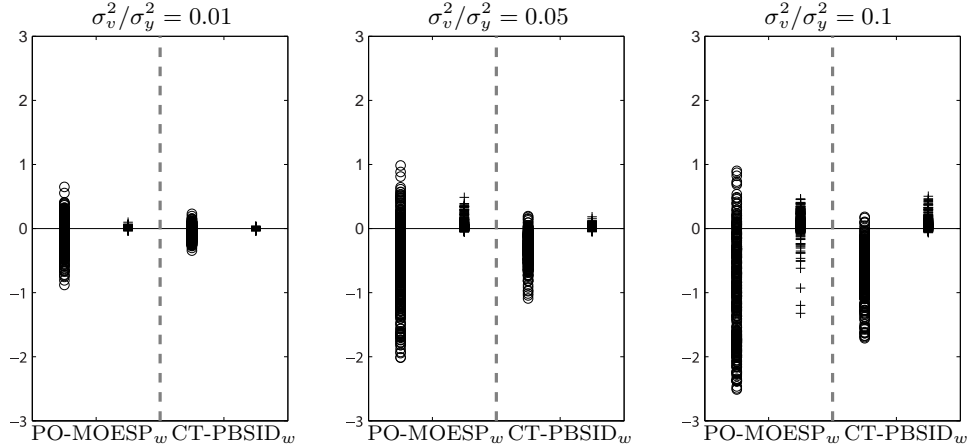


Figure 1.7: Eigenvalues estimation error (Real part) - open-loop experiments with $\Delta t = 0.0005$ s.

| σ_v^2/σ_y^2 | PO-MOESP _o | CT-PBSID _o |
|-------------------------|---|--|
| 0 | -0.0019 -0.0000 | -0.0005 0.0001 |
| 0.01 | -0.0058 ± (0.2209) 0.0018 ± (0.0180) | 0.0065 ± (0.1819) 0.0003 ± (0.0146) |
| 0.05 | -0.0338 + 0.0014 <i>i</i> ± (0.6044 + 0.0175 <i>i</i>) 0.0232 - 0.0014 <i>i</i> ± (0.0726 + 0.0175 <i>i</i>) | 0.0381 + 0.0007 <i>i</i> ± (0.4383 + 0.0145 <i>i</i>) 0.0044 - 0.0007 <i>i</i> ± (0.0400 + 0.0145 <i>i</i>) |
| 0.10 | -0.0328 + 0.0104 <i>i</i> ± (0.8385 + 0.0570 <i>i</i>) 0.0346 - 0.0104 <i>i</i> ± (0.0942 + 0.0570 <i>i</i>) | 0.0377 + 0.0032 <i>i</i> ± (0.5850 + 0.0345 <i>i</i>) 0.0066 - 0.0032 <i>i</i> ± (0.0565 + 0.0345 <i>i</i>) |

Table 1.4: Mean and standard deviation of the eigenvalue estimation error - open-loop experiments with $\Delta t = 0.0005$ s.

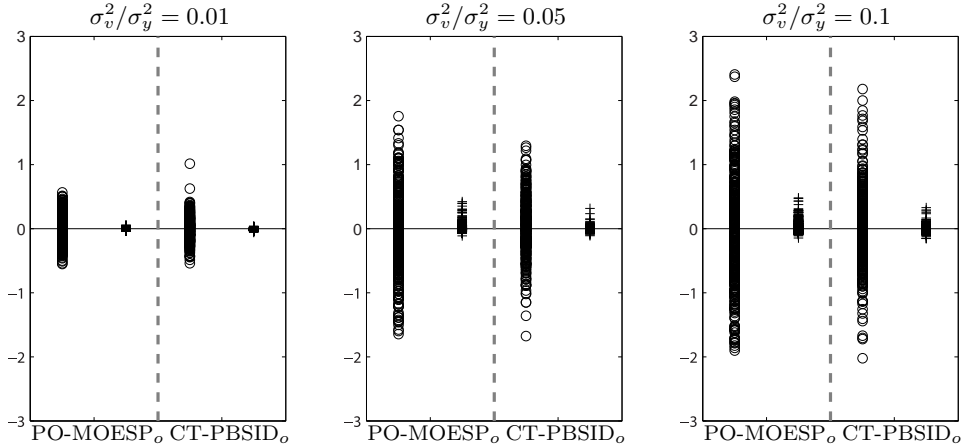


Figure 1.8: Eigenvalues estimation error (Real part) - open-loop experiments with $\Delta t = 0.0005$ s.

| σ_v^2/σ_y^2 | PO-MOESP _w | CT-PBSID _w |
|-------------------------|--|---|
| 0 | 0.0000 0.0000 | 0.0000 0.0000 |
| 0.01 | $-0.1896 + 0.0018i \pm (0.3887 + 0.0249i)$ $0.0179 - 0.0018i \pm (0.0357 + 0.0249i)$ | $-0.1258 \pm (0.1329)$ $0.0097 \pm (0.0176)$ |
| 0.05 | $-0.9359 + 0.1077i \pm (0.7776 + 0.1783i)$ $0.0768 - 0.1077i \pm (0.1612 + 0.1783i)$ | $-0.6548 + 0.0047i \pm (0.3046 + 0.0355i)$ $0.0857 - 0.0047i \pm (0.0823 + 0.0355i)$ |
| 0.10 | $-1.6784 + 0.2203i \pm (0.7083 + 0.2226i)$ $-0.4586 - 0.2203i \pm (1.3915 + 0.2226i)$ | $-1.3461 + 0.1878i \pm (0.4376 + 0.2210i)$ $0.2057 - 0.1878i \pm (0.1405 + 0.2210i)$ |

Table 1.5: Mean and standard deviation of the eigenvalue estimation error - open-loop experiments with $\Delta t = 0.001$ s.

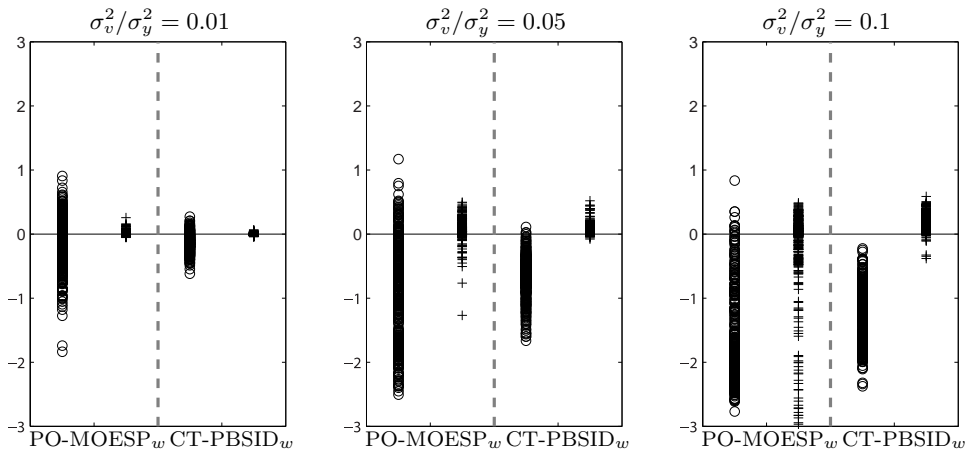


Figure 1.9: Eigenvalues estimation error (Real part) - open-loop experiments with $\Delta t = 0.001$ s.

1.6 Simulation examples

| σ_v^2/σ_y^2 | PO-MOESP _o | CT-PBSID _o |
|-------------------------|---|--|
| 0 | -0.0066 -0.0001 | -0.0016 0.0002 |
| 0.01 | -0.0140 ± (0.3535) 0.0056 ± (0.0302) | 0.0149 ± (0.2566) 0.0012 ± (0.0214) |
| 0.05 | -0.0455 + 0.0198 <i>i</i> ± (0.8888 + 0.0846 <i>i</i>) 0.0377 - 0.0198 <i>i</i> ± (0.0984 + 0.0846 <i>i</i>) | 0.0314 + 0.0012 <i>i</i> ± (0.6166 + 0.0134 <i>i</i>) 0.0128 - 0.0012 <i>i</i> ± (0.0639 + 0.0134 <i>i</i>) |
| 0.10 | 0.1159 + 0.0560 <i>i</i> ± (1.4410 + 0.1498 <i>i</i>) 0.0296 - 0.0560 <i>i</i> ± (0.1489 + 0.1498 <i>i</i>) | 0.0846 + 0.0075 <i>i</i> ± (0.8357 + 0.0506 <i>i</i>) 0.0174 - 0.0075 <i>i</i> ± (0.0834 + 0.0506 <i>i</i>) |

Table 1.6: Mean and standard deviation of the eigenvalue estimation error - open-loop experiments with $\Delta t = 0.001$ s.

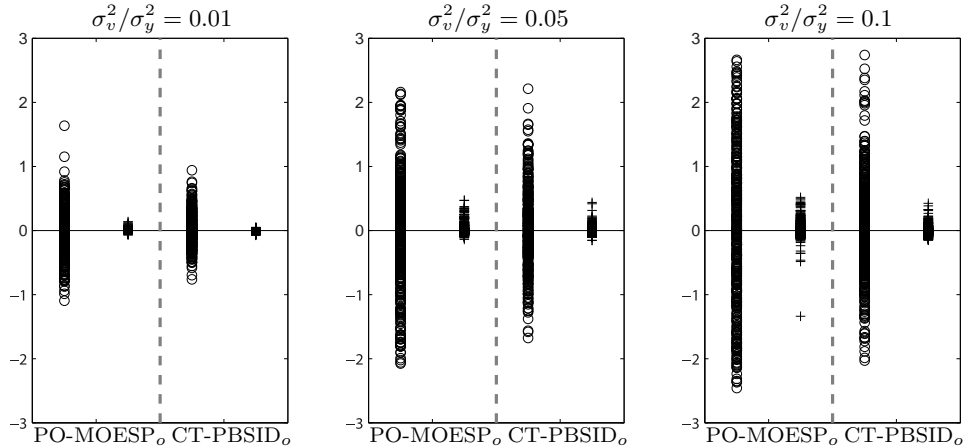


Figure 1.10: Eigenvalues estimation error (Real part) - open-loop experiments with $\Delta t = 0.001$ s.

| σ_v^2/σ_y^2 | PO-MOESP _w | CT-PBSID _w |
|-------------------------|--|--|
| 0 | 0.0000 0.0000 | 0.0000 0.0000 |
| 0.01 | -0.3359 + 0.0058 <i>i</i> ± (0.5329 + 0.0430 <i>i</i>) 0.0407 - 0.0058 <i>i</i> ± (0.0719 + 0.0430 <i>i</i>) | -0.2442 ± (0.1903) 0.0243 ± (0.0262) |
| 0.05 | -1.6712 + 0.2163 <i>i</i> ± (0.6731 + 0.2159 <i>i</i>) -0.2785 - 0.2163 <i>i</i> ± (0.9277 + 0.2159 <i>i</i>) | -1.3562 + 0.1799 <i>i</i> ± (0.4193 + 0.2230 <i>i</i>) 0.2075 - 0.1799 <i>i</i> ± (0.1434 + 0.2230 <i>i</i>) |
| 0.10 | -2.1092 + 0.1755 <i>i</i> ± (0.3743 + 0.2342 <i>i</i>) -2.0769 - 0.1755 <i>i</i> ± (2.7411 + 0.2342 <i>i</i>) | -2.1122 + 0.4583 <i>i</i> ± (0.3351 + 0.2113 <i>i</i>) -0.2596 - 0.4583 <i>i</i> ± (0.6856 + 0.2113 <i>i</i>) |

Table 1.7: Mean and standard deviation of the eigenvalue estimation error - open-loop experiments with $\Delta t = 0.002$ s.

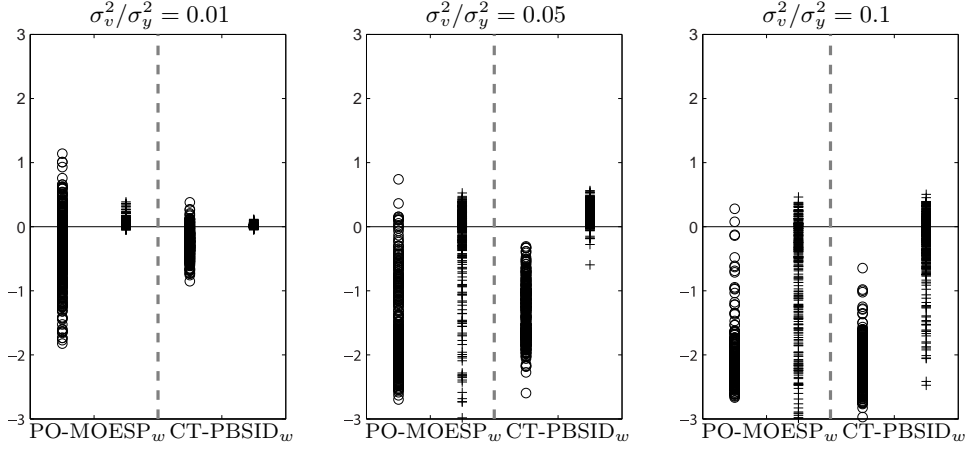


Figure 1.11: Eigenvalues estimation error (Real part) - open-loop experiments with $\Delta t = 0.002$ s.

| σ_v^2/σ_y^2 | PO-MOESP _o | CT-PBSID _o |
|-------------------------|---|--|
| 0 | -0.0119 0.0012 | -0.0024 0.0007 |
| 0.01 | -0.0086 + 0.0007 <i>i</i> ± (0.4765 + 0.0142 <i>i</i>) 0.0123 - 0.0007 <i>i</i> ± (0.0458 + 0.0142 <i>i</i>) | 0.0572 ± (0.4104) 0.0029 ± (0.0326) |
| 0.05 | 0.0211 + 0.0575 <i>i</i> ± (1.3199 + 0.1430 <i>i</i>) 0.0415 - 0.0575 <i>i</i> ± (0.1636 + 0.1430 <i>i</i>) | 0.0326 + 0.0086 <i>i</i> ± (0.8222 + 0.0510 <i>i</i>) 0.0207 - 0.0086 <i>i</i> ± (0.0935 + 0.0510 <i>i</i>) |
| 0.10 | 0.9662 + 0.0657 <i>i</i> ± (2.9287 + 0.1699 <i>i</i>) -0.0226 - 0.0657 <i>i</i> ± (0.2266 + 0.1699 <i>i</i>) | 0.1998 + 0.0276 <i>i</i> ± (1.2204 + 0.1029 <i>i</i>) 0.0261 - 0.0276 <i>i</i> ± (0.1307 + 0.1029 <i>i</i>) |

Table 1.8: Mean and standard deviation of the eigenvalue estimation error - open-loop experiments with $\Delta t = 0.002$ s.

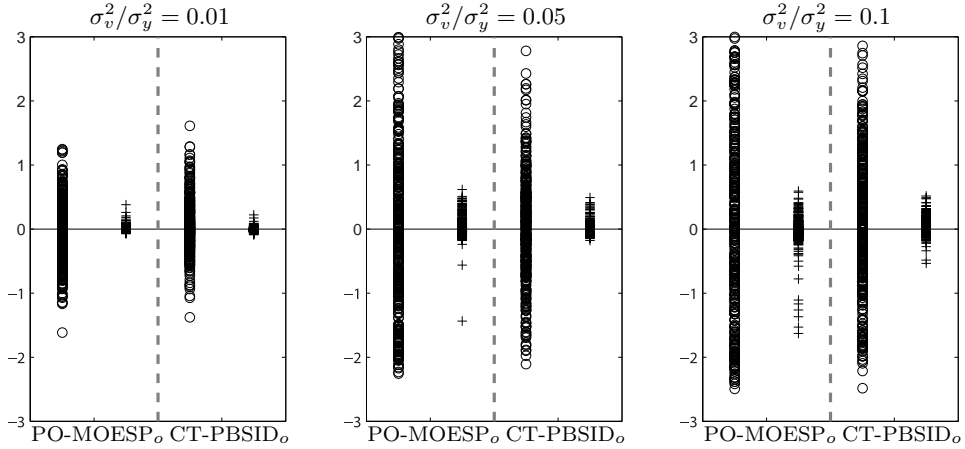
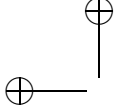
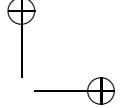


Figure 1.12: Eigenvalues estimation error (Real part) - open-loop experiments with $\Delta t = 0.002$ s.



|



for low signal-to-noise ratio the continuous-time PO-MOESP_w algorithm leads more frequently to complex estimates of the real eigenvalues. Both methods lead to larger variance of the fastest eigenvalue as expected.

1.6.2 Closed-loop case

The second considered example consists of the analysis of data generated by system (1.76)

$$S : \begin{cases} A = \begin{bmatrix} -2 & 1 \\ 0 & -4 \end{bmatrix} & B = \begin{bmatrix} 1 & 0.5 \\ 0 & 1 \end{bmatrix} \\ C = \begin{bmatrix} 1 & 0 \\ 4 & 1 \end{bmatrix} & D = \begin{bmatrix} 0 & 0 \\ 0 & 0 \end{bmatrix} \end{cases} \quad (1.77)$$

operating under feedback with the controller

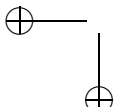
$$R : \begin{cases} A = \begin{bmatrix} -20 & 0 \\ 0 & -30 \end{bmatrix} & B = \begin{bmatrix} 1 & 0 \\ 0 & 1 \end{bmatrix} \\ C = \begin{bmatrix} 1 & 0 \\ 0 & 1 \end{bmatrix} & D = \begin{bmatrix} 0 & 0 \\ 0 & 0 \end{bmatrix} \end{cases} \quad (1.78)$$

which in turn operates on the basis of noisy measurements of the output. The identification experiments have been carried out using the same input sequence as in the open-loop case, again adding white Gaussian noise of increasing variance to the output to achieve the desired signal-to-noise ratio in closed-loop. The results obtained in this second example are summarised in Figure 1.19, in Tables 1.9-1.14 and in Figures 1.13-1.18.

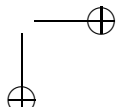
| σ_v^2/σ_y^2 | PO-MOESP _w | CT-PBSID _w |
|-------------------------|---|---|
| 0 | 0.0001 -0.0001 | 0.0000 -0.0001 |
| 0.01 | -0.0796 ± (0.2247) 0.0071 ± (0.0176) | -0.0635 ± (0.0891) 0.0053 ± (0.0113) |
| 0.05 | -0.3971 + 0.0118i ± (0.5490 + 0.0603i) 0.0424 - 0.0118i ± (0.0735 + 0.0603i) | -0.2933 ± (0.1908) 0.0275 ± (0.0289) |
| 0.10 | -0.8562 + 0.0781i ± (0.7617 + 0.1527i) 0.0791 - 0.0781i ± (0.1647 + 0.1527i) | -0.5754 + 0.0009i ± (0.2833 + 0.0175i) 0.0701 - 0.0009i ± (0.0672 + 0.0175i) |

Table 1.9: Mean and standard deviation of the eigenvalue estimation error - closed-loop experiments with $\Delta t = 0.0005$ s.

As can be seen from the results, both algorithms provide a very satisfactory performance in terms of eigenvalue estimation accuracy, with CT-PBSID_w leading to smaller variance of the estimated eigenvalues over a wide range of values for the Laguerre parameter a .



|



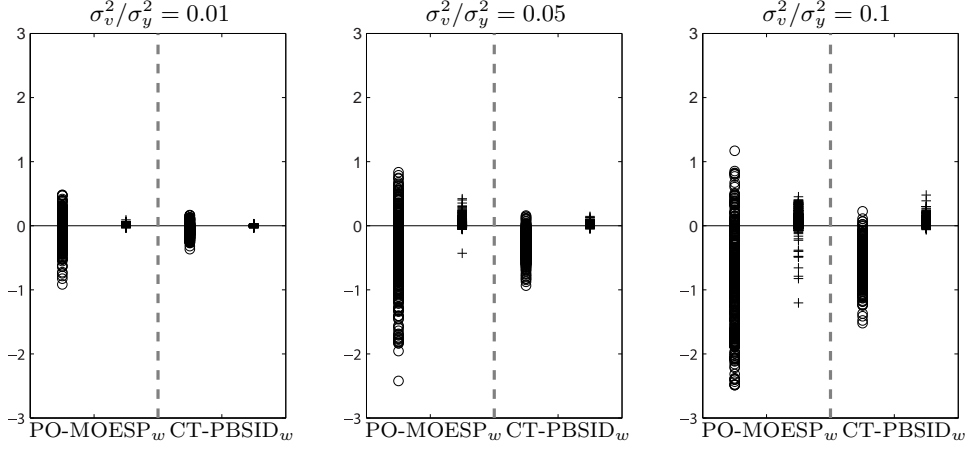


Figure 1.13: Eigenvalues estimation error (Real part) - closed-loop experiments with $\Delta t = 0.0005$ s.

| σ_v^2/σ_y^2 | PO-MOESP _w | CT-PBSID _w |
|-------------------------|---|--|
| 0 | -0.0018 -0.0002 | -0.0005 -0.0001 |
| 0.01 | $-0.0112 \pm (0.2279)$ $0.0038 \pm (0.0193)$ | $0.0090 \pm (0.1791)$ $0.0015 \pm (0.0161)$ |
| 0.05 | $0.0191 + 0.0028i \pm (0.5548 + 0.0283i)$ $0.0134 - 0.0028i \pm (0.0631 + 0.0283i)$ | $0.0349 \pm (0.3914)$ $0.0042 \pm (0.0352)$ |
| 0.10 | $-0.0137 + 0.0157i \pm (0.7780 + 0.0782i)$ $0.0274 - 0.0157i \pm (0.0872 + 0.0782i)$ | $0.0799 + 0.0018i \pm (0.5580 + 0.0291i)$ $0.0070 - 0.0018i \pm (0.0544 + 0.0291i)$ |

Table 1.10: Mean and standard deviation of the eigenvalue estimation error - closed-loop experiments with $\Delta t = 0.0005$ s.

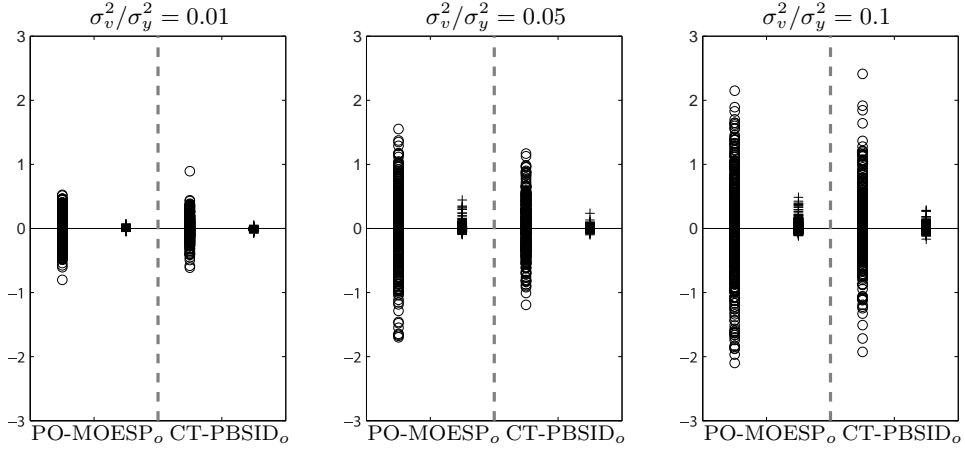


Figure 1.14: Eigenvalues estimation error (Real part) - closed-loop experiments with $\Delta t = 0.0005$ s.

| σ_v^2/σ_y^2 | PO-MOESP _w | CT-PBSID _w |
|-------------------------|--|---|
| 0 | 0.0001 -0.0002 | 0.0001 -0.0002 |
| 0.01 | -0.1472 + 0.0007 <i>i</i> ± (0.3484 + 0.0133 <i>i</i>) 0.0135 - 0.0007 <i>i</i> ± (0.0321 + 0.0133 <i>i</i>) | -0.1057 ± (0.1241) 0.0087 ± (0.0165) |
| 0.05 | -0.9007 + 0.0827 <i>i</i> ± (0.7185 + 0.1572 <i>i</i>) 0.0816 - 0.0827 <i>i</i> ± (0.1555 + 0.1572 <i>i</i>) | -0.6012 + 0.0050 <i>i</i> ± (0.3128 + 0.0461 <i>i</i>) 0.0710 - 0.0050 <i>i</i> ± (0.0694 + 0.0461 <i>i</i>) |
| 0.10 | -1.6069 + 0.2191 <i>i</i> ± (0.7358 + 0.2218 <i>i</i>) -0.2913 - 0.2191 <i>i</i> ± (0.0228 + 0.2218 <i>i</i>) | -1.2672 + 0.1508 <i>i</i> ± (0.4548 + 0.2109 <i>i</i>) 0.1889 - 0.1508 <i>i</i> ± (0.1408 + 0.2109 <i>i</i>) |

Table 1.11: Mean and standard deviation of the eigenvalue estimation error - closed-loop experiments with $\Delta t = 0.001$ s.

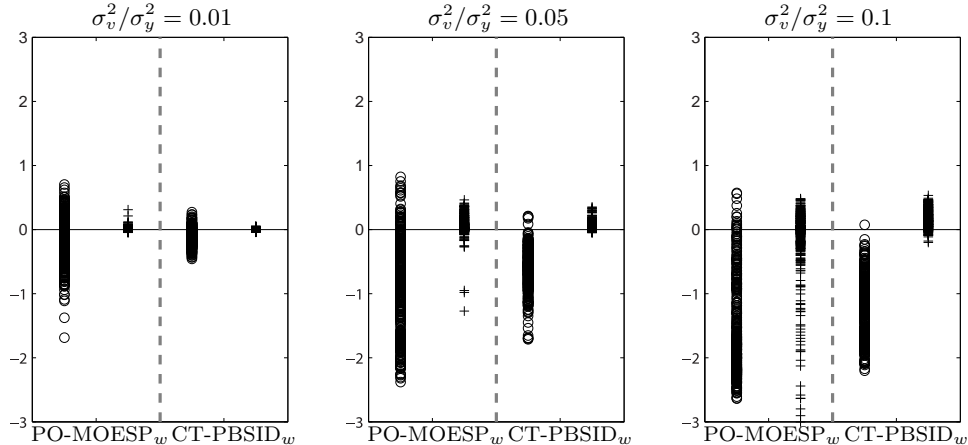


Figure 1.15: Eigenvalues estimation error (Real part) - closed-loop experiments with $\Delta t = 0.001$ s.

| σ_v^2/σ_y^2 | PO-MOESP _o | CT-PBSID _o |
|-------------------------|---|--|
| 0 | -0.0062 -0.0003 | -0.0018 0.0000 |
| 0.01 | -0.0013 ± (0.3115) 0.0034 ± (0.0252) | 0.0079 ± (0.2705) 0.0002 ± (0.0218) |
| 0.05 | -0.0750 + 0.0167 <i>i</i> ± (0.8044 + 0.0745 <i>i</i>) 0.0315 - 0.0167 <i>i</i> ± (0.0940 + 0.0745 <i>i</i>) | 0.0267 + 0.0017 <i>i</i> ± (0.5601 + 0.0246 <i>i</i>) 0.0099 - 0.0017 <i>i</i> ± (0.0639 + 0.0246 <i>i</i>) |
| 0.10 | 0.2085 + 0.0411 <i>i</i> ± (1.3649 + 0.1222 <i>i</i>) 0.0248 - 0.0411 <i>i</i> ± (0.1254 + 0.1222 <i>i</i>) | 0.0766 + 0.0101 <i>i</i> ± (0.7942 + 0.0606 <i>i</i>) 0.0138 - 0.0101 <i>i</i> ± (0.0912 + 0.0606 <i>i</i>) |

Table 1.12: Mean and standard deviation of the eigenvalue estimation error - closed-loop experiments with $\Delta t = 0.001$ s.

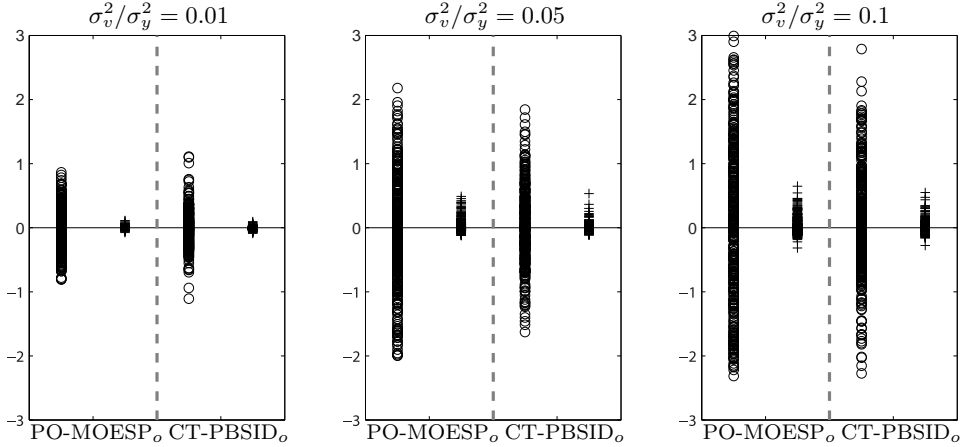


Figure 1.16: Eigenvalues estimation error (Real part) - closed-loop experiments with $\Delta t = 0.001$ s.

| σ_v^2/σ_y^2 | PO-MOESP _w | CT-PBSID _w |
|-------------------------|--|--|
| 0 | 0.0003 -0.0005 | 0.0002 -0.0003 |
| 0.01 | $-0.3457 + 0.0087i \pm (0.4916 + 0.0496i)$ $0.0380 - 0.0087i \pm (0.0664 + 0.0496i)$ | $-0.2265 \pm (0.1612)$ $0.0204 \pm (0.0260)$ |
| 0.05 | $-1.6185 + 0.1981i \pm (0.7177 + 0.2113i)$ $-0.2741 - 0.1981i \pm (1.1432 + 0.2113i)$ | $-1.2375 + 0.1240i \pm (0.4370 + 0.1899i)$ $0.1953 - 0.1240i \pm (0.1389 + 0.1899i)$ |
| 0.10 | $-2.0809 + 0.1634i \pm (0.4274 + 0.2218i)$ $-1.9502 - 0.1634i \pm (2.8723 + 0.2218i)$ | $-1.9974 + 0.4477i \pm (0.3425 + 0.2100i)$ $-0.1111 - 0.4477i \pm (0.5686 + 0.2100i)$ |

Table 1.13: Mean and standard deviation of the eigenvalue estimation error - closed-loop experiments with $\Delta t = 0.002$ s.

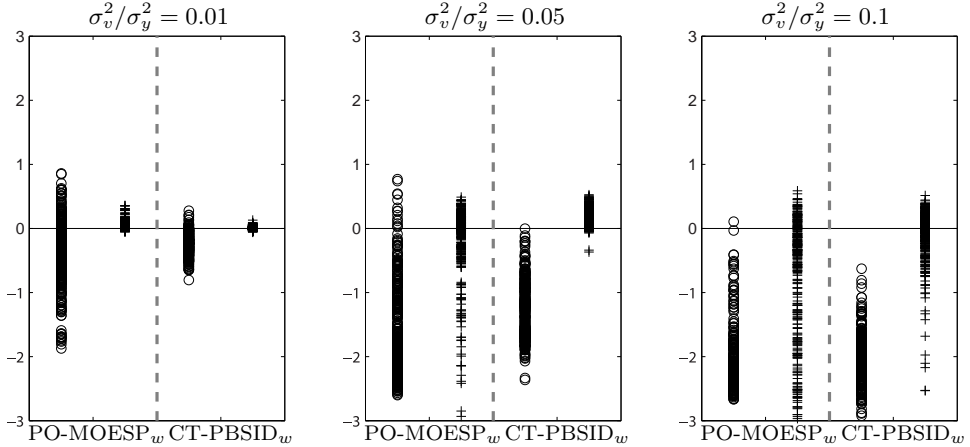


Figure 1.17: Eigenvalues estimation error (Real part) - closed-loop experiments with $\Delta t = 0.002$ s.

| σ_v^2/σ_y^2 | PO-MOESP _o | CT-PBSID _o |
|-------------------------|---|--|
| 0 | -0.0119 0.0008 | -0.0017 0.0002 |
| 0.01 | -0.0105 ± (0.4562) 0.0098 ± (0.0444) | 0.0440 ± (0.3471) 0.0017 ± (0.0312) |
| 0.05 | 0.0631 + 0.0501 <i>i</i> ± (1.3576 + 0.1340 <i>i</i>) 0.0282 - 0.0501 <i>i</i> ± (0.1568 + 0.1340 <i>i</i>) | 0.1111 + 0.0064 <i>i</i> ± (0.8161 + 0.0453 <i>i</i>) 0.0100 - 0.0064 <i>i</i> ± (0.0872 + 0.0453 <i>i</i>) |
| 0.10 | 0.8267 + 0.0697 <i>i</i> ± (2.7292 + 0.1609 <i>i</i>) -0.0509 - 0.0697 <i>i</i> ± (0.2717 + 0.1609 <i>i</i>) | 0.1706 + 0.0194 <i>i</i> ± (1.1706 + 0.0901 <i>i</i>) 0.0125 - 0.0194 <i>i</i> ± (0.1273 + 0.0901 <i>i</i>) |

Table 1.14: Mean and standard deviation of the eigenvalue estimation error - closed-loop experiments with $\Delta t = 0.002$ s.

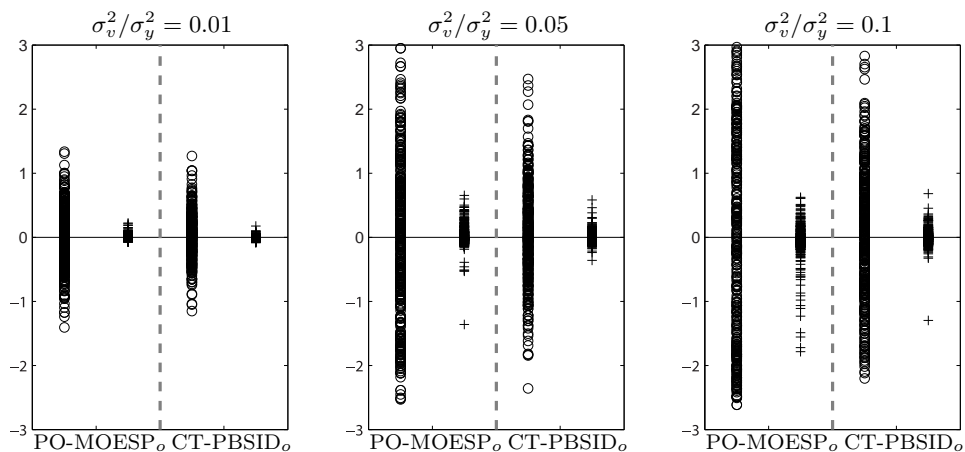


Figure 1.18: Eigenvalues estimation error (Real part) - closed-loop experiments with $\Delta t = 0.002$ s.

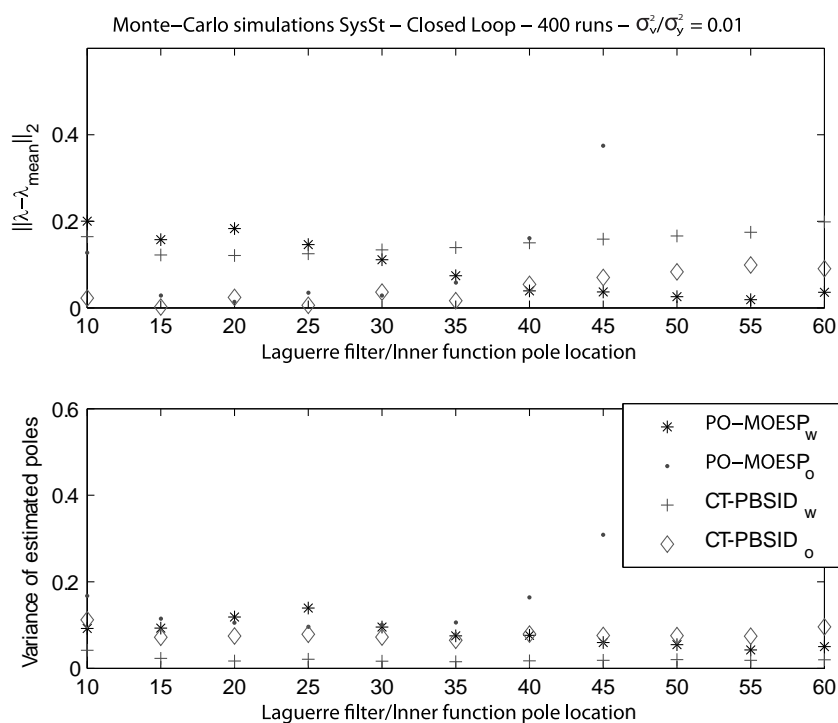
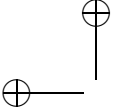
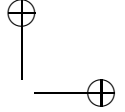


Figure 1.19: Bias and variance of the estimated eigenvalues - closed loop experiments.



|



1.6.3 Tuning parameters

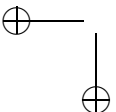
Finally, concerning the choice of the parameters f and p , the following general comments can be made. The same guidelines as in the case of the discrete-time PBSID algorithm apply. First of all, it is common practice to choose $f = p$, for the sake of simplicity. Then, one has to keep in mind that in view of the need to construct the extended controllability and observability matrices, one has to ensure that $p \geq n$, as a minimum. In addition, p must be sufficiently large to ensure that the term $\bar{A}_w^p x(t)$ is negligible (unfortunately, this can be verified *a posteriori* only). On the other hand, specific constraints on the choice of p arise due to the need of performing the filtering/projection operations over finite datasets using filters of order up to $2p$. Indeed, it is easy to verify that the impulse responses of the Laguerre-like filters defined in (1.7) have a settling time which is an increasing function of the filter order k . Since the implementation of both algorithms requires the computation of convolutions/correlations with the impulse response of such filters over time horizons determined by the length of the available dataset, the duration of the experiment provides an upper bound for the maximum value of the settling time of the highest order filter. An approximate value for the settling time of the filter

$$\mathcal{L}_k(s) = \sqrt{2a} \frac{(s-a)^k}{(s+a)^{k+1}}$$

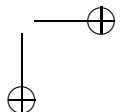
can be written as $(5 + 2k)/a$, which for $k = 2p$ gives $(5 + 4p)/a$. Therefore, denoting with t_N the duration of the available dataset and letting $\tau = 1/a$, one has the rough guideline $p \leq \frac{at_N-5}{4} \simeq \frac{1}{4} \frac{t_N}{\tau} - 1$ for CT-PBSID_w and $p \leq \frac{at_N/2-5}{4} \simeq \frac{1}{8} \frac{t_N}{\tau} - 1$ for CT-PBSID_o (the latter in view of the above described implementation (1.74) for the projection operation).

In order to understand the behavior of the proposed algorithms varying the windows length f, p and the Laguerre pole position a a numerical analysis is shown in Figures 1.20-1.27. The system (1.76) is in open-loop and only one simulation is considered. The input is the same as the one described in the previous Section. The distance between the estimated and the real eigenvalues is computed and it is expressed in a logarithmic way. The algorithms based on the Laguerre filtering achieve better results for high signal-to-noise ratio, while the algorithms based on the Laguerre projections exhibit good performance for low signal-to-noise ratio.

Figures 1.20 and 1.24 suggest that the estimates of the filter-based algorithms consistently converge for a wide range of p and a in the noise-free case. On the other hand the projection-based algorithms reach the same estimation error but for a smaller range of p and a . Now consider the



|



Figures 1.21-1.23 with decreasing signal-to-noise ratio and high sampling frequency. Note that the projection-based algorithms manage the measurement error in a better way, indeed they always achieve better estimation results. Another advantage of the projection-based algorithms is that they have a more regular behavior varying p and a , making simpler the choice of the above parameters. Same conclusions can be sketched considering the Figures 1.24-1.27 where lower sampling frequency is taken into account.

This suggests that the Laguerre projection have better numerical properties.

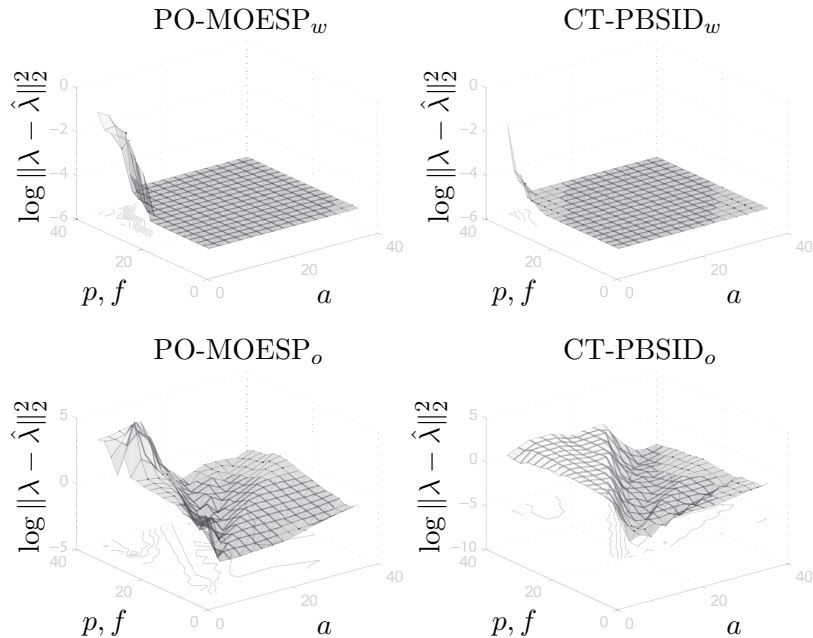


Figure 1.20: Eigenvalues estimation error varying the Laguerre pole position a and the windows length p, f ($\sigma_e^2/\sigma_y^2 = 0$, $\Delta t = 0.001$).

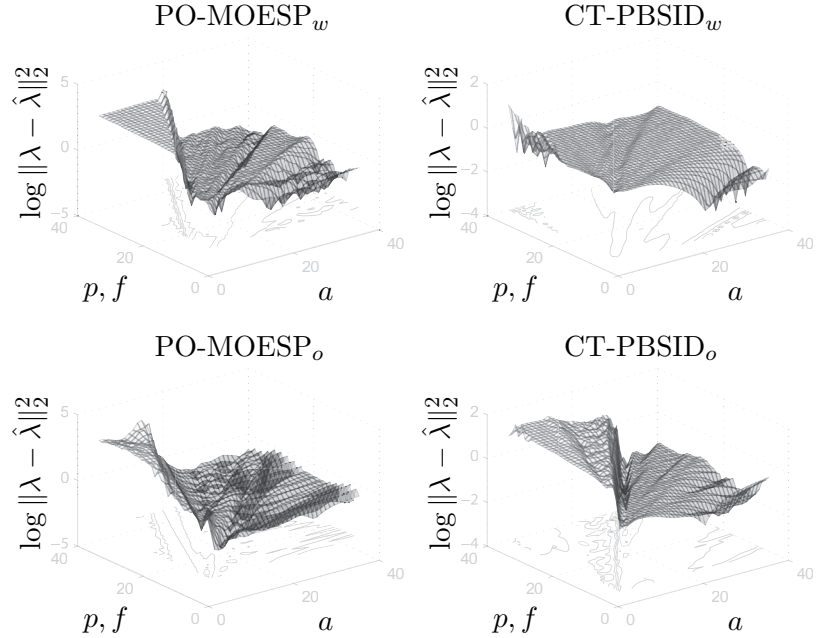


Figure 1.21: Eigenvalues estimation error varying the Laguerre pole position a and the windows length p, f ($\sigma_e^2/\sigma_y^2 = 0.01$, $\Delta t = 0.001$).

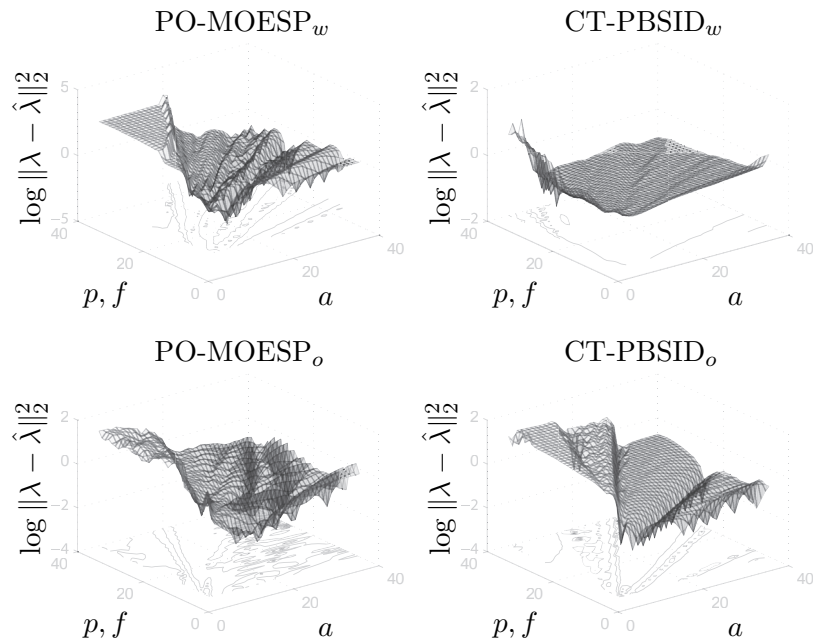


Figure 1.22: Eigenvalues estimation error varying the Laguerre pole position a and the windows length p, f ($\sigma_e^2/\sigma_y^2 = 0.05$, $\Delta t = 0.001$).

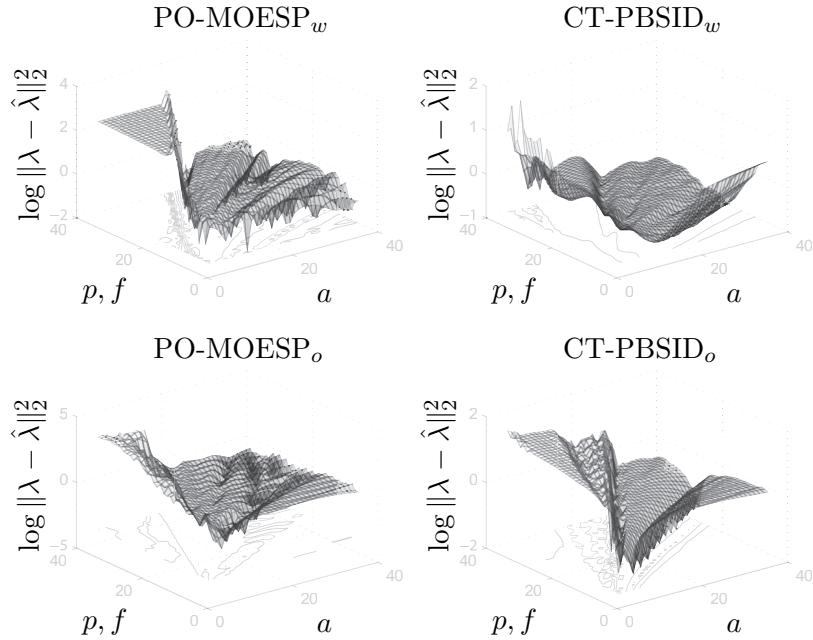


Figure 1.23: Eigenvalues estimation error varying the Laguerre pole position a and the windows length p, f ($\sigma_e^2/\sigma_y^2 = 0.1$, $\Delta t = 0.001$).

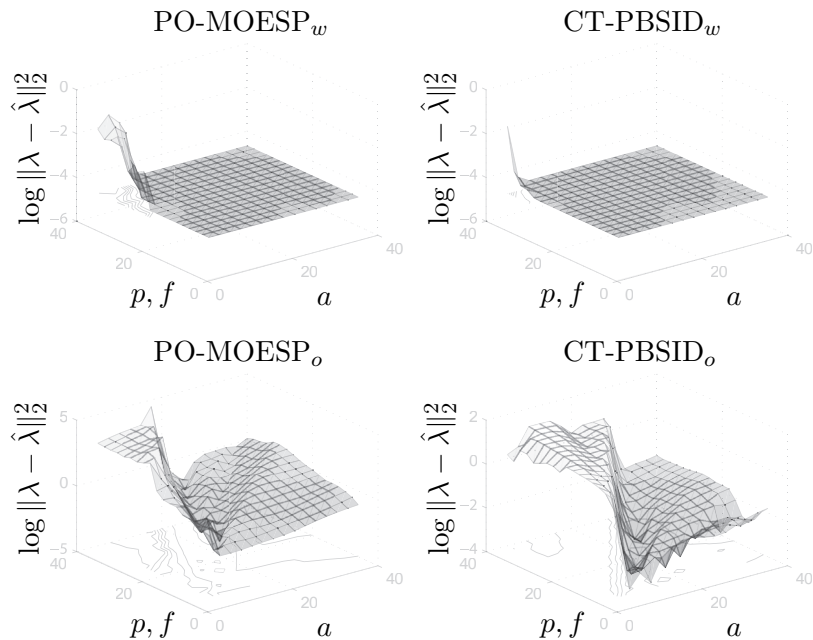


Figure 1.24: Eigenvalues estimation error varying the Laguerre pole position a and the windows length p, f ($\sigma_e^2/\sigma_y^2 = 0$, $\Delta t = 0.002$).

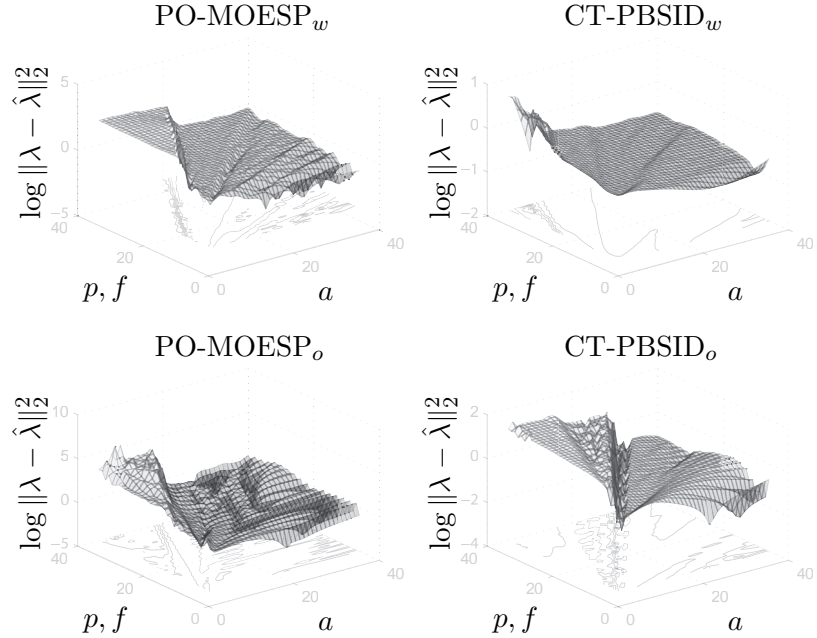


Figure 1.25: Eigenvalues estimation error varying the Laguerre pole position a and the windows length p, f ($\sigma_e^2/\sigma_y^2 = 0.01$, $\Delta t = 0.002$).

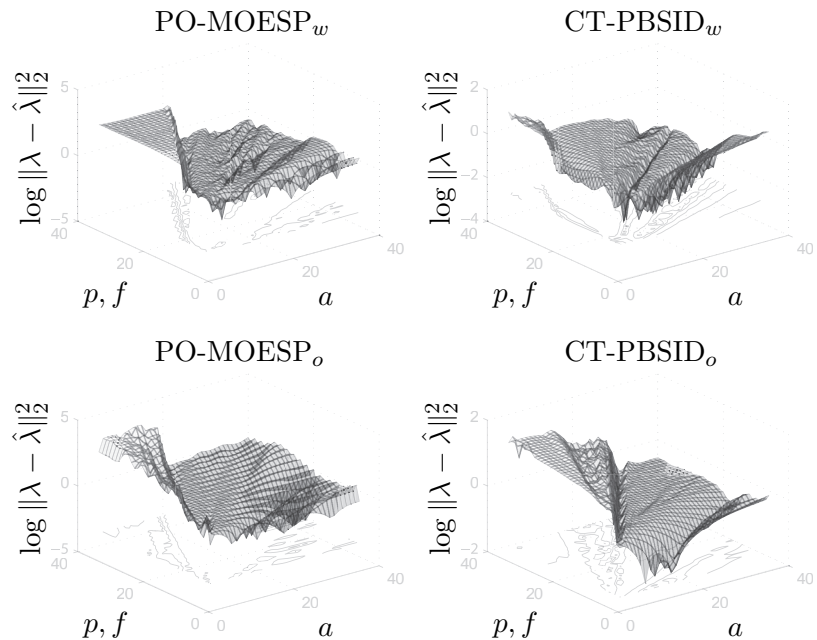


Figure 1.26: Eigenvalues estimation error varying the Laguerre pole position a and the windows length p, f ($\sigma_e^2/\sigma_y^2 = 0.05$, $\Delta t = 0.002$).

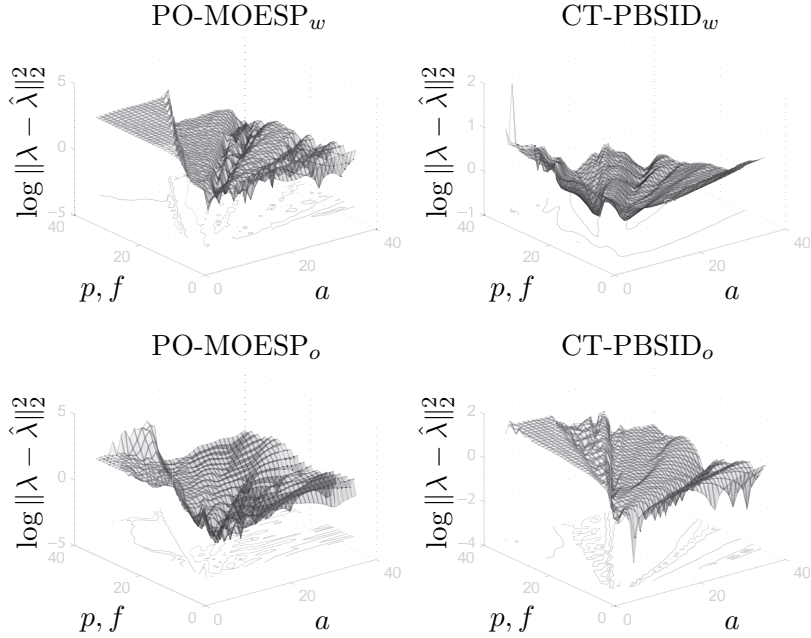
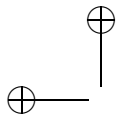


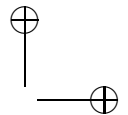
Figure 1.27: Eigenvalues estimation error varying the Laguerre pole position a and the windows length p, f ($\sigma_e^2/\sigma_y^2 = 0.1$, $\Delta t = 0.002$).

1.7 Concluding remarks

In this Chapter, the problem of continuous-time model identification has been studied and two subspace-based algorithms have been proposed. The algorithms are based on the reformulation of the identification problem from continuous-time to discrete-time by using either Laguerre filtering of the input-output data or projections of the same data onto the Laguerre basis for the appropriate signal space. In this framework, it has been shown along both lines that the PBSID_{opt} subspace identification algorithm, originally developed in the case of discrete-time systems, can be reformulated for the continuous-time case. Section 1.6 has shown that the algorithms based on the Laguerre projections outperform the algorithms based on the Laguerre filtering. In Ohta [2011] it has been shown that the Laguerre filtering technique PO-MOESP_w behaves poorly when the Laguerre filter pole a is close to the poles of the plants. This behavior can be explained by Remarks 1.3.4 and 1.3.6 in which it is shown that the poles of the discrete-time system tend to infinity for the Laguerre filtering techniques, while they tend to zero when the Laguerre projections are used. Of course in the first case the problem becomes rapidly ill-conditioned. Another point in favor of the Laguerre projections is that stable continuous-time systems remains stable,



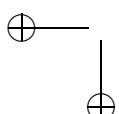
|



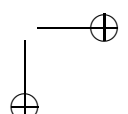
which is favorable from a numerical point of view. For all these reasons, only the CT-PBSID_o will be extended and used in the rest of this thesis.

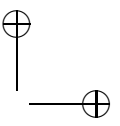
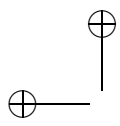
—

—



|

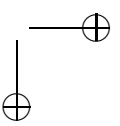
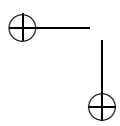




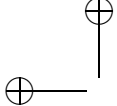
—

|

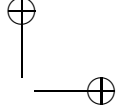
—



|



|



CHAPTER
TWO

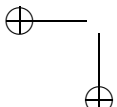
RECURSIVE CONTINUOUS-TIME SUBSPACE IDENTIFICATION

This Chapter deals with the problem of recursive model identification in continuous-time using subspace techniques. More precisely, the algorithm presented in Section 1.5 which relies on a system transformation using the Laguerre basis is considered and a recursive counterpart is developed.

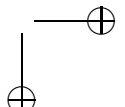
2.1 Introduction

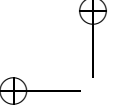
The problem of recursive subspace model identification (RSMI) in discrete-time has been an active area of research in recent years (see, *e.g.*, Verhaegen and Deprettere [1991], Cho et al. [1994], Gustafsson [1998], Lovera et al. [2000], Oku and Kimura [2002], Mercère et al. [2004]). Most RSMI algorithms are inspired by offline versions of SMI techniques and therefore rely on the availability of efficient updating methods for the numerical linear algebra algorithms used in batch SMI. In Mercère and Lovera [2007] the convergence properties of cited recursive subspace identification methods are investigated. While the above cited papers are concerned with the derivation of recursive versions for the MOESP class of SMI algorithms, more recently, two recursive implementations for the discrete-time PBSID algorithm have been proposed, in Houtzager et al. [2009], Chiuso et al. [2010], Houtzager et al. [2012].

Recursive implementation is particularly important in connection to continuous-time subspace methods in view of the significant computational burden associated with their implementation. In this respect, the recursive implementation of the continuous-time version of PO-MOESP first proposed in Ohta and Kawai [2004], Ohta [2011] has been presented in Kinoshita and

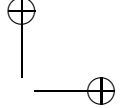


|





|



Ohta [2010], together with a novel set of orthonormal, Laguerre-like basis function with the specific feature of being compactly supported.

In view of the above discussion, the aim of this Chapter is to devise an algorithm for RSMI in continuous-time first proposed in Bergamasco et al. [2011], building on related results presented in Bergamasco and Lovera [2010a,b, 2011a] for the continuous-time counterpart of the PBSID method and on the recent advances in recursive identification presented in the above cited papers. More precisely, a recursive version of the algorithm in Section 1.5 is presented, and a comparison between conventional and compactly supported basis functions is carried out and discussed.

The Chapter is organised as follows. In Section 2.2 the problem statement is given and some definitions are provided. Section 2.3 provides a summary of the approach based on Laguerre projections used to convert continuous-time problems to equivalent discrete-time ones; subsequently, in Section 2.4 the proposed recursive algorithm is presented. Finally, some simulation results are presented in Section 2.5 to illustrate the performance of the proposed method.

2.2 Problem statement

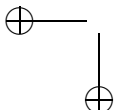
Consider the linear, time-invariant continuous-time system

$$\begin{aligned} dx(t) &= Ax(t)dt + Bu(t)dt + dw(t), \quad x(0) = x_0 \\ dz(t) &= Cx(t)dt + Du(t)dt + dv(t) \\ y(t)dt &= dz(t), \end{aligned} \tag{2.1}$$

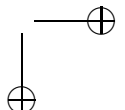
where $x \in \mathbb{R}^n$, $u \in \mathbb{R}^{n_u}$ and $y \in \mathbb{R}^{n_y}$ are, respectively, the state, input and output vectors and $w \in \mathbb{R}^n$ and $v \in \mathbb{R}^{n_y}$ are the process and the measurement noise, respectively, modelled as Wiener processes with incremental covariance given by

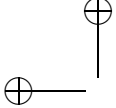
$$E \left\{ \begin{bmatrix} dw(t) \\ dv(t) \end{bmatrix} \begin{bmatrix} dw(t) \\ dv(t) \end{bmatrix}^T \right\} = \begin{bmatrix} Q & S \\ S^T & R \end{bmatrix} dt.$$

The system matrices A , B , C and D , of appropriate dimensions, are such that (A, C) is observable and $(A, [B, Q^{1/2}])$ is controllable. Assume that a dataset $\{u(t_i), y(t_i)\}$, $i \in [1, N]$ of sampled input/output data (possibly associated with a non equidistant sequence of sampling instants) obtained from system (2.1) is available. Then, the problem is to provide a *recursive estimator* of the state space matrices A , B , C and D (up to a similarity transformation) on the basis of the available data.

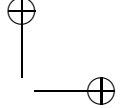


|





|



2.3 Recursive implementations of Laguerre projections

The continuous-time algorithms discussed in this Chapter are based on the results first presented in Section 1.5, which allow to obtain a discrete-time equivalent model starting from the continuous-time system (2.1). The projection technique is not directly applicable to the recursive estimate due to the computation of the infinity integrals as in (1.56). To avoid this problem two approaches are investigated. The former approach is based on the truncation of the infinity integrals exploiting the exponential decay of the Laguerre filters. The latter method is based on a reformulation of the Laguerre basis, used as generators of finitely-supported filter kernels.

2.3.1 Infinity integral truncation

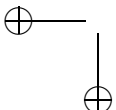
In discrete-time RSMI schemes the recursion is implemented directly with respect to the new discrete input-output sample acquired at the current sampling time. When dealing with the corresponding continuous-time counterpart the first step to be carried out is the (approximate) computation of the projections (1.56). In this respect, since the index k in the transformed system represents the order of the basis function on which the data has been projected, while the index i is related to the sampling instants t_i , the arrival of a new input-output sample leads to the addition of a new time instant at which the projections (1.56) have to be computed, which leads, in turn, to a new column to be added to the data matrices defined according to (1.63). In order to compute the projections (1.56) when dealing with the conventional (*i.e.*, with infinite support) Laguerre filters, the following approximation is introduced:

$$\begin{aligned}\tilde{u}_i(k) &= \int_0^\infty \Lambda_w^k \ell_0(\tau) u(t_i + \tau) d\tau \\ &= \int_{t_i}^\infty \Lambda_w^k \ell_0(\tau - t_i) u(\tau) d\tau \\ &\simeq \int_{t_i}^{t_F + t_i} \Lambda_w^k \ell_0(\tau - t_i) u(\tau) d\tau,\end{aligned}\tag{2.2}$$

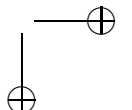
where t_F is the instant where the impulse response of the filter of maximum order can be considered approximately equal to zero. In other words

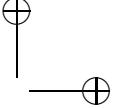
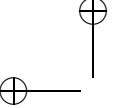
$$\begin{aligned}t_F &= \arg \min_\tau \tau \\ \text{s.t. } \Lambda_w^{2p-1} \ell_0(t) &\leq \epsilon \quad \forall t \geq \tau,\end{aligned}\tag{2.3}$$

where ϵ is a sufficiently small number. This approach is certainly very simple but it is not possible to directly choose the integral window length



|





t_F . As will be shown in the following Section, a method based on compact-supported filter kernels overcomes this problem.

2.3.2 Finitely-supported filter kernels generated from Laguerre basis functions

As remarked in Kinoshita and Ohta [2010] the above described projections based on Laguerre basis functions can only be computed in an approximate sense as the infinity integrals in (1.31) need to be truncated to finite intervals. In order to circumvent this difficulty, a novel set of basis functions, for which it can be proved that they are compactly supported, has been proposed in the same paper.

In this Section is shown that compact-supported filter kernels can be generated from Laguerre basis functions. These kernels are available as an alternative to Laguerre basis functions for the signal transformation, inducing the same system transformation as (1.33). The compactness of supports of the introduced kernels is shown as follows. Define coefficients $\alpha_0, \alpha_1, \dots, \alpha_\rho$ as satisfying the polynomial identity for x , i.e.,

$$\sum_{i=0}^{\rho} \alpha_i x^{\rho-i} = (x - e^{-a\tau})^\rho, \quad (2.4)$$

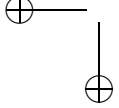
where τ is the delay constant, a is the Laguerre filter pole position, and ρ is the number of bases combined to obtain the filter kernels. Define the series of functions $\tilde{\ell}_k(t)$, $k = 0, \dots, \rho$ as

$$\tilde{\ell}_k(t) = \sum_{i=0}^{\rho} \alpha_i \Lambda_w^k \ell_0(t - i\tau). \quad (2.5)$$

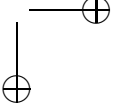
Proposition 2.3.1. (Kinoshita and Ohta [2010]) The functions $\tilde{\ell}_0(t), \tilde{\ell}_1(t), \dots, \tilde{\ell}_\rho(t)$ defined by (2.5) are supported on the compact interval $[0, \rho\tau]$.

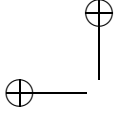
Proof. Consider the Laplace transform of functions $\tilde{\ell}_0(t), \tilde{\ell}_1(t), \dots, \tilde{\ell}_\rho(t)$,

$$\begin{aligned} \mathcal{L}[\tilde{\ell}_k(t)] &= \sum_{i=0}^{\rho} \alpha_i e^{-si\tau} \sqrt{2a} \frac{(s-a)^k}{(s+a)^{k+1}} \\ &= \left(\sum_{i=0}^{\rho} \alpha_i e^{s(\rho-i)\tau} \right) e^{-s\rho\tau} \sqrt{2a} \frac{(s-a)^k}{(s+a)^{k+1}} \\ &= (e^{s\tau} - e^{-a\tau})^\rho e^{-s\rho\tau} \sqrt{2a} \frac{(s-a)^k}{(s+a)^{k+1}}. \end{aligned}$$

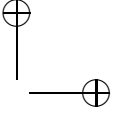


|





|



It is trivial to show that the term $(e^{s\tau} - e^{-a\tau})$ cancels the effect of the first Laguerre filter after $\rho\tau$ seconds. Then, if $\rho > k$, *i.e.*, the number of the combined Laguerre bases is greater than the maximum considered Laguerre filter order, $\tilde{\ell}_k(t)$ has a compact support. \square

The previous Proposition can be clarified using few numerical examples. For instance consider $\tau = 1$ s and $a = \frac{1}{2}$, then

$$\mathcal{L}[\tilde{\ell}_k(t)] = \left(e^s - e^{-\frac{1}{2}}\right)^\rho e^{-s\rho} \frac{(s - \frac{1}{2})^k}{(s + \frac{1}{2})^{k+1}}. \quad (2.6)$$

Taken $\rho = 1$ and $k = 0$, (2.6) becomes

$$\begin{aligned} \mathcal{L}[\tilde{\ell}_0(t)] &= \left(e^s - e^{-\frac{1}{2}}\right) e^{-s} \frac{1}{(s + \frac{1}{2})} \\ &= \left(1 - e^{-\frac{1}{2}} e^{-s}\right) \frac{1}{(s + \frac{1}{2})}, \end{aligned}$$

and applying the inverse Laplace transform

$$\tilde{\ell}_0(t) = e^{-\frac{1}{2}t} - e^{-\frac{1}{2}} e^{-\frac{1}{2}H(t-1)},$$

where H is the Heaviside function and $t \geq 0$. It is clear that the first Laguerre filter impulse response is deleted by the same filter shifted in time and scaled in the proper way, as shown in Figure 2.1 (Case 1). The following example cases are considered

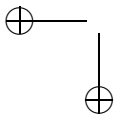
Case 1 - ($\rho = 1, k = 0$) $\mathcal{L}[\tilde{\ell}_0(t)] = \left(1 - e^{-\frac{1}{2}} e^{-s}\right) \frac{1}{(s + \frac{1}{2})} \rightarrow$
 $\tilde{\ell}_0(t) = e^{-\frac{1}{2}t} - e^{-\frac{1}{2}} e^{-\frac{1}{2}H(t-1)} = (1 - H(t-1)) e^{-\frac{1}{2}t},$

Case 2 - ($\rho = 2, k = 1$) $\mathcal{L}[\tilde{\ell}_1(t)] = \left(1 - 2e^{-\frac{5}{2}s} + e^{-1-2s}\right) \frac{s-\frac{1}{2}}{(s + \frac{1}{2})^2} \rightarrow$
 $\tilde{\ell}_1(t) = \left(1 - 4H(t-1) + 3H(t-2) - (1 - 2H(t-1) + H(t-2))t\right) e^{-\frac{1}{2}t},$

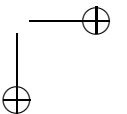
Case 3 - ($\rho = 3, k = 1$) $\mathcal{L}[\tilde{\ell}_1(t)] = \left(e^s - e^{-\frac{1}{2}}\right)^3 e^{-3s} \frac{(s-\frac{1}{2})}{(s + \frac{1}{2})^2},$

Case 4 - ($\rho = 3, k = 2$) $\mathcal{L}[\tilde{\ell}_2(t)] = \left(e^s - e^{-\frac{1}{2}}\right)^3 e^{-3s} \frac{(s-\frac{1}{2})^2}{(s + \frac{1}{2})^3},$

and their impulse responses are shown in Figure 2.1. Note that $\tilde{\ell}_1(t)$ (Case 3) and $\tilde{\ell}_2(t)$ (Case 4) are not reported in the time- domain because it is trivial and verbose.



|



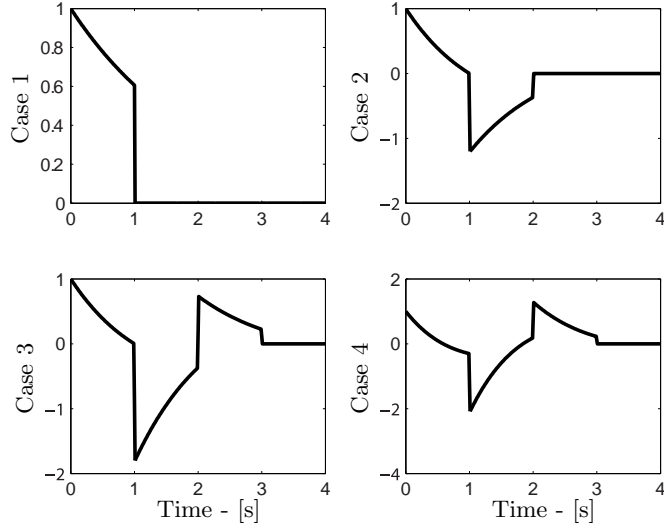
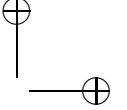
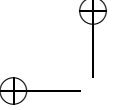


Figure 2.1: Impulse responses of finitely-supported filter kernels generated from Laguerre basis functions.

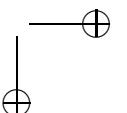
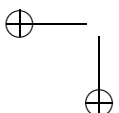
The signal transformation with the filter kernels (2.6) induces a system transformation that satisfies (1.32), (1.33) as it will be proved.

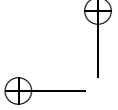
Consider the continuous-time linear time-invariant system (2.1). Let $0 \leq t_0 \leq t_1 \leq \dots \leq t_i \leq \dots \leq t_N$ be a sequence of equidistant time instants, i.e., $t_i = it_1, \forall i \geq 0$. Define

$$\begin{aligned}\tilde{u}_i(k) &= \int_0^\infty \tilde{\ell}_k(\nu) u(t_i + \nu) d\nu \\ \tilde{w}_i(k) &= \int_0^\infty \tilde{\ell}_k(\nu) dw(t_i + \nu) \\ \tilde{v}_i(k) &= \int_0^\infty \tilde{\ell}_k(\nu) dv(t_i + \nu) \\ \tilde{y}_i(k) &= \int_0^\infty \tilde{\ell}_k(\nu) y(t_i + \nu) d\nu,\end{aligned}\tag{2.7}$$

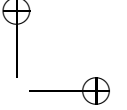
where $(\tilde{\cdot})$ is used with a slightly abuse of notation.

Proposition 2.3.2. (*Kinoshita and Ohta [2010]*) The signals (2.7) satisfy





|



the following discrete-time system

$$\begin{aligned}\xi_i(k+1) &= A_o \xi_i(k) + B_o \tilde{u}_i(k) + B_{ow} \tilde{w}_i(k), \quad \xi_i(0) = \sum_{j=0}^{\rho} \alpha_j x(t_i + j\tau) \\ \tilde{y}_i(k) &= C_o \xi_i(k) + D_o \tilde{u}_i(k) + D_{ow} \tilde{w}_i(k) + \tilde{v}_i(k).\end{aligned}\quad (2.8)$$

Proof. As shown in Section 1.3.2, considering the signals projections

$$\begin{aligned}\tilde{u}_{i,j}(k) &= \int_0^\infty \tilde{\ell}_k(\nu) u(t_i + j\tau + \nu) d\nu \\ \tilde{w}_{i,j}(k) &= \int_0^\infty \tilde{\ell}_k(\nu) dw(t_i + j\tau + \nu) \\ \tilde{v}_{i,j}(k) &= \int_0^\infty \tilde{\ell}_k(\nu) dv(t_i + j\tau + \nu) \\ \tilde{y}_{i,j}(k) &= \int_0^\infty \tilde{\ell}_k(\nu) y(t_i + j\tau + \nu) d\nu,\end{aligned}\quad (2.9)$$

the transformed system has the state space representation

$$\begin{aligned}\xi_{i,j}(k+1) &= A_o \xi_{i,j}(k) + B_o \tilde{u}_{i,j}(k) + B_{ow} \tilde{w}_{i,j}(k), \\ \tilde{y}_{i,j}(k) &= C_o \xi_{i,j}(k) + D_o \tilde{u}_{i,j}(k) + D_{ow} \tilde{w}_{i,j}(k) + \tilde{v}_{i,j}(k), \\ \xi_{i,j}(0) &= x(t_i + j\tau).\end{aligned}\quad (2.10)$$

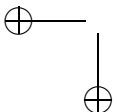
From (2.5) it holds that

$$\begin{aligned}\tilde{u}_i(k) &= \sum_{j=0}^{\rho} \alpha_j \tilde{u}_{i,j}(k) \quad \tilde{w}_i(k) = \sum_{j=0}^{\rho} \alpha_j \tilde{w}_{i,j}(k) \\ \tilde{v}_i(k) &= \sum_{j=0}^{\rho} \alpha_j \tilde{v}_{i,j}(k) \quad \tilde{y}_i(k) = \sum_{j=0}^{\rho} \alpha_j \tilde{y}_{i,j}(k).\end{aligned}$$

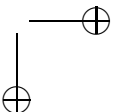
And then linearly combining the equations in (2.10) for $j = 0, \dots, \rho$ the state representation (2.8) is obtained. \square

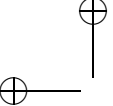
Summarizing, it has been shown that for suitably chosen scalars $\alpha_0, \alpha_1, \dots, \alpha_\rho$, i.e. the solution of (2.4), the functions

$$\tilde{\ell}_k(t) = \sum_{i=0}^{\rho} \alpha_i \Lambda_w^k \ell_0(t - i\tau) \quad (2.11)$$

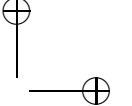


|





|



can be used to define the system transformations

$$\begin{aligned}\tilde{u}(k) &= \int_0^\infty \tilde{\ell}_k(t) u(t) dt \\ \tilde{y}(k) &= \int_0^\infty \tilde{\ell}_k(t) y(t) dt \\ \tilde{e}(k) &= \int_0^\infty \tilde{\ell}_k(t) d e(t),\end{aligned}\tag{2.12}$$

with the property that the signals obtained with the transformations (2.12) satisfy the discrete-time system (1.36) for suitably chosen initial states. Note that the system is directly considered in innovation form, since the steps to obtain the discrete-time system in this form are the same as the ones seen in 1.3.2. As shown, the support of the functions is compact if $\rho > k$.

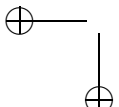
2.4 Recursive subspace model identification

In this Section the recursive implementation of the CT-PBSID_o algorithm is discussed, both using Laguerre basis functions according to Section 2.3.1 and their compactly supported counterparts described in Section 2.3.2.

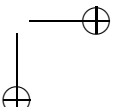
As far as the actual implementation of the recursive algorithm is concerned, the following steps have to be implemented (along the lines of the general template proposed in Chiuso et al. [2010] and of the algorithm in Houtzager et al. [2012]):

- Recursive update of the solution of the least squares problem (1.64), using a conventional recursive least square (RLS) scheme.
- Update of the estimate of the state sequence, *i.e.*, of the state estimate given by (1.70). In this respect, note that this is the most critical step in the implementation, as one has to ensure that the recursive state estimates are expressed in a consistent state space basis. One way of guaranteeing this is given by, *e.g.*, the scheme proposed in Houtzager et al. [2009], which is based on the so-called propagator method for the recursive update of the state sequence (see also Mercère et al. [2004, 2008a] for details).
- Recursive estimate of the state space matrices of the system, *i.e.*, update of the solution of the least squares problems (1.71) and (1.73), again by means of RLS.

The batch CT-PBSID_o algorithm involves some minimization problems that are usually solved using a SVD-approach. A least squares problems



|



can be reformulated as an iterative algorithm using several methods in the family of adaptive filtering, *e.g.*, least mean squares (LMS), recursive least squares (RLS), Kalman filtering (KF), etc. In this thesis the RLS approach is preferred for its good convergence properties (see Spall [2003]) and the fact that it is easily modifiable in order to track time-varying parameters.

In the following a brief review of the RLS scheme is given. Suppose that the multivariate model for a signal z_k is

$$z_k = \theta g_k + v_k,$$

where θ is the model parameters vector, g_k is the input data, v_k is a zero-mean noise vector with covariance matrix equal to λI . In order to estimate θ a least squares problem is posed as follows

$$\theta = \arg \min_{\theta} \|Z - \theta G\|_F^2$$

where $Z = [z_1 \ z_2 \ \dots \ z_k]$ and $G = [g_1 \ g_2 \ \dots \ g_k]$. Suppose that a new sample is available, *i.e.*, (z_{k+1}, g_{k+1}) , then the recursive estimation of the parameter θ can be computed as follows:

$$\begin{aligned} P_{k+1} &= P_k - P_k g_{k+1} (\lambda I + g_{k+1}^T P_k g_{k+1})^{-1} g_{k+1}^T P_k \\ \theta_{k+1} &= \theta_k + \frac{1}{\lambda} (z_{k+1} - \theta_k g_{k+1}) g_{k+1}^T P_{k+1}, \end{aligned} \quad (2.13)$$

with $\theta_0 = 0$ and $P_0 = \sigma I, \sigma \gg 0$. The tuning parameter λ can be seen as a *forgetting factor* the role of which is to increase the weight of the latest samples respect to the older ones. Therefore using $\lambda < 1$ it is possible to estimate time-varying parameters.

In the continuous-time recursive predictor based subspace model identification algorithm a new sample $(u(t_{N+1}), y(t_{N+1}))$ is not directly used to update the recursive least square problems. Indeed it is inserted in the sliding window for the computation of the projected signals using (2.2) or (2.7). The projected signals are stacked in vectors as follows:

$$\begin{aligned} Y_i^{p,p} &= [\tilde{y}_i(p) \ \tilde{y}_i(p+1) \ \dots \ \tilde{y}_i(2p)] \\ U_i^{p,p} &= [\tilde{u}_i(p) \ \tilde{u}_i(p+1) \ \dots \ \tilde{u}_i(2p)] \\ E_i^{p,p} &= [\tilde{e}_i(p) \ \tilde{e}_i(p+1) \ \dots \ \tilde{e}_i(2p)] \\ \Xi_i^{p,p} &= [\xi_i(p) \ \xi_i(p+1) \ \dots \ \xi_i(2p)] \\ \bar{Z}_i^{p,p} &= [Z_i^{0,p-1} \ Z_i^{1,p} \ \dots \ Z_i^{p,2p-1}]. \end{aligned} \quad (2.14)$$



Consider a reformulation of the least squares problem (1.64) in which the matrices $Y^{p,p}$, $\bar{Z}^{p,p}$, and $U^{p,p}$ are defined in different way with respect to (1.63), *i.e.*,

$$\begin{aligned} \min_{C_o \mathcal{K}^p, D_o} \|Y^{p,p} - C_o \mathcal{K}^p \bar{Z}^{p,p} - D_o U^{p,p}\|_F = \\ \min_{C_o \mathcal{K}^p, D_o} \|[Y_0^{p,p} \dots Y_N^{p,p}] - C_o \mathcal{K}^p [\bar{Z}_0^{p,p} \dots \bar{Z}_N^{p,p}] - D_o [U_0^{p,p} \dots U_N^{p,p}]\|_F = \\ \min_{C_o \mathcal{K}^p, D_o} \left\| [Y_0^{p,p} \dots Y_N^{p,p}] - [C_o \mathcal{K}^p \quad D_o] \begin{bmatrix} \bar{Z}_0^{p,p} & \dots & \bar{Z}_N^{p,p} \\ U_0^{p,p} & \dots & U_N^{p,p} \end{bmatrix} \right\|_F. \end{aligned} \quad (2.15)$$

Starting from (2.15) it is straightforward to derive the recursive formulation of the problem. Indeed when a new sample $(u(t_{N+1}), y(t_{N+1}))$ is available the new projected data $(U_{N+1}^{p,p}, Y_{N+1}^{p,p}, \bar{Z}_{N+1}^{p,p})$ can be computed and the estimation of $[C_o \mathcal{K}^p \ D_o]$ is update as follows:

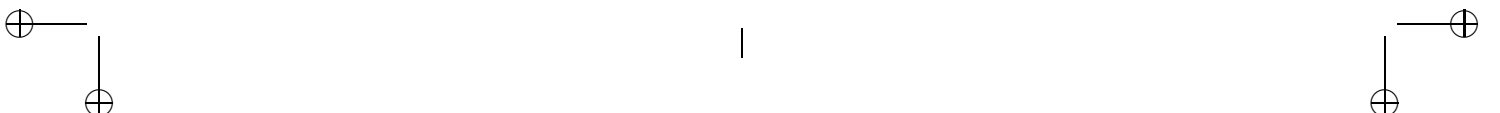
$$P_{N+1} = P_N - P_N \begin{bmatrix} \bar{Z}_{N+1} \\ U_{N+1} \end{bmatrix} \left(\lambda_1 I + \begin{bmatrix} \bar{Z}_{N+1} \\ U_{N+1} \end{bmatrix}^T P_N \begin{bmatrix} \bar{Z}_{N+1} \\ U_{N+1} \end{bmatrix} \right)^{-1} \begin{bmatrix} \bar{Z}_{N+1} \\ U_{N+1} \end{bmatrix}^T P_N$$

$$\begin{aligned} [C_o \mathcal{K}^p \ D_o]_{N+1} &= [C_o \mathcal{K}^p \ D_o]_N \\ &\quad + \frac{1}{\lambda_1} \left(Y_{N+1} - [C_o \mathcal{K}^p \ D_o]_N \begin{bmatrix} \bar{Z}_{N+1} \\ U_{N+1} \end{bmatrix} \right) \begin{bmatrix} \bar{Z}_{N+1} \\ U_{N+1} \end{bmatrix}^T P_{N+1}, \end{aligned} \quad (2.16)$$

where the superscript (p,p) is omitted for brevity. The estimate $\widehat{C_o \mathcal{K}^p}$ can be used to compute $\Gamma^p \mathcal{K}^p$ as in (1.66).

In the batch algorithm the state estimation is performed through the SVD as shown in (1.70). In the recursive algorithm this step becomes more delicate since using the SVD as in the batch case there is no guarantee that the state vector basis remains consistent. An estimate of the state sequence can be obtained from the recursive estimate of $\Gamma^p \mathcal{K}^p$ following the lines of Houtzager et al. [2012] in which the propagator method (Mercère et al. [2008a]) is used. First of all, the weighting matrix H is introduced, defined as

$$H = \begin{bmatrix} I & 0 & \dots & 0 \\ -C_o K_o & I & \ddots & \vdots \\ \vdots & \ddots & \ddots & 0 \\ -C_o \bar{A}_o^{p-2} K_o & -C_o \bar{A}_o^{p-3} K_o & \dots & I \end{bmatrix}. \quad (2.17)$$



In Houtzager et al. [2012] it is shown that H is invertible, and the following transformation holds

$$\tilde{\Gamma}^p = \begin{bmatrix} C_o \\ C_o A_o \\ \vdots \\ C_o A_o^{p-1} \end{bmatrix} = H^{-1} \Gamma^p = H^{-1} \begin{bmatrix} C_o \\ C_o \bar{A}_o \\ \vdots \\ C_o \bar{A}_o^{p-1} \end{bmatrix},$$

where $\tilde{\Gamma}^p$ is the extended observability matrix of the open-loop discrete time system. Using (1.70) the estimate of the state is

$$\begin{aligned} \Xi_i^{p,p} &= W_i H_i^{-1} \Gamma^p \mathcal{K}^p \bar{Z}_i^{p,p} \\ &= W_i \tilde{\Gamma}^p \mathcal{K}^p \bar{Z}_i^{p,p}, \end{aligned} \quad (2.18)$$

where W_i is a weighting matrix equal to $\Sigma_n^{-\frac{1}{2}} U_n^T$ in the batch case. Of course in the recursive case that weighting matrix is not available and then another solution has to be considered. Note that H_i^{-1} is time varying since it is computed using the updated estimation of $C_o \mathcal{K}^p$. The propagator method (PM) is based on the idea that as the system of order n is observable, its observability matrix has at least n linearly independent rows. If the order n is known it is possible to consider a constant selection matrix S such that

$$\begin{aligned} \Xi_i^{p,p} &= S H_i^{-1} \Gamma^p \mathcal{K}^p \bar{Z}_i^{p,p} \\ &= S \tilde{\Gamma}^p \mathcal{K}^p \bar{Z}_i^{p,p}. \end{aligned} \quad (2.19)$$

As pointed out in Houtzager et al. [2012] the PM fails to converge with the PBSID algorithm since Γ^p depends on the Kalman gain K which can be time varying. For this reason the matrix H^{-1} is considered, indeed pre-multiplying the observability matrix of the closed-loop system Γ^p with H^{-1} , the observability matrix of the open-loop system $\tilde{\Gamma}^p$ is obtained. $\tilde{\Gamma}^p$ does not depend on K , then it is time invariant and the PM converges. For the single-input single-output case a suitable S can be

$$S = [I_n \ 0_{n \times (pn_y - n)}], \quad (2.20)$$

while for the multi-input multi-output case a more complicated formulation of S have to be taken into account, as shown in Mercère et al. [2008a]. From the estimation of the state $\Xi_{N+1}^{p,p}$ an estimate of C_o can be computed by solving the recursive version of (1.71), *i.e.*,

$$\begin{aligned} M_{N+1} &= M_N - M_N \hat{\Xi}_{N+1} \left(\lambda_2 I + \hat{\Xi}_{N+1}^T M_N \hat{\Xi}_{N+1} \right)^{-1} \hat{\Xi}_{N+1}^T M_N \\ [C_o]_{N+1} &= [C_o]_N + \frac{1}{\lambda_2} \left(Y_{N+1} - \hat{D}_o U_{N+1} - [C_o]_N \hat{\Xi}_{N+1} \right) \hat{\Xi}_{N+1}^T M_{N+1}, \end{aligned} \quad (2.21)$$



where the superscript (p,p) is omitted for brevity. The final steps consist of the estimation of the innovation $E_{N+1}^{p,p}$, *i.e.*,

$$E_{N+1}^{p,p} = Y_{N+1}^{p,p} - \hat{C}_o \hat{\Xi}_{N+1}^{p,p} - \hat{D}_o U_{N+1}^{p,p}, \quad (2.22)$$

and of the entire set of the state space matrices for the system in the transformed domain, which can be obtained by solving the recursive version of the least squares problem (1.73), *i.e.*,

$$\begin{aligned} L_{N+1} &= L_N \\ &- L_N \begin{bmatrix} \hat{\Xi}_{N+1}^{p,p-1} \\ U_{N+1}^{p,p-1} \\ E_{N+1}^{p,p-1} \end{bmatrix} \left(\lambda_3 I + \begin{bmatrix} \hat{\Xi}_{N+1}^{p,p-1} \\ U_{N+1}^{p,p-1} \\ E_{N+1}^{p,p-1} \end{bmatrix}^T L_N \begin{bmatrix} \hat{\Xi}_{N+1}^{p,p-1} \\ U_{N+1}^{p,p-1} \\ E_{N+1}^{p,p-1} \end{bmatrix} \right)^{-1} \begin{bmatrix} \hat{\Xi}_{N+1}^{p,p-1} \\ U_{N+1}^{p,p-1} \\ E_{N+1}^{p,p-1} \end{bmatrix}^T L_N \end{aligned}$$

$$[A_o \ B_o \ K_o]_{N+1} = [A_o \ B_o \ K_o]_N \quad (2.23)$$

$$+ \frac{1}{\lambda_3} \left(\hat{\Xi}_{N+1}^{p+1,p} - [A_o \ B_o \ K_o]_N \begin{bmatrix} \hat{\Xi}_{N+1}^{p,p-1} \\ U_{N+1}^{p,p-1} \\ E_{N+1}^{p,p-1} \end{bmatrix} \right) \begin{bmatrix} \hat{\Xi}_{N+1}^{p,p-1} \\ U_{N+1}^{p,p-1} \\ E_{N+1}^{p,p-1} \end{bmatrix}^T L_{N+1}.$$

Finally, the state space form for the original continuous-time system can be recovered by means of equations (1.33).

The overall recursive algorithm is summarised in Table 2.1.



Algorithm CT-RPBSID_o

For t_i with $i = 1, \dots, N$

1. Compute $\tilde{u}_i(k)$ and $\tilde{u}_i(k)$ for $k = 0, \dots, 2p$ using (2.2) or (2.7).
2. Build the matrices $Y_i^{p,p}$, $U_i^{p,p}$ and $\bar{Z}_i^{p,p}$ according to (2.14).
3. Update the recursive estimation of $C_o \mathcal{K}^p$ and D_o using (2.16).
4. According to (1.66) an estimate of $\Gamma^p \mathcal{K}^p$ is obtained using $C_o \mathcal{K}^p$.
5. Compute the updated H_i using the estimate of $C_o \mathcal{K}^p$ as shown in (2.17).
6. Obtain an estimate of the state sequence from (2.19).
7. Update the recursive least-squares (2.21) obtaining C_o .
8. Compute $E_i^{p,p}$ with (2.22).
9. Update the recursive least-squares (2.23) obtaining A_o , B_o and K_o .
10. Use the matrix relations (1.33) and (1.38) to obtain A , B , C , D , and K .

end

Table 2.1: Summary of the CT-RPBSID_o algorithm.

2.5 Simulation examples

In this Section some simulation results obtained with the application of the proposed algorithms (recursive PBSID both with conventional and modified Laguerre bases) and of the algorithm in Kinoshita and Ohta [2010] to data generated by systems operating both in open-loop and in closed-loop are presented and discussed.

2.5.1 Open-loop case

The considered example is the single-input single-output continuous-time system given by the state space matrices

$$A = \begin{bmatrix} -0.5 & a_1 & 0 \\ -a_1 & -0.5 & 0 \\ 0 & 0 & a_2 \end{bmatrix} \quad B = \begin{bmatrix} 1.5 \\ 1.8 \\ 1.6 \end{bmatrix} \quad (2.24)$$

$$C = [1.5 \ 1.3 \ 1.6] \quad D = 0, \quad (2.25)$$

where a_1 and a_2 are initially equal to 10 and -2 respectively and change to 15 and -5 after 150s. The simulated data has been collected by applying to the input of the system a piece-wise constant signal with base period $T_p = 0.01$ s, for a duration of 300s. The input magnitude is chosen randomly according to a Gaussian distribution with zero mean and unit variance. White Gaussian noise of increasing variance has been added to the output in order to assess the influence of decreasing signal-to-noise ratio on the quality of the computed estimates. For the input and output variables the sampling interval $\Delta t = 0.001$ s has been considered. The pole of the Laguerre filters has been chosen as $a = 10$, while different choices have been made concerning the implementation of the projection operators associated with the system transformations. In the case of the conventional Laguerre basis, according to (2.4) a window of 2.6s have been used, while for the modified basis a shorter window of 0.8s only (in view of the compact support) has been employed. Figures 2.2-2.3 illustrate the estimation errors of the real and imaginary parts of the system eigenvalues as computed by running the algorithm in Kinoshita and Ohta [2010] (black line) and the one proposed herein, both using conventional Laguerre bases (pale gray line) and finitely supported ones (dark gray line), for two different values of the signal-to-noise ration at the output. Apart from occasional overshoots in transients, which are likely to be reduced by a more refined implementation, it appears that algorithms based on the modified Laguerre basis can provide good performance while requiring a shorter time window for the integration, which leads to a potentially faster operation.

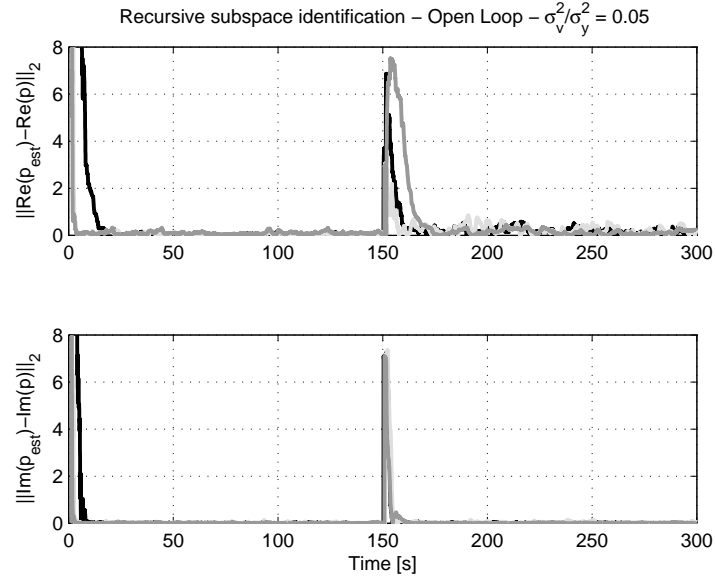


Figure 2.2: Real and imaginary part of the estimated eigenvalues - open loop experiment
- $\frac{\sigma_v^2}{\sigma_y^2} = 0.05$.

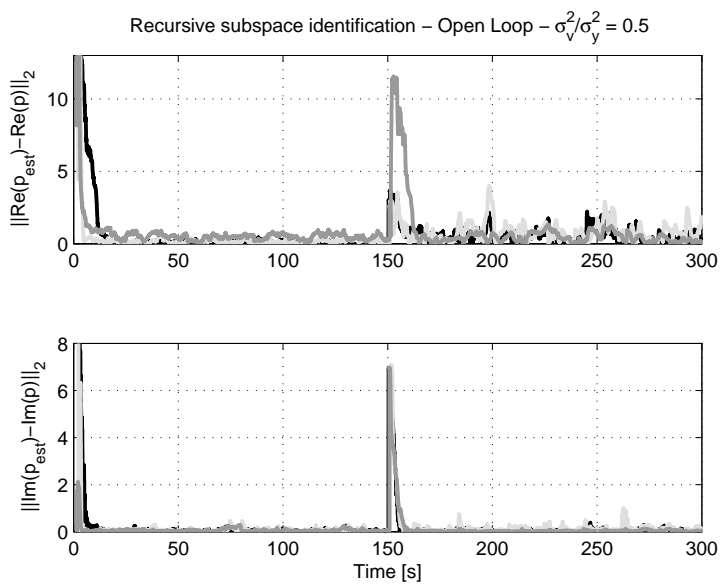


Figure 2.3: Real and imaginary part of the estimated eigenvalues - open loop experiment
- $\frac{\sigma_v^2}{\sigma_y^2} = 0.5$.



The tuning parameters λ_1 , λ_2 , and λ_3 in (2.15), (2.21), and (2.23) have been chosen equal to 0.999. They affect the regressions speed of convergence and the steady-state variances, as in the classic recursive linear regression algorithm.

2.5.2 Closed-loop case

In the second example the same system is considered, but data are now collected during closed-loop operation, subject to the control law $u = Ky$, $K = 1$. Again, Figures 2.4-2.5 illustrate the estimation errors of the real and imaginary parts of the system eigenvalues as computed by running the algorithm in Kinoshita and Ohta [2010] (black line) and the one proposed herein, both using conventional Laguerre basis (pale gray line) and finitely supported ones (dark gray line), for two different values of the signal-to-noise ration at the output. Similar comments as in the open-loop case apply to the results obtained in this situation.

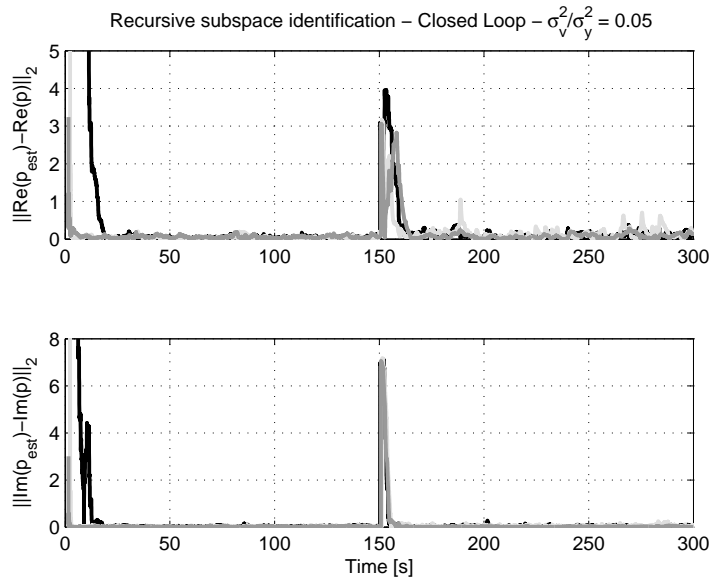


Figure 2.4: Real and imaginary part of the estimated eigenvalues - closed loop experiment
- $\frac{\sigma_v^2}{\sigma_y^2} = 0.05$.



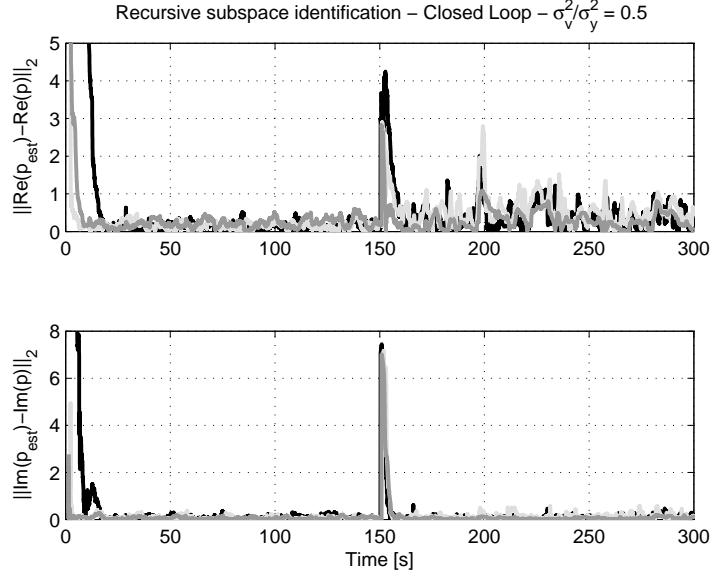
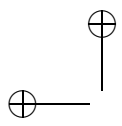


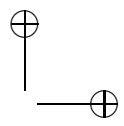
Figure 2.5: Real and imaginary part of the estimated eigenvalues - closed loop experiments
- $\frac{\sigma_v^2}{\sigma_y^2} = 0.5$.

2.6 Concluding remarks

The problem of recursive continuous-time subspace model identification has been considered and an updating scheme for a batch algorithm based on Laguerre projections of the input-output variables followed by a PBSID identification step has been proposed. In particular, the role of classical and compactly supported Laguerre basis functions has been considered. Simulation results show that the proposed schemes are viable and can be therefore applied to either relieve the computational burden and memory storage requirements of the corresponding batch algorithms when dealing with large scale and/or fast sampling problems or to compute on-line updates of the system matrices for slowly varying systems.

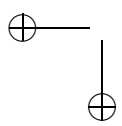


|

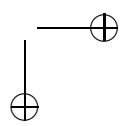


—

—



|



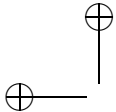
CHAPTER THREE

CONTINUOUS-TIME LINEAR PARAMETER VARYING MODEL IDENTIFICATION

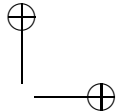
In the engineering field most of the systems are described by nonlinear models, but a very common approximation is to linearize them around a point of interest and consequently the controllers are designed in this nominal condition. The use of linear models are favorable due to their simplicity and the effectiveness and the robustness of the available control theory. A convenient extension of the linear models are the Linear Parameter Varying (LPV) models in which the dynamics of the system is locally linear but it changes over the time according to a varying scheduling parameter. In this Chapter an approach, formulated in the subspace model identification framework, is proposed for deriving continuous-time Linear Parameter Varying (LPV) models in state-space form starting from sampled measurements of input, output and scheduling variables, using a local approach.

3.1 Introduction

In many control engineering applications a single control system must be designed to guarantee stability and performance requirements for a given plant in many different operating conditions. The gain scheduling approach, which has been part of the engineering practice for decades, can be roughly summarised as follows: find one or more *scheduling variables* which can completely parameterise the operating space of interest for the system to be controlled; define a parametric *family* of linearised models for the plant associated with the set of operating points of interest; finally, design a *parametric* controller which can both ensure the desired control objectives in each operating point and an acceptable behaviour during (slow) transients between



|

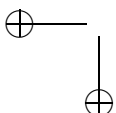


one operating condition and the other. As is well known, a wide body of design techniques is now available for this problem (see, *e.g.*, Shamma and Athans [1990], Kaminer et al. [1995], Apkarian and Adams [1998]), which can be reliably solved, provided that a suitable model in parameter-dependent form has been derived.

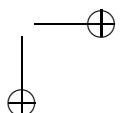
This modelling problem can be formulated in a number of different perspectives, which consequently lead to a number of different approaches. More precisely, two broad classes of methods can be identified in the literature (see, *e.g.*, Lovera et al. [2011]): *analytical* methods based on the availability of (relatively) reliable nonlinear equations for the dynamics of the plant, from which suitable control-oriented representations can be derived (see Leith and Leithead [2000], Rugh and Shamma [2000] and Marcos and Balas [2004]); *experimental* methods based entirely on identification, *i.e.*, aiming at deriving LPV models for the plant directly from input/output data. The methods belonging to the first class aim at developing LPV models for the plant to be controlled by resorting, broadly speaking, either to suitable extensions of the notion of linearisation, developed in order to take into account off-equilibrium operation of the system, or to interpolation schemes applied to local numerical linearisations. As far as identification methods are concerned, a number of algorithms has been proposed in the literature in the last ten years or so, aiming at the estimation of the parameters for both input/output and state-space models, the latter either in affine or Linear Fractional Transformation (LFT) form (Nemani et al. [1995], Lovera et al. [1998], Lee and Poolla [1999], Bamieh and Giarré [2002], Verdult [2002], Previdi and Lovera [2003], van Wingerden and Verhaegen [2009], Toth [2010]).

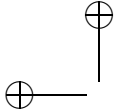
Most LPV identification techniques are based on the assumption that the identification procedure can rely on one *global* identification experiment in which both the control input and the scheduling variables are (persistently) excited in a simultaneous way. This assumption may not be a reasonable one in many applications, in which it would be desirable to try and derive a parameter-dependent model on the basis of *local* experiments only, *i.e.*, experiments in which the scheduling variable is held constant and only the control input is excited.

Such a viewpoint has been considered in Steinbuch et al. [2003], van Helvoort et al. [2004], Groot Wassink et al. [2005], Pajmans et al. [2008], where numerical procedures for the construction of parametric models for gain scheduling on the basis of local experiments and for the interpolation of local controllers have been proposed. In Steinbuch et al. [2003], van Helvoort et al. [2004], i) input-output local models are identified using a frequency-domain approach; ii) the identified models are written in state-space repre-

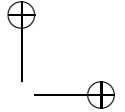


|





|

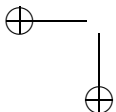


sentation using a canonical controllability form; iii) an interpolation step for the elements of the state-space matrices completes the identification procedure. In Groot Wassink et al. [2005], a similar approach is adopted, followed by a conversion of the identified model to LFT form. Finally, in Pajjmans et al. [2008], De Caigny et al. [2009] methods for the identification of LPV SISO models are proposed, based on the decomposition of the system in first and second order subsystems and the subsequent interpolation of the parameter-dependent gain, zeros and poles of each subsystem. An extension to the MIMO case has been presented in De Caigny et al. [2011, 2012]. All the above methods are clearly based on the idea of following a two stage procedure, which consists in deriving a set of local models and performing some kind of interpolation between them. A number of issues deserve attention as far as this general procedure is concerned. First of all, performing the interpolation on input-output models directly might lead to significant problems if the obtained LPV model is to be eventually used in a state-space representation (see, *e.g.*, Toth [2010] for a detailed discussion of the equivalence between input-output and state-space representations for LPV systems). Similarly, numerical issues might turn out to be critical in the interpolation problem if an ill-conditioned parameterisation for the model class is chosen (*e.g.*, numerator and denominator coefficients in a high order transfer function). Finally, when dealing with the problem of interpolating black-box local models in state-space form, the challenging problem of realizing all the models with respect to the same state variables comes into play. Indeed, interpolating such state-space models without taking this issue into account may lead to inaccurate LPV models, even if the local LTI models are consistent. Quantifying the modelling errors associated with this aspect is, to our best knowledge, an open problem.

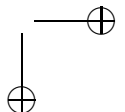
In view of the above discussion, the aim of this Chapter is to further elaborate on the existing approaches and on preliminary results presented in Lovera and Mercère [2007], in order to provide a number of extensions, namely:

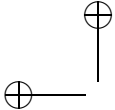
- the identification of local models is performed using the developed subspace technique of the predictor-based class for continuous-time models CT-PBSID_o presented in Section 1.5, so enabling the straightforward treatment of MIMO as well as SISO continuous-time modelling problems, in state-space form;
- in addition, the ability to deal with data generated in closed-loop is obtained as a benefit of the predictor-based framework.

In the light of the above discussion, in this Chapter the identification of the local models will be carried out using the continuous-time SMI schemes,

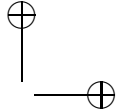


|





|



proposed in Section 1.5, based on the derivation of PBSID-like algorithms within the transformation theory proposed in Ohta and Kawai [2004] and relying on Laguerre projections of the sampled input-output data. Note that even though the proposed approach is capable of dealing with some of the limitations of the existing methods, the state-space basis issue remains open and will be dealt with in the present study only by means of simulations at the model validation stage.

The Chapter is organised as follows. In Section 3.2 the problem statement is given and some definitions are provided. Section 3.3 provides a summary of the balanced subspace approach. Finally, some simulation results are presented in Section 3.4 to illustrate the performance of the proposed method.

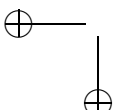
3.2 Problem statement

The system identification problem considered in this Chapter can be summarised as follows. Consider the MIMO linear parametrically-varying system given by

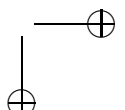
$$\begin{aligned}\dot{x} &= A(\theta)x + B(\theta)u \\ y &= C(\theta)x + D(\theta)u\end{aligned}\tag{3.1}$$

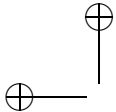
where $u \in \mathbb{R}^{n_u}$, $y \in \mathbb{R}^{n_y}$, $x \in \mathbb{R}^n$ and $\theta \in \mathbb{R}^{n_p}$ and assume that the results of N_θ identification experiments are available, associated with the operation of the system near N_θ different values of the parameter vector θ . The aim of the identification procedure proposed in this Chapter is to determine a set of parameter dependent matrices $\hat{A}(\theta)$, $\hat{B}(\theta)$, $\hat{C}(\theta)$ and $\hat{D}(\theta)$ either in affine or LFT form which can provide a good approximation of the system (3.1) over the considered range of operating points.

Note that in (3.1) no noise terms have been taken into account, as the above equations are just intended to illustrate the parameter dependent structure of the considered system. Since the actual identification experiments will be performed near operating points characterised by a constant value of the parameter vector, *i.e.*, assuming that the system can be considered as LTI, the same noise assumptions introduced in Section 1.2 are valid (see Bergamasco and Lovera [2011b] for further details).

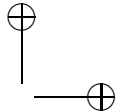


|





|



3.3 A balanced subspace approach to identification for gain scheduling

The approach to the problem of identification for gain scheduling proposed in this Section can be summarised in the following steps:

- linear continuous-time state-space models are estimated for each operating point, using the CT-PBSID_o algorithm (see Section 1.5).
- The identified models are balanced using the numerical algorithm of Laub et al. [1987] (as implemented in the Matlab Control Toolbox).
- Finally, the parameter-dependent model is obtained by direct interpolation of the state-space matrices of the local models, made possible by the unique properties of balanced realizations (see Laub et al. [1987]), and can eventually be converted to LFT form using results from the LPV identification literature (see Lee and Poolla [1999]).

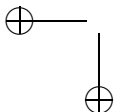
The above mentioned steps will be described in detail in the following Sections.

3.3.1 Balancing of the identified models

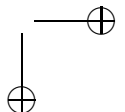
One of the main advantages and reasons of the success of subspace identification methods is the fact that, contrary to lots of identification methods applied to MIMO systems, no canonical forms are considered and no structural decision is explicitly made since this approach allows to estimate the system order during the identification procedure. On the other hand, this leads to the fact that the basis in which the estimated state-space matrices are given by the algorithm depends on the system itself as well as the input spectrum and cannot be enforced a priori by the user.

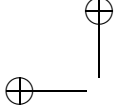
This characteristic can be used as a benefit if a particular basis is considered: the balanced coordinates first proposed in Moore [1981]. Once N_θ local models have been obtained, the problem of recovering the whole parameter-dependent system has to be faced. It turns out that this task is greatly simplified if the local models are converted to a suitable balanced form. In order to clarify this point, the main properties of internally balanced forms are recalled in Appendix A.2 (see Moore [1981], Moonen and Ramos [1993]).

In order to improve the numerical performance of the subsequent interpolation algorithm, it is proposed to fix the state-space basis of the estimated matrices by finding a similarity transformation T such that the

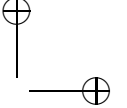


|





|



system $\{T^{-1}\hat{A}T, T^{-1}\hat{B}, \hat{C}T, \hat{D}\}$ is in internally balanced form. To this purpose, the algorithm first derived in Laub et al. [1987] is used, which consists of the following steps:

1. compute the Gramians \mathcal{W}_o and \mathcal{W}_c of the identified model;
2. apply a Cholesky factorisation to obtain $\mathcal{W}_o = L_o L_o^T$, $\mathcal{W}_c = L_c L_c^T$, where L_o and L_c are the lower triangular factors of the Gramians;
3. compute the SVD $L_o^T L_c = U \Sigma V^T$.

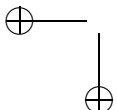
The balancing transformation is then defined by

$$\begin{aligned} T &= L_c V \Sigma^{-1/2} \\ T^{-1} &= \Sigma^{-1/2} U^T L_o^T. \end{aligned}$$

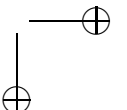
The most interesting property of balanced realizations, as far as this contribution is concerned, is associated with the *uniqueness* of the balancing transformation (see Moore [1981] and Laub et al. [1987] for details). Essentially, the question turns on the eigenvalues (real and nonnegative) of the product of the reachability and observability Gramians, and their corresponding eigenvectors, *i.e.*, the columns of the balancing transformation T . If these eigenvalues are distinct, then the corresponding eigenvectors are uniquely determined to within sign, *i.e.*, T is essentially unique. If, on the other hand, two or more eigenvalues are repeated, then their corresponding eigenvectors can be rotated arbitrarily in the corresponding eigenspace. This, in turn, implies that as long as the eigenvalues are distinct, if the true system exhibits a smooth dependence from the scheduling parameter p , then the overall parameter dependent model can be directly reconstructed from the identified local models.

Since, in general, the assumption of distinct eigenvalues cannot be guaranteed a priori, as far as our identification problem is concerned, the following situations may arise:

- if the elements of the state-space matrices of the identified local models exhibit a smooth variation as a function of the parameter θ , then the overall parameter-dependent model can be directly recovered using the interpolation techniques outlined in the following.
- If, instead, the behaviour of the elements of the state-space matrices exhibit abrupt sign changes (associated with sign changes in the columns of the balancing transformations), then one should check for situations in which the eigenvalues of the balanced Gramians are not



|



distinct. If signs changes are present but the eigenvalues are distinct, then a "mild" nonuniqueness is occurring, which can be corrected by adjusting the signs of the "stray" matrix elements, and the proposed procedure is applicable.

3.3.2 Model interpolation

In this Section the interpolation of the local models, in order to obtain an LPV model, is discussed. The problem of interpolating local models derived from jacobian linearisation of a nonlinear simulator is a subject of active research, see for example Groot Wassink et al. [2005], Pfifer and Hecker [2011]. Once the elements of the state-space matrices of the system have been estimated following the above steps, and set of N_θ local linear time-invariant state space models has been obtained, a number of options are available as far as the derivation of the actual parameter dependent model is concerned. The first, and simplest, would be to directly fit to the system matrices of the local models using suitable regressors formed from the scheduling parameter $\theta \in \mathbb{R}^{n_p}$. This would directly yield a parameter dependent model in so-called *affine* form, *i.e.*,

$$\begin{aligned}\dot{x} &= A(\gamma)x + B(\gamma)u \\ y &= C(\gamma)x + D(\gamma)u\end{aligned}\tag{3.2}$$

where $\gamma \in \mathbb{R}^{n_\gamma}$ is the vector of regressors (formed from linear or nonlinear combinations of the elements of θ) such that the parameter dependent matrices can be written as

$$A(\gamma) = A_0 + A_1\gamma_1 + A_2\gamma_2 + \dots + A_{n_\gamma}\gamma_{n_\gamma}$$

and similarly for $B(\gamma)$, $C(\gamma)$ and $D(\gamma)$. The state space matrices are represented as transfer functions

$$G_k(s) = C(\gamma(k))(sI - A(\gamma(k)))^{-1}B(\gamma(k)) + D(\gamma(k)), \quad k = 1, \dots, N_\theta$$

where k is the scheduling index of the k^{th} identified local model. The matrices are also aggregated in the following form

$$F(\gamma(k)) = \begin{bmatrix} A(\gamma(k)) & B(\gamma(k)) \\ C(\gamma(k)) & D(\gamma(k)) \end{bmatrix}, \quad k = 1, \dots, N_\theta.\tag{3.3}$$

In Figure 3.1 a scheme of the model interpolation problem is shown.

The polynomial interpolation of the elements of matrix F is performed by solving a least squares problem as $Y = \Phi\Theta$, where Y contains the elements f_{ij} of F , Φ contains the regressors γ , and Θ contains the polynomial

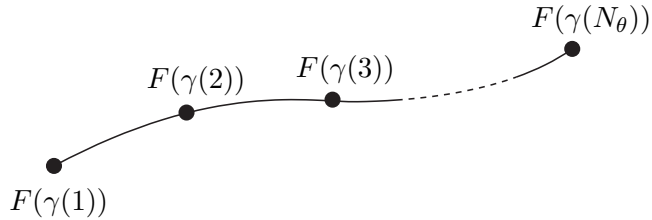


Figure 3.1: Interpolation of the state-space matrices of the local models.

coefficients. The root means square error (RMS_e) is defined as

$$RMS_e = \frac{\|Y - \Phi\hat{\Theta}\|_2}{\|Y\|_2}, \quad (3.4)$$

and it expresses the fitting error.

In order to reduce the model complexity, as suggested in Pfifer and Hecker [2011] and reported here for the sake of completeness, the fitting procedure is divided in two steps: the sensitivity analysis and the polynomial fitting.

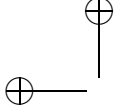
The H_∞ -norm sensitivity (note that in Pfifer and Hecker [2011] the ν -gap metric is instead used as a measure of sensitivity), defined as

$$S_{ij} = \max_k \frac{\|G_k - G_{kij}\|_\infty}{\|G_k\|_\infty}, \quad (3.5)$$

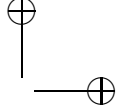
is computed for each element f_{ij} of the matrix $F(\gamma(k))$ where G_{kij} is equal to G_k except for the element f_{ij} that is substituted with the mean of the N_θ values $f_{ij}(\gamma(k))$. If the influence of an element f_{ij} on the transfer functions is lower than a (user-defined) bound $\underline{S} \in [0, 1]$, its mean value is used instead of performing a polynomial fitting. It is also possible to define an upper bound \overline{S} beyond which the maximum polynomial degree is used. If S_{ij} is in the interval $[\underline{S}, \overline{S}]$ a linear function of the influence is considered in order to obtain the most reasonable trade-off between model complexity, *i.e.*, polynomial degree, and fitting error. In other words, the coefficient ζ_{ij} is defined for each (i, j) as a function of the sensitivity S_{ij} as follows

$$\zeta_{ij} = \begin{cases} \infty & S_{ij} < \underline{S} \\ \frac{K_e - 1}{\underline{S} - \overline{S}} S_{ij} + \frac{\underline{S} - K_e \overline{S}}{\underline{S} - \overline{S}} & \underline{S} \leq S_{ij} \leq \overline{S} \\ 1 & S_{ij} > \overline{S}, \end{cases} \quad (3.6)$$

where $K_e > 1$ is the value of ζ_{ij} when S_{ij} is equal to \underline{S} . The value for this parameter suggested in Pfifer and Hecker [2011] is 2, which corresponds to twice the absolute and the relative tolerances than their original values,



|



and in this way the low sensitivity of the parameter (i, j) is taken into account. The absolute and the relative tolerances of the mean square error are respectively $\zeta_{ij}\varepsilon_a$ and $\zeta_{ij}\varepsilon_r$.

The algorithm increases the polynomial degree of the approximation and computes the new polynomial coefficients by solving the least squares problem until the RMS_e drops below the absolute tolerance $\zeta_{ij}\varepsilon_a$ or the improvement in the RMS_e becomes less than the relative tolerance $\zeta_{ij}\varepsilon_r$. The interpolation algorithm is summarized in Table 3.1.

Remark. *This algorithm can suffer by the curse of dimensionality, because of the dimension of γ , n_γ , that is*

$$n_\gamma = \binom{M + n_p}{M} \quad (3.7)$$

where M is the maximum degree of the polynomial and n_p is the dimension of θ .

Finally, in some applications it is desirable to obtain as output of the system identification procedure a model in so-called LPV-LFT form, *i.e.*, in which the state-space matrices are expressed as a linear fractional transformation over a suitable linear operator representing time-varying parameters:

$$\dot{x} = Ax + B_0w + B_1u \quad (3.8)$$

$$z = C_0x + D_{00}w + D_{01}u \quad (3.9)$$

$$y = C_1x + D_{10}w + D_{11}u \quad (3.10)$$

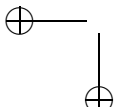
$$w = \Gamma z, \quad \Gamma = \text{diag}(\gamma_1 I_{r_1} \dots \gamma_{n_\gamma} I_{r_{n_\gamma}}) \quad (3.11)$$

and $w, z \in \mathbb{R}^r$, $r = r_1 + \dots + r_{n_\gamma}$.

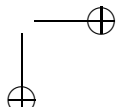
As is well known in the robust control literature and also pointed out in Lovera et al. [1998], Lee and Poolla [1999], LPV-A and LPV-LFT representations are related to each other. Denoting the composition of the system matrices as

$$M(\gamma) = \begin{bmatrix} A(\gamma) & B(\gamma) \\ C(\gamma) & D(\gamma) \end{bmatrix} = M_0 + M_1\gamma_1 + \dots + M_{n_\gamma}\gamma_{n_\gamma},$$

by expressing each of the M_i 's, $i = 1, \dots, n_\gamma$ by means of a rank r_i decomposition as $M_i = U_i V_i$ one can write $M(\gamma)$ as $M(\gamma) = M_0 + U \Gamma V$, where $U = [U_1 \dots U_{n_\gamma}]$, $V = [V_1^T \dots V_{n_\gamma}^T]^T$ and Γ is given by equation (3.11). The obtained form for the system matrices coincides with the one which is obtained in the special case of a linear fractional transformation characterised by having $D_{00} = 0$, hence the transformation between the two forms.



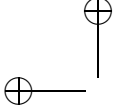
|



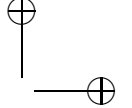
Interpolation Algorithm

- Input parameters: $\underline{S}, \bar{S}, \varepsilon_a, \varepsilon_r, K_e$
- For each $i = 1, \dots, n + p$ $j = 1, \dots, n + m$
 1. Compute S_{ij} according to (3.5)
 2. According to (3.6) compute ζ_{ij}
 3. Set the polynomial order equal to 0
 4. Solve the least squares problem obtaining an estimate of the polynomial coefficients and compute the RMS_e according to (3.4)
 5. Increase the polynomial order by 1
 6. If $RMS_e > \zeta_{ij}\varepsilon_a$ and the difference between two sequential RMS_e is larger than $\zeta_{ij}\varepsilon_r$ then return to the step 4

Table 3.1: Outline of the local model interpolation algorithm.



|



3.3.3 Implementation issues

The *mild* nonuniqueness problem of the balancing transformation T derived from a sign change, explained in Section 3.3.1, can be solved using the following method. Consider $F(\gamma(k))$ and $\tilde{F}(\gamma(k+1))$ with $F(\gamma(k))$ internally balanced and $\tilde{F}(\gamma(k+1))$ not internally balanced. Therefore a unique balancing transformation T can be found solving the problem

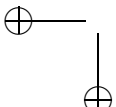
$$\begin{aligned}
 T = \arg \min_T & \|A(\gamma(k)) - T^{-1}\tilde{A}(\gamma(k+1))T\|_F \\
 & + \|B(\gamma(k)) - T^{-1}\tilde{B}(\gamma(k+1))\|_F \\
 & + \|C(\gamma(k)) - \tilde{C}(\gamma(k+1))T\|_F \\
 \text{s.t. } \mathcal{W}_o = & \int_0^{\infty} e^{(T^{-1}\tilde{A}(\gamma(k+1))T)^T \tau} (\tilde{C}(\gamma(k+1))T)^T \\
 & \cdot \tilde{C}(\gamma(k+1))T e^{T^{-1}\tilde{A}(\gamma(k+1))T \tau} d\tau \\
 \mathcal{W}_c = & \int_0^{\infty} e^{T^{-1}\tilde{A}(\gamma(k+1))T \tau} T^{-1}\tilde{B}(\gamma(k+1)) \\
 & \cdot (T^{-1}\tilde{B}(\gamma(k+1)))^T e^{(T^{-1}\tilde{A}(\gamma(k+1))T)^T \tau} d\tau \\
 \mathcal{W}_o = \mathcal{W}_c = \Sigma. &
 \end{aligned} \tag{3.12}$$

This optimization problem is solved using dynamic programming, *i.e.*, matrix T is first computed using the algorithm presented in Section 3.3.1 and then all the signs changes are tested in order to find the solution of (3.12). This method requires 2^{n-1} functions evaluation which is an affordable cost in most situations.

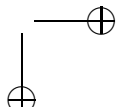
Remark. *The transformation theory exposed in Section 1.3.2 preserves the Gramians, i.e., the continuous-time system (1.4) and the transformed system (1.32) have the same Gramians and so the identified system can be balanced in any of both domains.*

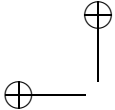
3.4 Simulation examples

In this Section the results obtained by applying the above described approach to a numerical example are presented. More precisely, both open-loop and closed-loop operating conditions are considered and the performance obtained in both situations by using either the continuous-time PB-SID algorithm presented in Section 1.5 or the equivalent approach based on the PO-MOESP algorithm (see Ohta and Kawai [2004]) is discussed.

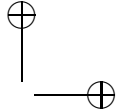


|





|



The parameter-dependent system used in this example (considered in De Filippi and Lovera [2011] in an LPV control design framework) is given by the equations

$$\begin{aligned}\dot{x}_1 &= (-2 + \theta)x_1 - 2x_2 + d + 3u \\ \dot{x}_2 &= x_1 - 2x_2 + d + u \\ z_1 &= x_1 \\ z_2 &= x_2 \\ z_3 &= x_1 + x_2 + u,\end{aligned}$$

where $\theta \in [\theta_{min}, \theta_{max}]$, with $\theta_{min} = 0$ and $\theta_{max} = 2.8$. The eigenvalues of the system strongly depend on θ . For the system the $N_\theta = 8$ local operating points corresponding to the values $\{0, 0.4, 0.8, 1.2, 1.6, 2, 2.4, 2.8\}$ have been considered. Simulated data has been collected near each of the considered local operating points by applying to the system a sequence of filtered white Gaussian noise as input, for a duration of 10s. White Gaussian noise of increasing variance has been added to the output in order to assess the influence of decreasing signal-to-noise ratio on the quality of the computed estimates. For the input and output variables two values of the sampling interval Δt have been considered, *i.e.*, $\Delta t = 0.001s$ and $\Delta t = 0.005s$. Similar choices for the p and f parameters have been made in the two algorithms, namely $p = f = 10$. As mentioned above, both open-loop and closed-loop operating conditions have been considered. In the latter case, the system is operating under feedback with a controller given by

$$K(\theta) = K_0 + \theta K_1$$

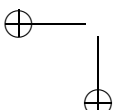
where

$$K_0 = \begin{bmatrix} 1.1254 & 1.1878 & 0 \\ 1.1878 & 1.2537 & 0 \end{bmatrix}, \quad K_1 = \begin{bmatrix} -0.0345 & -0.0078 & 0 \\ -0.0078 & 0.6752 & 0 \end{bmatrix}.$$

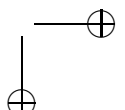
The Bode plots of the frequency responses associated with the system for different values of θ are given in Figure 3.2. As can be seen, the dynamics of the system is significantly affected by the parameter variations.

The singular values of the balanced Gramians for the local dynamics of the system are depicted in Figure 3.3. As can be seen, they are distinct for all the considered values of θ , so it can be anticipated that no major obstacles to the interpolation step of the procedure should be encountered.

Figures 3.4-3.6 show the elements of the matrices A , B , and C identified using noise-free datasets. It can be seen that the identified matrices do not have a smooth behavior varying θ , while the matrices of the internally



|



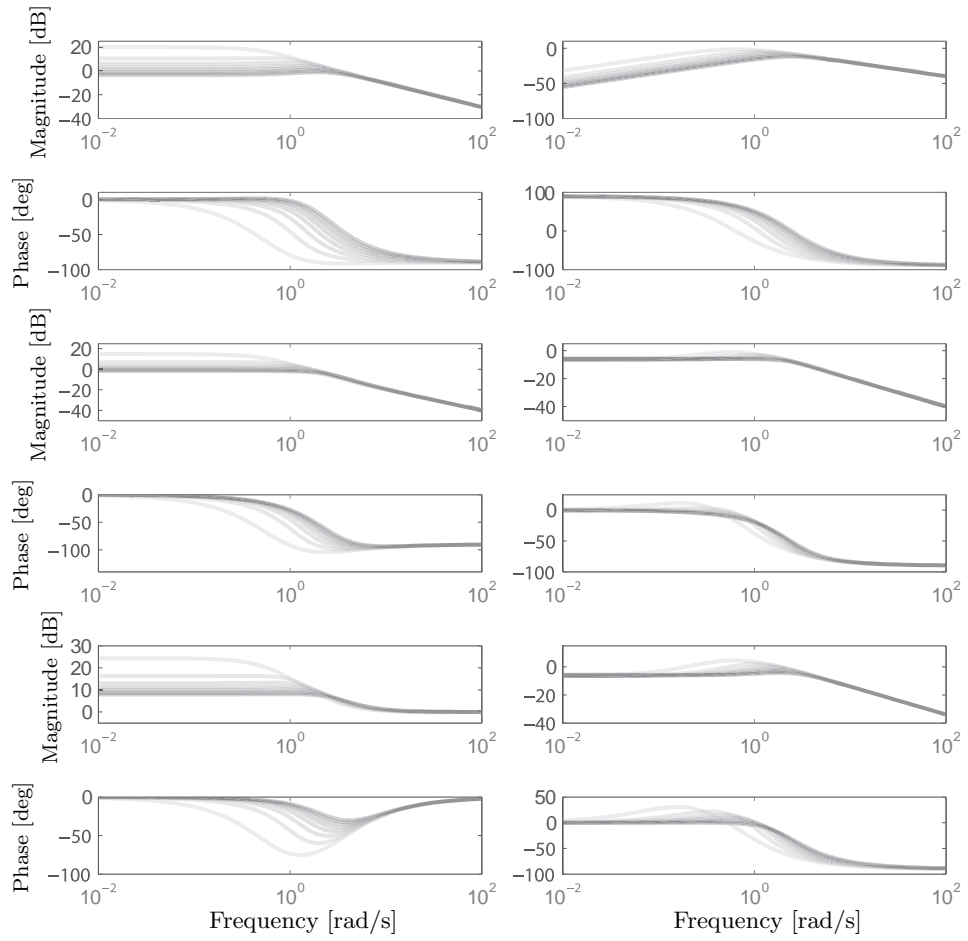


Figure 3.2: Bode plots of the frequency responses of the parameter dependent system for $\theta = (0 : 0.2 : 2.8)$.

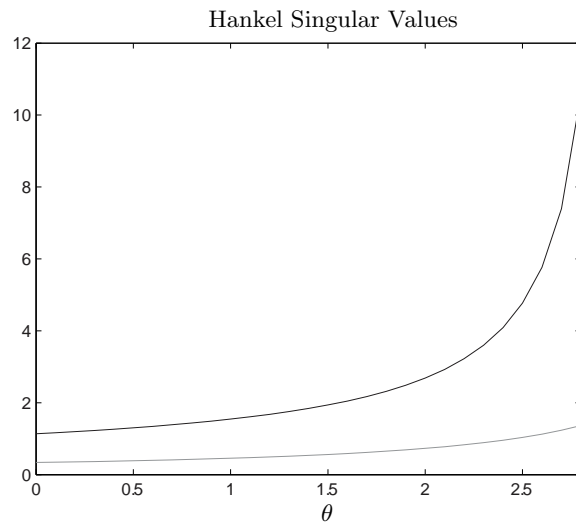


Figure 3.3: Eigenvalues of the balanced Gramian matrices, as function of θ .

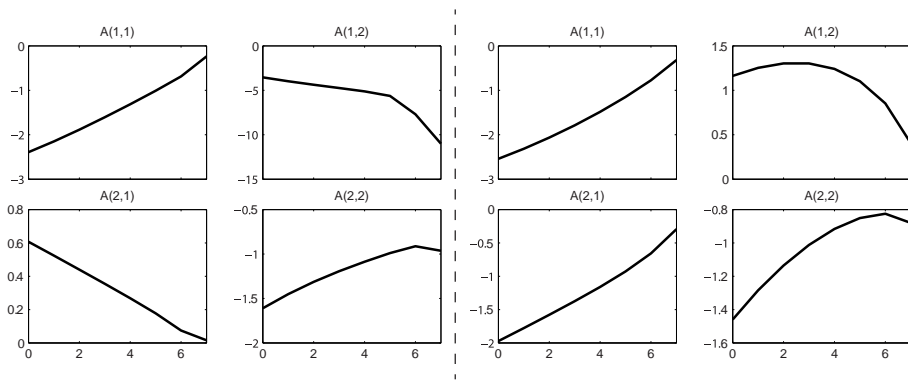


Figure 3.4: Comparison of elements of matrix $A(\theta)$ between the original identified models (left) and the balanced identified model (right).



3.4 Simulation examples

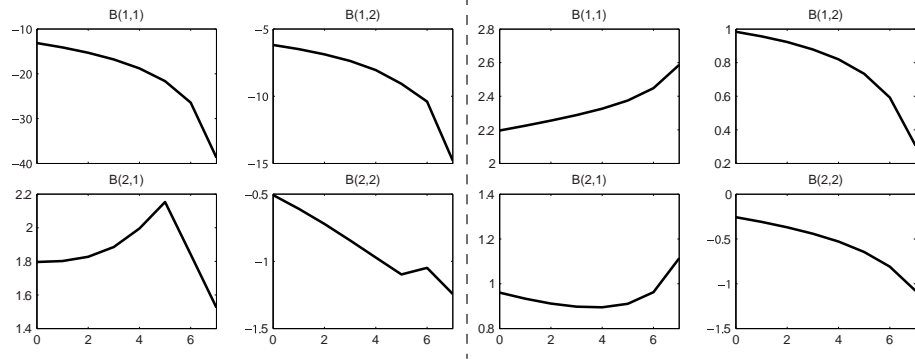


Figure 3.5: Comparison of elements of matrix $B(\theta)$ between the original identified models (left) and the balanced identified model (right).

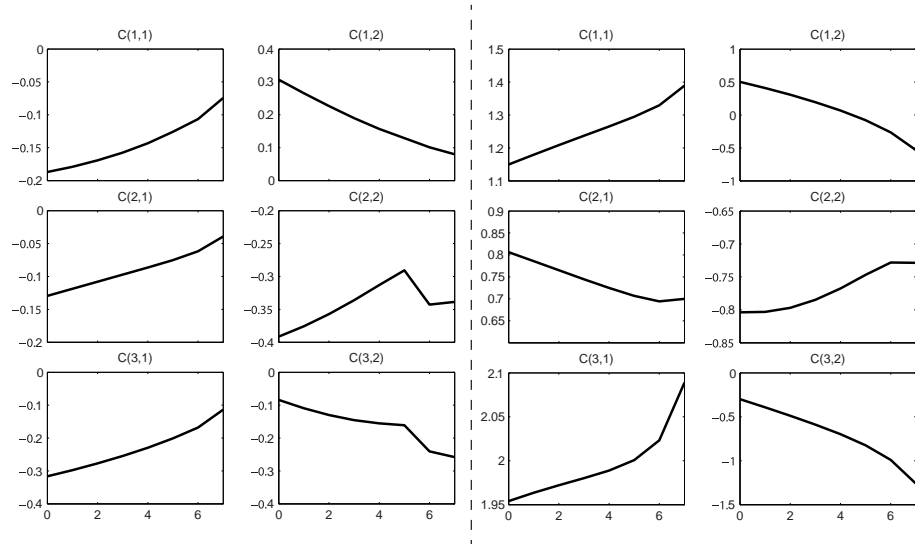
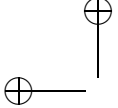
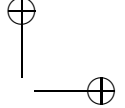


Figure 3.6: Comparison of elements of matrix $C(\theta)$ between the original identified models (left) and the balanced identified model (right).



|



balanced models on the right of the Figures are more smooth. Therefore the balanced identified local models are suitable for model interpolation.

Figure 3.7 shows an example of how the interpolation algorithm illustrated in Section 3.3.2 works. Most of the elements of the matrices are fixed to constant values by the interpolation algorithm since the associated sensitivities (3.5) are less than the lower bound $\underline{S} = 0.1$. The elements whose sensitivity is large enough are fitted using polynomials as suggested in 3.3.2.

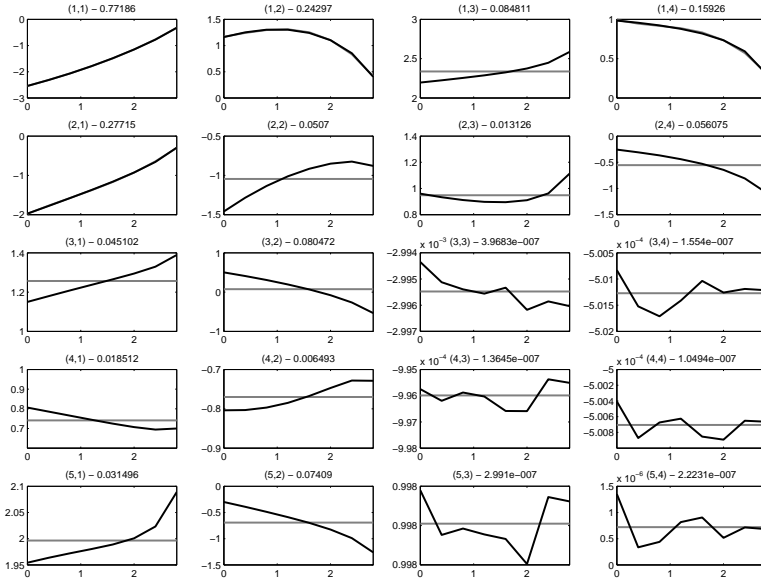


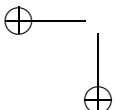
Figure 3.7: Example of how the interpolation algorithm works (identified model - black lines, interpolated model - grey lines).

The results obtained in the validation of the identified model can be summarised as follows, by referring to Figures 3.8-3.14 for the achieved values of the Variance-Accounted-For (VAF) in a Monte-Carlo study with 100 simulations for each case. The VAF of the i -th output is defined as follows

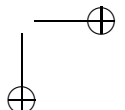
$$\text{VAF}_i = \left(1 - \frac{\text{Var}[y_i - \hat{y}_i]}{\text{Var}[y_i]} \right) \cdot 100\%, \quad (3.13)$$

where y_i is the measured output and \hat{y}_i is the estimated output. If the system has two or more outputs the mean of the outputs VAFs is considered.

Concerning open-loop operation, a direct inspection of the box plots in Figures 3.8-3.9 shows that for the case of sampling interval given by



|



$\Delta t = 0.001\text{s}$ the two subspace algorithms provide essentially equivalent results both when carrying out the validation for a constant value of the scheduling parameter and by considering a time-varying trajectory for it, as shown in 3.15. A difference in performance becomes apparent when increasing the sampling interval to $\Delta t = 0.005\text{s}$, as depicted in Figures 3.10-3.11, from which the greater sensitivity of the continuous-time MOESP becomes visible. Finally, as one can anticipate, when turning to the results obtained in closed-loop operation, comparing the performance of the two approaches for the "fast" sampling case (see Figures 3.12-3.13) clearly shows a wide gap in performance; for $\Delta t = 0.005\text{s}$, the local models computed using the continuous-time PO-MOESP are not asymptotically stable, and therefore in Figure 3.14 only the performance obtained using the continuous-time PBSID is illustrated.

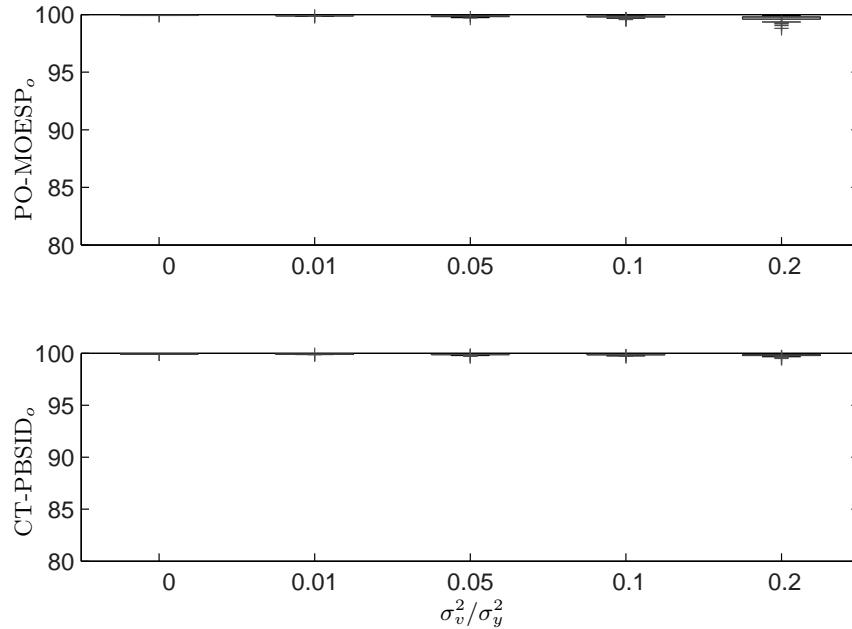


Figure 3.8: Open loop VAF - constant scheduling parameter with $\Delta t = 0.001\text{s}$.

As a conclusion, some representative time-domain validation results are presented in Figures 3.15-3.18, to illustrate the ability of the interpolated model to provide a satisfactory performance also in the case of a varying parameter.

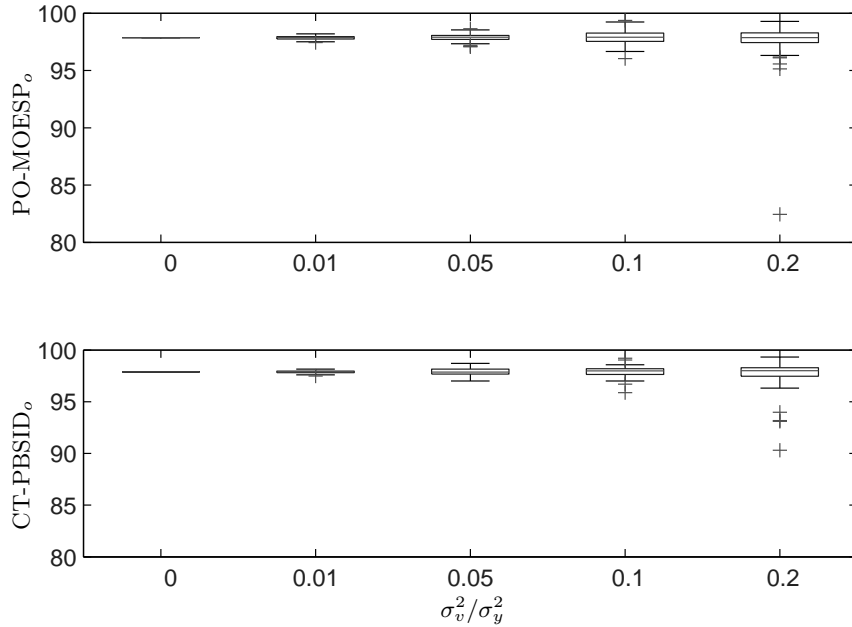


Figure 3.9: Open loop VAF - variable scheduling parameter with $\Delta t = 0.001\text{s}$.

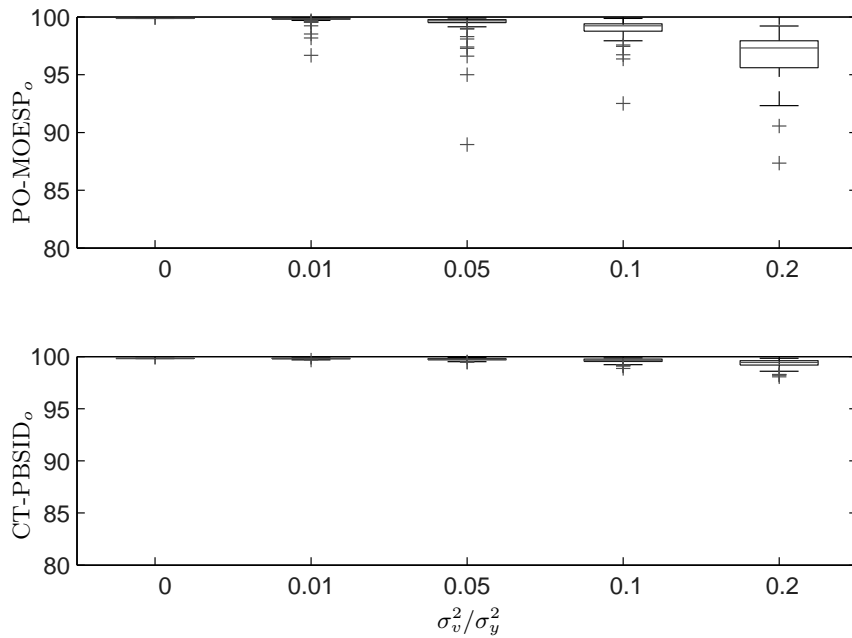
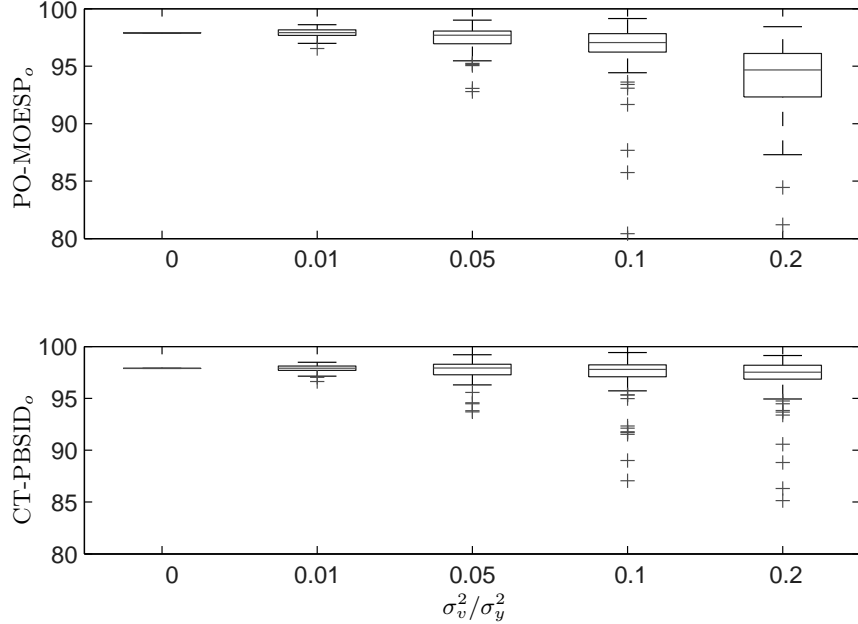
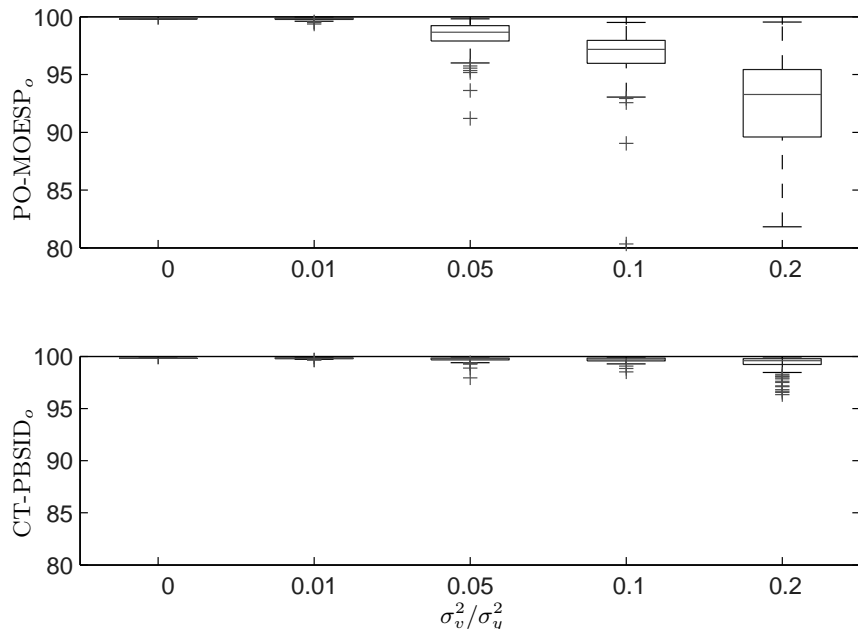


Figure 3.10: Open loop VAF - constant scheduling parameter with $\Delta t = 0.005\text{s}$.

Figure 3.11: Open loop VAF - variable scheduling parameter with $\Delta t = 0.005\text{s}$.Figure 3.12: Closed-loop VAF - constant scheduling parameter with $\Delta t = 0.001\text{s}$.

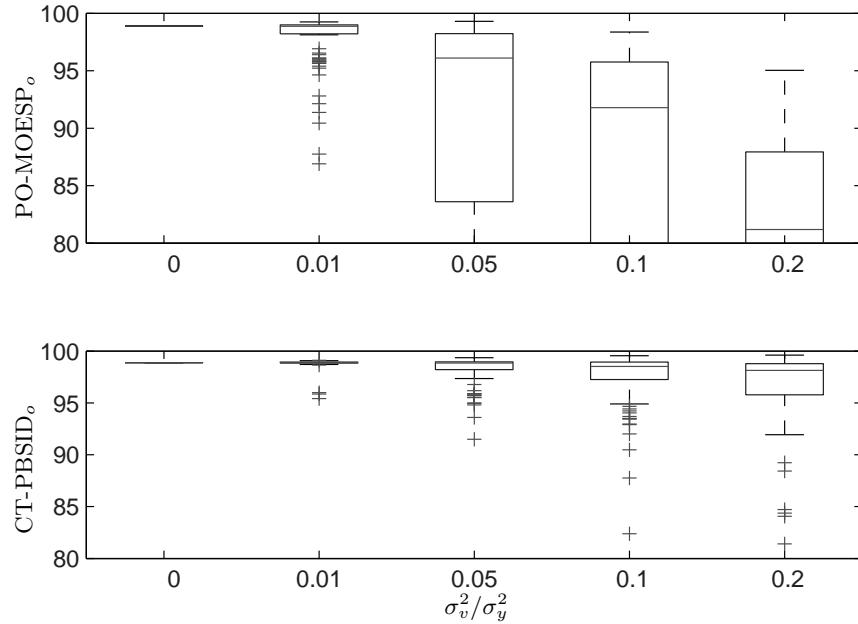


Figure 3.13: Closed-loop VAF - variable scheduling parameter with $\Delta t = 0.001s$.

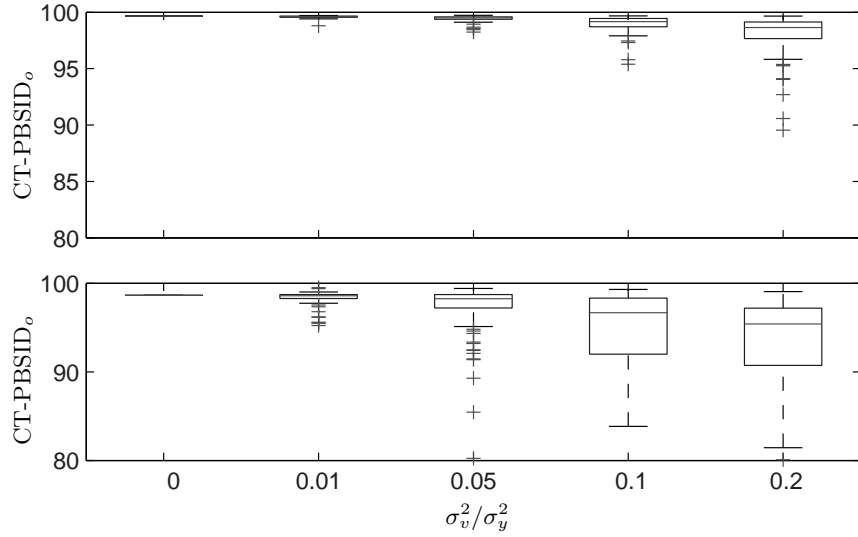


Figure 3.14: Closed-loop VAF - constant (top) and varying (bottom) scheduling parameter with $\Delta t = 0.005s$.

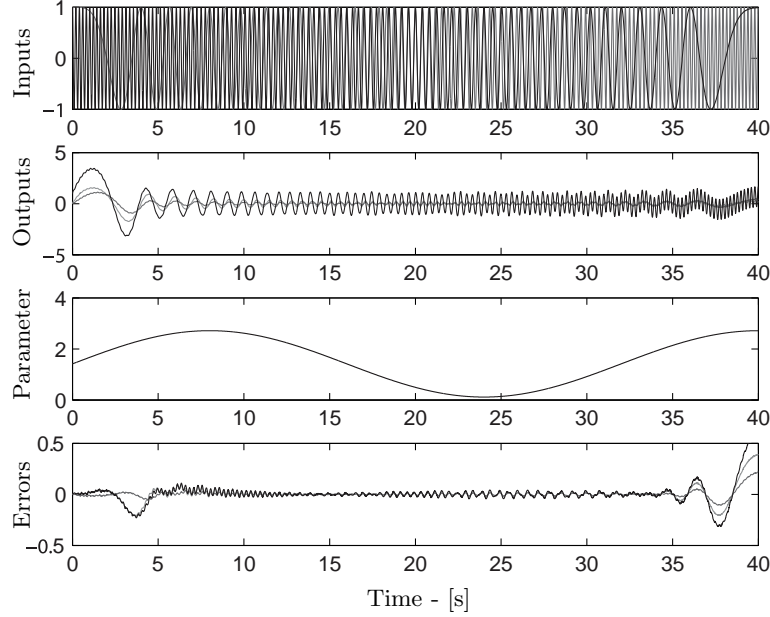


Figure 3.15: Validation performance with slowly-varying parameter θ , for CT-PBSID_o-based models identified in open-loop ($\Delta t = 0.005$ s, $\sigma_v^2/\sigma_y^2 = 0.05$).

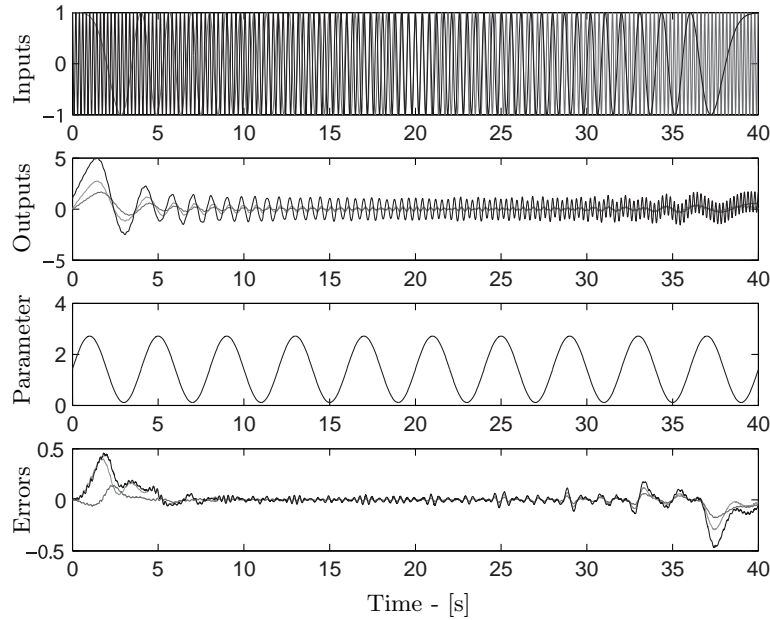


Figure 3.16: Validation performance with rapidly-varying parameter θ , for CT-PBSID_o-based models identified in open-loop ($\Delta t = 0.005$ s, $\sigma_v^2/\sigma_y^2 = 0.05$).

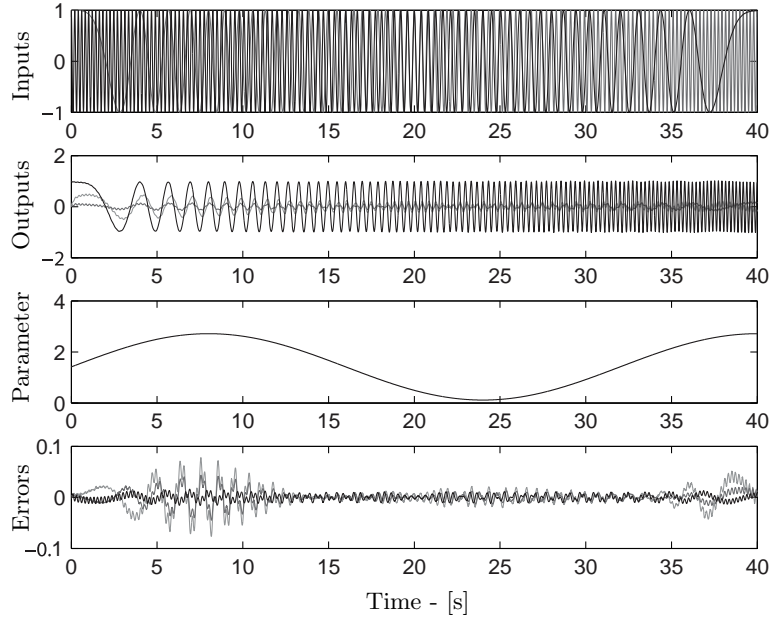


Figure 3.17: Validation performance with slowly-varying parameter θ , for CT-PBSID_o-based models identified in closed-loop ($\Delta t = 0.005\text{s}$, $\sigma_v^2/\sigma_y^2 = 0.05$).

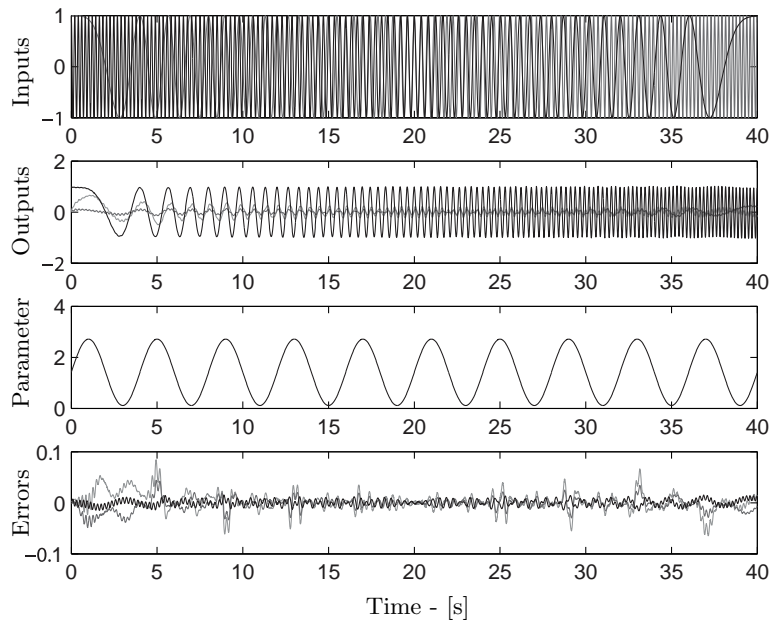
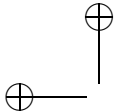
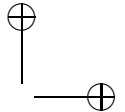


Figure 3.18: Validation performance with rapidly-varying parameter θ , for CT-PBSID_o-based models identified in closed-loop ($\Delta t = 0.005\text{s}$, $\sigma_v^2/\sigma_y^2 = 0.05$).



|



3.5 Concluding remarks

As mentioned in the Introduction, the proposed approach seems to offer a useful trade-off between the two classes of solutions to this problem which have been so far proposed in the literature.

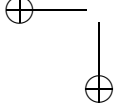
On one hand, subspace methods for the identification of LPV state-space models such as the ones in Verdult [2002], van Wingerden and Verhaegen [2009] provide a very general way of dealing with the problem, at the cost of critical requirements on the experimental conditions which might not be easily realizable in many applications.

On the other hand, the techniques of Steinbuch et al. [2003], van Helvoort et al. [2004], Groot Wassink et al. [2005] have the advantage of being much closer to the actual practice of system identification but suffer from the numerical drawbacks associated with the adoption of a fixed (generally not well conditioned) basis for the manipulation of state-space models and are restricted to SISO models.

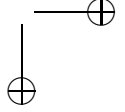
Finally, as far as the methods proposed in Paijmans et al. [2008], De Caigny et al. [2009] are concerned: the numerical issues associated with the use of the canonical observability form for the local models are circumvented by splitting the local models into first and second order submodels; however, a significant level of manual intervention is expected from the user, in order to choose the structure of the local submodels and formulate the interpolation problem, even more so when moving from SISO to MIMO models. The main advantage of this class of methods is the general applicability, as no specific preconditions must be met in order to use them.

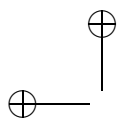
In this respect, the proposed method presents two advantages and one limitation. The advantages are that it is directly applicable to both SISO and MIMO systems (thanks to the use of subspace methods for the local identification) with an automatic intervention to deal with sign changes in the elements of the state space matrices (thanks to the adoption of the balanced form and the heuristic method shown in (3.12)). The limitation is due to the need to have distinct eigenvalues of the balanced Gramians of the local models in order to ensure that the interpolation problem is well posed. Note, in passing, that this issue has also been resolved by manual intervention on the local models in a few examples, but no systematic approach to it is available at present.

Simulation results show that the proposed approach are suitable to identify LPV models.

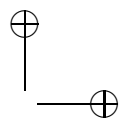


|



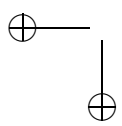


|

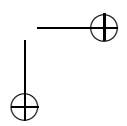


—

—



|



CHAPTER
FOUR

MODEL UNCERTAINTY ESTIMATION: BOOTSTRAP APPROACH

For the purpose of control design it is desirable to have information about the reliability of the identified model. The aim of this Chapter is to present an approach to the evaluation of the uncertainty of the identified models based on the application of the methods of computational statistics. More precisely, a procedure for the evaluation of the uncertainty associated with the frequency response of the estimated models is proposed. The statistical tool taken into account is the bootstrap method (see Efron and Tibshirani [1993], Shao and Tu [1995]), along the lines of the results in Bittanti and Lovera [2000].

4.1 Introduction

In recent years, in control theory many methods (see, *e.g.*, Zhou et al. [1996]) that require knowledge of the uncertainty of the models have been developed, because in addition of ensured stability and necessary performance, it must be ensured the safety of the controlled system by *any* modeling approximations. As well known, in the robust control the stability of the closed loop system is ensured in the worst-case, *i.e.*, when the uncertainty of the model is the *worst* among those considered. The model uncertainty is also useful in the stability and operation analysis using Monte Carlo methods, *e.g.*, the clearance of flight control laws where any flight conditions and uncertainties on aerodynamic coefficients are considered in order to avoid critical states (see Varga et al. [2012]).

The analysis of the variance of the estimated model in the subspace framework has been widely discussed in the literature (see, *e.g.*, Bauer

et al. [1997, 1999], Bauer and Jansson [2000], Knudsen [2001], Bauer [2005], Chiuso and Picci [2005], van Wingerden [2012]) and has led to the development of algorithms that minimize the variance of the estimation error in different cases, depending on the considered assumptions. In addition to analytical methods, numerical methods derived from the statistical literature have been studied for estimating the model uncertainty (see Bittanti and Lovera [2000]). The advantage of the latter methods is their ability to capture in a simple way the statistical distribution of the estimation error. The bootstrap method, originally introduced in Efron [1979], is here extended to the estimation of continuous-time model uncertainty using the CT-PBSID_o algorithm. This method falls in to the class of resampling algorithms since it uses several synthetic datasets created starting from the original data. The state space base among the various replicas used in the algorithm can not be fixed, therefore in the study of the uncertainty the focus will be in the frequency responses of the estimated models.

The Chapter is organised as follows: Section 4.2 introduces the bootstrap approach in the subspace model identification framework. The viability of the approach is verified using simulation results presented in Section 4.3. In Section 4.4 some conclusions remarks are sketched.

4.2 Quantifying model uncertainty: a bootstrap-based approach

4.2.1 The bootstrap

The bootstrap is a statistical method which was originally introduced in order to solve the following problem (Efron and Tibshirani [1993], Shao and Tu [1995]): given a random, independent, identically distributed (i.i.d.) sample $x = (x_1, x_2, \dots, x_n)$ drawn from an unknown distribution F , one computes an estimate $\hat{\theta}$ of the parameter $\theta = t(F) = t[x]$ on the basis of the available data, and would like to assess the accuracy of the obtained estimate, in terms of its standard deviation or its variance.

In general, the variance of $\hat{\theta}$ will be given by

$$var(\hat{\theta}) = \int \left[t[x] - \int t[y] d \prod_{i=1}^n F(y_i) \right]^2 d \prod_{i=1}^n F(x_i). \quad (4.1)$$

Obtaining explicit expressions for $var(\hat{\theta})$ is not always feasible, so one normally resorts to asymptotic results in order to simplify the analysis. For example, one can sometimes establish results of the form

$$\lim_{N \rightarrow \infty} N[var(\hat{\theta})] = \sigma_F^2 \quad (4.2)$$

where σ_F^2 is a simple function of F .

However, when a classical asymptotic analysis is not possible or too complex, or if the asymptotic approximation holds with satisfactory accuracy only for very (too) large values of N , then it may be useful and advantageous to resort to alternative techniques. The bootstrap is one of such methods. From a theoretical point of view, the bootstrap principle is based on the idea of replacing the (unknown) distribution F of the data with an estimate \hat{F} of it. For the case of variance estimation, the bootstrap estimate of variance is then given by:

$$\hat{\sigma}_{boot}^2 = \int \left[t[x] - \int t[y] d \prod_{i=1}^n \hat{F}(y_i) \right]^2 d \prod_{i=1}^n \hat{F}(x_i). \quad (4.3)$$

Whenever $\hat{\sigma}_{boot}^2$ is an explicit function of the sample x , one can compute the bootstrap estimate of variance in a direct way. Unfortunately, in general $\hat{\sigma}_{boot}^2$ cannot be evaluated exactly and one has to make use of approximation methods, such as, *e.g.*, the Monte Carlo approach. Suppose for a moment that the distribution F is known. Then, it would be easy to estimate σ_{boot}^2 by repeatedly drawing new random data sets from F , computing new estimates of θ from such data sets and approximating σ_{boot}^2 with the sample variance of the obtained estimates. As F is normally not known, one has to replace it with a data-based estimate \hat{F} .

Therefore, the bootstrap approach to the problem of variance estimation proceeds as follows:

1. Obtain an estimate \hat{F} of F . The estimate can be either parametric or non parametric, according to the assumptions in the statistical model underlying the analysis.
2. From the distribution \hat{F} , draw (with replacement) B samples of size n each, which it is indicated by $x^{*(i)}$, $i = 1, \dots, B$.
3. From each of the obtained samples, compute a *replication* of the estimate of the statistic of interest, $\hat{\theta}^{*(i)}$, $i = 1, \dots, B$.
4. The estimate of standard error is then given by

$$\hat{\sigma}_{boot} = \frac{1}{\sqrt{B-1}} \left(\sum_{i=1}^B (\hat{\theta}^{*(i)} - \bar{\hat{\theta}}^*)^2 \right)^{\frac{1}{2}} \quad (4.4)$$

where

$$\bar{\hat{\theta}}^* = \frac{\sum_{i=1}^B (\hat{\theta}^{*(i)})}{B}. \quad (4.5)$$

When no a priori assumptions on F can be made, \hat{F} is defined as the empirical discrete distribution, obtained by associating a probability of $\frac{1}{n}$ to each of the data points in sample x . On the other hand, whenever prior information on F is available, it is also possible to use a parametric approach for the estimation of F , by assuming that it belongs to some specified class of probability distributions. For example, assuming that F is gaussian, it can be determined in a straightforward way from the available data by estimating the corresponding sufficient statistics (mean and variance). The bootstrap is a well established tool in statistics, as it allows to work out numerical solutions to many problems which cannot be given a proper analytical treatment. In particular, the consistency of the bootstrap procedure can be proved for a large class of statistics of practical interest (see Shao and Tu [1995]). Unfortunately there is a price to be paid for the generality of the bootstrap method, in terms of the computational cost implied by the replication of the estimation procedure. The number of replications B required for the bootstrap estimate of standard error to converge is usually very large (see Shao and Tu [1995] for a discussion of the problem of choosing B), so that the application of the bootstrap can be considered in practice only if one is capable of computing the estimate $\hat{\theta}$ in a very efficient way.

4.2.2 Bootstrapping dynamic models: the residuals method

The definition of the bootstrap given in the previous Section applies only to the case of independent and identically distributed samples.

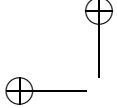
When dealing with more complicated data structures such as time series and dynamic models, different schemes have to be derived in order to obtain correct results from a bootstrap procedure. Various approaches have been proposed in order to apply the bootstrap for variance estimation in time series analysis (Shao and Tu [1995], Tjarnstrom [1999], Tjarnstrom and Ljung [2002]) and signal processing (Shamsunder [1998]).

In the following, a brief outline of the so-called bootstrapping residuals approach will be given. The idea is to turn the non i.i.d. problem into an i.i.d. one. It is a well known fact from the asymptotic theory of optimal linear prediction that the optimal one-step ahead prediction error

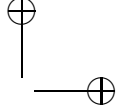
$$e(t) = y(t) - \hat{y}(t|t-1)$$

will be given by a white noise process with an (a priori unknown) probability distribution F_e , see Grewal and Andrews [2001].

Based on this key observation, one can devise the following bootstrapping scheme.



|

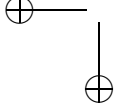


First perform the estimation of the parameters for the model and compute the prediction error based on the estimated model. Assuming subsequently that the sequence of the prediction error is a realisation of a white noise process, use it to approximate the distribution (either in a parametric or a non parametric way) of the true residual. Finally, resample from the estimated distribution in order to obtain replications of the residual and feed them to the estimated model, in order to obtain the required replications for the original data set. Repeating the estimation procedure for the replicated data and computing the standard deviation of the replicated estimates completes the procedure. The bootstrapping residuals method of dealing with time series data has been proved to be consistent for various kinds of correlation structures. In particular, a detailed proof of consistency for the case of subspace model identification has been given in Ridolfi and Lovera [2000], where the residual-based approach for the estimation of the standard error of frequency response estimates is analysed.

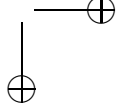
4.2.3 Bootstrap based estimates of uncertainty in SMI

For the present purposes and with reference to the problem of evaluating the standard deviation for the frequency response of the estimated model, the method of bootstrapping residuals can be synthesized as follows:

1. Estimate the continuous-time stochastic linear model in (1.6), *i.e.*, matrices $[\hat{A}, \hat{B}, \hat{C}, \hat{D}, \hat{K}]$, from the available input/output data (u, y) and compute the estimate for the points of interest of its frequency response $\hat{G}(j\omega_k)$, $k = 1, \dots, N$.
2. Compute the optimal one-step ahead prediction error for the identified model:
$$e(t) = y(t) - \hat{y}(t). \quad (4.6)$$
3. Obtain an estimate \hat{F}_e for the distribution F_e of the prediction error. In this thesis a parametric estimate will be considered and the normality assumption for the distribution of the residual will be made.
4. Generate B replications $(u^{*(i)}, y^{*(i)})$ of the original data set (u, y) , with $u^{*(i)} = u$ and $y^{*(i)}$ obtained by feeding the identified model $[\hat{A}, \hat{B}, \hat{C}, \hat{D}, \hat{K}]$ with the deterministic input $u^{*(i)} = u$ and the stochastic input $e^{*(i)}$, $k = 1, \dots, B$ where $e^{*(i)}$ is constructed by resampling (with replacement) from the distribution \hat{F}_e .
5. Estimate B replications of the identified model and of the points of interest for the frequency response $\hat{G}^{*(i)}(j\omega_k)$, $k = 1, \dots, N$.



|



6. The estimate of the standard error for the frequency response of the model is finally given by:

$$\hat{\sigma}_{\hat{G}(j\omega_k)} = \frac{1}{\sqrt{B-1}} \left(\sum_{i=1}^B (\hat{G}^{*(i)}(j\omega_k) - \bar{\hat{G}}^*(j\omega_k))^2 \right)^{\frac{1}{2}} \quad (4.7)$$

where

$$\bar{\hat{G}}^*(j\omega_k) = \frac{1}{B} \sum_{i=1}^B \hat{G}^{*(i)}(j\omega_k). \quad (4.8)$$

In a similar way one can obtain estimates of the standard deviation for the poles and zeros of the estimated model.

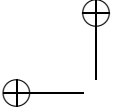
4.3 Simulation example

The considered stochastic system is given by the transfer function

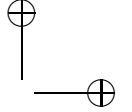
$$\begin{aligned} Y(s) &= \frac{1}{s-\alpha} U(s) + \frac{s-k}{s-\alpha} E(s) \\ &= \frac{1}{s+2} U(s) + \frac{s+12}{s+2} E(s). \end{aligned} \quad (4.9)$$

The simulated data has been collected by applying to input channel $u(t)$ a pseudo-random binary signal with a dwell time of 0.01 s. The noise $e(t)$ is a piece-wise constant signal with base period equal to the sample time which level is chosen randomly according to a Gaussian distribution with zero mean and increasing variance. For the measured variables the sampling interval $\Delta t = 0.0005$ s has been considered. About the tuning parameters of the CT-PBSID_o, the past and future windows lengths f and p have been chosen both equal to 10 and the Laguerre pole a has been placed in 50 rad/s.

As underlined in Qin [2006] in order to consistently estimate the stochastic part of the system, *i.e.*, the parameter k in the considered example, a large number of data is required and so the first issue to be investigated is about the length of the experiments. In order to study this problem four durations of the simulation are considered, *i.e.*, 10 s, 20 s, 40 s, and 100 s. The results of the Monte Carlo study comprising 1000 runs are shown in Tables 4.1 and 4.2. As expected the pole α of the system (4.9) is consistently estimated with a slight loss of accuracy, as meaning of the standard deviation, decreasing the signal-to-noise ratio. Increasing the number of samples the standard deviation of the estimate decreases for each signal-to-noise ratio.



|



4.3 Simulation example

| $\frac{\sigma_e^2}{\sigma_u^2}$ | Simulation duration | | | |
|---------------------------------|----------------------|----------------------|----------------------|----------------------|
| | 10s | 20s | 40s | 100s |
| 0.1 | -2.0015 ± 0.0565 | -2.0007 ± 0.0433 | -2.0005 ± 0.0221 | -1.9998 ± 0.0135 |
| 0.2 | -2.0030 ± 0.0776 | -1.9986 ± 0.0588 | -1.9997 ± 0.0312 | -2.0007 ± 0.0184 |
| 0.3 | -2.0021 ± 0.0939 | -2.0026 ± 0.0698 | -1.9978 ± 0.0401 | -2.0003 ± 0.0220 |

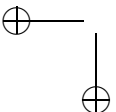
Table 4.1: Estimation results of the parameter α varying the simulation duration and the signal-to-noise ratio.

Different conclusions can be sketched about the estimation of the stochastic part of the system k , indeed the signal-to-noise ratio is substantially irrelevant for estimation purposes. From the Table 4.2 it is clear that the bias and the standard deviation errors of the estimates of k are both invariants to the signal-to-noise changes, while increasing the duration of the simulation the bias error tends to zero and the standard deviation error decreases.

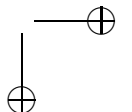
| $\frac{\sigma_e^2}{\sigma_u^2}$ | Simulation duration | | | |
|---------------------------------|-----------------------|-----------------------|-----------------------|-----------------------|
| | 10s | 20s | 40s | 100s |
| 0.1 | -10.3178 ± 2.2369 | -11.2357 ± 1.6706 | -11.7358 ± 1.2562 | -12.0127 ± 0.7785 |
| 0.2 | -10.2832 ± 2.4364 | -11.2325 ± 1.6685 | -11.6950 ± 1.2279 | -12.0037 ± 0.7768 |
| 0.3 | -10.2120 ± 2.2668 | -11.1458 ± 1.7156 | -11.6363 ± 1.2705 | -11.9695 ± 0.7970 |

Table 4.2: Estimation results of the parameter k varying the simulation duration and the signal-to-noise ratio.

In order to demonstrate the viability of the bootstrap method for the estimation of the model uncertainty, in Figures 4.1-4.4 are shown comparisons between the estimates of the pole of (4.9) using the bootstrap approach and the Monte Carlo method varying the signal-to-noise ratio. The experiment duration is fixed to 10 s, 20 s, 40 s, and 100 s and 1000 runs are taken into account in all cases. In the Figures the boxplots of the estimates are shown and under each boxplot the standard deviation is indicated. It can be noted that the bootstrap method achieves reliable estimate of the standard deviation of the pole of the system independently from the duration of the experiment. Although this result seems to contradict the analysis made above about the estimation of the stochastic part of the system, it suggests the robustness of the proposed approach. Indeed if the parameter k is poorly estimated the density function of the prediction error $e(t)$ changes in order to compensate the estimation error of K .



|



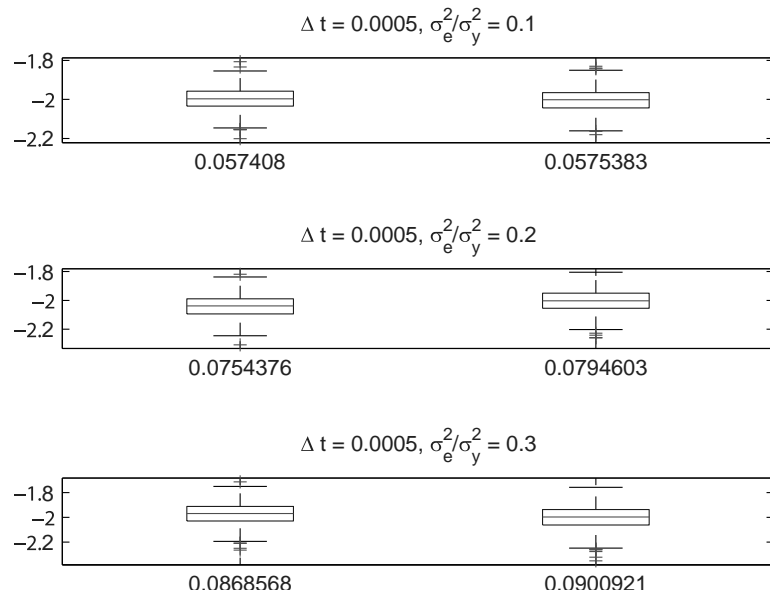


Figure 4.1: Pole estimation comparison between the bootstrap method (left) and the Monte Carlo method (right), with simulation durations $T = 10$ s.

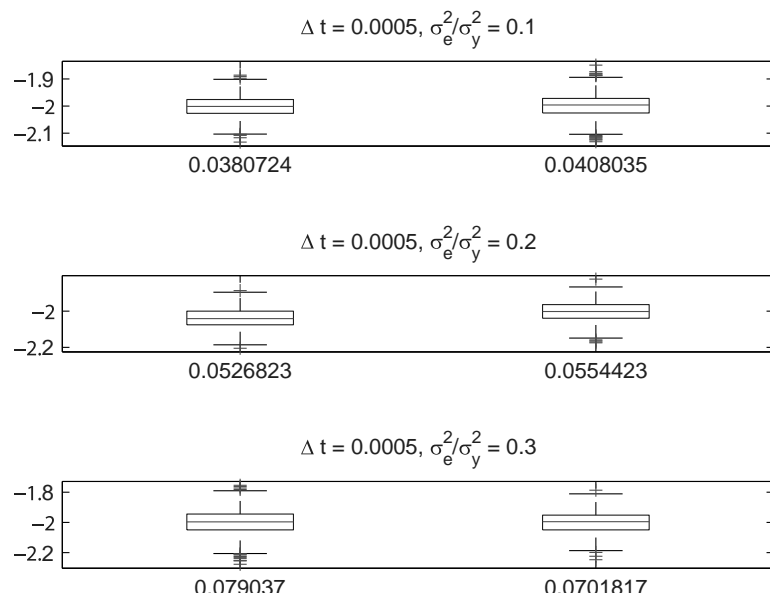
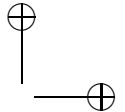
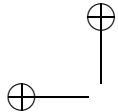


Figure 4.2: Pole estimation comparison between the bootstrap method (left) and the Monte Carlo method (right), with simulation durations $T = 20$ s.





4.3 Simulation example

107

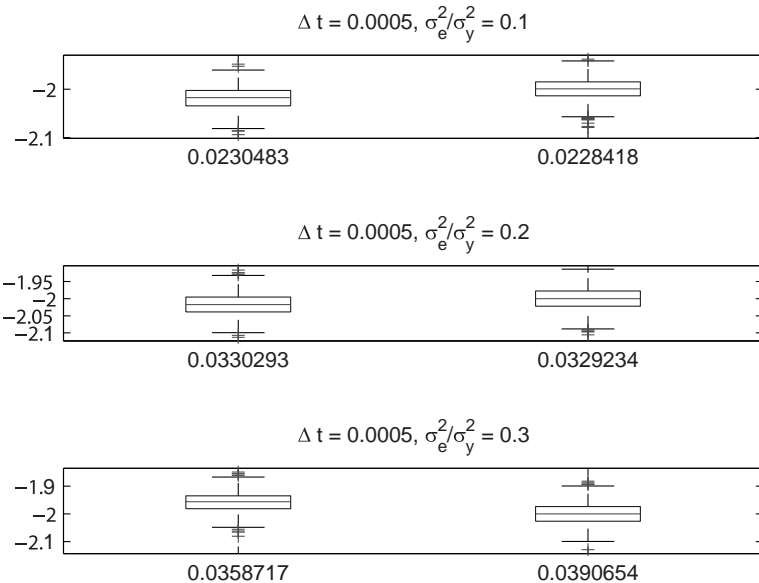


Figure 4.3: Pole estimation comparison between the bootstrap method (left) and the Monte Carlo method (right), with simulation durations $T = 40$ s.

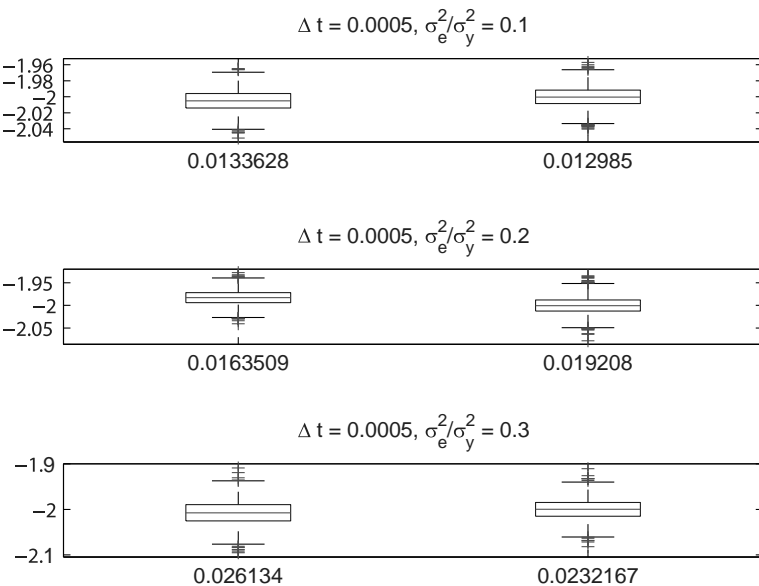
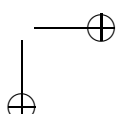
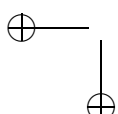


Figure 4.4: Pole estimation comparison between the bootstrap method (left) and the Monte Carlo method (right), with simulation durations $T = 100$ s.



4.4 Conclusions

In this Chapter a bootstrap method to the evaluation of the uncertainty of the identified models has been presented. The algorithm for the evaluation of the uncertainty associated with the frequency response or the poles and zeros of the estimated models has been introduced and a simulation study has been performed in order to demonstrate the viability of the approach.



CHAPTER
FIVE

FROM UNSTRUCTURED TO STRUCTURED
MODELS WITH AN \mathcal{H}_∞ APPROACH

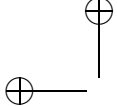
The Chapter deals with the problem of recovering the numerical values of the physical parameters of a structured representation of a linear system starting from a fully parameterised identified model as obtained by means of a subspace model identification method. It will be shown that this can be achieved without explicitly constructing the similarity transformation relating the unstructured model to the structured one, for linear time-invariant systems, linear time-periodic systems, and linear parameter-varying systems identified either from a periodic scheduling sequence or a generic one. Three numerical examples, one for each class of models, are presented to illustrate the proposed approach.

5.1 Introduction

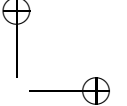
A well known downside of the subspace model identification approach to state space model identification is the impossibility to impose a fixed basis to the state space representation. This, in turn, implies that it is hard to impose a parameterisation to the state space matrices in this framework, and therefore difficulties in recovering physically-motivated models arise. This prevents the successful application of SMI methods to the problem of initialising iterative methods for the identification of structured state space representations.

The problem has been recently addressed in Prot and Mercère [2011], Prot et al. [2012], where the state space identification of a general black-box model of the same order as the physical system is assumed as a starting point and the physical and identified models are related to each other via a





|



similarity transformation. The bilinear equations resulting from the definition of the transformation are then converted into a null-space problem, the solution of which leads to a non-convex optimisation problem, for which uniqueness of the solution can be guaranteed by assuming that the user-defined physical state space form is identifiable and the identified black-box model is consistent.

In this Chapter the problem is addressed in a different perspective, with the aim of reducing the complexity of the non-convex optimisation problem to be addressed in order to match the structured and the unstructured state space representations. More precisely, the problem is formulated as an input-output model matching one, in terms of the \mathcal{H}_∞ norm of the difference between the two models. The solution of the problem is subsequently computing using recent results in non-smooth optimisation techniques, see Apkarian and Noll [2006], which yield effective computational tools (see Gahinet and Apkarian [2011]). The main advantage of this approach is that no explicit construction of the similarity transformation is needed, so the complexity of the non-convex optimisation task remains related to the number of uncertain parameter and is independent of the dimension of the model class. Furthermore, it can be applied to all instances of the problem corresponding to model classes for which the \mathcal{H}_∞ norm (or, rather, the \mathcal{L}_2 gain) can be computed, as illustrated in the case of linear time-invariant models, linear time-periodic (LTP) models, and linear parameter-varying (LPV) models identified using both a periodic scheduling sequence (see also Felici et al. [2007]) or a generic one.

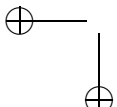
The Chapter is organised as follows: Section 5.2 introduces the problem as well as the considered model classes, while Section 5.3 shows the approaches employed for the parameter estimation problem. Simulation results are presented in Section 5.4. Finally, in Section 5.5 some conclusions and remarks are sketched.

5.2 Problem statement

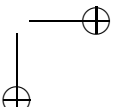
Consider the linear continuous-time system \mathcal{M}_{ns} belonging to one of the following model classes

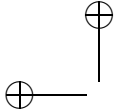
- linear time-invariant (LTI);
- linear time-periodic (LTP);
- linear parameter-varying (LPV).

\mathcal{M}_{ns} has been estimated from a dataset of sampled input/output data using a consistent estimator, *e.g.*, a subspace model identification algorithm

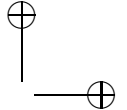


|





|



for the relevant model class. Consider also the model structure $\mathcal{M}_s(\theta)$, belonging to the same model structure of \mathcal{M}_{ns} , parameterized by the vector $\theta \in \mathbb{R}^{n_\theta}$. The problem is to provide estimates of θ such that the input-output behaviors of \mathcal{M}_{ns} and $\mathcal{M}_s(\theta)$ are equivalent under some criterion.

Identifiability is an important issue in system identification problems; a number of results are available, in particular, as far as nonlinearly parameterised models are concerned, as is the case here (see, *e.g.*, Dotsch and Van den Hof [1996] and the more recent Van Doren et al. [2008]). For the purpose of this study the following definitions of identifiability is adopted:

Definition 5.2.1. *Let $\theta^o \in \Theta \subset \mathbb{R}^{n_\theta}$, the model structure is said to be locally identifiable in θ^o if $\forall \theta_1, \forall \theta_2$ in the neighborhood of θ^o it holds that*

$$\mathcal{M}_s(\theta_1) = \mathcal{M}_s(\theta_2) \Rightarrow \theta_1 = \theta_2.$$

Definition 5.2.2. *The model structure $\mathcal{M}_s(\theta)$ is said to be globally identifiable if it is locally identifiable $\forall \theta \in \Theta$, i.e., over the entire parameter space.*

In the following the model structure $\mathcal{M}_s(\theta)$ is considered globally identifiable.

5.3 Approach

As discussed in the Introduction, the problem can be faced in a computationally effective way by defining the input-output operators associated with \mathcal{M}_{ns} and $\mathcal{M}_s(\theta)$ and seeking the values of the parameters corresponding to the solution of the optimisation problem

$$\theta^* = \arg \min_{\theta} \|\mathcal{M}_{ns} - \mathcal{M}_s(\theta)\| \quad (5.1)$$

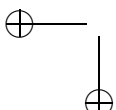
for a suitably chosen norm. In the following, the \mathcal{L}_2 gain is considered, see Appendix A for further details.

5.3.1 Linear time-invariant systems

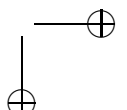
Consider the linear, time-invariant continuous-time system \mathcal{M}_{ns}

$$\begin{aligned} \dot{x}(t) &= \hat{A}x(t) + \hat{B}u(t) \\ y(t) &= \hat{C}x(t) + \hat{D}u(t) \end{aligned} \quad (5.2)$$

where $x \in \mathbb{R}^n$, $u \in \mathbb{R}^{n_u}$ and $y \in \mathbb{R}^{n_y}$ are, respectively, the state, input and output vectors. The system matrices \hat{A} , \hat{B} , \hat{C} and \hat{D} have been estimated



|





from a dataset $\{u(t_i), y(t_i)\}$, $i \in [1, N]$ of sampled input/output data. The model class $\mathcal{M}_s(\theta)$ is defined in terms of its state space matrices $A(\theta)$, $B(\theta)$, $C(\theta)$ and $D(\theta)$ as

$$\begin{aligned}\dot{x}(t) &= A(\theta)x(t) + B(\theta)u(t) \\ y(t) &= C(\theta)x(t) + D(\theta)u(t),\end{aligned}\quad (5.3)$$

and it is assumed of the same order as the model (5.2).

In the linear time-invariant case, the \mathcal{L}_2 gain reduces to the familiar notion of the \mathcal{H}_∞ norm and the input-output operators can be represented as the transfer functions $\hat{G}_{ns}(s)$ and $G_s(s; \theta)$, so that the model matching problem can be recast as

$$\theta^* = \arg \min_{\theta} \|\hat{G}_{ns}(s) - G_s(s; \theta)\|_\infty. \quad (5.4)$$

If the system (5.2) has eigenvalues with positive real part or equal to zero, then the \mathcal{H}_∞ norm is undefined. In this case the eigenvalues of $\mathcal{M}_s(\theta)$ and \mathcal{M}_{ns} are shifted on the real axis of a proper value μ as follows

$$\begin{aligned}\tilde{G}_s(s; \theta) &= C(\theta)((s - \mu)I - A(\theta))^{-1}B(\theta) + D(\theta) \\ \tilde{G}_{ns}(s) &= \hat{C}((s - \mu)I - \hat{A})^{-1}\hat{B} + \hat{D},\end{aligned}\quad (5.5)$$

where μ is chosen in order to all eigenvalues of \mathcal{M}_{ns} have negative real part. Then the model matching problem is reformulated as

$$\theta^* = \arg \min_{\theta} \|\tilde{G}_{ns}(s) - \tilde{G}_s(s; \theta)\|_\infty. \quad (5.6)$$

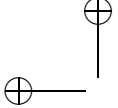
As mentioned in the Introduction, this is a non-convex, non-smooth optimisation problem, which has been studied extensively in recent years in the framework of the fixed-structured controller design problem and for which reliable computational tools (see Gahinet and Apkarian [2011]) are presently available.

5.3.2 Linear time-periodic systems

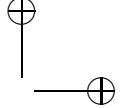
The \mathcal{L}_2 gain formulation of the problem can be readily extended to more general situations for which the gain can be computed explicitly. One such case is the class of linear time-periodic systems. In this Section some basic definitions associated with LTP systems are provided (see, *e.g.*, Bittanti and Colaneri [2009] for an in-depth treatment of this topic) and a framework extending frequency domain analysis to continuous-time LTP systems is reviewed. Consider the LTP system

$$\begin{aligned}\dot{x}(t) &= A(t)x + B(t)u(t) \\ y(t) &= C(t)x + D(t)u(t),\end{aligned}\quad (5.7)$$





|



where matrix $A(\cdot)$ is T -periodic, namely $A(t+T) = A(t)$ and similarly for $B(t)$, $C(t)$ and $D(t)$. As for stable LTI systems, a frequency response operator can be defined for stable LTP systems. The frequency domain representation for LTI systems is related to the fact that sinusoidal inputs are mapped into sinusoidal outputs at the same frequency with possibly different amplitude and phase. This notion can be extended to LTP systems by resorting to a more general class of signals: the set of exponentially-modulated periodic signals, *i.e.*,

$$h(t) = \sum_{k \in \mathbb{Z}} h_k e^{s_k t},$$

where $s_k = s + jk\Omega$, $\Omega = 2\pi/T$, which can be arranged as follows

$$\mathcal{H} = [\dots \ h_{-2}^T \ h_{-1}^T \ h_0^T \ h_1^T \ h_2^T \ \dots]^T.$$

The key idea, see Wereley and Hall [1990], further developed and formalized in Zhou and Hagiwara [1990], is to expand the complex Fourier series of the dynamics matrices

$$A(t) = \sum_{m \in \mathbb{Z}} A_m e^{jm\Omega t} \quad (5.8)$$

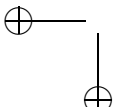
and similarly for $B(t)$, $C(t)$, and $D(t)$, and perform a harmonic balance approach. It was shown that defining

$$\mathcal{A} = \begin{bmatrix} \ddots & \vdots & \vdots & \vdots \\ \dots & A_0 & A_{-1} & A_{-2} & \dots \\ \dots & A_1 & A_0 & A_{-1} & \dots \\ \dots & A_2 & A_1 & A_0 & \dots \\ \vdots & \vdots & \vdots & \ddots \end{bmatrix}$$

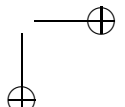
and similarly \mathcal{B} , \mathcal{C} , and \mathcal{D} , the harmonic transfer function $\mathcal{G}(s)$ that describes the input-output relation is

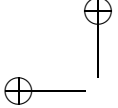
$$\mathcal{G}(s) = \mathcal{C} [s\mathcal{I} - (\mathcal{A} - \mathcal{N})]^{-1} \mathcal{B} + \mathcal{D}, \quad (5.9)$$

where $\mathcal{N} = blkdiag \{jn_\Omega \Omega I\}, n_\Omega \in \mathbb{Z}$. Note that the operator defined in (5.9) is a doubly-infinite dimensional one. On the other hand, it is no longer time-varying and this fact can be exploited to obtain input-output information related with system (5.7) without numerical integration. For practical purposes, however, truncation must be, of course, considered. However, given a stable system, performance measures such as the \mathcal{H}_∞ or the \mathcal{H}_2 norm

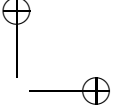


|





|



can be thus computed using a suitably truncated frequency response operator, see, *e.g.*, Zhou and Hagiwara [2002a] or Zhou and Hagiwara [2002b] for details.

Having established an approach to the computation of the \mathcal{H}_∞ norm for LTP operators, the approach outlined in the previous subsection for the case of linear time-invariant systems can be readily extended to this more general case.

Remark. *It is interesting to point out that even though the above outline approach requires the definition of an LTI model with a large number of states, inputs and outputs, this has a limited impact as similarity transformations in the state space are never computed explicitly.*

Remark. *Recently (see Felici et al. [2007]) an approach to the identification of LPV models in state space form under the assumption that the scheduling parameters are excited in a periodic fashion (such as, *e.g.*, when studying the dynamics of helicopter rotors or wind turbines) has been proposed. The outcome of the identification procedure is an LPV model which, when evaluated along the periodic scheduling sequence, is entirely equivalent to the class of LTP models studied in this Section. Therefore, the proposed approach can be applied also to the problem of recovering structured LPV state space models from unstructured ones, when the scheduling parameter can be excited with a periodic sequence.*

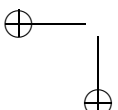
5.3.3 Linear parameter-varying systems

As extension of the LTI case, consider the affine LPV system $\mathcal{M}_{ns}(p)$

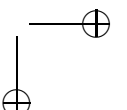
$$\begin{aligned}\dot{x}(t) &= \sum_{i=0}^{N_p} p_i(t) \left(\hat{A}_i x(t) + \hat{B}_i u(t) \right) \\ y(t) &= \sum_{i=0}^{N_p} p_i(t) \left(\hat{C}_i x(t) + \hat{D}_i u(t) \right),\end{aligned}\quad (5.10)$$

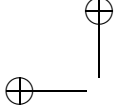
where $p_0 = 1$, and p_i , $i = 1, \dots, N_p$ are the scheduling parameters. As can be noticed the system matrices are affine functions of the scheduling parameters. The structured model $\mathcal{M}_s(p; \theta)$ is defined as follow

$$\begin{aligned}\dot{x}(t) &= \sum_{i=0}^{N_p} p_i(t) (A_i(\theta)x(t) + B_i(\theta)u(t)) \\ y(t) &= \sum_{i=0}^{N_p} p_i(t) (C_i(\theta)x(t) + D_i(\theta)u(t))\end{aligned}\quad (5.11)$$

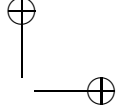


|





|



where $A_i(\theta)$, $B_i(\theta)$, $C_i(\theta)$, and $D_i(\theta)$ are functions of the parameter vector θ . In this case the problem is to solve the following optimization problem

$$\begin{aligned} \theta^* = \arg \min_{\theta} \gamma \\ \text{s.t. } \|\mathcal{M}_{ns}(p) - \mathcal{M}_s(p; \theta)\|_{L_2} < \gamma, \quad \forall p \in \mathcal{P}. \end{aligned} \quad (5.12)$$

where \mathcal{P} is the convex domain of the scheduling parameter p . As is well known in the LPV literature, (5.12) can be solved as an LMI problem evaluating the constraints only in the vertices of the polytopic domain \mathcal{P} .

5.4 Simulation examples

In this Section the results obtained by applying the above described approaches to numerical examples are presented. In order to evaluate the performance of the proposed methods the relative estimation error is defined as follow

$$\theta_{err} = \frac{\hat{\theta} - \bar{\theta}}{\bar{\theta}}, \quad (5.13)$$

where $\hat{\theta}$ and $\bar{\theta}$ are respectively the estimated and the actual value of the parameter θ .

5.4.1 A linear time-invariant system

The first example considered in this Chapter is the printer belt drive modeling problem recently studied in a similar perspective in Prot et al. [2012]. Most low-cost computer printers use a belt drive to move the printing device across the printed page (see Figure 5.1). In Dorf and Bishop [2011] a model

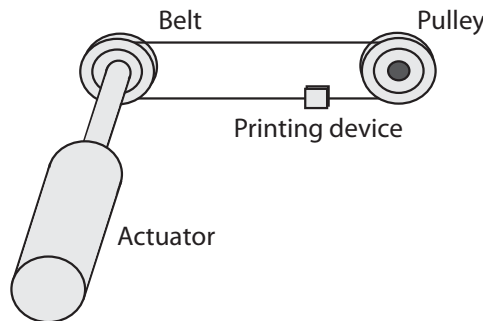
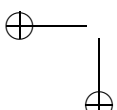
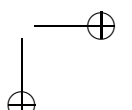


Figure 5.1: Printer belt-drive system.



|





of the belt-drive system is provided, which can be described as follows

$$\begin{aligned}\dot{x}(t) &= \begin{bmatrix} 0 & -1 & r \\ \frac{2k}{m} & 0 & 0 \\ -\frac{2kr}{J} & -\frac{K_r}{J} & -\frac{b}{J} \end{bmatrix} x(t) + \begin{bmatrix} 0 \\ 0 \\ -\frac{1}{J} u(t) \end{bmatrix} \\ y(t) &= [0 \ 1 \ 0] x(t),\end{aligned}$$

where r and m are known, while b , J , k and K_r are unknown parameters to be estimated. In Table 5.1 the real parameters of the system are shown.

| | |
|-------------------------------|--|
| Pulley radius r | 0.15 m |
| Pulley and motor inertia J | 0.01 kg m ² rad ⁻² |
| Belt elasticity k | 20 N m ⁻¹ |
| Printing device mass m | 0.2 kg |
| Pulley and motor friction b | 0.25 N m s rad ⁻¹ |
| Controller gain K_R | 0.1 |

Table 5.1: Physical parameters of the considered printer belt-drive.

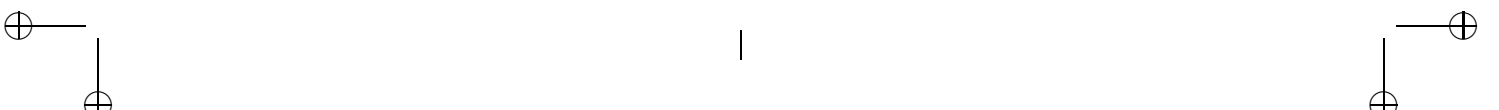
Similarly to Prot et al. [2012], the CT-PBSID_o is used to identify a fully parameterised state space model of the system from a given dataset of input/output measurements. The comparison in Table 5.2 between the eigenvalues of the simulator and the identified model shows that the algorithm is able to capture the system dynamics in the proper way.

| | Simulator | | | | Identified Model | | | |
|-----------------|-----------|---------|---------|--------|------------------|---------|---------|--------|
| | Real | Imag | Omega | Zeta | Real | Imag | Omega | Zeta |
| $\lambda_{1/2}$ | -1.2204 | 15.2790 | 15.3277 | 0.0796 | -1.2204 | 15.2790 | 15.3277 | 0.0796 |
| λ_3 | -22.5592 | 0 | 22.5592 | 0 | -22.5591 | 0 | 22.5591 | 0 |

Table 5.2: Comparison between simulator and identified eigenvalues.

A Monte Carlo study in the reconstruction of the structured state space representation given above has been carried out, by applying to the identified model 100 randomly generated coordinate changes and subsequently applying the approach described in Section 5.3 to estimate the relevant parameters.

The result obtained in the study, expressed in terms of the relative errors as defined in (5.13), is shown in Figure 5.2. As can be seen from the Figure, an extremely accurate reconstruction of the parameters can be achieved. Note that the result is independent of the conditioning of the applied coordinate transformation, which is never computed explicitly in this approach.



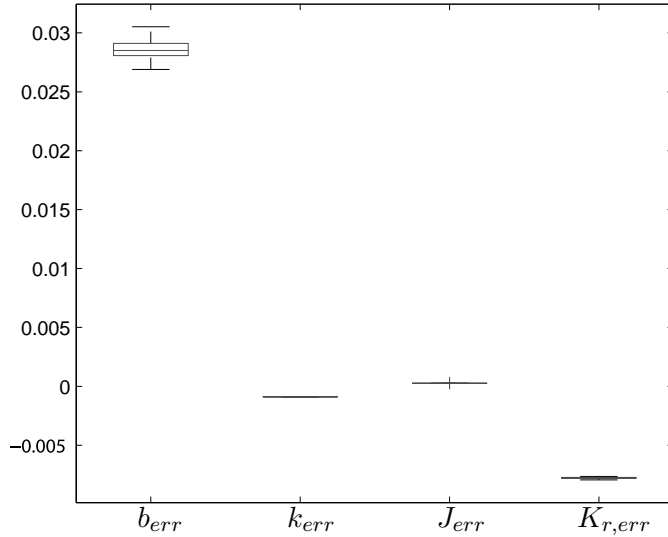


Figure 5.2: Printer belt example: boxplot of the relative errors of the estimated parameters.

5.4.2 A linear time-periodic system

As a second example, the dynamic response of a helicopter rotor blade is considered, assuming that the helicopter is performing steady level flight for a constant forward velocity (or advance ratio). It is well known (see, *e.g.*, Johnson [1980]) that in this case the response can be characterised by a linear time-periodic model, as outlined in the following.

Overview of the rotor blade model

This Section gives a brief overview of the model for the out-of-plane bending dynamics of a helicopter rotor blade which has been used in this study, as derived in Johnson [1980]. Although very simple, this model retains the main characteristics of the full blade dynamics. For a more detailed discussion the reader is referred to the above reference or to Bittanti and Lovera [1996].

Linear out-of plane bending can be described by the equation

$$M(r, t) = E(r)I(r) \frac{d^2 z(r, t)}{dr^2}, \quad (5.14)$$

where $M(r, t)$ is the total bending moment (inertial, centrifugal and aerodynamic) acting at radial station $r \in (0, R)$ of the blade at time t , $z(r, t)$ is the out-of plane blade deflection and $E(r)I(r)$ defines the local bending stiffness. Let now $m(r)$ be the mass per unit length of the blade and introduce



a modal expansion for z

$$z(r, t) = \sum_{i=1}^{\infty} \eta_i(r) q_i(t),$$

where

$$\int_0^R \eta_i(r) \eta_j(r) m(r) dr = 0, \quad \forall i \neq j,$$

and

$$\eta_i(R) = R.$$

Then, it is possible to show that the partial differential equation (5.14) is equivalent to the set of ordinary differential equations

$$I_{q_k}(\ddot{q}_k(t) + \nu_k^2 q_k(t)) = \int_0^R \eta_k(r) F_Z(r, t) dr, \quad k = 1, 2, \dots$$

where ν_k is the natural frequency associated with the k th bending mode, $F_Z(r, t)$ is the aerodynamic load acting at radial station r and

$$I_{q_k} = \int_0^R m(r) \eta_k^2(r) dr.$$

For the purpose of this study, the pitch angle of the blade (ϑ) and the vertical shear force at the root of the blade are respectively considered as input and output signals, defined as:

$$\begin{aligned} S_Z(t) &= \int_0^R F_Z(r, t) dr - \int_0^R m(r) \ddot{z}(r, t) dr = \\ &= \int_0^R F_Z(r, t) dr - \sum_k \ddot{q}_k(t) \int_0^R m(r) \eta_k(r) dr. \end{aligned}$$

So, the dynamics of one blade of a helicopter rotor can be described by a time-varying linear state-space system of the form

$$\begin{aligned} \dot{x}(t) &= A(t)x(t) + B(t)u(t) \\ y(t) &= C(t)x(t) + D(t)u(t), \end{aligned} \tag{5.15}$$

where $x \in \mathbb{R}^n$ is the state, $u \in \mathbb{R}$ is the input and $y \in \mathbb{R}$ is the output. The dimension of the state vector n equals twice the number of out-of-plane bending modes q that are taken into account in the modal expansion for the blade dynamics ($n = 2q$).

In particular, the system matrices in this model are periodic functions of time and vary according to the value of the advance ratio μ .



| | |
|----------------------------------|----------------------------------|
| Rotor angular frequency Ω | 40 rad/s |
| Rotor radius R | 5.5 m |
| Mass per unit length m | 5 kg/m |
| Stiffness EI | $1.8 \cdot 10^3$ Nm ² |
| Lift-curve slope a | 5.7 rad ⁻¹ |
| Lock number γ | 7.84 |
| Blade chord c | 0.3 m |

Table 5.3: Mechanical and aerodynamical characteristics of the considered rotor blade.

Numerical results

A rotor blade with the characteristics given in Table 5.3 has been considered and simulated experiments have been carried out applying to the original model $N = 100$ randomly generated coordinate changes and subsequently applying the approach described in Section 5.3 for the computation of the \mathcal{H}_∞ norm and the estimation of the relevant parameters. Only one out-of-plane bending mode has taken into account, *i.e.*, $q = 1$ and $n = 2$. The complex Fourier series (5.8) is truncated at the second order. In particular, two cases have been considered, where in the former only the Lock number γ and the flapping hinge offset e are estimated, while in the latter the advance ratio μ is also worked out.

Again, the relative errors shown in Figures 5.3 and 5.4 are defined as in (5.13).

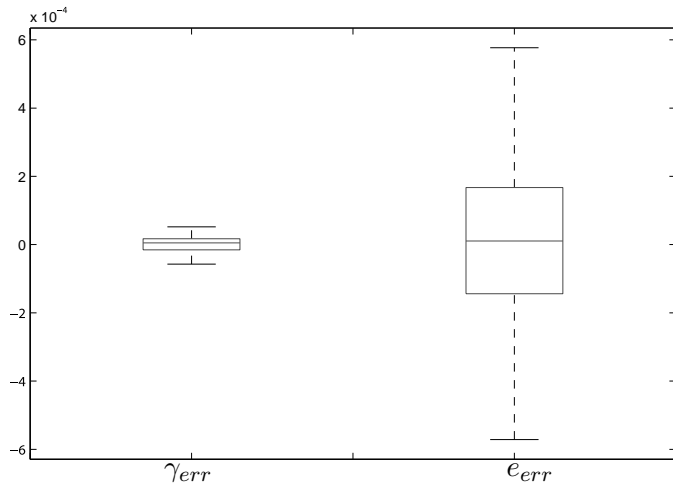


Figure 5.3: Rotor blade example: boxplot of the relative errors of the estimated parameters.

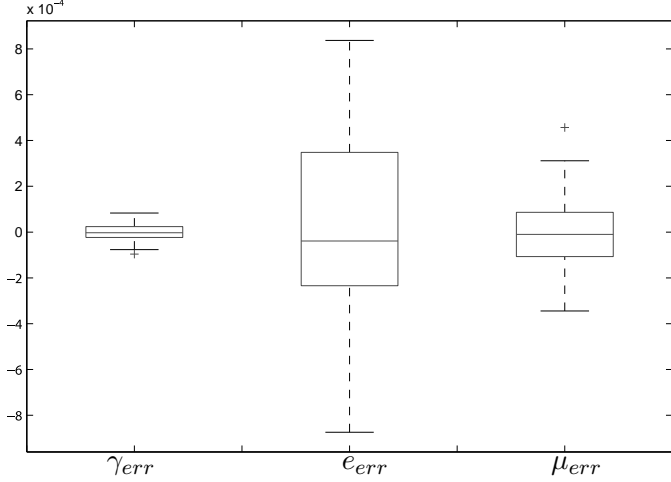


Figure 5.4: Rotor blade example: boxplot of the relative errors of the estimated parameters.

As can be seen from the Figures 5.3-5.4, the results are quite satisfactory and demonstrate that also in this, more complex, situation, the structured state space representation can be reliably recovered.

5.4.3 A linear parameter varying system

The last example involves a parameter-dependent system (considered in De Filippi and Lovera [2011] in an LPV control design framework) that is given by the equations

$$\begin{aligned}\dot{x}_1 &= (\theta_1 + p)x_1 + \theta_1x_2 + \theta_2u \\ \dot{x}_2 &= \theta_3x_1 + \theta_1x_2 + \theta_3u \\ y_3 &= \theta_3x_1 + \theta_3x_2 + u,\end{aligned}\tag{5.16}$$

where $p \in [p_{min}, p_{max}]$, with $p_{min} = 0$ and $p_{max} = 2.8$. The eigenvalues of the system strongly depend on p . The nominal values of θ_i are $\{\theta_1, \theta_2, \theta_3\} = \{-2, 3, 1\}$. Also in this example the black-box system identification is performed in open-loop using the CT-PBSID_o algorithm. For the system (5.16) the two local operating points corresponding to the values $\{p_{min}, p_{max}\}$ have been considered. Simulated data has been collected near each of the considered local operating points by applying to the system a pseudo-random binary signal as input, for a duration of 10s and with a dwell time of 0.01s. White Gaussian noise of increasing variance has been added to the output in order to assess the influence of decreasing signal-to-noise ratio on the quality of the computed estimates. For the input and output variables the sampling interval is $\Delta t = 0.001$ s. The Monte Carlo study is

performed considering 100 runs for each signal-to-noise ratio. In the Figures 5.5-5.7 are shown the estimation errors of the parameters θ_i , defined as in (5.13). The estimate of the parameters θ_i is satisfactory also for low signal-to-noise ratio; the reduced quality of estimation is due to the identification algorithm as denoted in Bergamasco and Lovera [2011b].

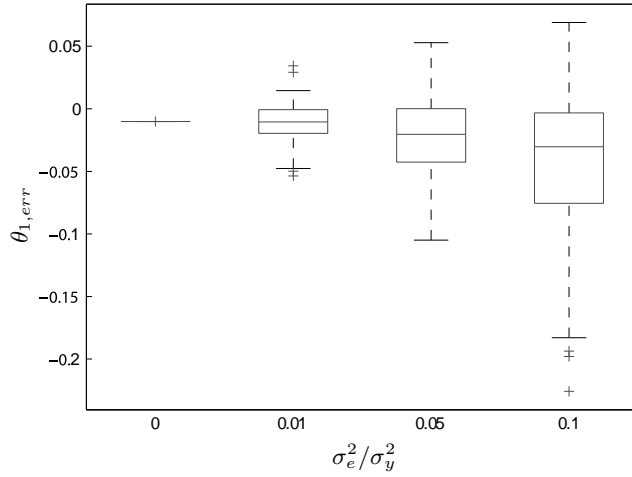


Figure 5.5: LPV example: boxplot of the relative errors of the estimated parameter θ_1 varying the signal-to-noise ratio.

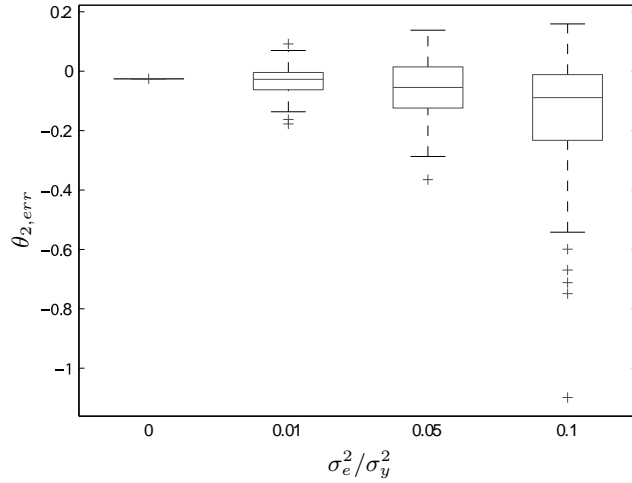


Figure 5.6: LPV example: boxplot of the relative errors of the estimated parameter θ_2 varying the signal-to-noise ratio.

This simulation example demonstrates the capability of the proposed approach to recover the parameters of a linear parameter varying structured

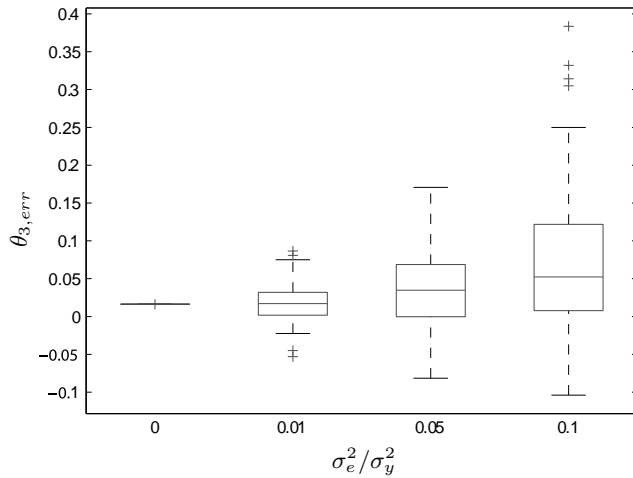
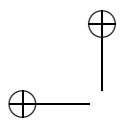


Figure 5.7: LPV example: boxplot of the relative errors of the estimated parameter θ_3 varying the signal-to-noise ratio.

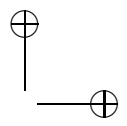
model even with low signal-to-noise ratio.

5.5 Concluding remarks

The problem of recovering the numerical values of the physical parameters of a structured representation starting from a fully parameterised identified model has been studied and an approach based on \mathcal{H}_∞ model matching has been proposed. This formulation can benefit from the availability of reliable computational tools (see Gahinet and Apkarian [2011]), it does not require an explicit construction of the similarity transformation and it can be applied to linear time-invariant systems, to affine linear parameter varying systems, to linear time-periodic systems, and to linear parameter-varying systems identified from a periodic scheduling sequence. Three numerical examples have been presented to illustrate the approach.

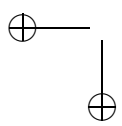


|

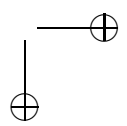


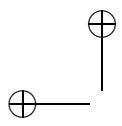
—

—

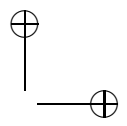


|



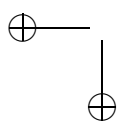


|

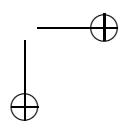


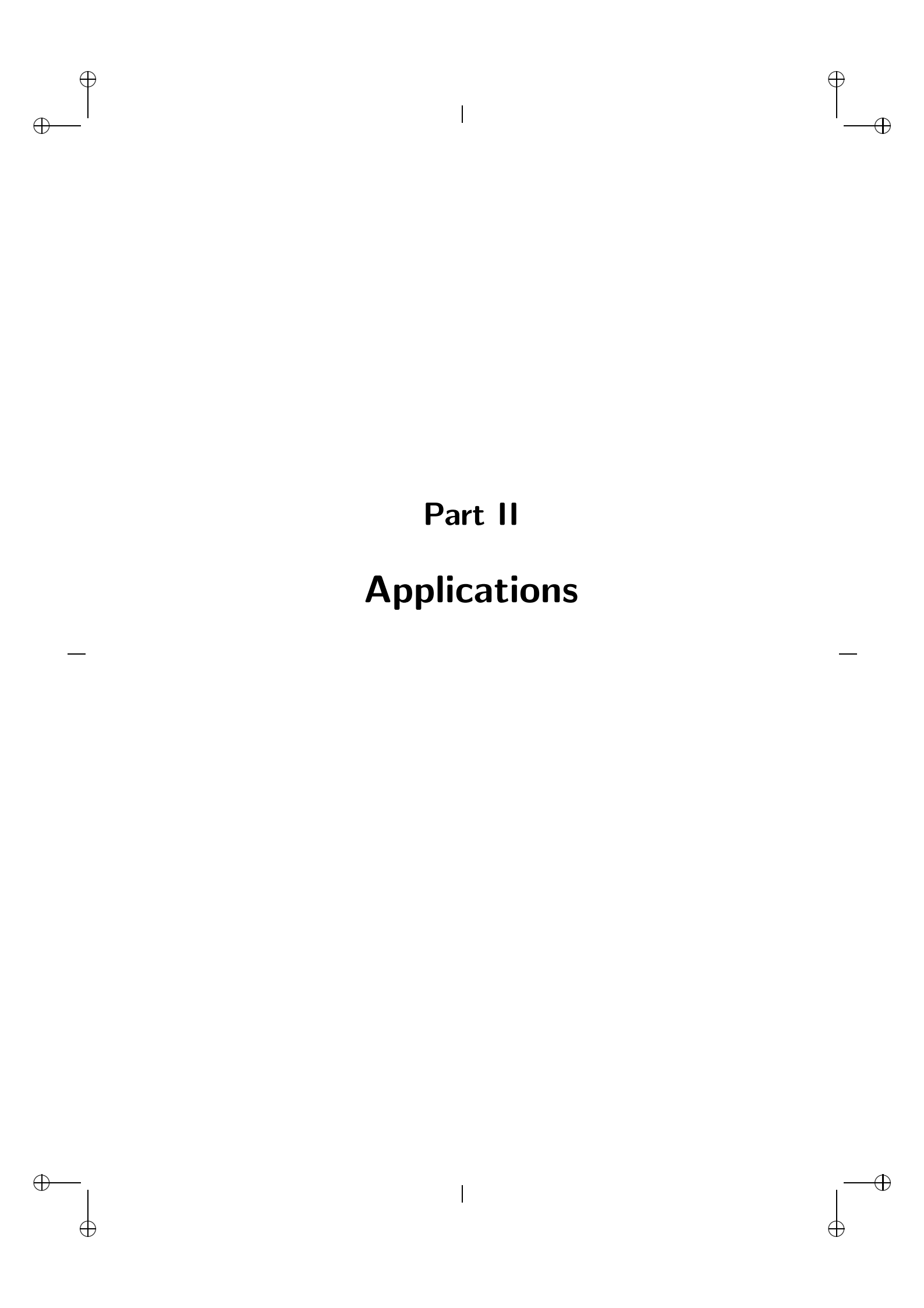
—

—



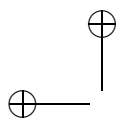
|



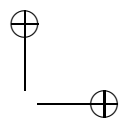


Part II

Applications

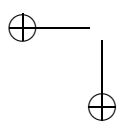


|

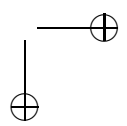


—

—



|



CHAPTER SIX

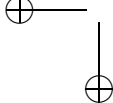
ROTORCRAFT SYSTEM IDENTIFICATION

Model identification has been exploited extensively in the rotorcraft community, precisely in order to overcome the difficulties associated with the accurate description of the most sensitive issues in helicopter dynamics, *i.e.*, the complexity of the interaction between dynamics and aerodynamics. The aim of this Chapter is to provide a concise overview of the relevant literature, with the aim of defining the current state-of-the-art in the field of rotorcraft model identification, and to analyze the potential of the continuous-time subspace model identification methods in this area.

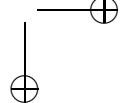
6.1 Introduction

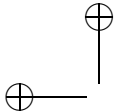
In helicopter engineering, system identification in time and frequency domain has emerged because physical models for rotorcraft dynamics include a number of uncertain parameters which are very difficult to determine (see, *e.g.*, Tischler and Kaletka [1987]); as an example, fluid dynamics is necessary to describe helicopter motion but the associated mathematical modelling is very complex and is affected by a number of unmeasurable physical parameters, *e.g.*, wake interferences with the empennage and tail rotor.

Rotorcraft dynamics usually involves multiple inputs and multiple outputs (MIMO) models, indeed it is described by the interaction of inertial and aerodynamic forces as well as control forces acting on the rotor and the airframe. The relative interactions and interferences between these forces and their effects on the rotorcraft dynamic response change both with flight condition and configuration. The parameter identification of helicopter models requires wind-tunnel and flight test validation experiments. Because of aerodynamic scale effects, wind-tunnel model deficiencies and constrained *free*

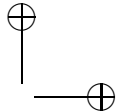


|





|

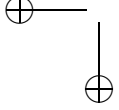


flight capabilities, some limitations must always be envisaged in the quality and applicability of rotorcraft wind-tunnel model data. Therefore, flight tests are necessary to isolate limitations and assess uncertainties in prediction techniques of rotorcraft aeromechanics, as well explained in Hamel and Kaletka [1997].

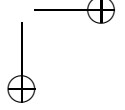
Frequency-domain system identification in helicopter engineering has been developed during the last two decades, so there is a number of contributions in the literature describing the relevant approaches and case studies. The procedure starts with the reconstruction of a nonparametric model using the test data. The frequency response data curve constitutes the nonparametric model, indeed it characterizes the input-to-output process at a large number of discrete frequencies. Then, a parametric frequency response curve is matched with the nonparametric model to find the parameters. First applied to lightly coupled, low bandwidth articulated rotors (Tischler and Kaletka [1987]), this technique has been applied to more highly coupled, higher bandwidth rotor systems (Tischler and Cauffman [1992], Tischler and Tomashoski [2002], Lawler et al. [2006]).

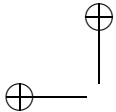
Time-domain system identification is another approach to rotorcraft system identification, which has been intensely developed by German Aerospace Center DLR (Hamel and Kaletka [1997]). In this technique the model, written in state-space form, is matched directly with the test data using least squares and/or maximum likelihood methods. The helicopter cannot generally be considered as a single rigid body and must be modelled as a coupled multibody dynamic system. There is strong coupling between the dynamics of the rotor blades and the dynamics of the air flow passing through the rotor with those of the fuselage, control system, and engine, so that as many as 13 degrees of freedom, or even more, are often necessary to accurately model the dynamic response, as shown in Tischler and Remple [2006].

As already explained in the first part of this thesis the subspace identification methods (SMI) fall into the category of the time-domain system identification algorithms, but in spite of the ease with which SMI can be exploited in dealing with Multiple-Inputs Multiple-Outputs (MIMO) modelling problems, until recently these methods have received limited attention from the rotorcraft community, with the partial exception of some contributions such as Verhaegen and Varga [1994], Bittanti and Lovera [1997], Lovera [2003]). The inapplicability of the SMI algorithms in the rotorcraft field is more ideological than technical, because the helicopter community wants physically interpretable models. A possible solution to this problem can be the \mathcal{H}_∞ model matching algorithm presented in Chapter 5. In any case, the SMI methods are particularly well suited for rotorcraft problems, for a number of reasons. First of all, the subspace approach can deal in a

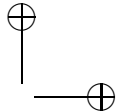


|





|



very natural way with MIMO problems; in addition, all the operations performed by subspace algorithms can be implemented with numerically stable and efficient tools from numerical linear algebra. Finally, information from separate data sets (such as generated during different experiments on the system) can be merged in a very simple way into a single state space model.

Identification techniques obviously require the availability of the actual aircraft, and therefore cannot be easily used at the preliminary design stage.

In this Chapter a brief introduction about the system identification of rotorcraft is done in Section 6.2, with some remarks on the practical problems like model structure selection, test procedure, and data consistency. In Section 6.3 the time- and frequency- domain identification methods available in the rotorcraft literature are briefly revised and the advantages of a SMI method, *e.g.*, CT-PBSID_o algorithm, are underlined in Section 6.4.

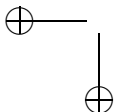
6.2 Challenges of rotorcraft system identification

6.2.1 Models of rotary-wing aircraft dynamics

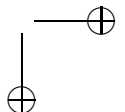
With a few exceptions the rotorcraft model identification literature focuses on the engineering relevant problem of estimating the parameters of linear models representing the system near a given flight condition, see Tischler and Remple [2006] and the reference therein. In this respect, the main choice is between internal, *i.e.*, state space, or external, *i.e.*, transfer function, representation. This tradeoff occurs ubiquitously in the systems and control literature and is generally resolved by noting that external representations are practical and reliable only as far as SISO systems of limited order are concerned, while internal representations are usually recommended whenever MIMO, possibly high order systems have to be dealt with.

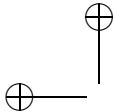
As far as model order is concerned, it is well known that rotary wing aircraft are characterized by high order dynamics, see, *e.g.*, Lawler et al. [2006]. The large number of degrees of freedom associated with the coupled rotor-fuselage dynamics leads to a high number of unknowns to be estimated, making system identification for such systems a potentially challenging problem. A conventional 6-DOF model may be adequate for handling qualities evaluations, whereas higher order model structures are required for simulation validation or flight control system design.

The paper Tischler and Cauffman [1992], analyzing the BO-105 helicopter dynamics, shows that a 9-DOF hybrid model that includes coupled body/rotor-flapping and lead-lag dynamics is accurate for frequencies up to 30 rad/sec, even if at low frequencies (below 13 rad/sec), the hybrid model response reduces to the 6-DOF quasi-steady response. In the paper

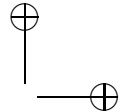


|





|



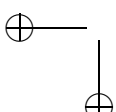
is stated that an advanced flight control designs for helicopters must be based on models that include the flapping and lead-lag dynamics. Similar results are found during the SH-2G system identification in Tischler and Tomashoski [2002]. The SH-2G model must include fuselage rigid body dynamics, rotor regressive flapping dynamics, rotor coning dynamics, dynamic inflow, and an engine response to match accurately the SH-2G responses in the frequency range of interest. Another result achieved in Tischler and Tomashoski [2002] is that, using a common model structure and a limited number of flight test condition, is possible to characterize the aircraft dynamics in all flight speed conditions. This method allows the interpolation for continuous flight simulation and the control system gain scheduling design at any speeds. In Fletcher [1995] a 14-DOF model for the UH-60 has been developed: 6-DOF fuselage rigid body, longitudinal and lateral main rotor regressive flapping, longitudinal and lateral regressive lead/lag, vertical dynamic inflow, main rotor/engine angular rate, engine torque, and engine fuel flow. The resulting model is accurate over a broad frequency range without being over-parameterized.

A generic model structure is not suitable for all cases and it must be chosen each time according top the helicopter configuration and the final application of the model. This choice can be considered an integral part of the system identification process and is left to the experience and competence of the modeller.

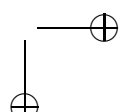
6.2.2 Flight test procedure

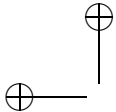
System identification approaches rely on the information content about the system under test, provided by the amplitude and phase relationships between the measured control inputs and the measured system responses. The test input is one of the major factor that influence the identified model parameters accuracies. It should at least meet the following requirements:

- all helicopter modes within the frequency range of interest must be properly excited;
- the flight test duration must be long enough to provide sufficient low frequency information;
- when linear models are estimated, the aircraft response should stay within small perturbations limits from trim so that linearity assumptions are met;
- no or only minor additional pilot inputs are allowed, *e.g.*, for keeping the response small.

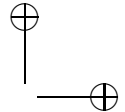


|





|



Furthermore, it is often desired that the test input sequence can be actually flown by the pilot.

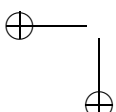
Generally speaking, all the standard excitation input sequences described in the classical system identification literature are applicable for rotorcraft model identification. The relevant literature, however, reports some dedicated developments which stem from the application of either time-domain or frequency-domain methods taking into account the additional requirements associated with flight testing. More precisely, a number of specific input sequences have been developed for the purpose of helicopter model identification, which have been widely applied in case studies reported in the available literature, ranging from simple doublets, to the DLR 3211 sequence, a kind of custom-designed Pseudo-Random Binary Sequence (PRBS), and finally to various types of frequency sweeps (linear, logarithmic, Schroeder-phased) as commonly adopted for frequency domain estimation, see Klein and Morelli [2006] for further details. In Hamel and Kaletka [1997] some general tendencies are described: pilot-flown control inputs are preferable rather than electronically generated inputs but it is very important that the test starts and ends in trim flight condition. The test input sequence should be applied separately to each control channel. A test should be repeated to provide redundant data for the evaluation.

When dealing with the problem of identifying high order models taking also into account some of the rotor modes, it is important to underline that direct excitation of the lower frequency rotor modes and structural coupling modes must be avoided, as it can severely damage the helicopter, as explained in Johnson [1980]. In this respect, the estimation of parametric coupled rotor-fuselage dynamic models is particularly challenging, as information about rotor dynamics can only be gathered using data associated with input-output behaviour at lower frequencies, which typically gives rise to ill-conditioned estimation problems (see Tischler and Cauffman [1992]).

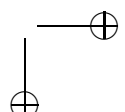
Finally, in Ham et al. [1993], Williams et al. [1995] are described in detail the practical aspects of frequency domain rotorcraft system identification including the measurement instrumentation, the safety considerations and the pilot instructions.

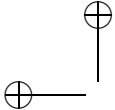
6.2.3 Data consistency

In order to check the data consistency and to remove measurement errors from data prior to the actual estimation step, an algorithm, originally described in Bach [1991], has been presented in Tischler and Remple [2006]. This preliminary data analysis is necessary because the results of system identification are highly influenced by data quality and could be severely

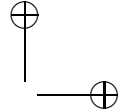


|





|



distorted by systematic errors. The post processing of the measured data is used to check the consistency of measured aircraft responses, to remove the instrumental errors, *i.e.*, biases and drifts, and to reconstruct some of the state variables and their first derivatives that are not directly measured. The mathematical model used is formed by the 6-DOF kinematic equations with the measured accelerations and angular rates considered as input variables, as described in Klein and Schiess [1977].

In Chapter 7 the data consistency problem is summarized and two novel approaches, based on the Unscented Kalman Filter and the Expectation Maximization, are proposed.

6.3 Classical rotorcraft identification methods

6.3.1 Time domain system identification

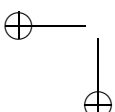
Regardless of the actual approach chosen for parameter estimation, a time domain processing step is initially applied to the data to check the compatibility and consistency of the measurements. This technique is usually adopted also in frequency domain system identification to remove data inconsistencies resulting from calibration errors, drifts, or instrumental failures. It can be used on-line and it helps to ensure that only consistent data are used in the system identification.

Apart from data consistency analysis and pre-processing, time domain system identification is a technique for the direct estimation of state-space models from flight test data. The data is not manipulated as in frequency-domain system identification, *i.e.*, Fourier transformation, then the errors occurring in the time-frequency transformation are avoided.

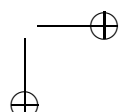
The Maximum likelihood (ML) technique is generally accepted as one of the most suitable time-based methods for aircraft parameter identification. The main characteristics of ML estimation can be summarised as follows:

- it yields asymptotically unbiased and consistent estimates for linear systems;
- it provides the Cramer-Rao bound, which is a measure of the reliability of each estimate;
- it yields the correlation between the identified parameters.

The Cramer-Rao bound (see Klein and Morelli [2006] for further details) and the parameter correlation help to find an appropriate model structure and to avoid over-parameterization. A nonlinear maximum likelihood method developed by DLR was utilized for time-domain identification of the XV-15



|



(Tischler and Kaletka [1987]). Time domain system identification requires to consider bias errors, for each differential equation added to the model, and the initial state vector. So a high order model requires many unknown terms to be estimated.

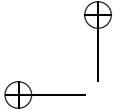
Two studies comparing the application of both time and frequency domain system identification techniques to the same flight test database have been conducted (Bell XV-15 tilt-rotor Tischler and Kaletka [1987] and the BO-105 Hamel and Kaletka [1997]). In Jategaonkar et al. [2004] a recent overview of the time-domain approaches for the rotorcraft system identification is presented. Finally, note that while the model is identified in state space form, it can be easily presented in frequency domain using the well known transformations, as shown in Appendix A.

6.3.2 Frequency domain system identification

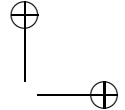
Rotorcraft model identification can be equivalently handled with the frequency domain identification approach. In the helicopter field it is common to analyze the behaviour of the system with a frequency point of view, *i.e.*, frequency response, eigenvalues, transfer function. Therefore a system identification method that uses data in the frequency domain can be suitable.

Frequency domain identification techniques allow the reduction both in the number of unknown parameters, *i.e.*, bias errors and initial state vector, and the number of required data points. The difficulty in determining correcting bias terms in the time domain is avoided in the frequency domain as no bias terms are present. Moreover it is avoided the estimation of the initial state vector, necessary in a time-domain ML method; note that it can be problematic due to the unstable dynamics of the helicopter. In literature there are some examples about frequency domain system identification, as the Bell XV-15 Tischler and Kaletka [1987], Sikorsky UH-60 Blackhawk Fletcher [1995], BO-105 Tischler and Cauffman [1992], Hamel and Kaletka [1997], R-MAX Cheng et al. [2006], SH2G Tischler and Tomashoski [2002], Fire Scout MQ-8B, S-76, and ARH-70A Ivler and Tischler [2008], MH-47G Link et al. [2011], and Unmanned K-MAX Mansur et al. [2011]. A frequency domain system identification procedure applied to helicopters is well described in Lawler et al. [2006] and Tischler and Remple [2006] and can be summarised as follows.

Frequency domain identification uses dynamic response time-history test data generated by pilot or computer generated inputs, such as sine sweeps or other inputs with good spectral content. These inputs excite the system vehicle dynamics, which could be an aircraft or any other physical system or subsystem of interest. The frequency sweep begins at low frequency and



|



increases smoothly in frequency until the maximum frequency is reached. The aim of this input type is to excite all dynamics within the frequency range of interest.

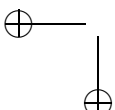
The next step is to perform a multi-variable spectral analysis of the data. This analysis, which is a MIMO matrix generalization of the SISO Fast Fourier Transform (FFT), is necessary for most aircraft system identification applications since real flight-test data inevitably involve multiple, partially correlated, control inputs during a single excitation manoeuvre. The MIMO frequency response matrix constitutes a nonparametric model of the aircraft response. An important by-product of this analysis is the coherence function, which provides key information about the frequency response accuracy. When the dynamics contain nonlinear behaviour, the extracted frequency response function using the Fourier transform can be interpreted as a describing function, which is the linear model that best characterizes the nonlinear behaviour of the system (see Lawler et al. [2006]) and its coherence function measures how much of the output power is linearly related with the input power.

In Tischler and Kaletka [1987], Tischler and Remple [2006] have been proved that the frequency response is well computed if the chirp z-transform and the composite window optimization are used. The chirp z-transformation is an advanced and flexible FFT algorithm that provides an accurate frequency response over the frequency range of interest. Spectral windowing is a process by which the time history data are segmented, and the frequency response is determined for each segment or window. By averaging the frequency responses from individual window segments, the effect of noise is reduced significantly. The state space model structure is formulated as

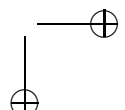
$$\begin{aligned}\dot{x}(t) &= Ax(t) + Bu(t) \\ y(t) &= Cx(t) + Du(t)\end{aligned}$$

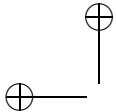
whose frequency responses match the measured MIMO frequency response data. Static trim data can also be included in the model structure to ensure its consistency. The complexity of the selected state space model structure depends on the aircraft dynamics and the intended application, as previously discussed. The accuracy of the identified model is quantified as a cost function, which is the weighted sum of the frequency response magnitude and phase errors. Initial guesses for the model parameters can be obtained from equation error regression methods as shown in Lawler et al. [2006].

Finally, an optimization algorithm is used to tune the parameters in the model structure minimizing the cost function and driving the model responses to the best match. At this stage the frequency domain system

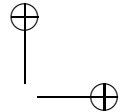


|





|



identification has achieved a state space model that best matches the MIMO frequency response database.

6.3.3 Comparison between frequency and time domain identification techniques

Both time and frequency domain system identification are able to identify the model that best matches the test data but they work in different ways, as explained, so it is important to summarize these differences.

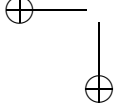
Frequency domain system identification uses spectral analysis that assumes input-to-output linearity. The initial data consists of frequency responses derived from time history data, but note that the time-frequency data transformation introduces some errors. The model reduction can start with the nonparametric model analyzing the coherence functions.

Time domain system identification is suited to MIMO identification since the model can be of arbitrary order and structure. Data consistency, drop out tests and signal reconstruction methods are an integral part of the time domain identification procedure. The noise models must be identified, indeed, if the presence of noise is ignored, it will introduce biases in the identification results. This technique requires shorter record lengths than frequency domain system identification. This is a big advantage of this technique forasmuch as the test cost. Extended maximum-likelihood techniques can be used to identify parametric nonlinearities which are especially important in low frequency dynamics of hovering rotorcraft. The major problem of these techniques, evidenced in Tischler and Kaletka [1987], is its sparse prediction capability in the frequency domain indeed time domain method inherently weights phase errors more heavily than magnitude errors. This characteristic makes the extracted state space model very sensitive to pure time delays and unmodelled high frequency dynamics. Also, the method inherently weights low-frequency dynamics much more than high-frequency dynamics.

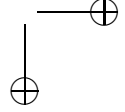
Similarities between the methods (as well as between all the system identification algorithms) are:

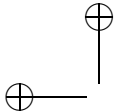
- the good results depends on satisfactory excitation of key dynamics modes;
- multiple inputs must not be fully correlated;
- the models are ultimately verified in the time domain.

Comparative studies of time and frequency domain methods were conducted under U.S./German memorandum of understanding using flight-test data

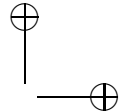


|



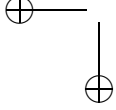


|

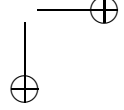


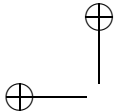
from the XV-15 tilt-rotor aircraft Tischler and Kaletka [1987] and the BO-105 helicopter Hamel and Kaletka [1997]. The methods in the time or frequency domain have shown to be suitable for rotorcraft identification. Both provide results of similar quality. Quoting from the conclusions of the cited study Hamel and Kaletka [1997], let's review them point wise, to get a clear picture of what system identification entails and can provide, also placing the conclusions of the 1997 AGARD studies in perspective, in view of the subsequent 15 years of research in the field.

- *Flight tests must meet specific identification requirements, mainly with respect to control inputs and response information content, accurate trim, small perturbation responses, and repeated tests for data redundancy. Therefore, a dedicated flight test program for the identification purpose should be conducted.* This point is of utmost importance, as it is often assumed that meaningful information can be extracted from routine flight test data, which is definitely not the case.
- *Data accuracy is the main prerequisite for a successful identification. Therefore, strong emphasis has to be placed on instrumentation, data quality checking, detection and correction of errors, and careful data processing. Correctly calibrated sensors easily provide the required accuracy, except for velocity measurements, which are still problematic, especially in the low speed regime.* The importance of accurate experiment planning and design and reliable measurements can be hardly overstated. As mentioned in the conclusions of the study Hamel and Kaletka [1997], however, it is expected that extensive experience in flight testing as routinely available in the rotorcraft industry should cover most of the relevant issues.
- *Identification techniques have reached a level of maturity that makes them powerful tools to support industry projects. From the techniques that have become standard, the least-squares method is appropriate for high quality data but usually it is applied to generate starting values. The more complex techniques in the time- or frequency-domain have shown to be suitable for rotorcraft identification. Both provide results of similar quality and it is more the skill and the experience of the analyst than the choice of the method that ensures the final success.* This is true for any application of system identification, which is ultimately a delicate exercise in the tuning of processing and estimation algorithms and in the interpretation of the results.
- *For the most part, the identification of classical 6-DOF rigid body models can be treated as a routine task. The determination of higher*

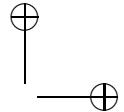


|



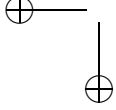


|

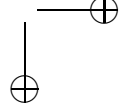


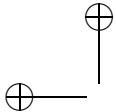
order models with rotor degrees of freedom is also done successfully, but it requires more effort in aircraft instrumentation, data processing, model structure definition and identification. This statement is not in fact entirely correct, as significant progress both in system identification and in the exploitation of identified models for control design purposes has taken place since the publication of that study. In this respect, also classical work related with 6-DOF models could be revised, with the aim of extracting much more information from data than was previously possible.

- *Higher order models can accurately characterize the higher frequency range. Therefore they are required for more demanding applications, such as high bandwidth control system design and high fidelity simulation. The need for reliable higher order mathematical models was clearly seen in the development of high quality In-Flight Simulators. The success of the simulation, demonstrated by the DLR ATTHeS, has shown that identification approaches can provide the required models needed for the control system design.* In other words, the feasibility of high order rotorcraft modelling from experimental data has already been demonstrated in the literature. It should be added, however, that the parameter estimation and model validation techniques discussed in the classical rotorcraft system identification literature do not deal explicitly with a very important aspect, *i.e.*, the accurate characterisation of uncertainty associated with the nominal identified model. In particular, advanced methods for the characterisation of model uncertainty are currently available, which can be used to provide information about the actual reliability of the estimated system descriptions.
- *As system identification extracts the rotorcraft characteristics from flight data of the existing aircraft, it is an ideal tool to generate a 'true' mathematical description of the vehicle dynamics. However, for specific applications, the presently used derivative models may be a too global representation of the aircraft dynamics. Approaches that combine the advantages of system identification and the advantages of other modeling approaches, such as generic simulation or wind-tunnel measurements, still have to be found. It is a major research challenge to develop ideas and guidelines for combining the individual techniques and to provide a powerful tool for accurately modeling the characteristics of a helicopter from its design phase through the flight testing phase until the final production.* This statement summarises the true challenge facing system identification today. Note however that such

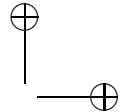


|





|



an ambitious goal may or may not prove achievable in practice depending on the specific application.

6.4 An underrated rotorcraft model identification method: the subspace approach

The subspace model identification algorithms have been already well introduced in this thesis, and so here the focus is on what problems of the rotorcraft system identification they are able to solve. Summarizing the challenges introduced in previous Sections, the main difficulties in rotorcraft model identification are

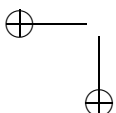
- intrinsically multivariable (MIMO) problem;
- high order dynamics;
- most rotorcraft vehicles are open loop unstable;
- rotorcraft community wants continuous-time models.

It is clear that a closed-loop continuous-time subspace model identification technique, like the CT-PBSID_o algorithm, is able to face all the listed problems. In fact the CT-PBSID_o approach, with the extensions explained in the first part of this thesis, can provide:

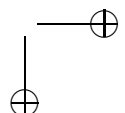
- unbiased model estimates from data generated during closed-loop operation, as is frequently the case in experiments for rotorcraft identification;
- the possibility to quantify model uncertainty using computational statistics for the variance of the estimates;
- the direct estimation of continuous-time models from (possibly non-uniformly) sampled input-output data;
- the transformation of the identified black-box model in a chosen gray-box one.

An unmentioned problem that is automatically solved by a subspace technique is the model structure selection, indeed the model order is directly extracted from the data.

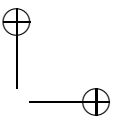
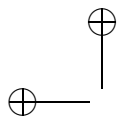
The performance of the CT-PBSID_o algorithm in the rotorcraft application will be analyzed in the next Chapters. In Chapter 8 the BO-105 helicopter will be considered and a black- and a gray- box model will be



|



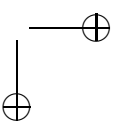
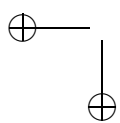
estimated starting from simulated data. In Chapter 9 a quadrotor will be taken into account in order to evaluate the viability of the continuous-time subspace method to deal with real experimental data. In addition an uncertainty model will be provided.



—

|

—



|

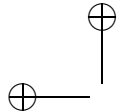
CHAPTER SEVEN

DATA CONSISTENCY ANALYSIS FOR ROTORCRAFT MODEL IDENTIFICATION

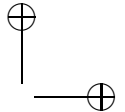
When rotorcraft measurements have to be used for system identification, all the possible error sources introduced by the sensors (gyroscopes, accelerometers, GPS, pressure sensors, etc) have to be deleted (or at least reduced), otherwise the identification procedure may introduce significant modelling errors. Data Compatibility Analysis (DCA) is a methodology that aims at cleaning up the measured data by the systematic measurement errors introduced by different sensors (see, *e.g.*, Klein and Morelli [2006]). Such a method can be reformulated as the parametric estimation of a nonlinear system, a well known problem typical when modeling physical systems for which some parameter is not known *a priori*. In this Chapter a comparison between the results obtained using different identification techniques is performed. The developed approaches are based on the following methods: Output Error (OE), Unscented Kalman Filter (UKF), and Particle Filter (PF), and they have been applied to DCA analysis of measured data for a small scale quadrotor Unmanned Aerial Vehicle (UAV).

7.1 Introduction

Rotorcraft system identification requires accurate measured data in order to maximise the reliability of the obtained models for the plant. Measurements from a typical research helicopter include data gathered by diverse sensors such as accelerometers, gyroscopes, dynamic pressure sensors, GPS, etc. In view of the heterogeneous nature of the information on the basis of which parameter estimation is performed, it is very important that some preliminary processing of the data is carried out, in order to ensure



|



that the simultaneous presence of various types of instrumental errors and inaccuracies does not lead to significant modelling errors.

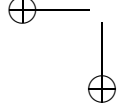
This step is known in the literature as data consistency (or data compatibility) analysis (DCA, see for example the recent textbooks Klein and Morelli [2006], Tischler and Remple [2006]), and consists of ensuring that the measured data are mutually consistent, by enforcing kinematic constraints among measured variables. More precisely, recalling that sensor measurement errors can be classified as either random or systematic, only the latter can be estimated and removed using kinematic relationships, while the former can only be dealt with in an average sense on the basis of the law of large numbers. In other words, a kinematically consistent data set is a prerequisite for the model structure determination and parameter estimation steps of the system identification process.

The general idea behind the kinematic approach to DCA can be summarised as follows. The set of measured variables is partitioned in two subsets: a subset of the measurements is used as inputs to the kinematic equations, which are solved and used with the output equations to generate reconstructed values for the second subset of the measurements. If all the measurements are compatible, the reconstructed outputs will match the measurements of the same output quantities, except for random measurement noise.

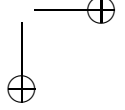
The problem of DCA can be recast as a parameter estimation problem for an uncertain nonlinear system. This problem is widely studied in the system identification literature because the potential benefits coming from a methodology capable of identifying a set of unknown parameters affecting a generic nonlinear model class are quite evident. A complete literature review can be found in Ljung [2003] and Ninness [2009].

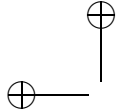
The aim of this Chapter is to provide some background on the approaches to data consistency which are currently available in the literature. In particular, the classic approach (*i.e.*, the Output Error method) is compared to innovative ones (*i.e.*, the Unscented Kalman Filter and the Particle Filter), their implementations are discussed and the relative strengths and weaknesses are compared.

The Chapter is organised as follows: Section 7.2 introduces the DCA problem as well the kinematic and measurement models, while Section 7.3 shows the approaches employed for the parameter estimation problem arising in the DCA. The experimental results are presented in Section 7.4 and in Section 7.5 some conclusions remarks are sketched.

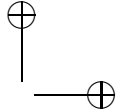


|





|



7.2 Problem Statement

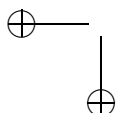
A helicopter has typically several onboard sensors, *e.g.*, gyroscopes, accelerometers, GPS, magnetometers, pressure sensors. The measurements of each sensor can be affected by systematic and random errors. When the measurements have to be used for system identification, the systematic errors introduced by the sensors have to be compensated, otherwise the identification procedure may introduce significant modelling errors too. The measurements from helicopter instrumentation can require three types of corrections: ground calibration, sensor alignment and position corrections, and systematic instrumentation error corrections. While the first two errors do not vary over the course of a flight-test program, systematic instrumentation errors can change with maneuver type and flight conditions. Then, these errors should be estimated for each individual maneuver or each type of maneuver. The aim of such a procedure, also called data consistency analysis, is to clean up the measured data from the systematic measurements errors introduced by the sensors. The basic idea is to couple the nonlinear kinematic equations that describe the aircraft motion with the output equations and their measurement models. An identification procedure is then applied in order to provide estimates of the unknown parameters (bias and scale factors). Once an estimate for such parameters is available, the measured data can be corrected and used for system identification purposes.

Kinematic equations

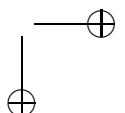
The kinematic equations are formed of translational and rotational kinematic equations. A derivation of these equations can be found in Klein and Morelli [2006]. The translational kinematic equations in body axes, derived from Newton's second law, are

$$\begin{aligned}\dot{u} &= rv - qw - g \sin(\theta) + a_x \\ \dot{v} &= pw - ru + g \cos(\theta) \sin(\phi) + a_y \\ \dot{w} &= qu - pv + g \sin(\theta) \cos(\phi) + a_z,\end{aligned}\tag{7.1}$$

where u , v , and w are respectively the components of the velocity along the x , y , and z body axes, while ϕ , θ , and ψ are respectively the roll, pitch, and yaw Euler angles. The accelerometer measurements are a_x , a_y , and a_z . The rotational kinematics equations, relating the rate of change of the Euler



|





angles to the body axes component of the angular velocities p , q , and r , are

$$\begin{aligned}\dot{\phi} &= p + \tan(\theta)(q \sin(\phi) + r \cos(\phi)) \\ \dot{\theta} &= q \cos(\phi) - r \sin(\phi) \\ \dot{\psi} &= \frac{q \sin(\phi) + r \cos(\phi)}{\cos(\theta)}.\end{aligned}\tag{7.2}$$

The aircraft kinematics is described by equations (7.1) and (7.2). The Euler angles ϕ , θ , and ψ can be provided by an Inertial Measurement Unit (IMU), while the translational velocities u , v , and w can be related to the air data measurements (if available) by the following equations

$$\begin{aligned}V &= \sqrt{u^2 + v^2 + w^2} \\ \alpha &= \arctan\left(\frac{w}{u}\right) \\ \beta &= \arcsin\left(\frac{v}{V}\right),\end{aligned}\tag{7.3}$$

where V is the airspeed, α is the angle of attack, and β is the sideslip angle.

For the kinematic data consistency check, the body axis angular rates (p , q , and r), and the measured acceleration at the centre of gravity (a_x , a_y , and a_z) are considered inputs in the state equations. The states are u , v , w , ϕ , θ , and ψ , and the outputs are V , α , β , ϕ , θ , and ψ .

Model equations for DCA

As shown in Klein and Morelli [2006], the typical systematic instrumentation errors can be modelled as

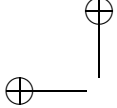
$$z(i) = (1 + \lambda)y(i) + b + \nu(i),$$

where $z(i)$ is the measurement at discrete-time i , $y(i)$ is the true value, $\nu(i)$ is a random noise, while λ and b are respectively scale factor and bias.

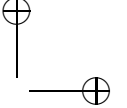
The size of the identification problem can be reduced by the sensors characteristics, considering that not all sensors are affected by both scale factor and bias error. In Table 7.1 the typical instrumentation errors for various sensors are shown (see Klein and Morelli [2006] for further details).

The state space form of the kinematic equations used for data consis-





|



| Sensor | Variables | Bias error | Scale factor error |
|-----------------------------|-----------------------------|------------|--------------------|
| Translational accelerometer | a_x, a_y, a_z | × | - |
| Rotational accelerometer | $\dot{p}, \dot{q}, \dot{r}$ | × | - |
| Rate gyro | p, q, r | × | - |
| Airflow angle vane | α, β | × | × |
| Dynamic pressure | V | × | × |
| Integrating gyro | ϕ, θ, ψ | × | × |
| Pressure altimeter | h | - | × |

Table 7.1: Typical instrumentation errors (Klein and Morelli [2006]).

tency analysis is

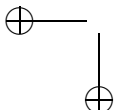
$$\begin{aligned}
 \dot{u} &= (r_m - b_r)v - (q_m - b_q)w - g \sin \theta + a_{x_m} - b_{a_x} \\
 \dot{v} &= (p_m - b_p)w - (r_m - b_r)u + g \cos \theta \sin \phi + a_{y_m} - b_{a_y} \\
 \dot{w} &= (q_m - b_q)u - (p_m - b_p)v + g \cos \theta \cos \phi + a_{z_m} - b_{a_z} \\
 \dot{\phi} &= (p_m - b_p) + \tan \theta ((q_m - b_q) \sin \phi + (r_m - b_r) \cos \phi) \\
 \dot{\theta} &= (q_m - b_q) \cos \phi - (r_m - b_r) \sin \phi \\
 \dot{\psi} &= \frac{(q_m - b_q) \sin \phi + (r_m - b_r) \cos \phi}{\cos \theta},
 \end{aligned} \tag{7.4}$$

where the subscript m indicates measured values. State and parameter estimation, either simultaneous or separate, would be an extremely difficult task. In Section 7.3 this problem is faced using different approaches.

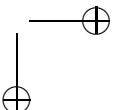
The measured output equations with the instrumentation errors are modeled as follows

$$\begin{aligned}
 V_m(i) &= (1 + \lambda_V) \sqrt{u^2(i) + v^2(i) + w^2(i)} + b_V \\
 \alpha_m(i) &= (1 + \lambda_\alpha) \tan^{-1} \left(\frac{w(i)}{u(i)} \right) + b_\alpha \\
 \beta_m(i) &= (1 + \lambda_\beta) \tan^{-1} \left(\frac{v(i)}{u(i)} \right) + b_\beta \\
 \phi_m(i) &= (1 + \lambda_\phi) \phi(i) + b_\phi \\
 \theta_m(i) &= (1 + \lambda_\theta) \theta(i) + b_\theta \\
 \psi_m(i) &= (1 + \lambda_\psi) \psi(i) + b_\psi.
 \end{aligned} \tag{7.5}$$

The rotorcraft equations of motion can be decoupled depending on the performed experiment, *e.g.*, the vertical motion does not significantly affect the rotational dynamics. Further simplifications can be achieved by separating the kinematic differential equations and the measured output equations



|



into longitudinal and lateral subsets when the flight test contains mainly longitudinal and lateral motions, as shown in Table 7.2. This property can be used in order to reduce the size and thus the computational complexity of the parameter further procedure.

| | <i>Longitudinal manoeuvre</i> | <i>Lateral manoeuvre</i> | <i>Full manoeuvre</i> |
|-------------------------------|---|--|--------------------------|
| <i>Instrumentation errors</i> | $b_{a_x}, b_{a_z}, b_q, \lambda_\alpha, \lambda_\theta$ | $b_{a_y}, b_p, b_r, \lambda_\beta, \lambda_\phi, \lambda_\psi$ | all |
| <i>Input variables</i> | $V, \phi, \psi, a_x, a_z, q$ | u, w, θ, a_y, p, r | a_x, a_y, a_z, p, q, r |
| <i>State variables</i> | u, w, θ | v, ϕ, ψ | all |
| <i>Output variables</i> | V, α, θ | β, ϕ, ψ | all |

Table 7.2: DCA variables for lateral, longitudinal and full manoeuvres.

7.3 Data compatibility analysis methods

In this Section the approaches employed for the DCA are introduced. In the presented methods the state space model of the system is described as

$$\begin{aligned} \dot{x}(t) &= f(x(t), u(t), \Theta) + \eta(t) \\ y(t) &= h(x(t), \Theta) \\ z(i) &= h(x(i), \Theta) + e(i), \quad i = 1, 2, \dots, N \end{aligned} \tag{7.6}$$

$$\begin{aligned} x &= [u \quad v \quad w \quad \phi \quad \theta \quad \psi \quad h]^T \\ u &= [a_x \quad a_y \quad a_z \quad p \quad q \quad r]^T \\ y &= [V \quad \beta \quad \alpha \quad \phi \quad \theta \quad \psi \quad h]^T \\ \Theta &= [b^T \quad \lambda^T]^T, \end{aligned}$$

where $\Theta \in \mathbb{R}^{n_\Theta}$ is the vector of unknown parameters, $x \in \mathbb{R}^n$ is the state vector, $u \in \mathbb{R}^{n_u}$ is the input vector, $y \in \mathbb{R}^{n_y}$ is the output vector, and $z \in \mathbb{R}^{n_y}$ is the measured output vector. Additive process and output noises $\eta(t) \sim p_\eta(\cdot)$ and $e(t) \sim p_e(\cdot)$ represent respectively the model uncertainty and output error measurements. The goal of each identification procedure is to find the value of the unknown parameter vector Θ that minimises a given cost function $J(\Theta, U_N, Z_N)$, where $U_N \in \mathbb{R}^{n_u \times N}$ and $Z_N \in \mathbb{R}^{n_y \times N}$ are input and output measurements coming from an experiment performed on the true system. The way the cost function is defined and minimised as well the assumptions introduced in the model (7.6) are the distinctive characteristics of each approach.

7.3.1 Output Error

The model (7.6) is a nonlinear function of the parameter vector, which can lead to significant difficulties in the formulation of the estimation problem. As described in Klein and Morelli [2006], these difficulties are circumvented in the Output Error (OE) method assuming that the dynamic system under study is deterministic, *i.e.*, the process is not affected by random noise ($\eta(t) = 0, \forall t$) while the output noise is assumed to be a zero mean gaussian noise $e(t) \sim p_e(\cdot) = \mathcal{N}(0, R)$. The parameters are estimated minimizing the cost function given by

$$\min_{\Theta} J = \frac{1}{2} \sum_{i=1}^N \nu^T(i; \Theta) R^{-1} \nu(i; \Theta), \quad (7.7)$$

where the error $\nu(i; \Theta)$ is defined as

$$\nu(i; \Theta) = z(i) - h(x(i), \Theta). \quad (7.8)$$

The optimisation problem (7.7) can be solved using a Newton-Raphson algorithm (see Nocedal and Wright [2006]).

A block diagram of the output error method is shown in Figure 7.1, where the parameter estimation is performed using the error ν and the sensitivity functions of the cost function to the parameters variation.

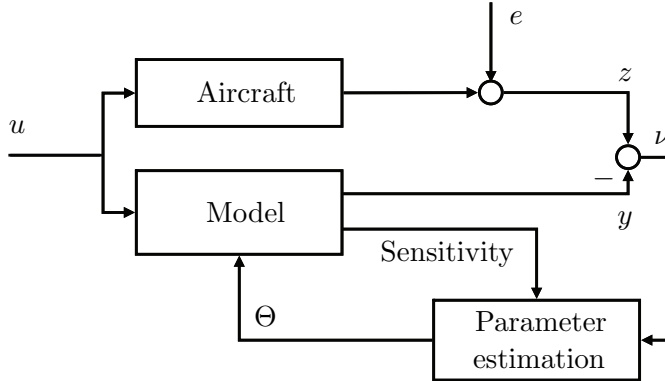


Figure 7.1: Block diagram of Output Error method.

This approach is very simple and the computational complexity is low even if the system is nonlinear, but the underlying assumption that the state equations are not affected by noise and uncertainty might be overly restrictive in practice. To avoid local minima a good initialization of the model parameters is required.

7.3.2 Unscented Kalman Filter

While the simplification introduced in the OE method is frequently adopted in practice, in view of the nonlinear nature of the system another approach is preferable whenever process noise driving the state equations is not negligible, *e.g.*, in the case of rotorcraft models in which higher order dynamics are not negligible and have to be approximated by means of a stochastic noise on the model states. The state and output equations for DCA are considered as in (7.6), where the dynamics of the state is affected by a zero-mean white Gaussian noise. In this context the problem of using an appropriate filtering scheme arises, thus a nonlinear version of the Kalman Filter (KF) is preferable. The classical choice considered in the literature to overcome the limitations of the linear KF is the Extended Kalman Filter (EKF), as shown in Grewal and Andrews [2001]. The EKF operates on the local linearisation of the nonlinear model computed in the neighborhood of the current state estimate. The EKF uses only the first order terms of the Taylor series expansion of the nonlinear functions; this can introduce large errors in the estimated second order statistics of the estimated state vector probability distribution. The proposed approach considers instead the Unscented Kalman Filter (UKF), which is an increasingly used nonlinear filtering scheme (see Julier and Uhlmann [1997] and Van der Merwe and Wan [2000]) based on the application of the so-called Unscented Transformation. Using such a filtering technique some of the approximation issues of the EKF can be addressed.

This is especially true when the models are highly nonlinear and the local linearity assumption breaks down, *i.e.*, the effects of the higher order terms of the Taylor series expansion become significant. Unlike the EKF, the UKF does not explicitly approximate the model equations; it uses the true nonlinear model (7.6), and approximates linearly the distribution of the state. The state is represented as a non Gaussian random variable, the distribution of which is modelled non parametrically using a set of points known as sigma points. Using the sigma points, *i.e.*, by propagating a suitable number of state realisations through the state and output equations, the mean and the covariance of the state can be captured in a consistent way, as proved in Julier and Uhlmann [1997]. However the favorable properties of the UKF are to be paid in terms of an increased computational cost. Finally, the uncertain parameters are estimated by minimizing the cost function (7.7) in which the error is defined as

$$\nu(i; \Theta) = z(i) - h(\hat{x}(i), \Theta), \quad (7.9)$$

where $\hat{x}(i)$ is the estimate of the state $x(i)$ for each time step i . A block diagram of the Unscented Kalman Filter method is shown in Figure 7.2,

where the sensitivity is the influence of the parameters variations on the outputs, as explained in Klein and Morelli [2006].

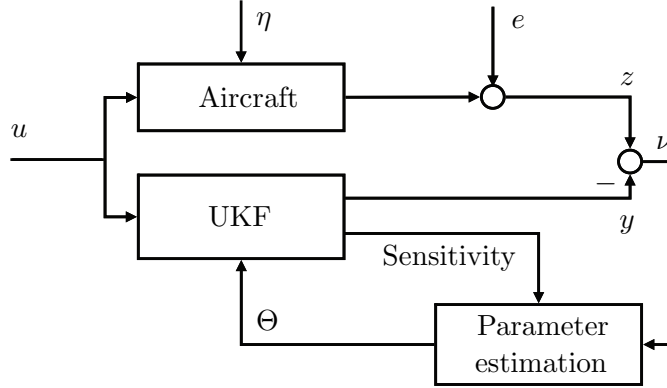


Figure 7.2: Block diagram of Unscented Kalman Filter method.

7.3.3 Expectation Maximisation with Particle Filter

The last approach here presented is the coupling between the Expectation Maximisation (EM) algorithm (see Dempster et al. [1977]), together with particle filtering (PF) (see Doucet et al. [2000, 2001]). Such an idea, investigated in Shön et al. [2011], Gopaluni [2008], has been shown as a promising methodology for the parameter estimation of nonlinear state space systems. The EM algorithm is designed to compute the Maximum-Likelihood (ML) estimate $\hat{\Theta}$ of a parameter vector Θ on the basis of an observed data set $Z_N = z(i) : i = 1, 2, \dots, N$. The likelihood of Z_N is $p_\Theta(Z|I)$ where I denotes a general information available. In other words, $p_\Theta(Z|I)$ is the probability to observe Z_N given the available information I and a suitable value for Θ . The EM algorithm aims at finding

$$\hat{\Theta} \in \{\Theta \in \mathbb{R}^p : p_\Theta(Z|I) \geq p_{\Theta_k}(Z|I) \quad \forall \Theta_k \in \mathbb{R}^p\}, \quad (7.10)$$

where $p_\Theta(\cdot|\cdot)$ is a conditional probability density function that is parameterised by Θ . The traditional approach to the problem is to recognise (7.10) as a particular case of a general class of optimization problems where the cost is smooth enough for a gradient-based search algorithm. The EM algorithm, instead of exploiting any smoothness of $p_\Theta(\cdot|\cdot)$, takes a different approach by utilising a fundamental characteristic of the cost function that arises by the virtue of it being a probability density function.

$$\int p_\Theta(Z|I)dZ = 1. \quad (7.11)$$



The EM method, using the property (7.11) together with Bayes' rule, introduces a function $Q(\cdot)$ that can be employed to infer the log-likelihood of the observed data Z_N , and thus retrieve information about the accuracy of the parameter estimate (see Shön et al. [2011] for further details). The function $Q(\cdot)$ is defined by the sum of three integrals, each one depending on the smoothing probabilities $p(x(i)|Z_N)$, *i.e.*, the probability to observe the state at a time step i given all the measurements Z_N . In the proposed framework, this probability distribution is retrieved by means of a Particle Filter (PF).

Particle filters are model-based state estimators useful in the case of strongly nonlinear models for which the posterior probability distribution cannot be satisfactorily approximated with a Gaussian one (*e.g.*, it is better described by a bi-modal distribution). The main idea underlying PF is to employ a Monte Carlo method for facing the problem of the state estimation and providing a description of the filtering and smoothing density probabilities, as explained in Doucet et al. [2000, 2001].

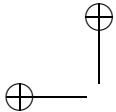
$$\begin{aligned}
 & \{x_k(i), k = 1 \dots N\} && \text{particles} \\
 & \{w_k(i), k = 1 \dots N\} && \text{weights} \\
 & p(x(i)|y_{1:i}) = && \text{approximation} \\
 & \sum_{k=1}^{n_p} w_k(i) \delta(x(i) - x_k(i)) &&
 \end{aligned}$$

At each time step i the state $x(i)$ is assumed to be distributed as a discrete random variable. Such a distribution is described by a set of n_p (randomly generated) particles $x_k(i)$ with associated weights $w_k(i)$. The particles are propagated according to the state equation (7.6) while the weights are updated at each step according to the output measurements $z(i)$. The interested reader can find more details concerning features and implementation issues of this method in Kitagawa [1996], Doucet et al. [2000, 2001], Arulampalam et al. [2002]. Once the descriptions of the posterior filtering and smoothing distributions are available, a numerical approximation $\hat{Q}(\cdot)$ of the function $Q(\cdot)$ can be computed and thus the EM algorithm can iteratively converge to the best approximation of Θ .

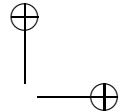
7.4 Experimental results

This Section presents the results obtained in the application of the presented approaches to the data consistency analysis on two sets of measurements coming from a small-scale quadrotor UAV. For each case the state estimation problem and the parameter identification are faced.





|



7.4.1 System description

The quadrotor used in this thesis is a modified version of the Mikrokopter platform, an open source project developed and distributed by HiSystems GmbH (Germany). The Mikrokopter consists of a frame composed by four tubes held together by a metal cross as shown in Figure 7.3, with the four motors placed at the end of the tubes. The onboard electronics are piled up at the centre of the cross in order to maintain a good mass distribution. The size of the quadrotor is approximately $45 \times 45 \times 20$ cm and its mass is about 1 kg (with battery). The quadrotor is powered with a Lithium-ion polymer battery (11.1 V, 2200 mAh) that guarantees an autonomy of about 15 minutes. The original design provides three electronic boards:

Flight-Ctrl It is the main board of the quadrotor. It includes the AVR Atmel 8-bit microcontroller (20 MHz), a set of three MEMS accelerometers as well three gyroscopes. This board is the flight controller, indeed it uses the measurements of the sensors and the command inputs taken through the receiver to set the motors speed rates in the proper way. The sensors outputs are sampled using the internal ADC with a 10 bits resolution.

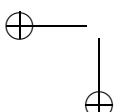
BL-Ctrl (x4) It is the driver of the motor. The microcontroller mounted on this board is an AVR Atmel 8-bit (8MHz) and it is dedicated to the generation of the PWM signal in order to control the motor angular rate according to the set-point communicated through the Inter Integrated Circuit (I^2C) bus by the Flight-Ctrl board. It is able to provide up to 5 A at 15 V.

Navi-Ctrl It is dedicated to record the flight data. This board mounts an AVR Atmel 16-bit microcontroller (25 MHz) and it communicates with the Flight-Ctrl through the Serial Peripherical Interface (*SPI*).

The original firmware has been modified in order to obtain flight data at a sampling frequency of 100 Hz. This data is stored in a microSD card during flight and downloaded for processing purposes after landing. As shown in Castillo et al. [2005], in the hover flying the quadrotor is an unstable system and so the identification tests must be performed in closed-loop.

7.4.2 Case study: rotational kinematics

For this case only the rotational kinematics has been taken into account, as the available experimental data regards rotational tests, *i.e.*, pitch, roll, and yaw manoeuvres. Looking at equations (7.2) the translational velocities do not appear, thus the translational kinematics (7.1) and air data



|

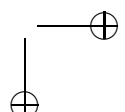




Figure 7.3: The Mikrokopter quadrotor used in this study.

measurements (7.3) can be disregarded. As noted in Section 7.2, the proposed approaches can be straightforwardly extended to the translational kinematics. The variables considered in this analysis are listed in Table 7.3. The states are a subset of the entire state vector, namely the Euler angles ϕ and θ . The output variables are the measured values of such angles ϕ_m and θ_m . The considered set of equations is (7.12), where the parameters that represent the measurement errors appear both in the state equations as well as in the output ones.

$$\begin{aligned}\dot{\phi} &= (p_m - b_p) + \tan \theta ((q_m - b_q) \sin \phi + (r_m - b_r) \cos \phi) \\ \dot{\theta} &= (q_m - b_q) \cos \phi - (r_m - b_r) \sin \phi \\ \phi_m &= (1 + \lambda_\phi)\phi + b_\phi \\ \theta_m &= (1 + \lambda_\theta)\theta + b_\theta\end{aligned}\tag{7.12}$$

7.4.3 Results

The comparison of the above described methods for DCA is performed upon a set of measurements coming from flight tests of the quadrotor in the hover condition. Two datasets are available in which different manoeuvres have been performed for system identification purposes. In view of the

| | |
|------------------------|--|
| State variables | ϕ and θ |
| Input variables | p_m, q_m and r_m |
| Output variables | ϕ_m and θ_m |
| Instrumentation errors | $b_p, b_q, b_r, \lambda_\phi, \lambda_\theta, b_\phi$, and b_θ |

Table 7.3: Variables involved in the rotational kinematic case.

application of time-domain identification methods (as in Chapter 9), the input signal adopted for identification experiments is the so-called 3211 piece-wise constant sequence. The numbers used in the designation refer to the relative time intervals between control reversals. As discussed in Hamel and Kaletka [1997], this input sequence, developed at the German Aerospace Center DLR, excites a wide frequency bandwidth within a short time period, so it is also suited for moderately unstable systems. Following the guideline in Klein and Morelli [2006], as the dominant dynamics of the quadrotor was expected to be around 5 rad/s, the duration of the second step has been set to half the period of the expected dominant mode. This choice led to a first step duration of 0.9 seconds, that is almost the maximum operable on a quadrotor without it flying too far away from trim. The amplitude of the steps has been chosen asymmetric in order to obtain tests ending with almost null velocity. For the purpose of the present study, two datasets are considered, corresponding to the application of 3211 sequences to the pitch and roll axes of the quadrotor:

- Pitch double 3211 – Test 1,
- Roll double 3211 – Test 2.

The available measurements are the angular rates (p, q, r) and the estimated attitude angles (ϕ, θ). The instrumental errors have been identified using the approaches introduced in the previous section: the Output Error method, the Unscented Kalman Filter, and Expectation Maximisation together with Particle Filtering.

Results provided by these methods, and with these datasets, show that a limited set of the unknown parameters listed in Table 7.3 are significant, *i.e.*, the scale factors λ_ϕ and λ_θ . The small influence of the biasing parameters depends on the limited duration (8 seconds) of the data set used for the identification, thus adding these parameters to the list of significant parameters increases the computational complexity without adding relevant information. Another important aspect is related to the specific manoeuvre performed in each experiment. The manoeuvre is a double 3211 performed respectively on the pitch and roll angles in the experiments. Such a manoeuvre excites the interested dynamics, without affecting the other ones.

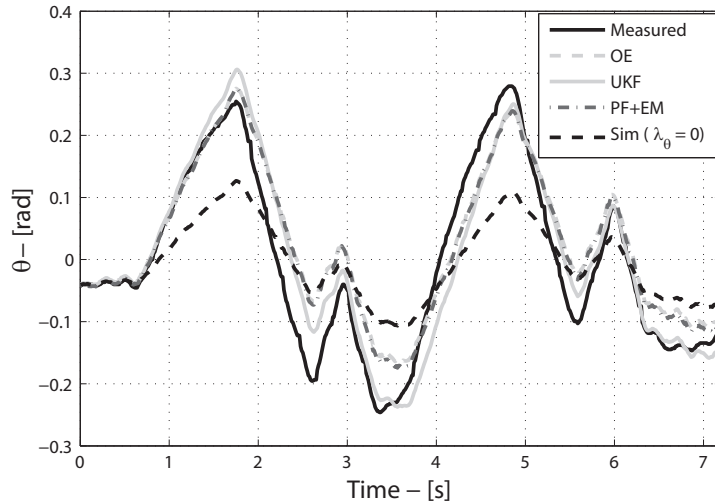


Figure 7.4: Measured, simulated (with $\lambda_\theta = 0$), and estimated outputs comparison – Test 1.

| | λ_θ | MSE |
|--------|------------------|----------------------|
| NONE: | 0 | $8.48 \cdot 10^{-2}$ |
| OE: | 0.8872 | $5.66 \cdot 10^{-2}$ |
| UKF: | 1.1653 | $4.64 \cdot 10^{-2}$ |
| PF+EM: | 0.9176 | $5.38 \cdot 10^{-2}$ |

Table 7.4: Experiment Test 1 – identified parameter

For this reason when using the first data set (Test 1) the pitch dynamics is the one mainly excited, thus the λ_θ parameter can be identified; for the same reason the λ_ϕ parameter can be better identified when using the second data set in which the roll dynamics is excited. The results coming from the identification of such parameters with the proposed approaches are summarized in Tables 7.4 and 7.5.

Results listed in Tables 7.4 and 7.5 show that there is a good agreement between the parameter estimation procedures. In order to compare the results obtained with the proposed approaches the Mean Square Error (MSE) is used as defined in (7.13),

$$MSE = \sqrt{\frac{1}{T} \sum_{i=1}^T \nu(i)^2}, \quad (7.13)$$

where $\nu(i)$ is defined as in (7.8) for the OE method and as in (7.9) for the UKF and the PF+EM methods. All methods provide good parameter

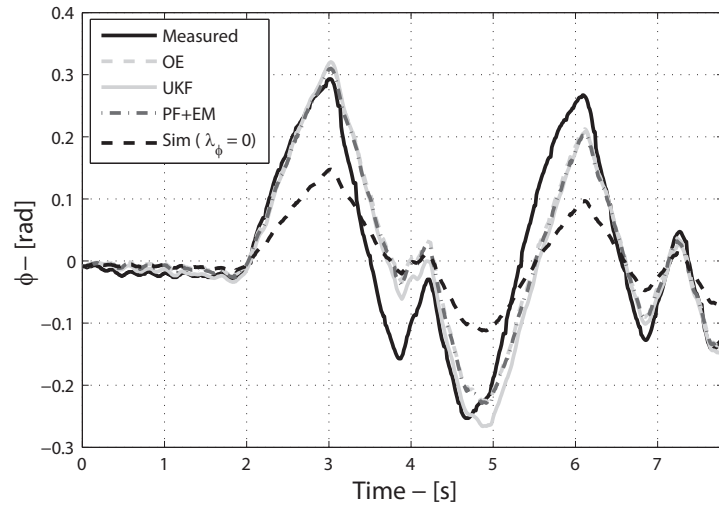


Figure 7.5: Measured, simulated (with $\lambda_\phi = 0$), and estimated outputs comparison – Test 2.

| | λ_ϕ | MSE |
|--------|----------------|----------------------|
| NONE: | 0 | $8.37 \cdot 10^{-2}$ |
| OE: | 1.0989 | $5.22 \cdot 10^{-2}$ |
| UKF: | 1.1510 | $5.18 \cdot 10^{-2}$ |
| PF+EM: | 1.0582 | $5.16 \cdot 10^{-2}$ |

Table 7.5: Experiment Test 2 – identified parameter

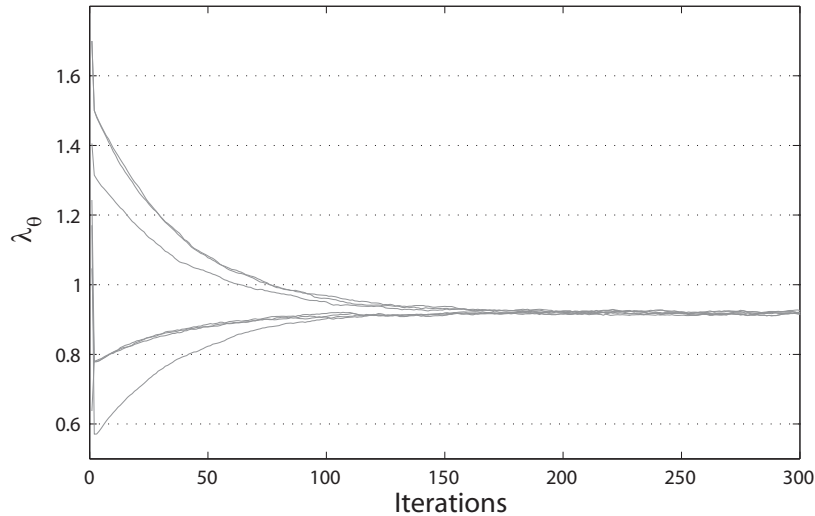


Figure 7.6: Example of different identification experiments for the dataset Test 1. Identified parameter λ_θ .

estimates since in each case the MSE is reduced with respect to the case in which the parameter is set to zero. In Figure 7.4 a comparison between the measured output and the estimated outputs using the proposed approaches is shown, for Test 1. In this case the UKF method outperforms the other two methods in the fitting of the output data. The same comparison is shown in Figure 7.5 where the Test 2 is considered. In this case the proposed approaches provide comparable results. It is clear that in these cases the instrumental errors play a relevant role, thus they have to be estimated with one of the proposed approaches in order to provide consistent datasets to further system identification stages. Due to the noisy data the UKF and the PF+EM methods provide better results than the OE method, particularly in Test 1.

Remark. Figure 7.6 shows the results of the identification of the scale factor affecting the measure of the θ angle (namely λ_θ) in Test 1 with the PF based approach. In this Figure, several identification experiments are reported where the initial guess of the parameter λ_θ is randomly changed; in all the experiments the same asymptotic value for the estimate is reached. Figure 7.7 shows similar results when the estimated parameter is λ_ϕ using the Test 2 dataset. Also in this case, starting from different assumptions on the initial value of λ_ϕ , the method converges to a unique value.

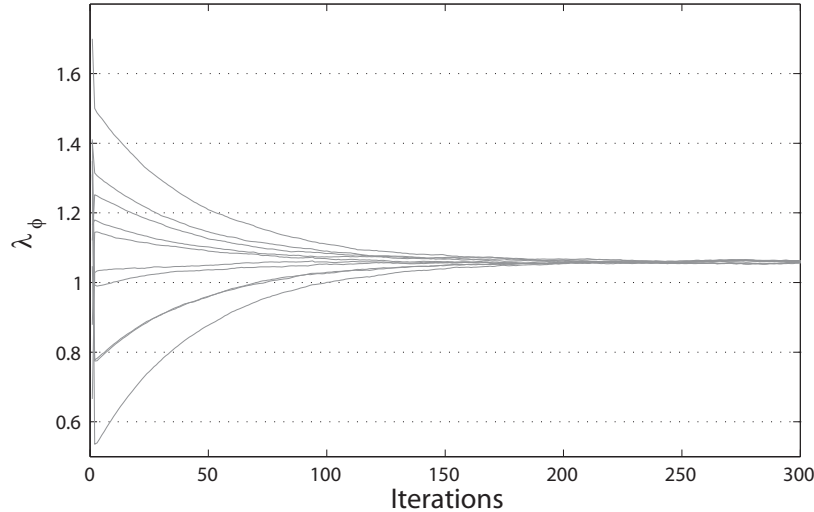
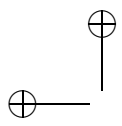


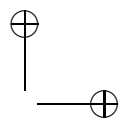
Figure 7.7: Example of different identification experiments for the dataset Test 2. Identified parameter λ_ϕ .

7.5 Conclusions

For system identification purposes, all the possible error sources introduced by the sensors have to be deleted, otherwise the identification procedure may introduce significant errors. Data compatibility analysis has been used as a methodology that aims at cleaning up the measured data by the systematic measurements errors. It has been shown that such a method can be reformulated as the parametric estimation of a nonlinear system. In this Chapter such a problem has been addressed with innovative approaches: Unscented Kalman filter and Expectation Maximisation together with particle filter. The proposed approaches have been compared with one classic solution in the context of DCA analysis (*i.e.*, the output error method). The comparison has been performed upon a set of measurements coming from an experimental setup: a small scale quadrotor Unmanned Aerial Vehicle. Even in this simple case, the results suggest that the proposed approaches give better results than the classical one, since they are able to manage the nonlinearities of the model and noisy measurements data in a more accurate way.

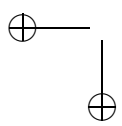


|

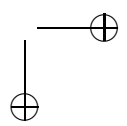


—

—



|



CHAPTER EIGHT

HELICOPTER DYNAMICS IDENTIFICATION: BLACK-BOX AND GRAY-BOX MODELLING

In this Chapter a first application is discussed. The continuous-time predictor based subspace algorithm CT-PBSIDO_o presented in Chapter 1 is proposed as a suitable method for time-domain continuous-time identification of rotorcraft dynamics. Besides starting from the black-box model the parameters of the BO-105 linear model are found using the approach presented in Chapter 5. The performance of the proposed techniques, which can deal with data generated under feedback, are illustrated by means of simulation results.

8.1 Introduction

The derivation of accurate dynamic models for helicopter aeromechanics is becoming more and more important, as progressively stringent requirements are being imposed on rotorcraft control systems: as the required control bandwidth increases, accurate models become a vital part of the design problem. In this respect, system identification has been known for a long time as a viable approach to the derivation of control-oriented dynamic models in the rotorcraft field (see for example the recent books Tischler and Remple [2006], Jategaonkar [2006] and the references therein).

Recently, see Li and Postlethwaite [2011], the interest in SMI for helicopter model identification has been somewhat revived and the performance of subspace methods has been demonstrated on flight test data. However, so far only methods and tools which go back 10 to 15 years in the SMI literature (such as the MOESP algorithm of Verhaegen [1994] and the bootstrap-based method for uncertainty analysis of Bittanti and Lovera [2000]) have been



considered. Therefore, the further potential benefits offered by the latest developments in the field have not been fully exploited. In view of the above discussion, this Chapter has the initial objective to illustrate the achievable model accuracy, using the CT-PBSIDO_o algorithm, by means of simulation results for a full-scale helicopter (previously presented in Bergamasco and Lovera [2011c]). As second goal of this Chapter, the parameters of the gray-box model of the BO-105 are successfully identified using the approach described in Chapter 5.

The Chapter is organised as follows. In Section 8.2 the problem statement is given. Section 8.3 gives an introduction of the BO-105 simulator. Finally, some simulation results are presented in Section 8.4 to illustrate the performance of the considered methods.

8.2 Black-box and gray-box modelling of the helicopter dynamics

In order to describe the dynamics of a rotorcraft in all possible flight envelope a nonlinear model should be taken into account. Unfortunately the use of this kind of models has some drawbacks. First of all a nonlinear model can be unsuitable for controller design. It is dependent on the physical parameters; most of the physical parameters are estimated using certain off-line procedures that can be long and expensive, as emphasized in Tischler and Remple [2006]. The resulting model can still describe the helicopter dynamics in an unsatisfactory way, therefore *a-posteriori* parameters tuning procedure based on flight-data is required.

From a controller design point of view a linear model derived directly from the flight-data is more suitable than the physical nonlinear model. Most rotorcraft vehicles are open-loop unstable and so closed-loop identification techniques are needed. Continuous-time identification techniques are preferable since the community wants continuous-time models. In the light of all these reasons, it is clear that the CT-PBSID_o algorithm can be an excellent way to provide a linear time-invariant continuous-time system suitable for control design, as defined in (1.4), since it overcomes all the described drawbacks of the nonlinear modeling. The system (1.4) describes a limited flight envelope, *i.e.*, the wind speed is assumed constant and the attitude angles vary around the trim values.

Another way to describe the system is exploiting the model structure by means of a gray-box model. In this case the problem is to provide an estimate of the parameter vector θ , defined in Chapter 5.2, on the basis of the identified black-box model.



As in Chapter 1, assume that a dataset $\{u(t_i), y(t_i)\}$, $i \in [1, N]$ of sampled input/output data (possibly associated with a non equidistant sequence of sampling instants) obtained from system (1.4) is available. Then, the first problem is to provide estimates of the state space matrices A , B , C , and D of the unstructured model on the basis of the available data. The second problem considered therein is the estimation of the parameters of the structured model.

Note that unlike most identification techniques, in this setting incorrelation between u and w, v is not required, so that this approach is viable also for systems operating under feedback as in the helicopter case.

8.3 BO-105 simulation model

The BO-105 helicopter is considered. Possibly it is the most studied helicopter in the rotorcraft system identification literature. The BO-105 is a light, twin-engine, multi-purpose utility helicopter shown in Figure 8.1.



Figure 8.1: Bölkow BO-105 (courtesy of André Karwath).

It is considered in forward flight at 80 knots, a flight condition which corresponds to unstable dynamics, with the aim of demonstrating the identification of a nine-DOF state-space model with test data extracted from a simulator based on the nine-DOF model from Tischler and Cauffman [1992]. As described in the cited reference, the model includes the classical six-DOF and some additional states to account for some additional effects, namely:

- the BO-105 exhibits highly coupled body-roll and rotor-flapping responses; their interaction is represented in the model with a dynamic



equation that describes the flapping dynamics using the cyclic controls;

- a second order dipole is appended to the model of roll rate response to lateral stick in order to account for the effect of lead-lag rotor dynamics.

Therefore, the simulator includes a nine-DOF linear model including the six-DOF quasi steady dynamics, the flapping equations and the lead-lag dynamics modelled with a complex dipole. Delays at the input of the model are also taken into account in the simulation, though they are not estimated. The state vector and the trim values are

$$x = [u \ v \ w \ p \ q \ r \ \phi \ \vartheta \ a_{1s} \ b_{1s} \ x_1 \ x_2]$$

and, respectively,

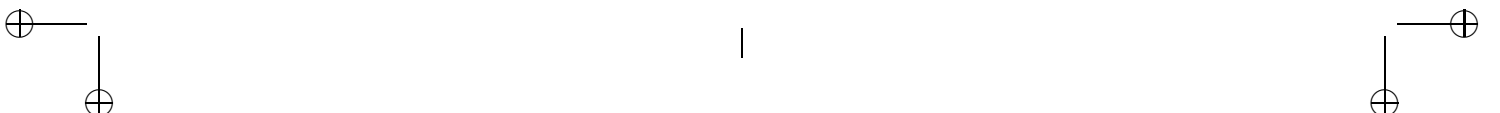
$$u_0 = 40 \text{ m/s}, \quad v_0 = 3 \text{ m/s}, \quad w_0 = -5 \text{ m/s}, \quad \phi_0 = 0 \text{ rad}, \quad \vartheta_0 = 0 \text{ rad}. \quad (8.1)$$

In details, the state vector includes the longitudinal flapping a_{1s} , the lateral flapping b_{1s} and two state variables x_1 and x_2 , coming from the lead-lag dynamics complex dipole. The corresponding dynamics equations are

$$\begin{aligned} \dot{u} &= X_u u + X_w w + X_p p + (X_q - w_0)q + v_0 r - g\vartheta + X_{\delta_{lon}} \delta_{lon} + X_{\delta_{col}} \delta_{col} \\ \dot{v} &= Y_v v + Y_w w + (Y_p + w_0)p + Y_q q + (Y_r - u_0)r - g\phi + Y_{\delta_{lat}} \delta_{lat} + Y_{\delta_{col}} \delta_{col} \\ \dot{w} &= Z_u u + Z_w w + (Z_p - v_0)p + u_0 q + Z_{\delta_{col}} \delta_{col} \\ \dot{p} &= L_u u + L_v v + L_w w + L_q q + L_{\delta_{b_{1s}}} b_{1s} + L_{\delta_{lon}} \delta_{lon} + L_{\delta_{ped}} \delta_{ped} + L_{\delta_{col}} \delta_{col} \\ \dot{q} &= M_v v + M_w w + M_p p + M_r r + M_{\delta_{a_{1s}}} a_{1s} + M_{\delta_{ped}} \delta_{ped} + M_{\delta_{col}} \delta_{col} \\ \dot{r} &= N_v v + N_w w + N_q q + N_r r + N_{\delta_{lon}} \delta_{lon} + N_{\delta_{lat}} \delta_{lat} + N_{\delta_{ped}} \delta_{ped} + N_{\delta_{col}} \delta_{col} \\ \dot{\phi} &= p \\ \dot{\vartheta} &= q \\ \dot{a}_{1s} &= -q - \frac{1}{\tau_f} a_{1s} + \frac{K_{a_{1s}}}{\tau_f} \delta_{lon}, \\ \dot{b}_{1s} &= -p - \frac{1}{\tau_f} b_{1s} + \frac{K_{b_{1s}}}{\tau_f} \delta_{lat} + K_{x_1} x_1 + K_{x_2} x_2 \\ \dot{x}_1 &= x_2 \\ \dot{x}_2 &= C_1 x_1 + C_2 x_2 + \delta_{lat}. \end{aligned} \quad (8.2)$$

Finally, the output vector is

$$y = [u \ v \ w \ p \ q \ r \ a_x \ a_y \ a_z \ \phi \ \vartheta],$$



where

$$\begin{aligned} a_x &= \dot{u} + w_0 q - v_0 r + g\dot{\theta} \\ a_y &= \dot{v} - w_0 p + u_0 r - g\dot{\phi} \\ a_z &= \dot{w} + v_0 p - u_0 q, \end{aligned}$$

i.e., the state variables related to quasi-steady dynamics and the linear accelerations are measured. Considering (8.2) the parameter vector θ contains the stability derivatives, the control derivatives, the flapping and lead-lag rotor dynamics parameters for a total of 47 parameters.

8.4 Model identification results

The identification experiment is performed in closed-loop because of the instability of the model, with the helicopter operating under feedback from a stabilising LQG controller. In the experiment, additive perturbations have been applied to the input variables ($\delta_{lat}, \delta_{lon}, \delta_{ped}, \delta_{col}$) computed by the controller; in particular, all the channels have been excited in the same experiment with pseudorandom binary signals with a duration of 60 s and a dwell time of 0.8 s. The perturbation of the control inputs has a 1% amplitude and the sampling time is 0.008s. The parameters of the CT-PBSID_o have been chosen as $p = 40$ and $a = 45$.

The obtained results are illustrated in Table 8.1.

| | Simulator | | | | Identified Model (CT-PBSID _o) | | | |
|--------------------|-----------|--------|--------|--------|---|--------|--------|--------|
| | Real | Imag | Omega | Zeta | Real | Imag | Omega | Zeta |
| Pitch phugoid | 0.119 | 0.278 | 0.302 | -0.394 | 0.119 | 0.278 | 0.302 | -0.394 |
| Dutch roll | -0.571 | 2.546 | 2.609 | 0.219 | -0.571 | 2.546 | 2.609 | 0.219 |
| Roll/flapping | -9.904 | 7.740 | 12.569 | 0.788 | -9.901 | 7.7399 | 12.568 | 0.788 |
| Lead-Lag | -0.868 | 15.567 | 15.592 | 0.0557 | -0.867 | 15.566 | 15.590 | 0.0556 |
| Spiral | -0.0510 | | | | -0.0507 | | | |
| Pitch ₁ | -0.448 | | | | -0.448 | | | |
| Pitch ₂ | -5.843 | | | | -5.844 | | | |
| Long. flapping | -15.930 | | | | -15.901 | | | |

Table 8.1: Comparison between simulator and black-box identified eigenvalues.

As can be seen from the Table the CT-PBSID_o algorithm is able to identify the dynamics of the system with a slight loss of accuracy at high frequency. Using the model estimated with the CT-PBSID_o algorithm a structured model is identified using the \mathcal{H}_∞ approach.

The study in the reconstruction of the structured state space representation given above has been carried out by applying the approach described in Chapter 5 to estimate the relevant parameters. In this example the relative errors, as defined in (5.13), of the estimated parameters in (8.2) are

below the 0.03%. It is clear from Table 8.2, where the eigenvalues of the real system and the identified gray-box model are shown, that using *a-priori* information, *i.e.*, the model structure, the estimation accuracy increases.

| | Simulator | | | | Identified Model (Gray-box) | | | |
|--------------------|-----------|--------|--------|--------|-----------------------------|--------|--------|--------|
| | Real | Imag | Omega | Zeta | Real | Imag | Omega | Zeta |
| Pitch phugoid | 0.119 | 0.278 | 0.302 | -0.394 | 0.119 | 0.278 | 0.302 | -0.394 |
| Dutch roll | -0.571 | 2.546 | 2.609 | 0.219 | -0.571 | 2.546 | 2.609 | 0.219 |
| Roll/flapping | -9.904 | 7.740 | 12.569 | 0.788 | -9.903 | 7.740 | 12.568 | 0.788 |
| Lead-Lag | -0.868 | 15.567 | 15.592 | 0.0557 | -0.868 | 15.566 | 15.590 | 0.557 |
| Spiral | -0.0510 | | | | -0.0507 | | | |
| Pitch ₁ | -0.448 | | | | -0.448 | | | |
| Pitch ₂ | -5.843 | | | | -5.843 | | | |
| Long. flapping | -15.930 | | | | -15.929 | | | |

Table 8.2: Comparison between simulator and gray-box identified eigenvalues.

Finally, a time-domain validation of the identified models has been also carried out, by measuring the accuracy of the models in response to a doublet input signal on each input channel. The input sequence used in the validation experiment is illustrated in Figure 8.2, while the time history for two of the outputs (u and w) is presented in Figure 8.3. Again, even though the open-loop system is unstable, the simulated outputs obtained from the identified models (dashed lines: black-box; cross: gray-box) match very well the ones computed from the simulation model (solid lines).

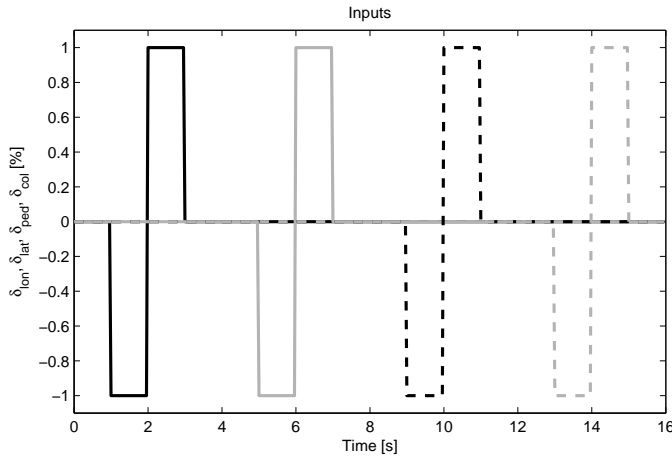


Figure 8.2: Doublet input signal used for model validation.

In quantitative terms, considering the root mean square error, defined

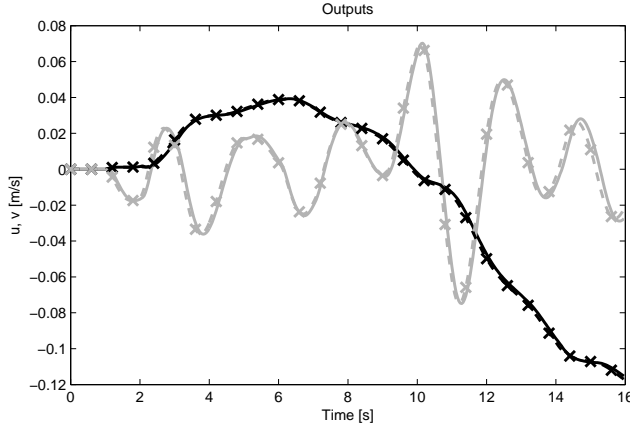


Figure 8.3: Doublet output signals (real: solid line; black-box: dashed line; gray-box: cross).

as

$$RMS = \sqrt{\frac{1}{N} \sum_{i=1}^N (y(i) - \hat{y}(i))^2}, \quad (8.3)$$

where y is the real output and \hat{y} is the estimated one. The RMS values are below 0.01 on all the considered output variables as shown in Table 8.3. Note that most of the error is due the unestimated input delays, as it clear in Figure 8.3.

| Output | $RMS_{CT-PBSID_o}$ | $RMS_{Gray-Box}$ |
|-------------|--------------------|------------------|
| u | 0.0013 | 0.0013 |
| v | 0.0044 | 0.0044 |
| w | 0.0026 | 0.0026 |
| p | 0.0002 | 0.0002 |
| q | 0.0003 | 0.0003 |
| r | 0.0003 | 0.0003 |
| a_x | 0.0013 | 0.0013 |
| a_y | 0.0017 | 0.0017 |
| a_z | 0.0077 | 0.0077 |
| ϕ | 0.0001 | 0.0001 |
| ϑ | 0.0001 | 0.0001 |

Table 8.3: Relative errors norm.

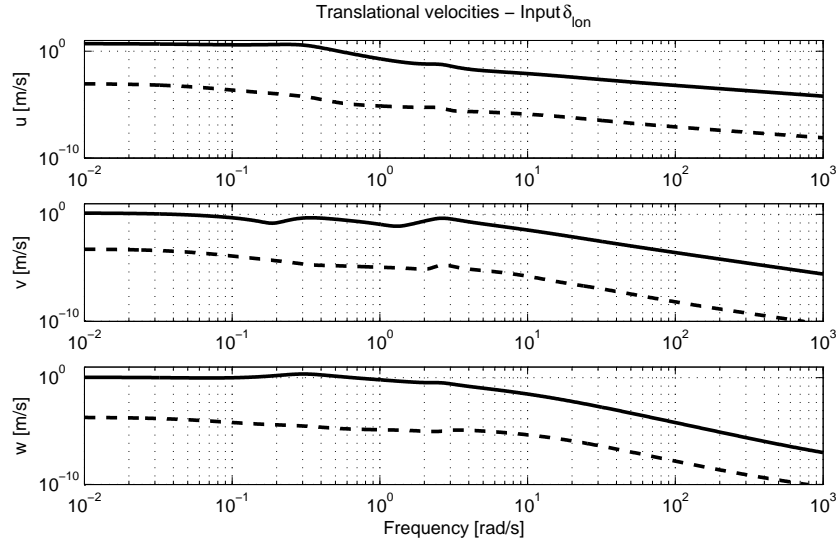


Figure 8.4: Frequency response from longitudinal input to linear velocities. (real: solid line; error: dashed line)

Finally, in Figures 8.4-8.19 the magnitude of the frequency response of the error transfer function defined as

$$E_s(s) = G_s(s; \theta^0) - G_s(s; \hat{\theta}),$$

is shown, where $G_s(s; \theta^0)$ is the real transfer function of the BO-105 and $G_s(s; \hat{\theta})$ is the gray-box estimated one. Note that the magnitude of the frequency response of the error is always several order of magnitude below the frequency response of the BO-105 simulation model.

8.5 Concluding remarks

Simulation results show that the CT-PBSID_o algorithm is viable for rotorcraft applications and can deal successfully with data generated during closed-loop experiments. It is also shown that the model obtained with the CT-PBSID_o algorithm results suitable to recover the parameters of the structured model of the BO-105 helicopter using an \mathcal{H}_∞ approach. In the next Chapters real flight data will be considered to underline the effectiveness of the CT-PBSID_o method for this kind of problem.



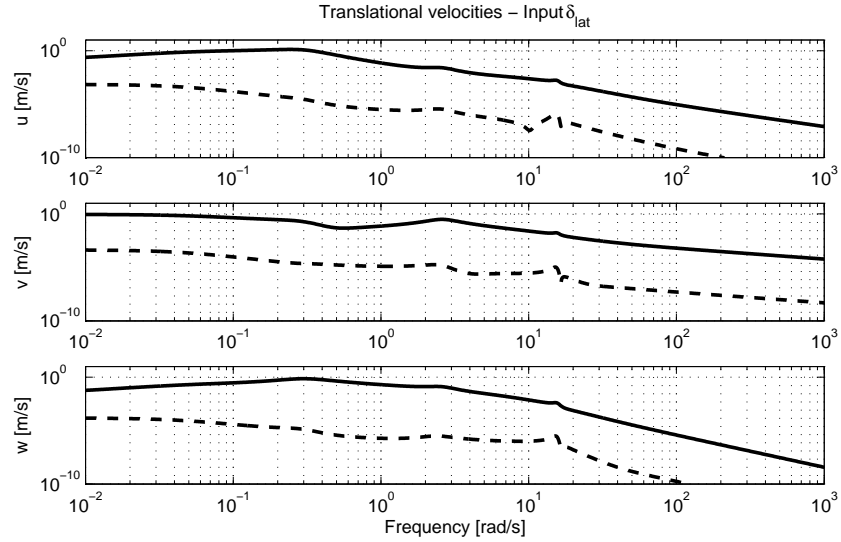


Figure 8.5: Frequency response from lateral cyclic input to linear velocities. (real: solid line; error: dashed line)

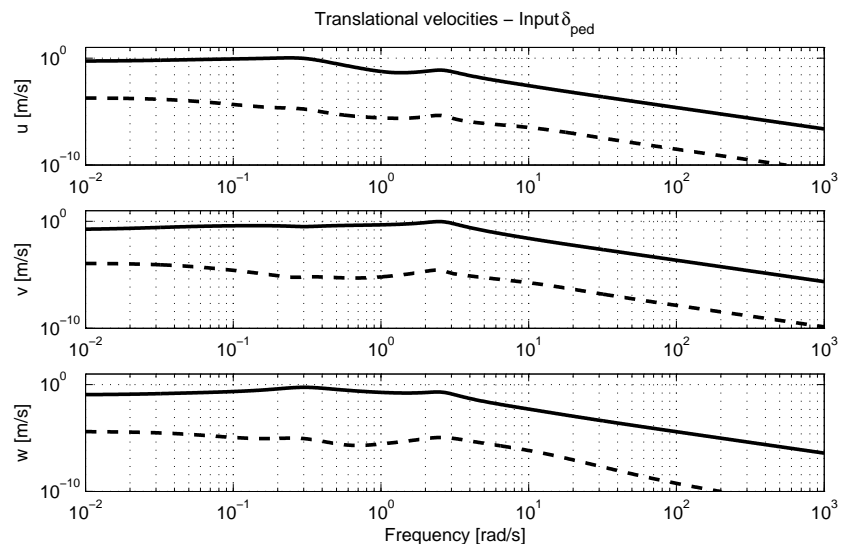


Figure 8.6: Frequency response from pedal cyclic input to linear velocities. (real: solid line; error: dashed line)



168 Chapter 8 Helicopter dynamics identification: black-box and gray-box modelling

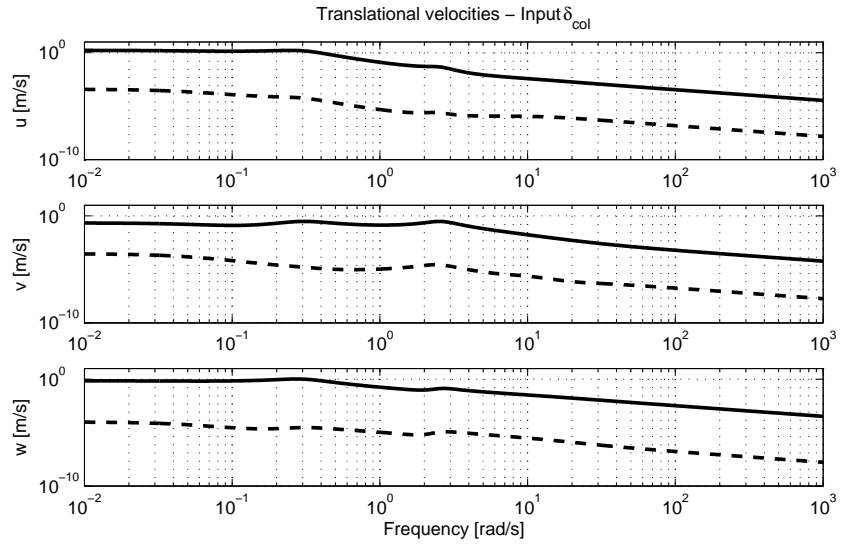


Figure 8.7: Frequency response from collective input to linear velocities. (real: solid line; error: dashed line)

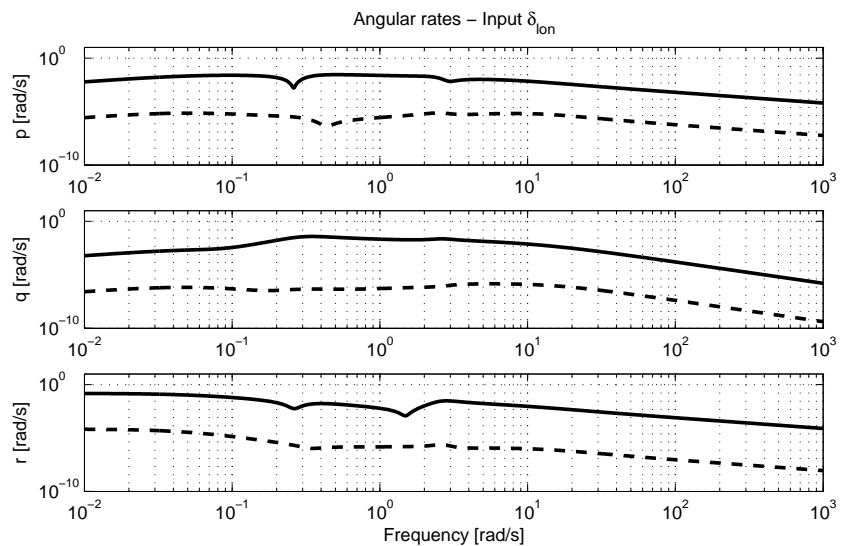
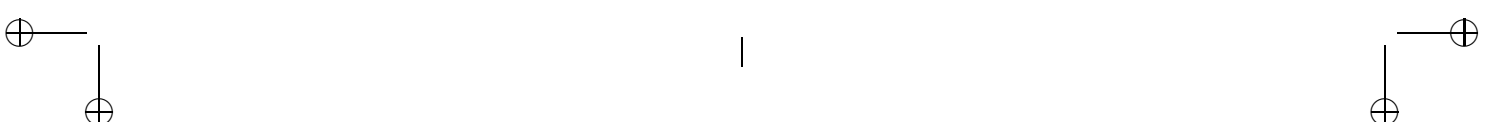


Figure 8.8: Frequency response from longitudinal input to angular velocities. (real: solid line; error: dashed line)



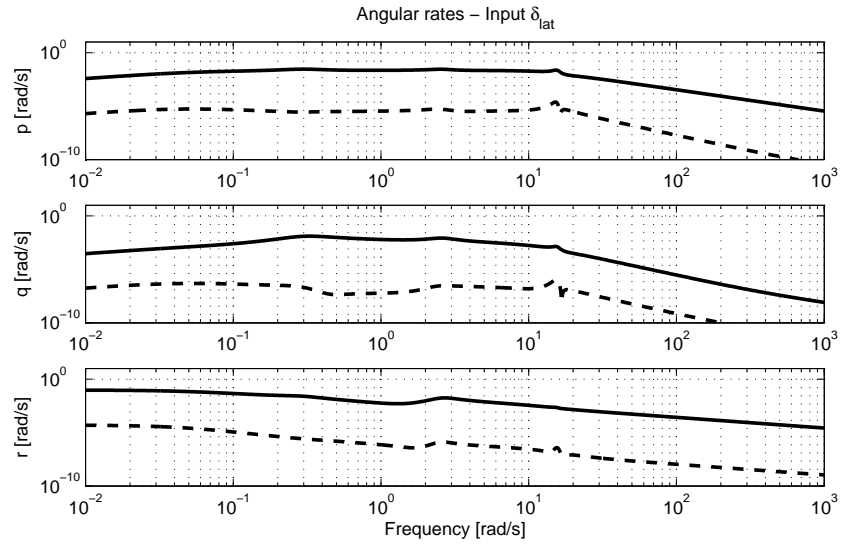


Figure 8.9: Frequency response from lateral cyclic input to angular velocities. (real: solid line; error: dashed line)

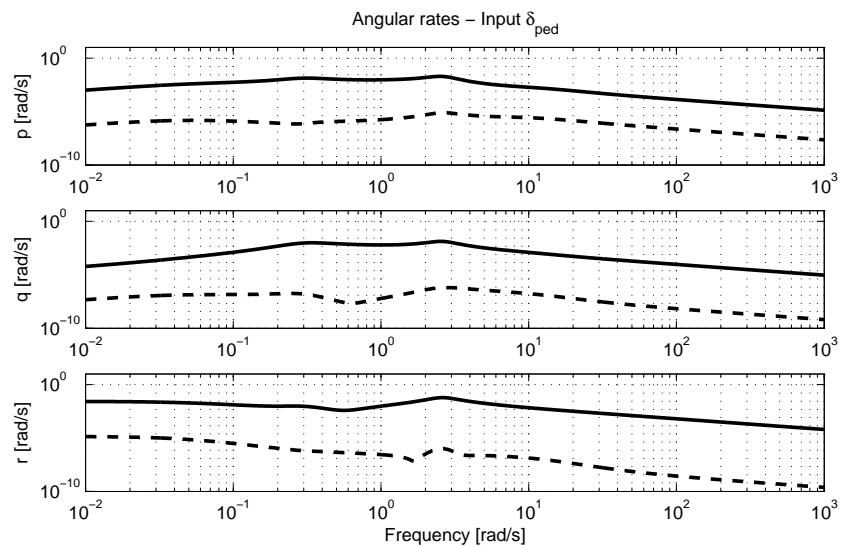


Figure 8.10: Frequency response from pedal cyclic input to angular velocities. (real: solid line; error: dashed line)



170 Chapter 8 Helicopter dynamics identification: black-box and gray-box modelling

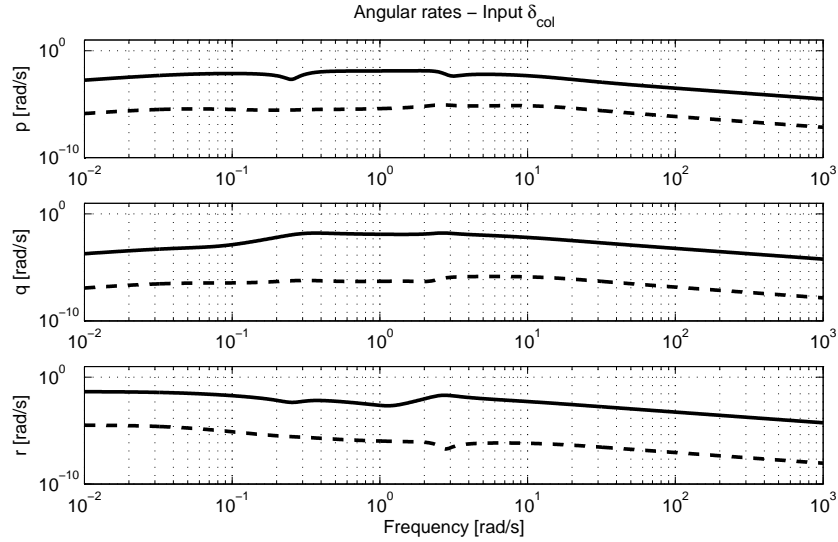


Figure 8.11: Frequency response from collective input to angular velocities. (real: solid line; error: dashed line)

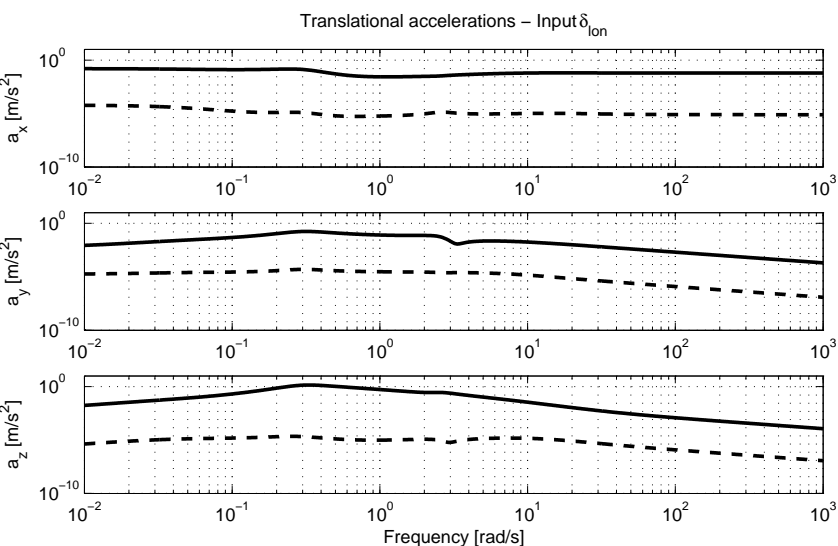


Figure 8.12: Frequency response from longitudinal input to linear accelerations. (real: solid line; error: dashed line)



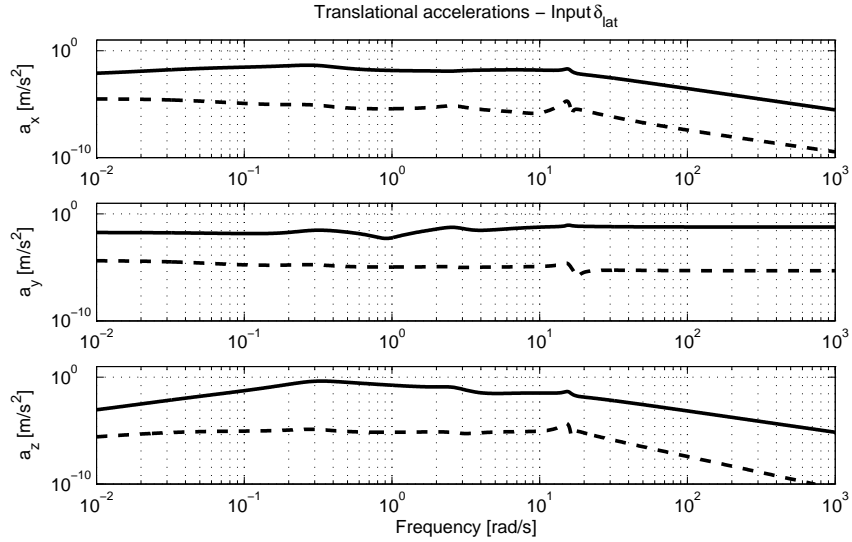


Figure 8.13: Frequency response from lateral cyclic input to linear accelerations. (real: solid line; error: dashed line)

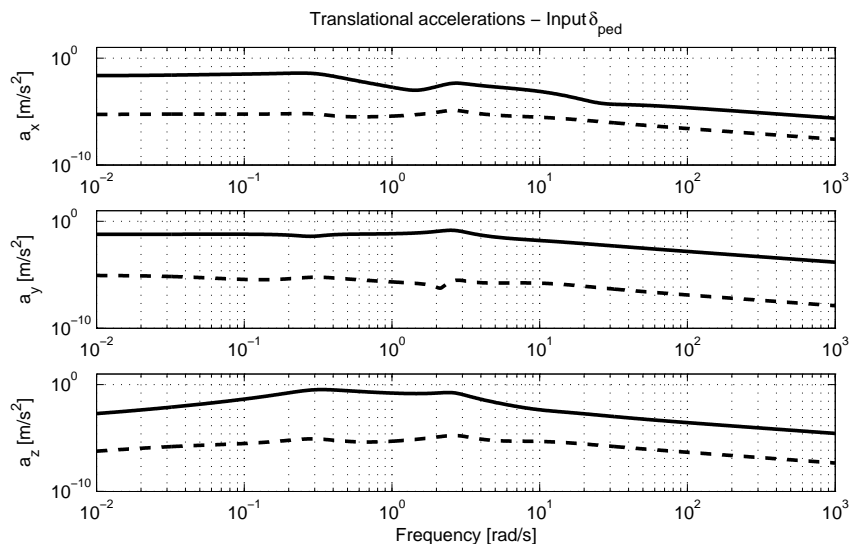


Figure 8.14: Frequency response from pedal cyclic input to linear accelerations. (real: solid line; error: dashed line)

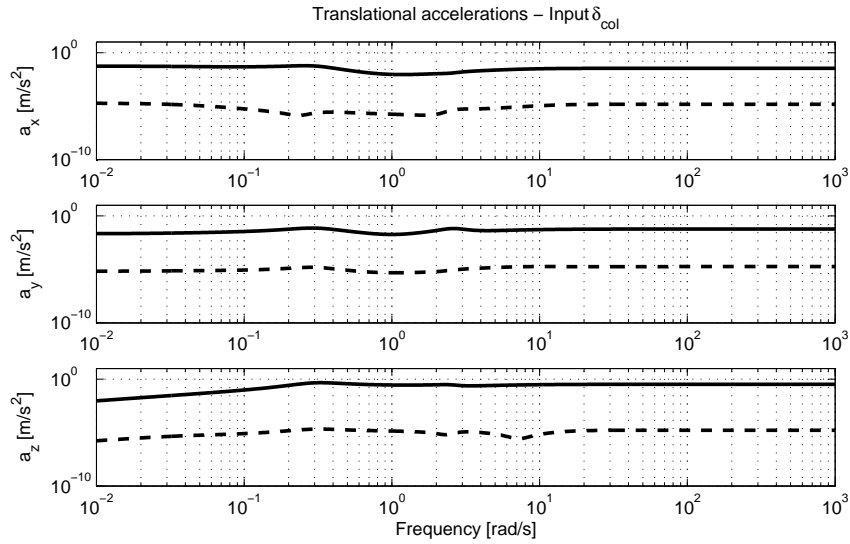


Figure 8.15: Frequency response from collective input to linear accelerations. (real: solid line; error: dashed line)

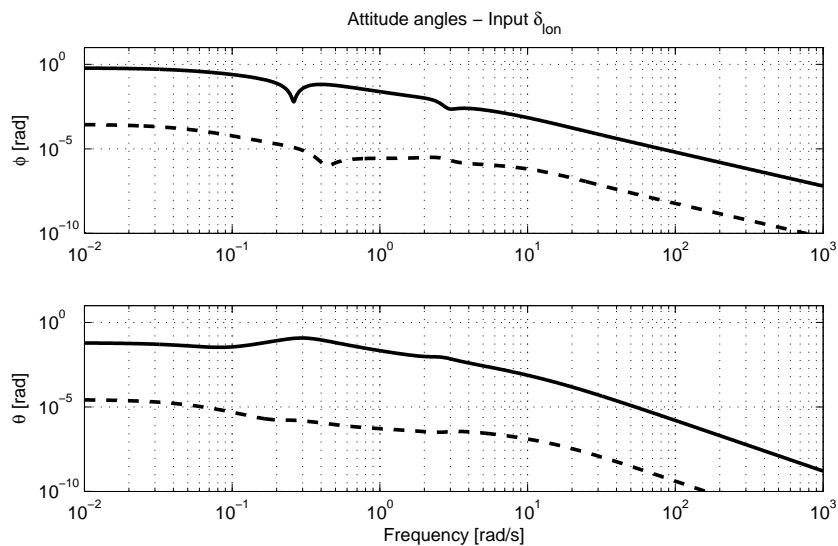


Figure 8.16: Frequency response from longitudinal input to attitude angles. (real: solid line; error: dashed line)

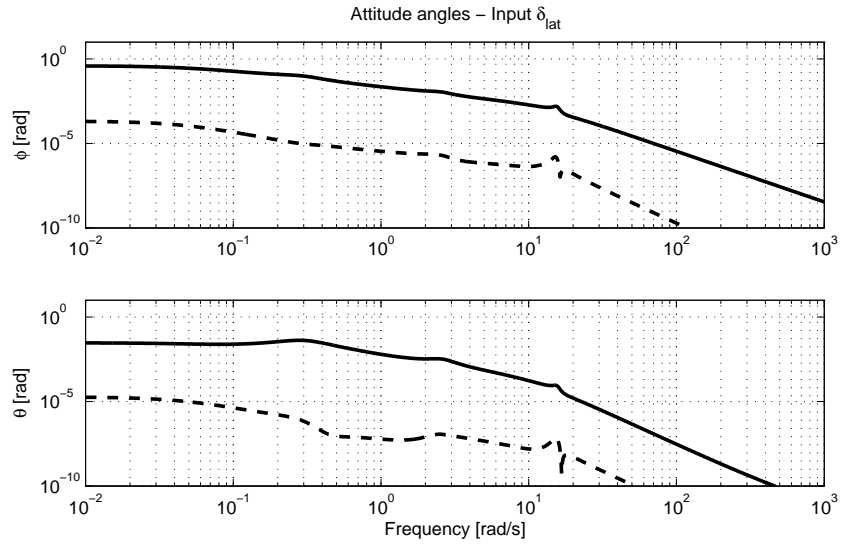
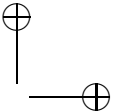
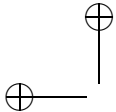


Figure 8.17: Frequency response from lateral cyclic input to attitude angles. (real: solid line; error: dashed line)

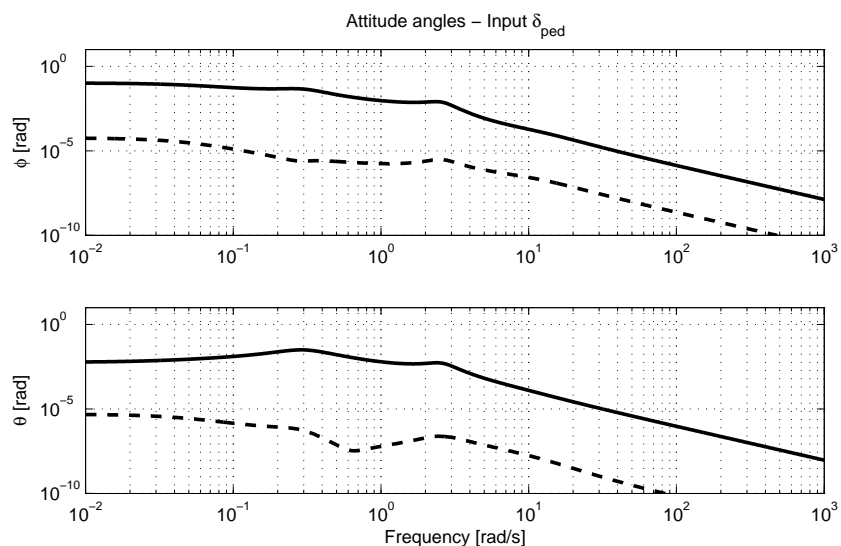
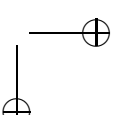
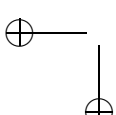
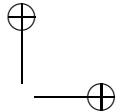
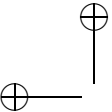


Figure 8.18: Frequency response from pedal cyclic input to attitude angles. (real: solid line; error: dashed line)





174 Chapter 8 Helicopter dynamics identification: black-box and gray-box modelling

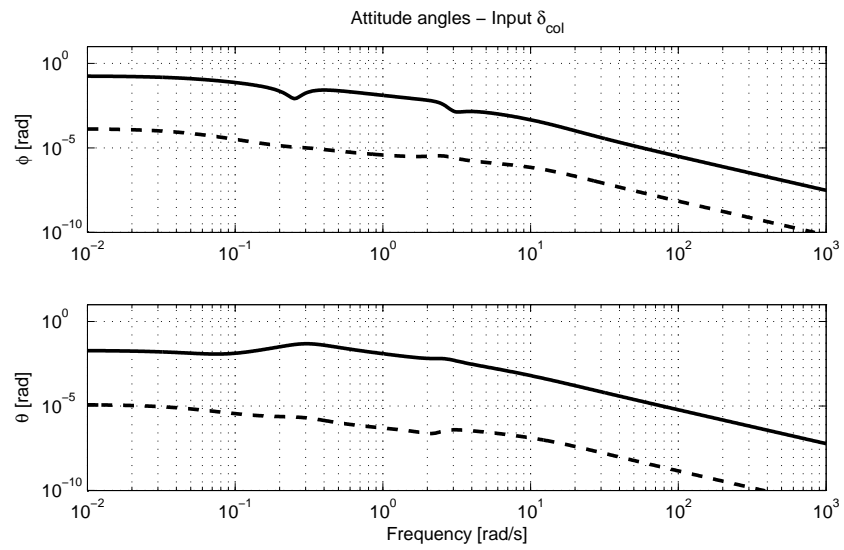
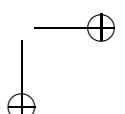
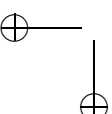


Figure 8.19: Frequency response from collective input to attitude angles. (real: solid line; error: dashed line)



CHAPTER
NINE

IDENTIFICATION OF LINEAR MODELS FOR THE DYNAMICS OF A HOVERING QUADROTOR

In this Chapter the problem of deriving continuous-time black-box models for the dynamics of a small-scale quadrotor helicopter is considered. More precisely, the continuous-time predictor-based subspace identification approach exposed in Chapter 1 and the model uncertainty estimation method introduced in Chapter 4 are adopted and the results obtained in an experimental study are presented and discussed.

9.1 Introduction

The quadrotor architecture is a very popular one for the development of rotorcraft UAV platforms (see, *e.g.*, Castillo et al. [2005], Bouabdallah et al. [2007] and the references therein), in view of its favorable dynamic characteristics (see Das et al. [2009]): indeed, although open-loop unstable, like most rotorcraft architectures, quadrotors exhibit a good degree of decoupling, which makes them easier to control. As discussed in, *e.g.*, Hamel et al. [2002], Pounds and Mahony [2009] and the references therein, mathematical models for the dynamics of quadrotors are easy to establish as far the kinematics and dynamics of linear and angular motion are concerned. In fact a significant portion of the literature dealing with quadrotor control is based on such models, probably also because of the elegant mathematical methods which can be deployed to design feedback controller on this basis. Unfortunately, characterising aerodynamic effects and additional dynamics such as, *e.g.*, the response of the controlled speed of the individual rotors, is far from trivial, and has led to the development of many approaches to the experimental characterisation of the dynamic response of the quadro-



tor. Broadly speaking, two classes of methods to deal with this problem can be defined. The first class of methods is based on the calibration of the parameters of detailed physical models, see for example Kim and Tilbury [2004], Derafa et al. [2006]. The second class of methods is based on a black-box identification approach and as such aims at extracting the information about the dynamics of the system directly (and solely) from measured input-output data (see for example La Civita et al. [2002], Heredia et al. [2008]). Note, in passing, that system identification has been known for a long time as a viable approach to the derivation of control-oriented dynamic models in the rotorcraft field (see for example the survey paper Hamel and Kaletka [1997], the recent books Tischler and Remple [2006], Jategaonkar [2006] and the references therein).

In view of the above discussion, the aim of this Chapter is to demonstrate by means of an experimental case study the applicability of SMI methods to the identification of a small-scale quadrotor helicopter. More precisely (see also the preliminary results presented in Sguanci et al. [2012], Bergamasco and Lovera [2013]), the continuous-time predictor-based subspace identification approach proposed in Chapter 4 is applied to flight data collected during dedicated identification experiments and a model for the hovering quadrotor is derived. Particular emphasis is placed on the analysis of the uncertainty associated with the identified model, both in the frequency domain and in the time domain, which provides useful information in a control design perspective.

The Chapter is organised as follows. The approach followed in the identification and validation experiments is presented in Section 9.2. The results obtained in the estimation of linear models for the hovering quadrotor and in the analysis of their characteristics are presented in Section 9.3.

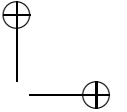
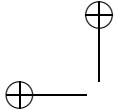
9.2 Identification-oriented quadrotor flight testing

The aim of this Section is to provide some information about the identification and validation experiments which have been carried out to characterise the dynamic response of the hovering Mikrokopter. The experimental set-up used in this study has been presented in Section 7.4.1.

9.2.1 Input-output variables selection

In this Chapter, the following input and output variables are considered. Concerning the inputs, since, as is well known, the forces and moments generated by the four rotors are quadratic functions of the rotors angular rates (see, *e.g.*, Castillo et al. [2005]), a change of variables is usually adopted





to define control inputs which enter linearly the equations of motion, namely

$$u = \begin{bmatrix} u_{col} \\ u_{lon} \\ u_{lat} \\ u_{ped} \end{bmatrix} = \begin{bmatrix} \Omega_1^2 + \Omega_2^2 + \Omega_3^2 + \Omega_4^2 \\ \Omega_4^2 - \Omega_2^2 \\ \Omega_3^2 - \Omega_1^2 \\ \Omega_2^2 + \Omega_4^2 - \Omega_1^2 - \Omega_3^2 \end{bmatrix},$$

where Ω_i , $i = 1, \dots, 4$ are the angular rates of the four rotors, u_{col} can be interpreted as a force along the vertical body axis and u_{lon} , u_{lat} and u_{ped} as, respectively, a pitching, rolling and a yawing moment around the body axes. The output vector, on the other hand, includes the measurements provided by the available inertial sensors, *i.e.*, $y = [a_x \ a_y \ a_z \ p \ q \ r]^T$, where a_x , a_y and a_z are the measurements of the acceleration along the three body axes and p , q and r are, respectively, the measurements of the components of the quadrotor's angular rate, again expressed in the body frame shown in Figure 9.1. Note that the single arrow indicates a linear movement/acceleration/force, while the double arrow is used for the angular quantities with the right-hand-rule.

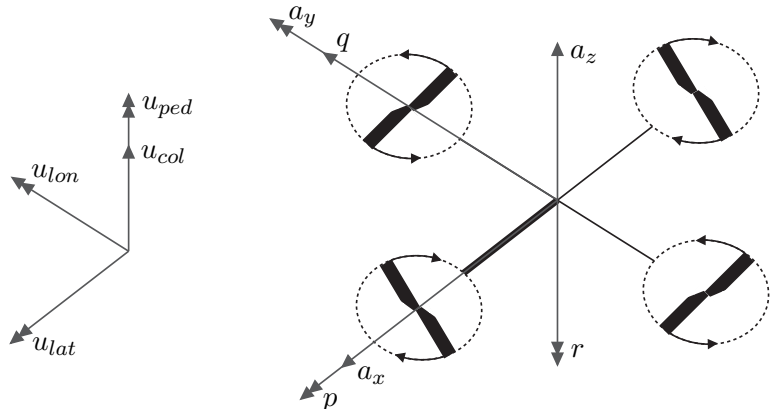
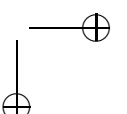
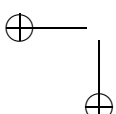


Figure 9.1: Reference frames of the inputs and the sensors (body frame).

9.2.2 Identification experiments

The problem of defining suitable approaches to the experimental testing of a rotorcraft platform has been studied extensively in the literature of piloted rotorcraft, see for example Hamel and Kaletka [1997], Tischler and Remple [2006]. The key aspect when planning the class of inputs to be applied to the vehicle is the domain in which data will be processed in the identification procedure. Indeed, for frequency-domain approaches such as the ones proposed in Tischler and Remple [2006] periodic excitation is desirable (*e.g.*,



frequency sweeps, so as to minimise leakage in the computation of frequency spectra). For time-domain identification, on the contrary, this requirement is not necessary so it is possible to employ input sequences which can excite a broad range of frequencies in shorter experiments than swept sines or multi-sines. Concerning the execution of identification experiments in flight, they can be carried out either manually, with the pilot exciting the dynamics of the helicopter using the remote control, or automatically, by implementing on-board functions to generate the input sequences for the experiments. In the case of a small-scale helicopter manual excitation is not sufficiently fast, so an automatic command generation function has been implemented.

In view of the application of the CT-PBSID_o method, the input signal adopted for identification experiments is the so-called 3211 piece-wise constant sequence. The numbers used in the designation refer to the relative time intervals between control reversals. As discussed in Hamel and Kaletka [1997], this input sequence, developed at the German Aerospace Center DLR, excites a wide frequency band within a short time period, so it is also suited for moderately unstable systems. Following the guideline in Klein and Morelli [2006], as the dominant dynamics of the quadrotor was expected to be around 5 rad/s, the duration of the second step has been set to half the period of the expected dominant mode. This choice led to a first step duration of 0.9 seconds, that is almost the maximum operable on a quadrotor without it flying too far away from trim. The amplitude of the steps has been chosen asymmetric in order to obtain tests ending with almost null velocity. This maneuver has been repeated twice in order to get more data.

The input signal used for the validation test is a so-called doublet, *i.e.*, a sequence of two opposite steps of equal duration and amplitude. For the identification phase multiple datasets have been used: three double 3211s for an overall duration of approximately 20 seconds. For the cross-validation phase a double 3211 has been used for a duration of approximately 6.5 seconds. Finally, for the validation phase a doublet has been used for a duration of approximately 4 seconds. All the data has been filtered with a lowpass filter with a cutoff frequency of 5Hz.

Finally, note that while experiments exciting u_{col} have been carried out in open-loop, the identification of the response to the other control inputs has been carried out using closed-loop data because of the open-loop unstable nature of the platform under study. As already explained before this is not a problem since the identification method considered in this study (see Chapter 4) can provide unbiased estimates of the dynamics of the system regardless of the input/output correlation introduced by feedback control.

9.3 Experimental results

9.3.1 Time-domain data

As an illustrative example, in Figure 9.2 the response of the vertical acceleration to a double 3211 applied to u_{col} is shown (the input command is expressed in terms of percentage of the trim value). As can be seen from

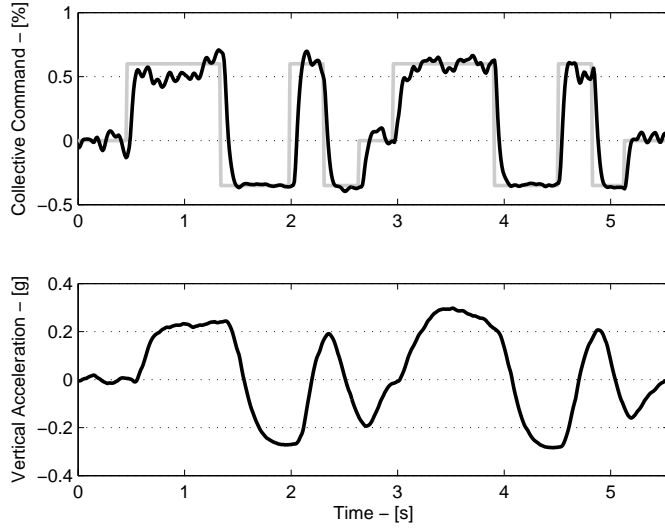


Figure 9.2: Example of identification data. Top: 3211 collective excitation (u_{col}); bottom: response of vertical acceleration (a_z).

the time history of the input in Figure 9.2, the actual input sequence applied by the on-board electronics is not exactly equal to the desired one, still the 3211 profile is clearly visible. Figure 9.3, on the other hand, shows the time histories of all the measured outputs during the same experiment, to motivate the choice of developing uncoupled models for individual DOFs of the quadrotor. Indeed, it is apparent from the figure that the excitation of u_{col} has a significant effect only on the vertical acceleration. Similar considerations can be made for the other input variables - the details have been omitted for brevity. Finally, correlation analysis between inputs and outputs has been used to assess the possible presence of delays in the quadrotor's response. Unlike what occurs typically in full scale helicopters, time delays in this case are negligible.

Remark. Since the dynamics of the quadrotor is open-loop unstable, in order to validate the identified models the estimation of the initial state is

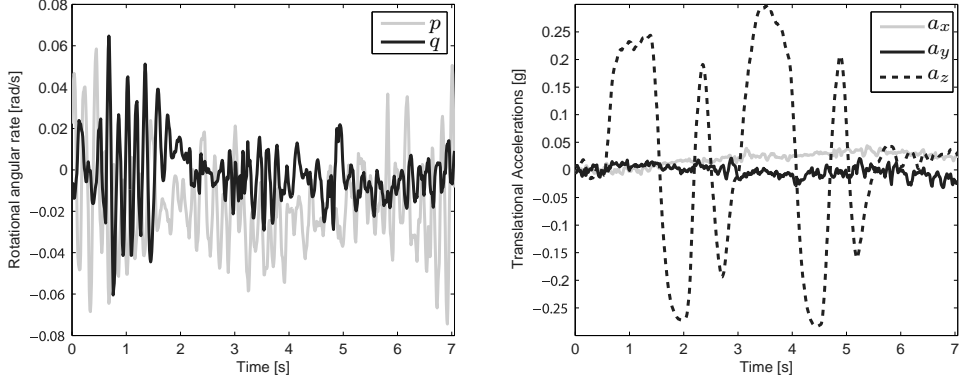


Figure 9.3: Response of measured variable to 3211 collective excitation. Left: pitch and roll rates; right: acceleration components.

necessary. This problem can be faced in the framework of the above described identification algorithm, as follows. The estimation is performed considering the simulation of the system model (1.4) where the estimated matrices are used and the noise is not taken into account. As shown in Appendix A.2, under these assumptions the output at each time instant t is given by

$$y(t) = Ce^{A(t-t_0)}x_0 + C \int_{t_0}^t e^{A(t-\tau)}Bu(\tau)d\tau + Du(t). \quad (9.1)$$

Therefore given the input and output data it is possible to solve a least squares problem to obtain an estimate of x_0 .

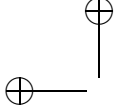
Remark. As is frequently the case with SMI algorithms, also the approach outlined above can use data gathered in different experiments simultaneously. Assuming that M datasets are available, they are independently projected using the transformation (1.56). The matrix $Y^{p,p}$ (see Section 1.5) is then built as

$$Y^{p,p} = [Y^{p,p,1} \quad Y^{p,p,\dots} \quad Y^{p,p,M}], \quad (9.2)$$

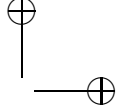
and similarly for the construction of $U^{p,p}$ and $\bar{Z}^{p,p}$.

9.3.2 Identification of uncoupled models for the individual DOFs

Both model order and the tuning parameters of the identification algorithm (*i.e.*, the position of the Laguerre pole a and the past and future windows lengths p , f , Section 1.6.3) have been selected using a cross-validation approach. More precisely, the model order has been selected by inspecting the singular values of $\Gamma^p K^p \bar{Z}^{p,p}$ (see (1.69)) while the selection of a and p



|



| Input | Model order (n) | Laguerre pole (a) | Window length (p) |
|--------------|---------------------|-----------------------|-----------------------|
| Collective | 3 | 16 | 25 |
| Pedal | 3 | 16 | 10 |
| Longitudinal | 3 | 21 | 14 |
| Lateral | 3 | 15 | 8 |

Table 9.1: Selected tuning parameters of the algorithm for the identification of each model.

has been carried out by checking the norm of the simulation error over the cross-validation dataset. The results of this step are shown in Table 9.1. Before the validation step, the identified models have been simplified by removing zeros occurring at frequencies well above the excitation bandwidth. For the sake of completeness, the identified models are reported hereafter in equations (9.3)-(9.6).

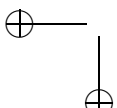
$$G_{col}(s) = \frac{a_z}{u_{col}} = \frac{1.2498(s + 0.3451)}{(s + 16.49)(s + 5.309)(s + 1.933)} \quad (9.3)$$

$$G_{yaw}(s) = \frac{r}{u_{ped}} = \frac{0.077646(s + 5.475)(s - 0.2086)}{(s + 11.03)(s^2 + 0.2838s + 0.06947)} \quad (9.4)$$

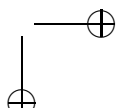
$$G_{lon}(s) = \begin{bmatrix} \frac{q}{u_{lon}} \\ \frac{a_x}{u_{lon}} \end{bmatrix} = \begin{bmatrix} \frac{0.22016(s+0.2579)(s-0.2596)}{(s+1.865)(s^2-1.285s+8.067)} \\ \frac{-0.011659(s-3.271)(s+3.681)}{(s+1.865)(s^2-1.285s+8.067)} \end{bmatrix} \quad (9.5)$$

$$G_{lat}(s) = \begin{bmatrix} \frac{p}{u_{lat}} \\ \frac{a_y}{u_{lat}} \end{bmatrix} = \begin{bmatrix} \frac{-0.20194(s^2+0.09235s+0.2532)}{(s+1.82)(s^2-1.388s+10.02)} \\ \frac{-0.00359(s-9.182)(s+4.164)}{(s+1.82)(s^2-1.388s+10.02)} \end{bmatrix}. \quad (9.6)$$

As can be seen from equation (9.3), the response of the quadrotor on the vertical axis is asymptotically stable and non-oscillatory, being characterised by real poles only. The dominant mode is located at about 2 rad/s, corresponding to a dominant time constant of approximately 0.5 s. Similarly, as can be seen from (9.4) the response of the yaw rate is also asymptotically stable, but with an oscillatory dominant mode. As expected, on the other hand, the response of the roll and pitch axes is characterised by an unstable, oscillatory mode. Note, in passing, the significant symmetry between the models for lateral and longitudinal response. In particular, the models have the same structure (up to the location of the zeros, on which more



|



comments will be made in subsections 9.3.4 and 9.3.5) corresponding to the overall symmetry of the quadrotor platform, which therefore has been successfully captured by the identified models. Small differences in the numerical values of the poles positions can be attributed to asymmetries such as, *e.g.*, different inertial properties due to the mounting of the battery on the quadrotor (aligned with the roll axis).

9.3.3 Time-domain validation

The performance of the identified models has been checked by comparing the simulated outputs with the measured response to a doublet excitation applied on each of the control variables. The results of the validation experiments are presented in Figure 9.4 for the response of the vertical acceleration to the collective input, Figure 9.5 for the response of the yaw rate to the pedal input and Figures 9.6 and 9.7 for, respectively, the response of the pitch (roll) rate and of the longitudinal (lateral) acceleration to the longitudinal (lateral) input.

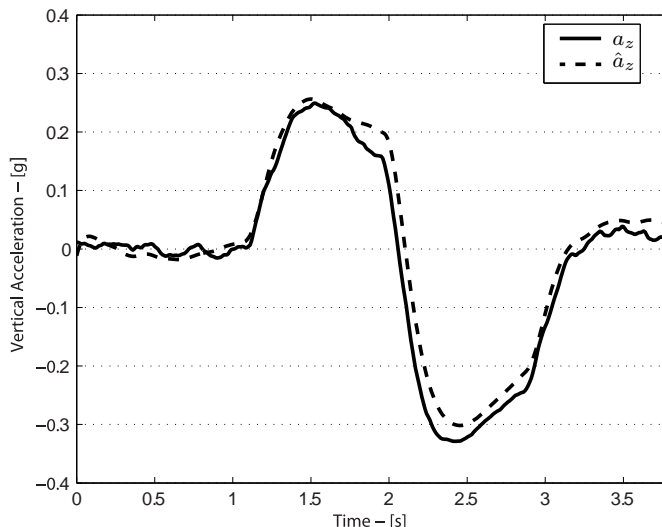


Figure 9.4: Response of vertical acceleration to collective doublet (measured: solid line; estimated: dashed line).

As can be seen from the Figures, the identified models capture the essential features of the response of the quadrotor along all the axes.

Finally, to complete the analysis of the results the bootstrap-based approach to uncertainty analysis introduced in Chapter 4 has been applied to both the frequency responses associated with the transfer functions in

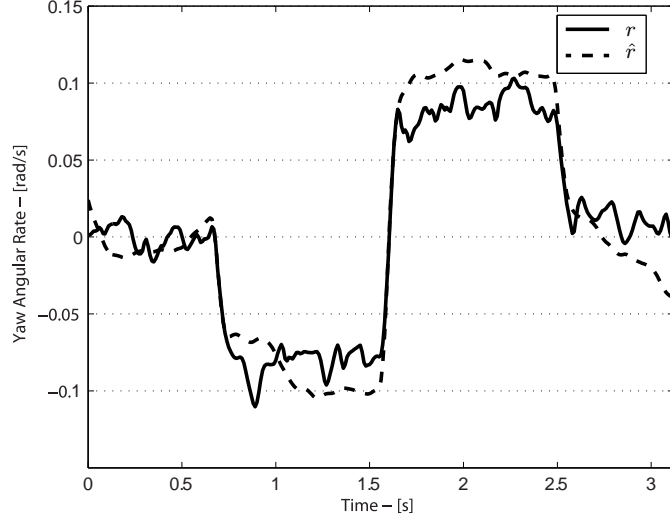


Figure 9.5: Response of yaw rate to pedal doublet (measured: solid line; estimated: dashed line).

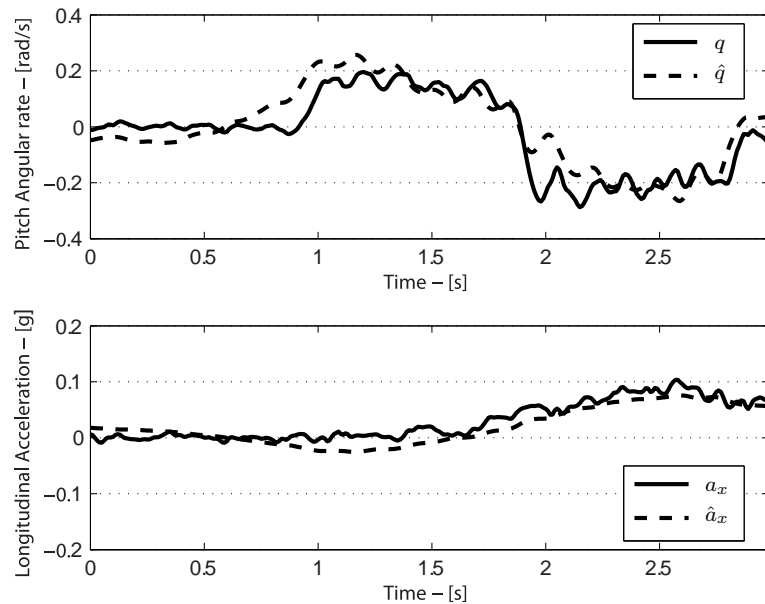


Figure 9.6: Response of pitch rate (top) and longitudinal acceleration (bottom) to longitudinal cyclic doublet (measured: solid line; estimated: dashed line).

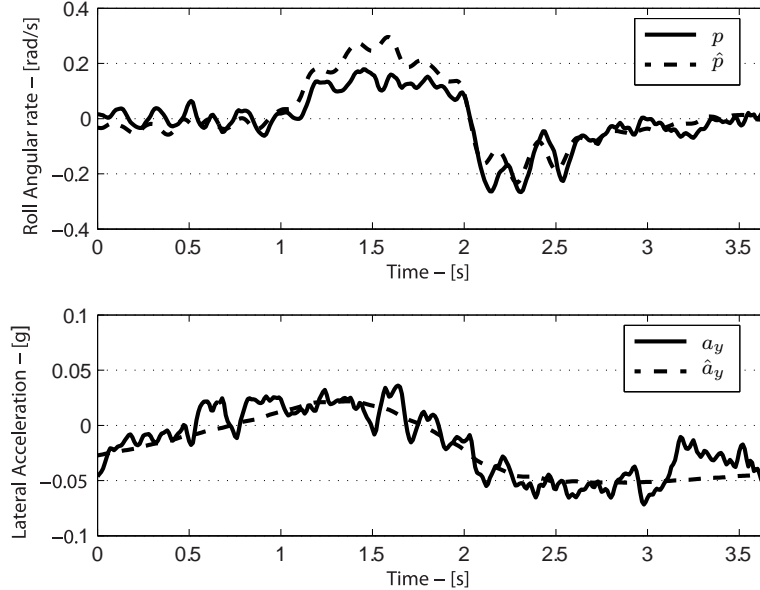


Figure 9.7: Response of roll rate (top) and lateral acceleration (bottom) to lateral cyclic doublet (measured: solid line; estimated: dashed line).

equations (9.3)-(9.6) and the corresponding positions of poles and zeros in the complex plane. The results are reported in the following subsections.

9.3.4 Uncertainty analysis: frequency responses

The results of the uncertainty analysis for the frequency responses of the identified models are reported in Figures 9.8-9.13, where the frequency responses corresponding to the identified models are compared with 1000 replications computed using the bootstrap.

As can be seen from Figure 9.8, the response of the vertical axis is captured by the model with very good accuracy, the uncertainty band having a very limited amplitude both in magnitude and phase over the excitation bandwidth (approximately 1-10 rad/s). Clearly some uncertainty is to be expected at low and high frequency, however since for the purpose of controller design what is really relevant is model accuracy around the crossover frequency, this level of model accuracy can be considered adequate. Similar comments can be made with reference to the response of the yaw axis, depicted in Figure 9.9. Figures 9.10 and 9.11 on the other hand represent the frequency responses for the longitudinal response of the quadrotor. In the responses one can readily recognise the unstable complex conjugate

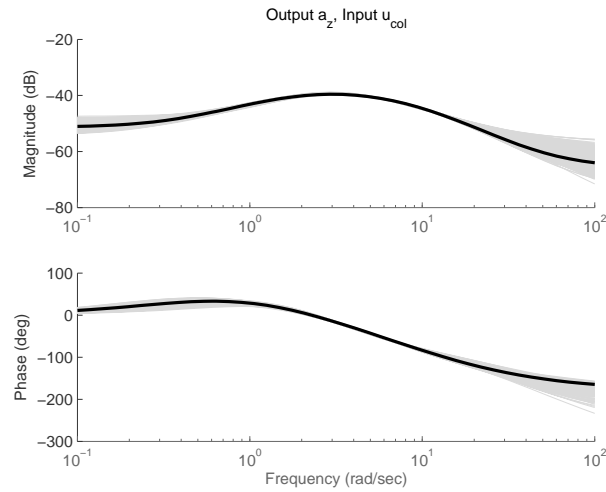


Figure 9.8: Frequency response of vertical acceleration to collective (black line: nominal model; grey lines: bootstrap replicas).

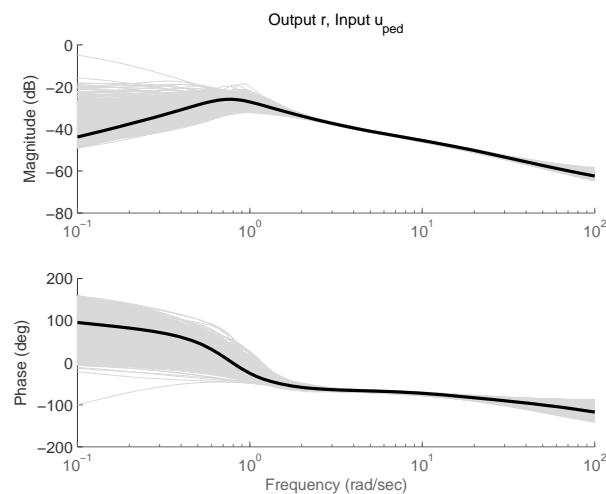


Figure 9.9: Frequency response of yaw rate to pedal (black line: nominal model; grey lines: bootstrap replicas).



186 Chapter 9 Identification of linear models for the dynamics of a hovering quadrotor

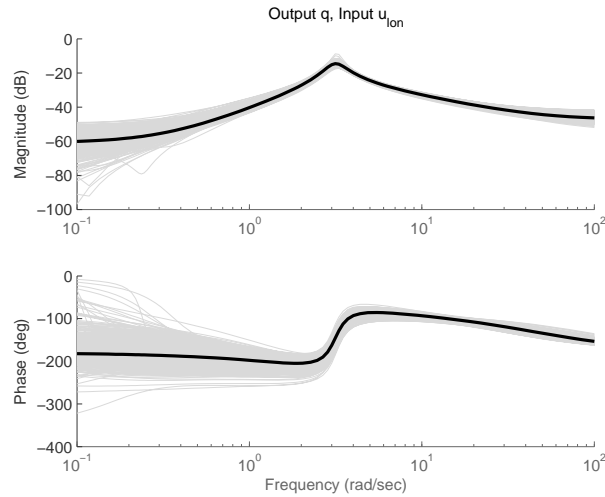


Figure 9.10: Frequency response of pitch rate to longitudinal cyclic (black line: nominal model; grey lines: bootstrap replicas).

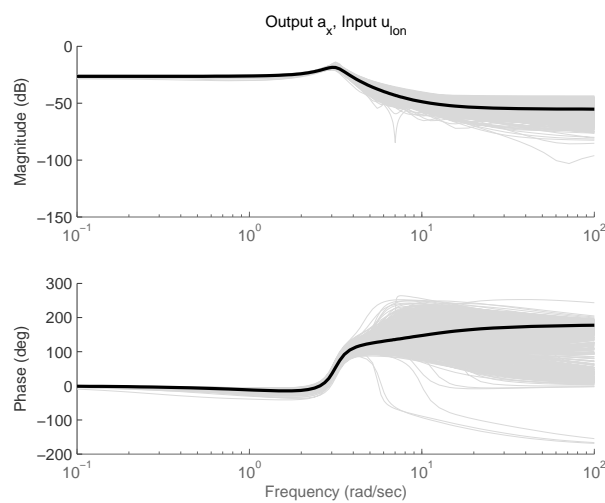


Figure 9.11: Frequency response of longitudinal acceleration to longitudinal cyclic (black line: nominal model; grey lines: bootstrap replicas).



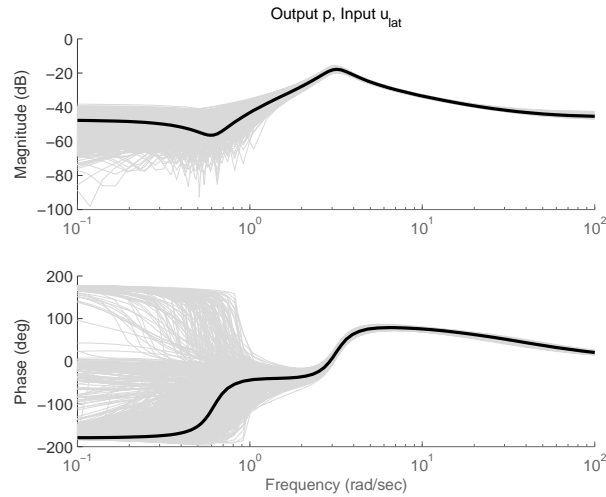


Figure 9.12: Frequency response of roll rate to lateral cyclic (black line: nominal model; grey lines: bootstrap replicas).

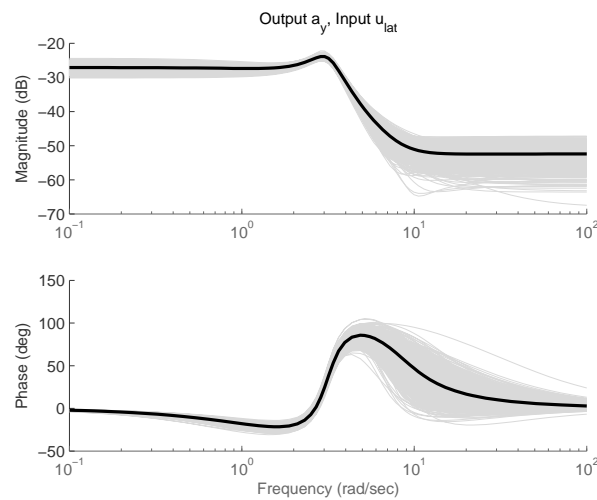


Figure 9.13: Frequency response of lateral acceleration to lateral cyclic (black line: nominal model; grey lines: bootstrap replicas).



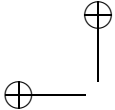
poles which dominate the response. In addition, note that in this case the uncertainty associated with the identification procedure is concentrated at low frequency for the response of the pitch rate and at high frequency for the response of the longitudinal acceleration. The lateral response of the quadrotor, reported in Figures 9.12 and 9.13, is qualitatively similar to the longitudinal one (again, confirming the essential symmetry of the considered configuration), except for the low frequency behaviour of the roll rate frequency response (Figure 9.12). Indeed in this case, the low frequency derivative character of the response is captured in the model by means of a complex conjugate pair of zeros, which leads to a significantly different phase curve with respect to the pitch rate one. Note however that this portion of the estimated response is associated with large uncertainty. Over the excitation bandwidth, however, the identified model appears to be accurate also in this case.

In summary, it can be concluded that the performance of the identified model is adequate for control systems design provided that the control loops are closed within the above mentioned excitation bandwidth. In order to further reduce the residual uncertainty in the models, additional experiments ought to be carried out.

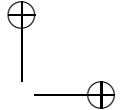
9.3.5 Uncertainty analysis: poles and zeros

A similar analysis, again based on the bootstrap method, can be carried out for the location of poles and zeros of the identified models. Note in particular that for the longitudinal and lateral responses the focus is on the zeros of the individual transfer functions rather than on the MIMO ones in view of the fact that conventional control architectures for quadrotor control would lead to separate loop closures on the individual transfer functions (angular rate for attitude control, acceleration for position control). As is well known, the position of zeros and poles in the complex plane plays a major role in determining the achievable closed-loop performance. In particular, for the case of unstable and/or non-minimum phase systems, the position of right-half plane zeros and poles imposes, respectively, upper and lower bounds to the closed-loop bandwidth (see, *e.g.*, the classical papers Freudenberg and Looze [1985], Stein [2003]). Along the lines of the previous subsection, the bootstrap method has been applied and 1000 replicas of the identified models have been obtained. For the vertical response of the quadrotor, the results are depicted in Figure 9.14, where the left panel shows a histogram of the position of the 1000 replicas of the poles, while the right one shows the same results for the zeros. It appears that all the 1000 replicated models remain asymptotically stable and the two dominant poles





|



(nominal locations at -1.933 and -5.309) are estimated with a very low uncertainty, while the "fast" pole located in the nominal model at -16.49 has a much more significant uncertainty associated with it (again, not surprising as its location is above the excited bandwidth). Similarly, the zero of the transfer function appears to be estimated very accurately and, most importantly, remains minimum phase for all the bootstrapped replicas. For

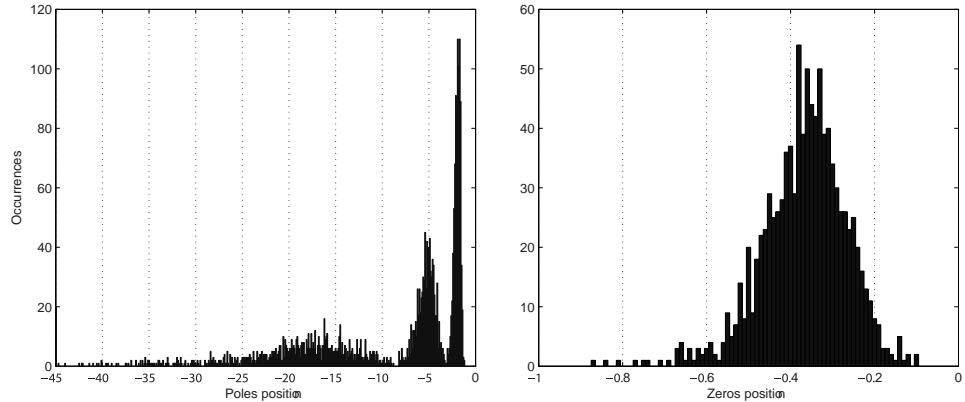
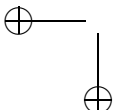


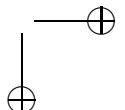
Figure 9.14: Histograms of poles (left) and zero (right) of the transfer function from collective to vertical acceleration.

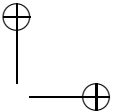
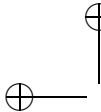
the response of the yaw axis, in Figure 9.15 the histograms for the natural frequencies and the damping factors of the poles are depicted, while the zeros are illustrated in Figure 9.16. Concerning the poles, the peaks in the histograms associated with the complex conjugate poles and the real pole are clearly visible; again, the dominant complex conjugate mode is captured with small dispersion, while the faster real pole is determined with larger uncertainty. As for the zeros, it is interesting to note that the (low frequency) non-minimum phase one is actually characterised by an uncertainty range which lies across the imaginary axis, which reflects the high level of uncertainty in the phase response of the yaw rate apparent from Figure 9.9.

Finally, the results for the response of the longitudinal axis are presented (the lateral response is omitted for brevity) in Figures 9.17-9.18 (poles) and 9.19 (zeros). Concerning the poles, it appears from Figure 9.17 that the dominant, unstable complex conjugate mode is identified with great accuracy, while there is some uncertainty associated with the real pole, for which a histogram is presented in Figure 9.18. The natural frequency of the unstable mode, which can be placed at 2.84 rad/s therefore provides information about the minimum bandwidth for the control of the longitudi-



|





190 Chapter 9 Identification of linear models for the dynamics of a hovering quadrotor

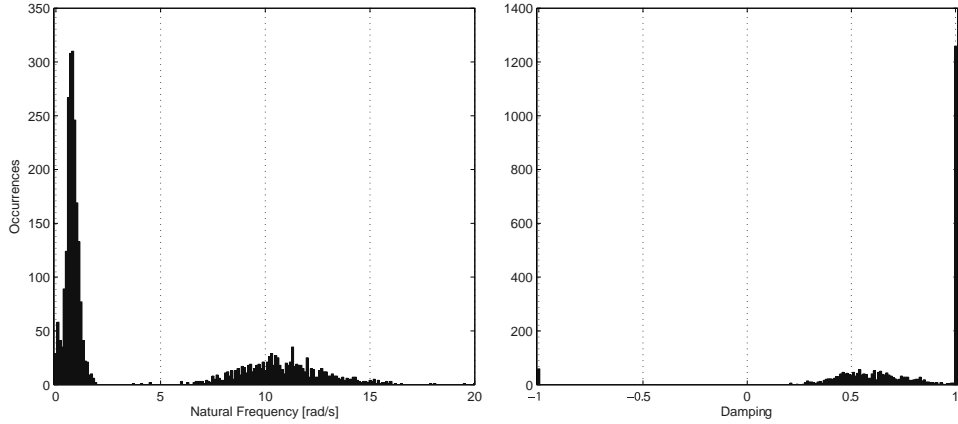


Figure 9.15: Histograms of poles of the transfer function from pedal to yaw rate. Left: natural frequencies; right: damping factors.

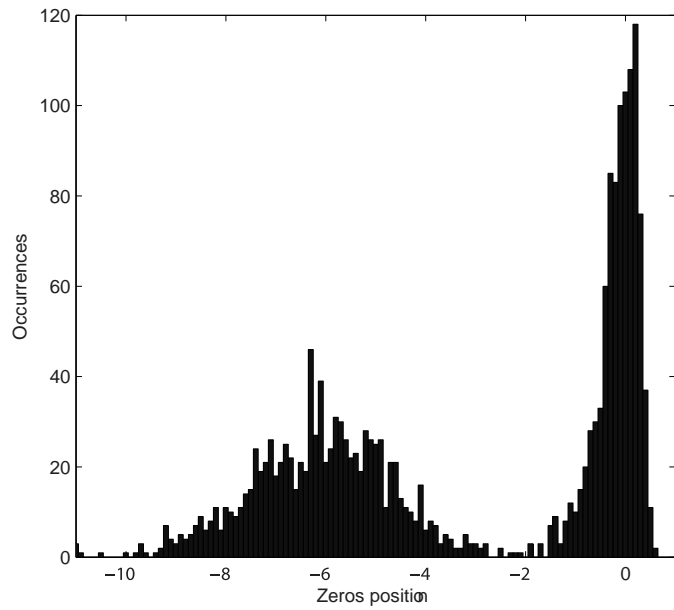
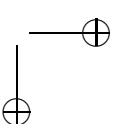
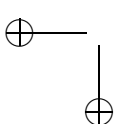
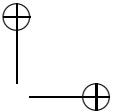
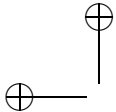


Figure 9.16: Histogram of zeros of the transfer function from pedal to yaw rate.





nal response. As for the zeros of the two transfer functions associated with the longitudinal axis, Figure 9.19 clearly shows the non-minimum phase of the responses, confirming also in a statistical sense the characteristics of the identified model. Note in particular that the estimation of the right-half plane zeros is quite accurate.

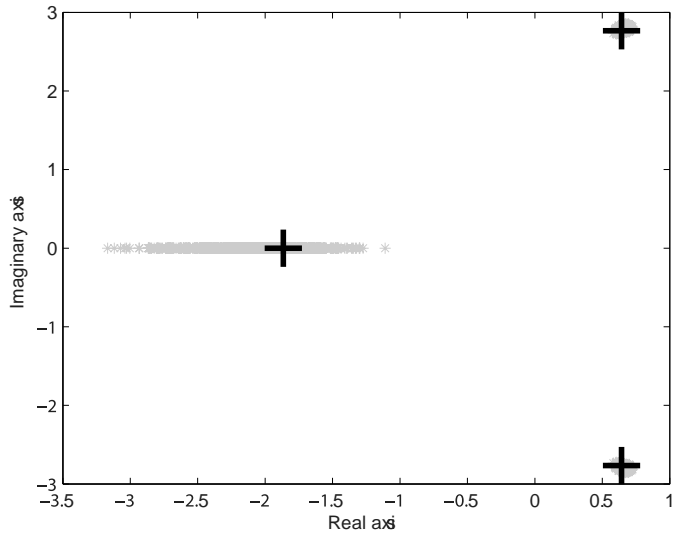
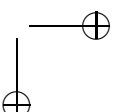
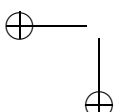


Figure 9.17: Poles of the transfer functions from longitudinal control to pitch rate and longitudinal acceleration.

9.4 Concluding remarks

The problem of black-box model identification of the dynamics of a quadrotor helicopter has been considered. In view of the open-loop instability of the quadrotor, closed-loop experiments have been carried out and a continuous-time subspace model identification approach capable of dealing with such experimental conditions has been adopted. Furthermore, a complete analysis of the uncertainty associated with the identified model has been performed, using tools from the field of computational statistics. The results of the study show that the considered approach is an effective one as far as the characterisation of the local dynamics of the quadrotor is concerned and can also provide useful uncertainty information for the purpose of robust control system design, both in the frequency-domain and in the time-domain. Future work will deal with the problem of optimising the input sequences used in the identification experiments (some preliminary results are avail-



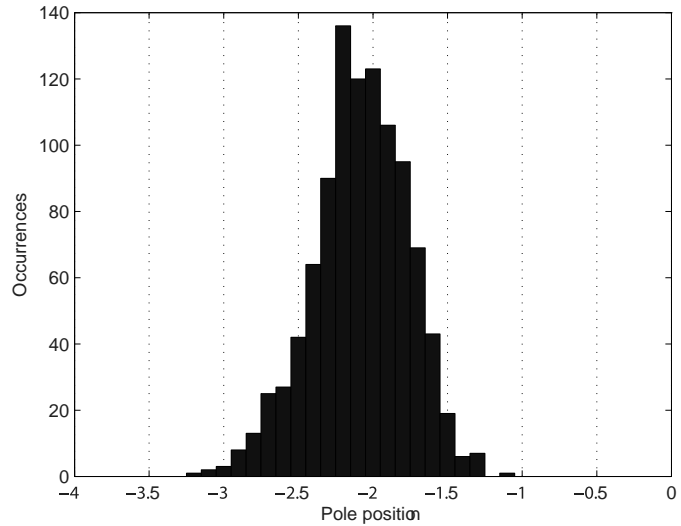


Figure 9.18: Histogram of real pole of the transfer functions from longitudinal control to pitch rate and longitudinal acceleration.

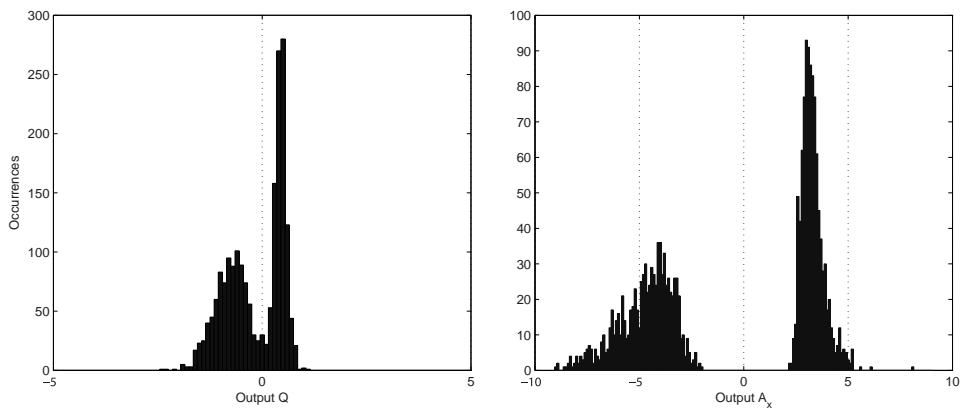
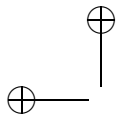
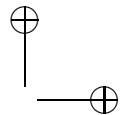


Figure 9.19: Histogram of zeros of the transfer functions from longitudinal control to pitch rate (left) and longitudinal acceleration (right).



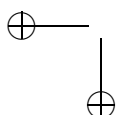
|



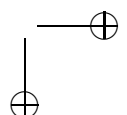
able in Beltramini et al. [2011]), which in turn will allow the analysis of the platform in more general flight conditions, and to consider additional sensors in the model identification.

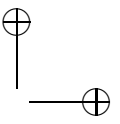
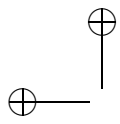
—

—



|

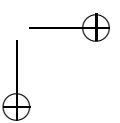
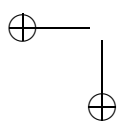




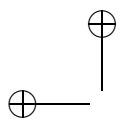
—

|

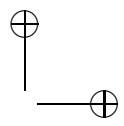
—



|

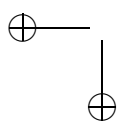


|

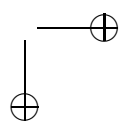


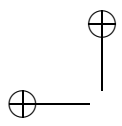
—

—

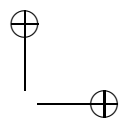


|



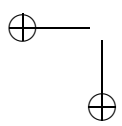


|

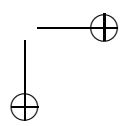


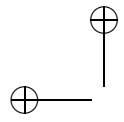
—

—

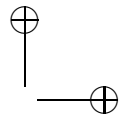


|





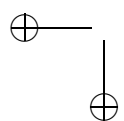
|



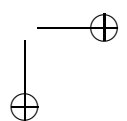
Appendix

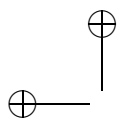
—

—

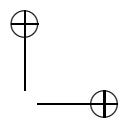


|



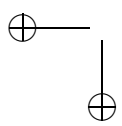


|

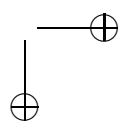


—

—



|





APPENDIX
A

SIGNALS AND SYSTEMS THEORY: SOME
PRELIMINARIES

In this Appendix some basic definitions and properties of signals and systems are introduced. The Lebesgue space $\mathcal{L}_2(0, \infty)$ is reviewed. The frequency domain Lebesgue space $\mathcal{L}_2(i\mathbb{R})$ and the Hardy space \mathcal{H}_2 are introduced. Definitions of causality, time-invariance, stability and linearity are given. The infinity norm is defined and the spaces $\mathcal{L}_\infty(i\mathbb{R})$ and \mathcal{H}_∞ are introduced. The properties of adjoint and all-pass systems are reviewed. These Sections do not attempt to provide a definitive or comprehensive treatment of signal and system theory, but only the concepts necessary to understand the transformation theory explained in Section 1.3.2. This Appendix is a summary of Chapter 3 in Green and Limebeer [1994]. More details can be found in the mentioned reference.

A.1 Signals

Definition A.1.1. *A signal is a (Lebesgue) measurable function that maps the real numbers \mathbb{R} to \mathbb{R}^n . The set of signals is*

$$\mathcal{S} = \{f : \mathbb{R} \mapsto \mathbb{R}^n\}$$

Signals form a natural vector space under addition and scalar multiplication, which are defined by

$$\begin{aligned}(f + g)(t) &= f(t) + g(t) \\ (\alpha f)(t) &= \alpha f(t).\end{aligned}$$





It is convenient to define the two subspaces

$$\begin{aligned}\mathcal{S}_+ &= \{f \in \mathcal{S} : f(t) = 0 \forall t < 0\} \\ \mathcal{S}_- &= \{f \in \mathcal{S} : f(t) = 0 \forall t > 0\}.\end{aligned}$$

A.1.1 Time-domain norms of signals

The size of a signal can be measured by a 2-norm defined over either a finite or infinite time interval. In the sequel, $\|x\| = \sqrt{x^T x}$ is the Euclidean norm.

Definition A.1.2. *Finite horizon* The finite-horizon 2-norm is defined by

$$\|f\|_{2,[0,T]} = \left\{ \int_0^T \|f(t)\|^2 dt \right\}^{\frac{1}{2}}. \quad (\text{A.1})$$

The set of signals for which this norm is finite is known as the finite-horizon Lebesgue 2-space

$$\mathcal{L}_2(0, T) = \{f \in \mathcal{S} : \|f\|_{2,[0,T]} < \infty\}. \quad (\text{A.2})$$

Any signal that is continuous on $[0, T]$ is bounded and is therefore in $\mathcal{L}_2(0, T)$. A signal f is in the finite-horizon space $\mathcal{L}_2(t_0, T)$ if and only if the time-shifted signal $g(t) = f(t + t_0)$ is in $\mathcal{L}_2(0, T - t_0)$.

Definition A.1.3. *Infinite horizon* The infinite-horizon Lebesgue 2-space is defined by

$$\mathcal{L}_2(-\infty, \infty) = \{f \in \mathcal{S} : \|f\|_2 < \infty\}. \quad (\text{A.3})$$

in which

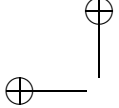
$$\|f\|_2 = \left\{ \int_{-\infty}^{\infty} \|f(t)\|^2 dt \right\}^{\frac{1}{2}}. \quad (\text{A.4})$$

The spaces $\mathcal{L}_2[0, \infty)$ and $\mathcal{L}_2(-\infty, 0]$ are defined by $\mathcal{L}_2[0, \infty) = \mathcal{S}_+ \cap \mathcal{L}_2(-\infty, \infty)$ and $\mathcal{L}_2(-\infty, 0] = \mathcal{S}_- \cap \mathcal{L}_2(-\infty, \infty)$.

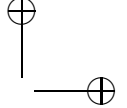
Definition A.1.4. Inner product The space $\mathcal{L}_2(-\infty, \infty)$ is a Hilbert space with inner product defined by

$$\langle f, g \rangle = \int_{-\infty}^{\infty} g^T(t) f(t) dt. \quad (\text{A.5})$$





|



Two signals f and g are orthogonal if $\langle f, g \rangle = 0$. This is a natural extension of orthogonality in \mathbb{R}^n . Note that $f \in \mathcal{L}_2[0, \infty)$ and $g \in \mathcal{L}_2(-\infty, 0]$ implies that $\langle f, g \rangle = 0$, which means that $\mathcal{L}_2[0, \infty)$ and $\mathcal{L}_2(-\infty, 0]$ are orthogonal subspaces of $\mathcal{L}_2(-\infty, \infty)$. The spaces $\mathcal{L}_2[0, \infty)$, $\mathcal{L}_2(-\infty, 0]$ and $\mathcal{L}_2[0, T]$ are all Hilbert spaces in their own right, with the inner product integral taken over the appropriate time interval. For example, for $\mathcal{L}_2[0, T]$ the inner product is defined by

$$\langle f, g \rangle_{[0, T]} = \int_0^T g^T(t) f(t) dt.$$

Note that $\|f\|_2^2 = \langle f, f \rangle$ and that the inner product here defined satisfies the Cauchy-Schwarz inequality (as any other inner product)

$$\langle f, g \rangle \leq \|f\|_2 \|g\|_2.$$

A.1.2 Signals in the frequency-domain

A frequency domain signal is a measurable function $f(j\omega)$ that has the property $f^*(j\omega) = f^T(-j\omega)$. The variable ω is the real frequency variable in radians per unit time and the superscript $(\cdot)^*$ denotes the complex conjugate transpose.

Definition A.1.5. *The frequency domain 2-norm is defined by*

$$\|f\|_2 = \left\{ \frac{1}{2\pi} \int_{-\infty}^{\infty} f^*(j\omega) f(j\omega) d\omega \right\}^{\frac{1}{2}}. \quad (\text{A.6})$$

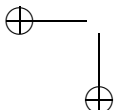
The frequency domain Lebesgue space $\mathcal{L}_2(i\mathbb{R})$ consists of those signals with finite norm

$$\mathcal{L}_2(i\mathbb{R}) = \{f : \|f\|_2 < \infty\}. \quad (\text{A.7})$$

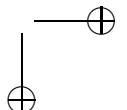
$\mathcal{L}_2(i\mathbb{R})$ is a Hilbert space under the inner product

$$\langle f, g \rangle = \frac{1}{2\pi} \int_{-\infty}^{\infty} g^*(j\omega) f(j\omega) d\omega. \quad (\text{A.8})$$

The same symbol for the norm and the inner product in both the time and frequency domains is used because the Fourier transform, which is a Hilbert space isomorphism between $\mathcal{L}_2(-\infty, \infty)$ and $\mathcal{L}_2(i\mathbb{R})$, preserves the inner product and the 2-norm. Two Hilbert spaces are isomorphic if there



|



is a bijective linear mapping from one to the other that preserves the inner product. For $f \in \mathcal{L}_2(-\infty, \infty)$, the Fourier transform of f is

$$\hat{f}(j\omega) = \mathcal{F}[f] = \int_{-\infty}^{\infty} f(t)e^{-j\omega t} dt. \quad (\text{A.9})$$

Furthermore,

$$\langle f, g \rangle = \langle \mathcal{F}[f], \mathcal{F}[g] \rangle = \langle \hat{f}, \hat{g} \rangle \quad (\text{A.10})$$

which is known as Parsevals identity. As a consequence of (A.10), $\|f\|_2 = \|\hat{f}\|_2$.

Definition A.1.6. The space \mathcal{H}_2 The Hardy 2-space \mathcal{H}_2 consists of functions of a complex variable that are analytic in the open right-half of the complex plane (ORHP) and such that the norm

$$\|f\|_2 = \left\{ \sup_{\alpha > 0} \frac{1}{2\pi} \int_{-\infty}^{\infty} f^*(\alpha + j\omega) f(\alpha + j\omega) d\omega \right\}^{\frac{1}{2}}. \quad (\text{A.11})$$

is finite. That is,

$$\mathcal{H}_2 = \{f : f(s) \text{ is analytic in } \operatorname{Re}(s) > 0 \text{ and } \|f\|_2 < \infty\}. \quad (\text{A.12})$$

Due to the analyticity of f in the ORHP, the supremum always occurs on the boundary $\alpha = 0$, e.g., as shown in Figure A.1. Therefore, the \mathcal{H}_2 norm can be evaluated by the formula

$$\|f\|_2 = \left\{ \frac{1}{2\pi} \int_{-\infty}^{\infty} f^*(j\omega) f(j\omega) d\omega \right\}^{\frac{1}{2}}. \quad (\text{A.13})$$

The Paley-Wiener theorem states that \mathcal{H}_2 is isomorphic to $\mathcal{L}_2[0, \infty)$ under the Laplace transform. For any signal $f \in \mathcal{S}$ the Laplace transform is defined by the integral

$$\hat{f}(s) = \int_{-\infty}^{\infty} f(t)e^{-st} dt. \quad (\text{A.14})$$

For any particular f , the domain of definition (allowable values of s) depends on the convergence of the integral. For $f \in \mathcal{L}_2[0, \infty)$ the domain of definition is $\operatorname{Re}(s) > 0$ and $\hat{f} \in \mathcal{H}_2$. The function \hat{f} is often defined outside this domain of convergence by analytic continuation. The space \mathcal{H}_2^\perp defined by

$$\mathcal{H}_2^\perp = \{f : f(-s) \in \mathcal{H}_2\}. \quad (\text{A.15})$$

is isomorphic to $\mathcal{L}_2(-\infty, 0]$ under the Laplace transform. It follows that the spaces \mathcal{H}_2 and \mathcal{H}_2^\perp are orthogonal and $\mathcal{L}_2(i\mathbb{R}) = \mathcal{H}_2 \oplus \mathcal{H}_2^\perp$.

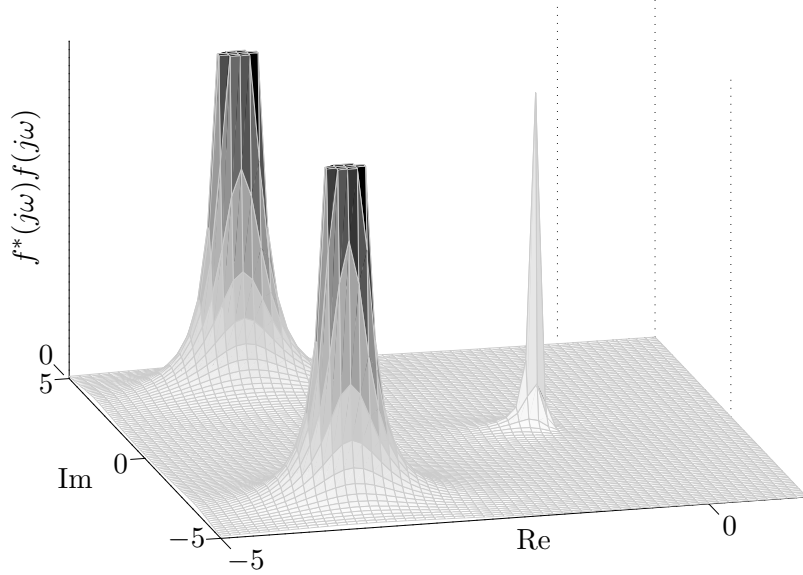
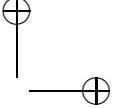
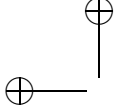


Figure A.1: $\|f\|^2$ of a f in \mathcal{H}_2 , i.e., $f(s) = \frac{2s+1}{(s+1)(s^2+7s+25)} \Big|_{s=\alpha+j\omega}$.

A.2 Systems

Definition A.2.1. A system is a mapping from one signal space, the input space, to another signal space, the output space:

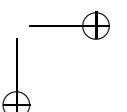
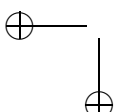
$$\begin{aligned} G : \mathcal{S}_1 &\mapsto \mathcal{S}_2 \\ &: u \mapsto y = Gu. \end{aligned}$$

Systems form a linear space under addition (parallel connection) and multiplication by a scalar, which are defined by

$$\begin{aligned} (G_1 + G_2)u &= G_1u + G_2u \\ (\alpha G_1)u &= \alpha(Gu). \end{aligned}$$

A system is called causal if the output up to time T depends only on the input up to time T , for every T . Let $y(t)$ be the response of a system G to input $u(t)$. If the response to the time-shifted input $u(t - T)$ is $y(t - T)$, the system is called time-invariant. Defining the time-shift operator S_T by

$$(S_T u)(t) = u(t - T), \quad (\text{A.16})$$



a system is time-invariant if it commutes with the time-shift operator, *i.e.*, if $GS_T = S_TG$, for every T . A system G is stable if $y = Gu \in \mathcal{L}_2[0, \infty)$, $\forall u \in \mathcal{L}_2[0, \infty)$.

A.2.1 Linear systems

Definition A.2.2. A system $g : \mathcal{S}_1 \mapsto \mathcal{S}_2$ is linear if

$$g(\alpha u_1 + \beta u_2) = \alpha gu_1 + \beta gu_2$$

for all scalars α, β and for all $u_1, u_2 \in \mathcal{S}_1$.

The space of linear systems forms an algebra under addition (parallel connection) and composition (series connection). For systems $g : \mathcal{S}_1 \mapsto \mathcal{S}_2$, this algebra has the identity $Iu = u$ for all u . Any linear system may be represented by the integral operator

$$y(t) = \int_{-\infty}^{\infty} g(t, \tau)u(\tau)d\tau.$$

The system is causal if and only if $g(t, \tau) = 0 \forall \tau > t$ and is time-invariant if $g(t, \tau) = g(t - \tau, 0) \forall t, \tau$. Thus any linear, time-invariant system may be represented as a convolution integral

$$y(t) = \int_{-\infty}^{\infty} g(t - \tau)u(\tau)d\tau \quad (\text{A.17})$$

in which it has been written $g(t - \tau)$ instead of $g(t - \tau, 0)$ to make the formula more compact.

Transfer function matrices

Definition A.2.3. Taking the Laplace transform of (A.17), it holds

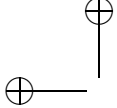
$$y(s) = G(s)u(s)$$

in which

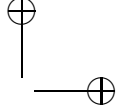
$$G(s) = \int_{-\infty}^{\infty} g(t)e^{-st}dt.$$

The function G is known as the transfer function matrix of the system.

Note that any system described by a transfer function matrix is linear and time-invariant. The transfer function is called proper if $\lim_{s \rightarrow \infty} G(s)$ exists and is finite.



|



A signal is a real-vector valued function of time. It follows that the impulse response matrix $g(t)$ is a real matrix-valued function and that the transfer function matrix $G(s)$ is a complex matrix-valued function of s such that

$$G^*(s) = G^T(\bar{s}).$$

State-space systems

Systems that are described by linear differential equations are our main concern.

Definition A.2.4. *These systems can be written as state-space equations:*

$$\begin{aligned}\dot{x}(t) &= Ax(t) + Bu(t), \quad x(t_0) = x_0 \in \mathbb{R}^n \\ y(t) &= Cx(t) + Du(t),\end{aligned}\tag{A.18}$$

where $u \in \mathbb{R}^m$ is the input vector, $x \in \mathbb{R}^n$ is the state vector and $y \in \mathbb{R}^p$ is the output vector. A , B , C and D are assumed constant real matrices with appropriate dimensions.

The equations (A.18) define a linear system

$$G : \mathbb{R}^n \oplus \mathcal{S}_1 \mapsto \mathcal{S}_2; \quad \begin{bmatrix} x_0 \\ u \end{bmatrix} \mapsto y.$$

The quadruple of matrices A , B , C and D is called a realization of the system. The following notation is also used

$$G = \begin{bmatrix} A & B \\ C & D \end{bmatrix}.$$

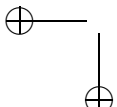
The realization is observable if the pair $(y(t), u(t))$, $t \in [t_0, T]$, uniquely determines $x(t_0)$, or also if $\mathcal{W}_o > 0$, in which \mathcal{W}_o is the observability Gramian defined as

$$\mathcal{W}_o = \int_0^\infty e^{AT\tau} C^T C e^{A\tau} d\tau.\tag{A.19}$$

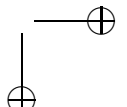
The realization is controllable if and only if, for any $x_T \in \mathbb{R}^n$, there exists a $u(t)$, $t \in [t_0, T]$, such that $x(T) = x_T$, or also if $\mathcal{W}_c > 0$, in which \mathcal{W}_c is the controllability Gramian defined as

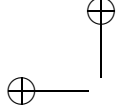
$$\mathcal{W}_c = \int_0^\infty e^{A\tau} B B^T e^{AT\tau} d\tau.\tag{A.20}$$

Controllability depends only on A and B and it can be shown that (A, B) is controllable if and only if (A^T, B^T) is observable.

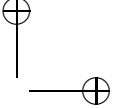


|





|



Definition A.2.5. Consider the observability and controllability Gramians of the state-space system (A.18). The state-space realization is internally balanced if

$$\mathcal{W}_o = \mathcal{W}_c = \Sigma = \text{diag}(\sigma_1 \dots \sigma_n), \quad (\text{A.21})$$

where $\{\sigma_i\}_{i=1}^n$ are the singular values of $\mathcal{W}_c \mathcal{W}_o$.

The realization is minimal if no other realization with the same input-output properties has a lower state dimension. It can be shown that the realization is minimal if and only if it is both controllable and observable. The output can be analytically computed as follows

$$y(t) = C e^{A(t-t_0)} x_0 + C \int_{t_0}^t e^{A(t-\tau)} B u(\tau) d\tau + D u(t).$$

Taking Laplace transforms it holds that

$$y(s) = C(sI - A)^{-1} x_0 + (C(sI - A)^{-1} B + D) u(s).$$

The matrix valued function $G(s) = C(sI - A)^{-1} B + D$ is the transfer function matrix of the system. The degree of the denominator of $G(s)$ is known as the McMillan degree of $G(s)$. The McMillan degree of $G(s)$ is equal to the dimension of the state vector in a minimal realization of the system.

The transfer function matrix $G(s) = C(sI - A)^{-1} B + D$ has no poles in the closed RHP if and only if G defines an asymptotically stable system. Realizations are not unique, indeed there always exists a state transformation such that the input-output behavior of G is the same. Consider the new state-space representation $\hat{x}(t) = T x(t)$ where T is a non-singular matrix, i.e., T^{-1} exists. Then, the system (A.18) becomes

$$\begin{aligned} \dot{\hat{x}}(t) &= T A T^{-1} \hat{x}(t) + T B u(t), \quad \hat{x}(t_0) = \hat{x}_0 = T x_0 \in \mathbb{R}^n \\ y(t) &= C T^{-1} \hat{x}(t) + D u(t). \end{aligned} \quad (\text{A.22})$$

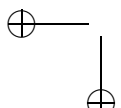
It is easy to show that the transfer functions of (A.18) and (A.22) are exactly the same.

A.2.2 The space $\mathcal{L}_\infty(j\mathbb{R})$

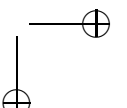
Because $\mathcal{L}_2(-\infty, \infty)$ is isomorphic to $\mathcal{L}_2(j\mathbb{R})$, a linear time-invariant system maps $\mathcal{L}_2(-\infty, \infty)$ to $\mathcal{L}_2(-\infty, \infty)$ if and only if the transfer function matrix G is such that $G u \in \mathcal{L}_2(j\mathbb{R})$, $\forall u \in \mathcal{L}_2(j\mathbb{R})$. A sufficient condition for this is

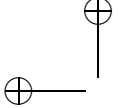
$$\sup_\omega \bar{\sigma}(G(j\omega)) < \infty.$$

where $\bar{\sigma}$ is the maximum singular value.

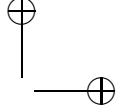


|





|



Definition A.2.6. *The class of systems for which the supremum is finite is known as $\mathcal{L}_\infty(j\mathbb{R})$*

$$\mathcal{L}_\infty(j\mathbb{R}) = \{G : \|G\|_\infty < \infty\},$$

in which the $\mathcal{L}_\infty(j\mathbb{R})$ -norm is defined by

$$\|G\|_\infty = \sup_{\omega} \bar{\sigma}(G(j\omega)). \quad (\text{A.23})$$

A.2.3 The space \mathcal{H}_∞

If G is the transfer function matrix of a linear, time-invariant system, then G defines a stable system if and only if $y = Gu \in \mathcal{H}_2$ whenever $u \in \mathcal{H}_2$. This is because $\mathcal{L}_2[0, \infty)$ is isomorphic to \mathcal{H}_2 .

Since $y \in \mathcal{H}_2$ requires that z is analytic in the ORHP, a necessary condition for stability is that G is analytic in the ORHP.

Definition A.2.7. *The class of systems for which G is analytic in the ORHP and its supremum is finite is known as \mathcal{H}_∞ :*

$$\mathcal{H}_\infty = \{G : G \text{ is analytic in } \text{Re}(s) > 0 \text{ and } \|G\|_\infty < \infty\}, \quad (\text{A.24})$$

in which

$$\begin{aligned} \|G\|_\infty &= \sup_{\alpha>0} \left\{ \sup_{\omega} \bar{\sigma}(G(\alpha + j\omega)) \right\} \\ &= \sup_{\omega} \bar{\sigma}(G(j\omega)). \end{aligned} \quad (\text{A.25})$$

A system that has a transfer function matrix in \mathcal{H}_∞ is a stable system. In fact, a transfer function matrix G defines a stable system if and only if $G \in \mathcal{H}_\infty$. \mathcal{H}_∞ is a closed subspace of $\mathcal{L}_\infty(j\mathbb{R})$.

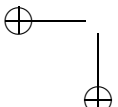
In the case that G is rational, $G \in \mathcal{H}_\infty$ if and only if G has no poles in the closed RHP.

The \mathcal{H}_∞ norm is equal to the L_2 gain when the system is linear time-invariant.

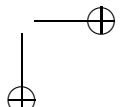
Definition A.2.8. *A system has a finite L_2 gain if there exists a $\gamma > 0$ such that*

$$\inf_{t>T} \int_T^t \{\gamma^2 |u(\tau)|^2 - |y(\tau)|^2\} d\tau > -\infty \quad \forall T \in \mathbb{R}$$

for every input/output pair (u, y) . The L_2 gain is the infimum of such $\gamma > 0$.



|





A.2.4 Adjoint systems

Definition A.2.9. Suppose $G : \mathcal{S}_1 \mapsto \mathcal{S}_2$ is a linear system and \mathcal{S}_1 and \mathcal{S}_2 are Hilbert spaces such as $\mathcal{L}_2[0, T]$ or $\mathcal{L}_2[0, \infty)$. The adjoint system is the linear system $G^\sim : \mathcal{S}_2 \mapsto \mathcal{S}_1$ that has the property

$$\begin{aligned} <Gu, y>_{\mathcal{S}_2} &= <u, G^\sim y>_{\mathcal{S}_1}, \quad \forall u \in \mathcal{S}_1, \forall y \in \mathcal{S}_2 \\ G^\sim G &= I. \end{aligned} \tag{A.26}$$

G^\sim is uniquely defined by equations (A.26).

If G is a transfer function matrix mapping $\mathcal{L}_2(j\mathbb{R})$ to $\mathcal{L}_2(j\mathbb{R})$, which is to say $G \in \mathcal{L}_\infty(j\mathbb{R})$, the adjoint system has transfer function matrix

$$G^\sim(s) = G^T(-s).$$

If G has realization (A, B, C, D) then G^\sim has realization $(-A^T, -C^T, B^T, D^T)$. Note that if the complex variable s is limited to the imaginary axis, i.e., $s = j\omega$, then

$$G^\sim(s) = G^*(s).$$

A.2.5 All-pass/Inner systems

An all-pass system has the property that the norm of the output is equal to the norm of the input. The term *all-pass* derives from the fact that, by definition, all-pass systems pass all signals with unchanged magnitude, in contrast to other systems of interest such as low-pass, high-pass or band-pass systems, which attenuate the magnitude of certain signals. All-pass systems are also known as *inner* systems.

Definition A.2.10. Suppose \mathcal{S}_1 and \mathcal{S}_2 are normed signal spaces, e.g., $\mathcal{L}_2[0, T]$ or $\mathcal{L}_2(-\infty, \infty)$, with the norms on these spaces denoted $\|\cdot\|_{\mathcal{S}_i}$. If $G : \mathcal{S}_1 \mapsto \mathcal{S}_2$ is linear, then G is all-pass if

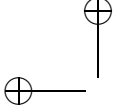
$$\|Gu\|_{\mathcal{S}_2} = \|u\|_{\mathcal{S}_1}, \quad \forall u \in \mathcal{S}_1. \tag{A.27}$$

It also holds that when the spaces \mathcal{S}_i are Hilbert spaces, G is an all-pass if and only if

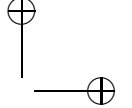
$$<Gu, Gw>_{\mathcal{S}_2} = <u, w>_{\mathcal{S}_1}, \quad \forall u, w \in \mathcal{S}_1.$$

which means an all-pass system between two Hilbert spaces preserves the inner product.





|



Consequently, G is an all-pass system between two Hilbert spaces if and only if

$$G^\sim G = I. \quad (\text{A.28})$$

If an all-pass system is a bijection, then the spaces \mathcal{S}_i are necessarily of the same dimension and $G^\sim = G^{-1}$. This implies that $GG^\sim = I$.

A.3 Basis of $\mathcal{L}_2(j\mathbb{R})/\mathcal{L}_2(-\infty, \infty)$

In this Section some preliminaries on the $\mathcal{L}_2(-\infty, \infty)$ basis are introduced. It is shown (see Oliveira e Silva [1999] for detailed proofs) that using an inner system as operator applied to $\mathcal{L}_2(-\infty, \infty)$, a basis of the whole space can be obtained.

Definition A.3.1. Given $\phi \in \mathcal{H}_\infty$ an inner function such that $\phi(j\omega)^\sim \phi(j\omega) = I$ almost everywhere on the imaginary axis, unless ϕ is constant, the space $\phi\mathcal{L}_2(j\mathbb{R})$ is a proper closed subspace of $\mathcal{L}_2(j\mathbb{R})$, and hence the orthogonal complement of the subspace $\phi\mathcal{L}_2(j\mathbb{R})$, i.e., $S = \mathcal{L}_2(j\mathbb{R}) \ominus \phi\mathcal{L}_2(j\mathbb{R})$, is a non-zero subspace Ohta [2010].

Using the subspace S , the spaces $\mathcal{L}_2(j\mathbb{R})$, \mathcal{H}_2^\perp , and \mathcal{H}_2 are written as

$$\mathcal{L}_2(j\mathbb{R}) = \bigoplus_{k=-\infty}^{\infty} \phi^k S, \quad \mathcal{H}_2^\perp = \bigoplus_{k=-\infty}^{-1} \phi^k S, \quad \mathcal{H}_2 = \bigoplus_{k=0}^{\infty} \phi^k S \quad (\text{A.29})$$

where $\phi^k = (\phi^\sim)^k$ for $k < 0$.

In view of Parseval's identity (A.10), similar results can be found for the space $\mathcal{L}_2(-\infty, \infty)$, and its subspaces $\mathcal{L}_2(-\infty, 0]$ and $\mathcal{L}_2[0, \infty)$.

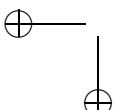
Definition A.3.2. The multiplication operator $\mathcal{L}_2(-\infty, \infty) \mapsto \mathcal{L}_2(-\infty, \infty)$, denoted by Λ_ϕ , is defined as

$$\Lambda_\phi u = \mathcal{F}^{-1}[\phi\mathcal{F}[u]] \in \mathcal{L}_2(-\infty, \infty), \quad u \in \mathcal{L}_2(-\infty, \infty). \quad (\text{A.30})$$

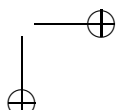
Then, applying the Fourier transformation to (A.29), it holds

$$\mathcal{L}_2(-\infty, \infty) = \bigoplus_{k=-\infty}^{\infty} \Lambda_\phi^k S, \quad \mathcal{L}_2(-\infty, 0] = \bigoplus_{k=-\infty}^{-1} \Lambda_\phi^k S, \quad \mathcal{L}_2[0, \infty) = \bigoplus_{k=0}^{\infty} \Lambda_\phi^k S \quad (\text{A.31})$$

where $S = \mathcal{L}_2[0, \infty) \ominus \Lambda_\phi \mathcal{L}_2[0, \infty)$, with a slightly abuse of notation.



|



Note that (A.31) implies that any $u \in \mathcal{L}_2(-\infty, \infty)$ can be represented as $u = \sum_{k=-\infty}^{\infty} \Lambda_{\phi}^k u_k$, where $u_k \in S$.

Hence the map

$$u \mapsto \{\dots, u_{-1}, u_0, u_1, \dots\} \quad (\text{A.32})$$

from $\mathcal{L}_2(-\infty, \infty)$ to the space of square summable sequences in S is a norm-preserving bijection. The Fourier transform induces a frequency domain counter-part of (A.32)

$$\hat{u} \mapsto \{\dots, \hat{u}_{-1}, \hat{u}_0, \hat{u}_1, \dots\}.$$

Remark. Given an inner function ϕ , (A.29) and (A.31) suggest that it is sufficient knowing the basis of S to obtain an orthonormal basis of the spaces.

As example consider the inner function $\phi(s) = e^{-sh}$ that corresponds to a delay of h seconds in the time domain. It is easy to prove that $\phi(s) \in \mathcal{H}_{\infty}$ ($\phi^*(s)\phi(s) = e^{sh}e^{-sh} = 1, \forall s$, so it is bounded and it is analytic in $\text{Re}(s) > 0$).

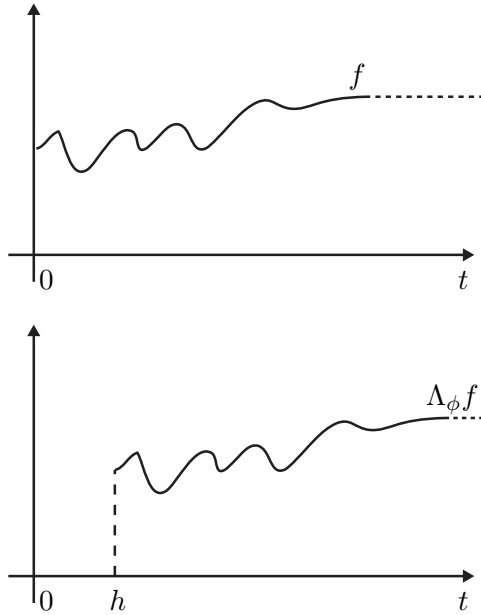


Figure A.2: Example of decomposition of the space $\mathcal{L}_2[0, \infty)$ in two subspaces, $\mathcal{L}_2[0, h]$ and $\mathcal{L}_2[h, \infty)$, using the inner function $\phi(s) = e^{-sh}$.

As shown in Figure A.2, applying Λ_{ϕ} to a signal $f \in \mathcal{L}_2[0, \infty)$, the signal is translated in time of h seconds, then its new support is $\mathcal{L}_2[h, \infty)$,



or $\Lambda_\phi f \in \mathcal{L}_2[h, \infty)$. The orthogonal space of $\Lambda_\phi \mathcal{L}_2[h, \infty)$ is clearly $S = \mathcal{L}_2[0, h)$, indeed

$$\mathcal{L}_2[0, \infty) = \mathcal{L}_2[0, h) \oplus \mathcal{L}_2[h, \infty) = S \oplus \Lambda_\phi \mathcal{L}_2[0, \infty).$$

Applying the inner function to the space $\mathcal{L}_2[h, \infty)$ a new space is defined, $\mathcal{L}_2[2h, \infty)$, which is a closed subspace of $\mathcal{L}_2[h, \infty)$, indeed

$$\begin{aligned} \mathcal{L}_2[h, \infty) &= \mathcal{L}_2[h, 2h) \oplus \mathcal{L}_2[2h, \infty) \\ &= \mathcal{L}_2[h, 2h) \oplus \Lambda_\phi \mathcal{L}_2[h, \infty) \\ &= \Lambda_\phi S \oplus \Lambda_\phi^2 \mathcal{L}_2[0, \infty). \end{aligned}$$

This means that

$$\mathcal{L}_2[0, \infty) = S \oplus \Lambda_\phi S \oplus \Lambda_\phi^2 \mathcal{L}_2[0, \infty).$$

Iterating this result, the space $\mathcal{L}_2[0, \infty)$ can be defined as follows

$$\mathcal{L}_2[0, \infty) = \bigoplus_{k=0}^{\infty} \mathcal{L}_2(kh, (k+1)h) = \bigoplus_{k=0}^{\infty} \Lambda_\phi^k S,$$

and this result can be extended to the space $\mathcal{L}_2(-\infty, \infty)$ which is defined as

$$\mathcal{L}_2(-\infty, \infty) = \bigoplus_{k=-\infty}^{\infty} \mathcal{L}_2(kh, (k+1)h) = \bigoplus_{k=-\infty}^{\infty} \Lambda_\phi^k S.$$

A.3.1 Continuous-time generalized orthonormal basis function (CT-GOBF)

The projection theory exposed in Section 1.3.2 is based on the CT-GOBF, see Oliveira e Silva [1999] for further details. When ϕ is a rational inner function, the space $S = \mathcal{H}_2 \ominus \phi \mathcal{H}_2$ is finite dimensional.

As suggested by the previous remark, in order to have a basis of the space \mathcal{H}_2 , a basis of S is necessary. Suppose that

$$\phi(s) = C_\phi(sI - A_\phi)^{-1} B_\phi \quad (\text{A.33})$$

is a balanced realization with order n_ϕ . Define

$$\hat{v}(s) = [\hat{v}_1(s) \ \hat{v}_2(s) \ \dots \ \hat{v}_{n_\phi}(s)] = C_\phi(sI - A_\phi)^{-1}. \quad (\text{A.34})$$



Then $\{\hat{v}_1 \hat{v}_2 \dots \hat{v}_{n_\phi}\}$ is an orthonormal basis of $S \subset \mathcal{H}_2$. Notice that S is a n_ϕ dimensional space. For the time domain the basis is found using the Fourier transformation, indeed

$$v(t) = \mathcal{F}^{-1}[\hat{v}(s)] = [v_1(t) \ v_2(t) \ \dots \ v_{n_\phi}(t)] = C_\phi e^{A_\phi t} \quad (\text{A.35})$$

is an orthonormal basis of $S \subset \mathcal{L}_2[0, \infty)$. Knowing a basis of S , an orthonormal basis of \mathcal{H}_2 is

$$[\hat{v}(s) \ \phi\hat{v}(s) \ \phi^2\hat{v}(s) \ \dots]. \quad (\text{A.36})$$

Including negative powers of ϕ , *i.e.*, $\phi^k = (\phi^\sim)^k$ for $k < 0$, an orthonormal basis of $\mathcal{L}_2(j\mathbb{R})$ is obtained,

$$[\dots \ \phi^{-2}\hat{v}(s) \ \phi^{-1}\hat{v}(s) \ \hat{v}(s) \ \phi\hat{v}(s) \ \phi^2\hat{v}(s) \ \dots]. \quad (\text{A.37})$$

By the inverse Fourier transform, an orthonormal basis of $\mathcal{L}_2[0, \infty)$ is obtained

$$[v(t) \ \Lambda_\phi v(t) \ \Lambda_\phi^2 v(t) \ \dots], \quad (\text{A.38})$$

and an orthonormal basis of $\mathcal{L}_2(-\infty, \infty)$

$$[\dots \ \Lambda_\phi^{-2}v(t) \ \Lambda_\phi^{-1}v(t) \ v(t) \ \Lambda_\phi v(t) \ \Lambda_\phi^2 v(t) \ \dots]. \quad (\text{A.39})$$

A.3.2 The Laguerre basis

The Laguerre basis and its generalisations to wider classes of orthonormal basis functions (see, *e.g.*, the classical references (Wahlberg [1991], Wahlberg and Mäkilä [1996], Heuberger et al. [2005])) have been used extensively in the system identification literature in order to formulate the system identification problem for continuous-time input-output models as a linear-in-the-parameters one.

In the following the focus will be on the first order inner function

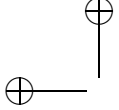
$$\phi(s) = w(s) = \frac{s-a}{s+a}, \quad (\text{A.40})$$

$a > 0$, together with the associated balanced realisation

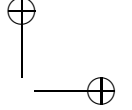
$$w(s) = \frac{c_w b_w}{s - a_w} + d_w, \quad (\text{A.41})$$

where $a_w = -a$, $b_w = -\sqrt{2a}$, $c_w = \sqrt{2a}$, $d_w = 1$. Then the orthogonal complement of $w(s)\mathcal{H}_2$ is denoted as $S = \mathcal{H}_2 \ominus w(s)\mathcal{H}_2$. Following the CT-GOBF theory,

$$\mathcal{L}_0(s) = \frac{c_w}{s+a} = \frac{\sqrt{2a}}{s+a} \quad (\text{A.42})$$



|



is a basis of the (one-dimensional) subspace S and the set

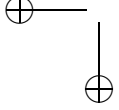
$$\{\mathcal{L}_0, \mathcal{L}_1, \dots, \mathcal{L}_i, \dots\} = \{\mathcal{L}_0, w(s)\mathcal{L}_0, \dots, w(s)^i\mathcal{L}_0, \dots\} \quad (\text{A.43})$$

is an orthonormal basis of \mathcal{H}_2 , *i.e.*, $\mathcal{H}_2 = \bigoplus_{i=0}^{\infty} w^i S$. Equivalently, letting $\ell_0 = \mathcal{F}^{-1}[\mathcal{L}_0]$, the set

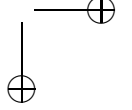
$$\{\ell_0, \ell_1, \dots, \ell_i, \dots\} = \{\ell_0, \Lambda_w \ell_0, \dots, \Lambda_w^i \ell_0, \dots\} \quad (\text{A.44})$$

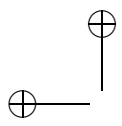
is an orthonormal basis of $\mathcal{L}_2(0, \infty)$, *i.e.*, $\mathcal{L}_2(0, \infty) = \bigoplus_{i=0}^{\infty} \Lambda_w^i S$. The basis defined starting with the first order inner function is called Laguerre basis, in time- and frequency- domain.

— —

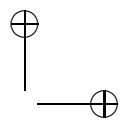


|



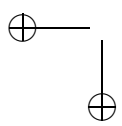


|

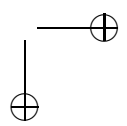


—

—



|

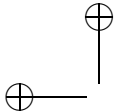




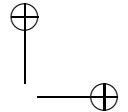
BIBLIOGRAPHY

- P. Apkarian and R. J. Adams. Advanced gain-scheduling techniques for uncertain systems. *IEEE Transactions on Control System Technology*, 6(1):21–32, 1998.
- P. Apkarian and D. Noll. Nonsmooth H_∞ synthesis. *IEEE Transactions on Automatic Control*, 51(1):71–86, 2006.
- M. Arulampalam, S. Maskell, N. Gordon, and T. Clapp. A tutorial on particle filters for online nonlinear/non-gaussian bayesian tracking. *IEEE Transactions on Signal Processing*, 50(2):174 –188, 2002.
- K. J. Astrom and R. M. Murray, editors. *Feedback Systems: An Introduction for Scientists and Engineers*. Princeton University Press, 2008.
- R. Bach. State estimation applications in aircraft flight-data analysis. Technical Report NASA Reference Publication 1252, 1991.
- B. Bamieh and L. Giarré. Identification of linear parameter-varying models. *International Journal of Robust and Nonlinear Control*, 12(9):841–853, 2002.
- T. Bastogne, H. Garnier, and P. Sibille. A PMF-based subspace method for continuous-time model identification. Application to a multivariable winding process. *International Journal of Control*, 74(2):118–132, 2001.
- D. Bauer. Asymptotic properties of subspace estimators. *Automatica*, 41(3):359–376, 2005.
- D. Bauer and M. Jansson. Analysis of the asymptotic properties of the MOESP type of subspace algorithms. *Automatica*, 36(4):497–509, 2000.

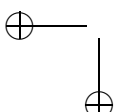




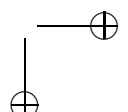
|



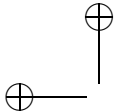
- D. Bauer, M. Deistler, and W. Scherrer. The analysis of the asymptotic variance of subspace algorithms. *11th IFAC Symposium on System Identification, Fukuoka, Japan*, pages 1087–1097, 1997.
- D. Bauer, M. Deistler, and W. Scherrer. Consistency and asymptotic normality of some subspace algorithms for systems without observed inputs. *Automatica*, 35(7):1243–1254, 1999.
- F. Beltramini, M. Bergamasco, and M. Lovera. Experiment design for MIMO model identification, with application to rotorcraft dynamics. In *IFAC World Congress, Milano, Italy*, 2011.
- M. Bergamasco and M. Lovera. Continuous-time subspace identification in closed-loop using Laguerre filters. In *49th IEEE Conference on Decision and Control (CDC)*, pages 2023–2028, Atlanta, USA, 2010a.
- M. Bergamasco and M. Lovera. Continuous-time subspace identification in closed-loop. In *19th International Symposium on Mathematical Theory of Networks and Systems (MTNS)*, pages 1359–1365, Budapest, Hungary, 2010b.
- M. Bergamasco and M. Lovera. Continuous-time predictor-based subspace identification using Laguerre filters. *IET Control Theory Applications*, 5 (7):856–867, 5 2011a.
- M. Bergamasco and M. Lovera. Subspace identification of continuous-time state-space lpv models. In P. Lopes dos Santos, T. P. Azevedo Perdigolos, C. Novara, J. A. Ramos, and D. E. Rivera, editors, *Linear Parameter-Varying System Identification: New Developments and Trends*, volume 14, pages 233–262. World Scientific, 2011b.
- M. Bergamasco and M. Lovera. Continuous-time predictor-based subspace identification for helicopter dynamics. In *37th European Rotorcraft Forum, Gallarate, Italia*, 2011c.
- M. Bergamasco and M. Lovera. Identification of linear models for the dynamics of a hovering quadrotor. *submitted*, 2013.
- M. Bergamasco, M. Lovera, and Y. Ohta. Recursive continuous-time subspace identification using Laguerre filters. In *50th IEEE Conference on Decision and Control (CDC)*, pages 6469–6474, Orlando, USA, 2011.
- S. Bittanti and P. Colaneri. *Periodic systems - filtering and control*. Springer, 2009.



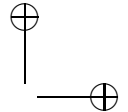
|



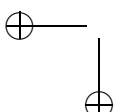
- S. Bittanti and M. Lovera. On the zero dynamics of helicopter rotor loads. *European Journal of Control*, 2(1):57–68, 1996.
- S. Bittanti and M. Lovera. Identification of linear models for a hovering helicopter rotor. In *11th IFAC Symposium on system identification, Fukuoka, Japan*, 1997.
- S. Bittanti and M. Lovera. Bootstrap-based estimates of uncertainty in subspace identification methods. *Automatica*, 36(11):1605–1615, 2000.
- S. Bouabdallah, M. Becker, and R. Siegwart. Autonomous miniature flying robots: coming soon! *IEEE Robotics & Automation Magazine*, 14(3):88–98, 2007.
- P. Castillo, R. Lozano, and A. Dzul. *Modelling and control of mini-flying machines*. Springer-Verlag New York Inc, 2005.
- R. Cheng, M. Tischler, and G. Schulein. R-max helicopter state-space model identification for hover and forward-flight. *Journal of the American Helicopter Society*, 51(2):202–210, 2006.
- A. Chiuso. The role of vector autoregressive modeling in predictor based subspace identification. *Automatica*, 43(6):1034–1048, 2007.
- A. Chiuso and G. Picci. Consistency analysis of certain closed-loop subspace identification methods. *Automatica*, 41(3):377–391, 2005.
- A. Chiuso, R. Muradore, and E. Marchetti. Dynamic calibration of adaptive optics systems: A system identification approach. *IEEE Transactions on Control Systems Technology*, 8(3):705–713, 2010.
- Y. Cho, G. Xu, and T. Kailath. Fast recursive identification of state space models via exploitation displacement structure. *Automatica*, 30(10):45–60, 1994.
- C. Chou and M. Verhaegen. Subspace algorithms for the identification of multivariable dynamic error-in-variables state space models. *Automatica*, 33(10):1857–1869, 1997.
- S. Chouaba, A. Chamroo, R. Ouvrard, and T. Poinot. Continuous-time identification of linear parameter varying model using an output-error technique. In *18th IFAC World Congress, Milano, Italy*, 2011.
- A. Das, K. Subbarao, and F. Lewis. Dynamic inversion with zero-dynamics stabilisation for quadrotor control. *IET Control Theory & Applications*, 3(3):303–314, 2009.



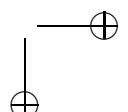
|

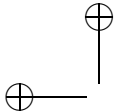


- J. De Caigny, J. F. Camino, and J. Swevers. Interpolating model identification for SISO Linear Parameter Varying systems. *Mechanical Systems and Signal Processing*, 23(8):2395–2417, 2009.
- J. De Caigny, J. F. Camino, and J. Swevers. Interpolation-based modelling of MIMO LPV systems. *IEEE Transactions on Control Systems Technology*, 19(1):46–63, 2011.
- J. De Caigny, R. Pintelon, J. F. Camino, and J. Swevers. Interpolated modeling of lpv systems based on observability and controllability. In *16th IFAC Symposium on System Identification*, 2012.
- P. De Filippi and M. Lovera. Linear parameter-varying state feedback synthesis with hierarchical performance requirements. In *2011 IFAC World Congress, Milano, Italy*, 2011.
- T. J. de Hoog, Z. Szab, P. S. Heuberger, P. M. V. den Hof, and J. Bokor. Minimal partial realization from generalized orthonormal basis function expansions. *Automatica*, 38(4):655 – 669, 2002.
-
- A. Dempster, N. Laird, and D. Rubin. Maximum likelihood from incomplete data via the EM algorithm (with discussion). *Journal of the Royal Statistical Society B*, 39(1):1–38, 1977.
- L. Derafa, T. Madani, and A. Benallegue. Dynamic modelling and experimental identification of four rotors helicopter parameters. In *IEEE International Conference on Industrial Technology*, pages 1834–1839. IEEE, 2006.
- R. Dorf and R. Bishop. *Modern Control Systems*. Prentice Hall, 2011.
- H. Dotsch and P. Van den Hof. Test for local structural identifiability of high-order non-linearly parameterised state space models. *Automatica*, 32(6):875–883, 1996.
- A. Doucet, S. Godsill, and C. Andrieu. On sequential monte carlo sampling methods for bayesian filtering. *Statistics and Computing*, 10(3):197–208, 2000.
- A. Doucet, N. de Freitas, and N. Gordon. *Sequential Monte Carlo Methods in Practice*. Springer Verlag, 2001.
- B. Efron. Bootstrap methods: Another look at the Jackknife. *The Annals of Statistics*, 7(1):1–26, 1979.

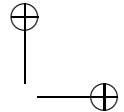


|





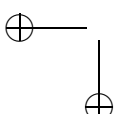
|



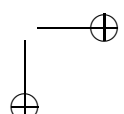
BIBLIOGRAPHY

219

- B. Efron and R. Tibshirani. *An introduction to the bootstrap*. Chapman and Hall, 1993.
- F. Felici, J. van Wingerden, and M. Verhaegen. Subspace identification of MIMO LPV systems using a periodic scheduling sequence. *Automatica*, 43(10):1684–1697, 2007.
- J. Fletcher. Identification of uh-60 stability derivative models in hover from flight test data. *Journal of the American Helicopter Society*, 40(1):32–46, 1995.
- J. Freudenberg and D. Looze. Right half plane poles and zeros and design tradeoffs in feedback systems. *IEEE Transactions on Automatic Control*, 30(6):555–565, 1985.
- P. Gahinet and P. Apkarian. Decentralized and fixed-structure H_∞ control in matlab. In *50th IEEE Conference on Decision and Control and European Control Conference, Orlando, USA*, 2011.
- H. Garnier and L. Wang, editors. *Identification of continuous-time models from sampled data*. Springer, 2008.
-
- M. Gevers. A personal view of the development of system identification: a 30-year journey through an exciting field. *IEEE Control Systems Magazine*, 26(6):93–105, 2006.
- R. Gopaluni. A particle filter approach to identification of nonlinear processes under missing observations. *The Canadian Journal of Chemical Engineering*, 86(6):1081–1092, 2008.
- M. Green and D. Limebeer. *Linear Robust Control*. Prentice Hall Information and System Sciences, 1994.
- M. Grewal and A. Andrews. *Kalman filtering: theory and practice using Matlab*. Wiley, 2001.
- W. Groot Wassink, M. van de Wal, C. Scherer, and O. Bosgra. LPV control for a wafer stage: beyond the theoretical solution. *Control Engineering Practice*, 13(2):231–245, 2005.
- R. Guidorzi. Canonical structures in the identification of multivariable systems. *Automatica*, 11(4):361–374, 1975.
- T. Gustafsson. Instrumental variable subspace tracking using projection approximation. *IEEE Transactions on Signal Processing*, 46(3):669–681, 1998.



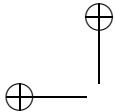
|



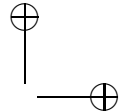
- J. Ham, C. Gardner, and M. Tischler. Flight testing and frequency domain analysis for rotorcraft handling qualities characteristics. Technical Report American Helicopter Society Specialists' Meeting on Piloting Vertical Flight Aircraft, San Francisco, CA, 1993.
- P. Hamel and J. Kaletka. Advances in rotorcraft system identification. *Progress in Aerospace Sciences*, 33(3-4):259–284, 1997.
- T. Hamel, R. Mahony, R. Lozano, and J. Ostrowski. Dynamic modelling and configuration stabilisation for an X4-flyer. In *IFAC World Congress, Barcelona, Spain*, 2002.
- B. R. J. Haverkamp. *State space identification: theory and practice*. PhD thesis, Delft University of Technology, 2001.
- G. Heredia, A. Ollero, M. Bejar, and R. Mahtani. Sensor and actuator fault detection in small autonomous helicopters. *Mechatronics*, 18(2):90–99, 2008.
- P. Heuberger, P. Van den Hof, and O. Bosgra. A generalized orthonormal basis for linear dynamical systems. *IEEE Transactions on Automatic Control*, 40(3):451–465, 1995.
- P. Heuberger, P. Van den Hof, and O. Bosgra. A generalized orthonormal basis for linear dynamical systems. *IEEE Transactions on Automatic Control*, 40(5):451–465, 2005.
- P. S. C. Heuberger, T. J. d. Hoog, P. M. J. Van, d. Hof, and B. Wahlberg. Orthonormal basis functions in time and frequency domain: Hambo transform theory. *SIAM Journal Control Optimzation*, 42(4):1347–1373, 2003.
- I. Houtzager, J. van Wingerden, and M. Verhaegen. Fast-array recursive closed-loop subspace model identification. In *15th IFAC Symposium on System Identification, Saint Malo, France*, 2009.
- I. Houtzager, J. van Wingerden, and M. Verhaegen. Recursive predictor-based subspace identification with application to the real-time closed-loop tracking of flutter. *IEEE Transactions on Control Systems Technology*, 20(4):934–949, 2012.
- B. Huang, S. Ding, and S. Qin. Closed-loop subspace identification: an orthogonal projection approach. *Journal of Process Control*, 15(1):53–66, 2005.

- C. Ivler and M. Tischler. System identification modeling for flight control design. In *RAeS Rotorcraft Handling-Qualities Conference, University of Liverpool, UK*, 2008.
- R. Jategaonkar. *Flight Vehicle System Identification*. AIAA, 2006.
- R. Jategaonkar, D. Fischenberg, and W. von Gruenhagen. Aerodynamic modeling and system identification from flight data - recent applications at dlr. *Journal of the American Helicopter Society*, 41(4):681–691, 2004.
- R. Johansson, M. Verhaegen, and C. Chou. Stochastic theory of continuous-time state-space identification. *IEEE Transactions on Signal Processing*, 47(1):41–51, 1999a.
- R. Johansson, M. Verhaegen, B. J. Haverkamp, and C. Chou. Correlation methods of continuous-time state-space model identification. In *European Control Conference (ECC'99), Karlsruhe, Germany*, 1999b.
- W. Johnson. *Helicopter theory*. Princeton University Press, 1980.
- S. Julier and J. Uhlmann. A new extension of the kalman filter to non-linear systems. In *International Symposium Aerospace/Defense Sensing, Simulation and Controls*, Orlando, FL, 1997.
- I. Kaminer, A. M. Rascoal, P. P. Karghonekar, and E. E. Coleman. A velocity algorithm for the implementation of gain-scheduled controllers. *Automatica*, 31(8):1185–1191, 1995.
- S. K. Kim and D. Tilbury. Mathematical modeling and experimental identification of an unmanned helicopter robot with flybar dynamics. *Journal of Robotic Systems*, 21(3):95–116, 2004.
- Y. Kinoshita and Y. Ohta. Continuous-time system identification using compactly supported filter kernels generated from Laguerre basis functions. In *49th IEEE Conference on Decision and Control, Atlanta, USA*, 2010.
- G. Kitagawa. Monte Carlo filter and smoother for non-gaussian nonlinear state space models. *Journal of Computational and Graphical Statistics*, 5 (1):1–25, 1996.
- V. Klein and E. Morelli. *Aircraft System Identification: Theory And Practice*. AIAA, 2006.

- V. Klein and J. Schiess. Compatibility check of measured aircraft responses using kinematic equations and extended kalman filter. Technical Report NASA TN D-8514, 1977.
- T. Knudsen. Consistency analysis of subspace identification methods based on a linear regression approach. *Automatica*, 37(1):81–89, 2001.
- M. La Civita, W. Messner, and T. Kanade. Modelling of small-scale helicopters with integrated first-principles and system identification techniques. In *Proceedings of the 58th American Helicopter Society Annual Forum*, 2002.
- A. Laub, M. Heath, C. Paige, and R. Ward. Computation of system balancing transformations and other applications of simultaneous diagonalization algorithms. *IEEE Transactions on Automatic Control*, 32(2):115–122, 1987.
- V. Laurain, R. Toth, M. Gilson, and H. Garnier. Direct identification of continuous-time lpv input/output models. *IET Control Theory and Applications*, 5(7):878–888, 2011.
- M. Lawler, C. Ivler, M. Tischler, and Y. Shtessel. System identification of the longitudinal/heave dynamics for a tandem-rotor helicopter including higher-order dynamics. In *AIAA Atmospheric Flight Mechanics Conference and Exhibit, Colorado*, 2006.
- L. Lee and K. Poolla. Identification of linear parameter-varying systems using nonlinear programming. *ASME Journal of Dynamic Systems, Measurement and Control*, 121(1):71–78, 1999.
- D. J. Leith and W. E. Leithead. Survey of gain-scheduling analysis and design. *International Journal of Control*, 73(11):1001–1025, 2000.
- P. Li and I. Postlethwaite. Subspace and bootstrap-based techniques for helicopter model identification. *Journal of the American Helicopter Society*, 56(1):012002, 2011.
- D. Link, B. Kashawlic, B. Fujizawa, and M. Tischler. Influence of frequency response analysis on mh-47g dafcs development and flight test. In *American Helicopter Society 67th Annual Forum, Virginia Beach, VA*, 2011.
- L. Ljung. Bode lecture: Challenges of nonlinear system identification. In *42nd IEEE Conference on Decision and Control, Maui, Hawaii, USA*, 2003.



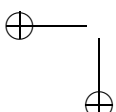
|



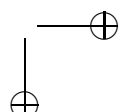
BIBLIOGRAPHY

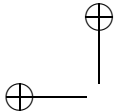
223

- L. Ljung and T. McKelvey. Subspace identification from closed loop data. *Signal Processing*, 52(2):209–215, 1996.
- M. Lovera. Identification of MIMO state space models for helicopter dynamics. In *13th IFAC Symposium on System Identification, Rotterdam, The Nederlands*, 2003.
- M. Lovera and G. Mercère. Identification for gain-scheduling: a balanced subspace approach. In *2007 American Control Conference*, New York, USA, 2007.
- M. Lovera, M. Verhaegen, and C. T. Chou. State space identification of MIMO linear parameter varying models. In *International Conference on Mathematical Theory of Networks and Systems*, Padova, Italy, 1998.
- M. Lovera, T. Gustafsson, and M. Verhaegen. Recursive subspace identification of linear and non linear Wiener state space models. *Automatica*, 36(11):1639–1650, 2000.
- M. Lovera, C. Novara, P. Lopes, and D. Rivera. Guest editorial special issue on Applied LPV modelling and identification. *IEEE Transactions on Control Systems Technology*, 19(1):1–4, 2011.
-
- C. Lyzell, M. Enqvist, and L. Ljung. Handling certain structure information in subspace identification. In *15th IFAC Symposium on System Identification, Sain Malo, France*, 2009.
- P. M. Makila. Approximation of stable systems by Laguerre filters. *Automatica*, 26(2):333 – 345, 1990.
- M. Mansur, M. Tischler, M. Bielefield, J. Bacon, K. Cheung, M. Berrios, and K. Rothman. Full flight envelope inner-loop control law development for the unmanned k-max. In *American Helicopter Society 67th Annual Forum, Virginia Beach, VA*, 2011.
- A. Marcos and G. Balas. Development of linear-parameter-varying models for aircraft. *Journal of Guidance, Control and Dynamics*, 27(2):218–228, 2004.
- G. Mercère and M. Lovera. Convergence analysis of instrumental variable recursive subspace identification algorithms. *Automatica*, 43(8):13771386, 2007.

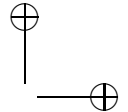


|

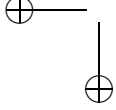




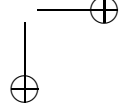
|

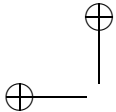


- G. Mercère, S. Lecœuche, and M. Lovera. Recursive subspace identification based on instrumental variable unconstrained quadratic optimization. *International Journal of Adaptive Control and Signal Processing*, 18(9):771–797, 2004.
- G. Mercère, L. Bako, and L. S. Propagator-based methods for recursive subspace model identification. *Signal Processing*, 88(3):468 – 491, 2008a.
- G. Mercère, R. Ouvrard, M. Gilson, and H. Garnier. Identification de systèmes multivariables à temps continu par approche des sous-espaces. *Journal Européen des Systèmes Automatisés*, 42(2-3):261–285, 2008b.
- G. Mercère, H. Palsson, and T. Poinot. Continuous-time linear parameter-varying identification of a cross flow heat exchanger: A local approach. *IEEE Transactions on Control Systems Technology*, 19(1):64–76, 2011.
- R. Mohd-Moktar and L. Wang. Continuous-time state space model identification using closed-loop data. In *Second Asia International Conference on Modelling & Simulation, Kuala Lumpur, Malaysia*, 2008.
- M. Moonen and J. Ramos. A subspace algorithm for balanced state space system identification. *IEEE Transactions on Automatic Control*, 38(11):1727–1729, 1993.
- B. Moore. Principal component analysis in linear systems: controllability, observability and model reduction. *IEEE Transactions on Automatic Control*, 26(1):17–32, 1981.
- M. Nemanic, R. Ravikanth, and B. Bamieh. Identification of linear parameter-varying systems. In *34th IEEE Conference on Decision and Control*, 1995.
- B. Ninness. Some system identification challenges and approaches. In *15th IFAC Symposium on System Identification*, pages 1–20, 2009.
- J. Nocedal and S. Wright. *Numerical Optimization*. Springer, 2006.
- A. Ohsumi, K. Kameyama, and K. Yamagushi. Subspace identification for continuous-time stochastic systems via distribution-based approach. *Automatica*, 38(1):63–79, 2002.
- Y. Ohta. Hankel singular values and vectors of a class of infinite-dimensional systems: Exact hamiltonian formulas for control and approximation problems. *Mathematics of Control, Signals, and Systems (MCSS)*, 12(4):361–375, 1999.

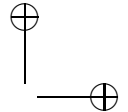


|





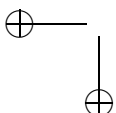
|



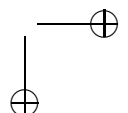
BIBLIOGRAPHY

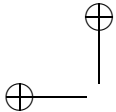
225

- Y. Ohta. Realization of input-output maps using generalized orthonormal basis functions. *Systems & Control Letters*, 22(6):437–444, 2005.
- Y. Ohta. A study on stochastic system transformation using generalized orthonormal basis functions. In *46th IEEE Conference on Decision and Control*, pages 3114–3119, 2007.
- Y. Ohta. From lifting to system transformation. In J. Willems, S. Hara, Y. Ohta, and H. Fujioka, editors, *Perspectives in Mathematical System Theory, Control, and Signal Processing*, volume 398, pages 207–216. Springer Berlin / Heidelberg, 2010.
- Y. Ohta. Stochastic system transformation using generalized orthonormal basis functions with applications to continuous-time system identification. *Automatica*, 47(5):1001 – 1006, 2011.
- Y. Ohta and T. Kawai. Continuous-time subspace system identification using generalized orthonormal basis functions. In *16th International Symposium on Mathematical Theory of Networks and Systems, Leuven, Belgium*, 2004.
-
- H. Oku and H. Kimura. Recursive 4SID algorithms using gradient type subspace tracking. *Automatica*, 38(6):1035–1043, 2002.
- T. Oliveira e Silva. Rational orthonormal functions on the unit circle and on the imaginary axis, with applications in system identification, August 1999. URL <http://www.ieeta.pt/~tos/bib/8.2.pdf>.
- B. Paijmans, W. Symens, H. V. Brussel, and J. Swevers. Identification of interpolating affine LPV models for mechatronic systems with one varying parameter. *European Journal of Control*, 14(1):16–29, 2008.
- P. Parrilo and L. Ljung. Initialization of physical parameter estimates. In *13th IFAC Symposium on System Identification, Rotterdam, The Netherlands*, 2003.
- H. Pfifer and S. Hecker. Generation of optimal linear parametric models for LFT-based robust stability analysis and control design. *IEEE Transactions on Control Systems Technology*, 19(1):118–131, 2011.
- P. Pounds and R. Mahony. Design principles of large quadrotors for practical applications. In *IEEE International Conference on Robotics and Automation, Kobe, Japan*, 2009.

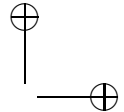


|

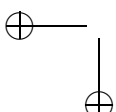




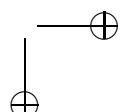
|

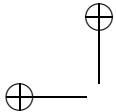


- F. Previdi and M. Lovera. Identification of a class of nonlinear parametrically varying models. *International Journal on Adaptive Control and Signal Processing*, 17(1):33–50, 2003.
- O. Prot and Mercère. Initialization of gradient-based optimization algorithms for the identification of structured state-space models. In *18th IFAC World Congress, Milan, Italy*, 2011.
- O. Prot, G. Mercère, and J. Ramos. A null-space-based technique for the estimation of linear-time invariant structured state-space representations. In *16th IFAC Symposium on System Identification, Brussels, Belgium*, 2012.
- S. Qin. An overview of subspace identification. *Computers & Chemical Engineering*, 30(10-12):1502–1513, 2006.
- A. Ridolfi and M. Lovera. Consistency of bootstrap estimates of model uncertainty in subspace identification methods. In *International Symposium on Mathematical Theory of Networks and Systems, Perpignan, France*, 2000.
-
- W. Rugh and J. Shamma. Research on gain scheduling. *Automatica*, 36(10):1401–1425, 2000.
- D. Saha and G. Rao. A general algorithm for parameter identification in lumped continuous systems—the poisson moment functional approach. *IEEE Transactions on Automatic Control*, 27(1):223–225, 1982.
- M. Sguanci, M. Bergamasco, and M. Lovera. Continuous-time model identification for rotorcraft dynamics. In *16th IFAC Symposium on System Identification, Brussels, Belgium*, Brussels, Belgium, 2012.
- J. S. Shamma and M. Athans. Analysis of Gain-Scheduled Control for Nonlinear Plants. *IEEE Transactions on Automatic Control*, 35(8):898–907, 1990.
- S. Shamsunder. Signal processing applications of the bootstrap. *IEEE Signal Processing Magazine*, 15(1):38, 1998.
- J. Shao and D. Tu. *The jackknife and bootstrap*. Springer, 1995.
- T. Schön, A. Wills, and B. Ninness. System identification of nonlinear state-space models. *Automatica*, 47(1):39–49, 2011.

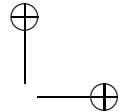


|





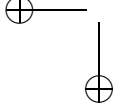
|



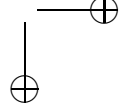
BIBLIOGRAPHY

227

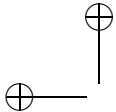
- V. Sima and S. Van Huffel. Efficient numerical algorithms and software for subspace-based system identification. In *IEEE International Symposium on Computer-Aided Control System Design*, 2000.
- N. Sinha and G. Rao, editors. *Identification of continuous-time systems*. Kluwer Academic Publishers, 1991.
- J. C. Spall, editor. *Introduction to Stochastic Search and Optimization: Estimation, Simulation, and Control*. Wiley, 2003.
- H. Stark and J. Woods. *Probability and Random Processes with Applications to Signal Processing*. Prentice Hall, 2002.
- G. Stein. Respect the unstable. *IEEE Control Systems*, 23(4):12–25, 2003.
- M. Steinbuch, R. van de Molengraft, and A. van der Voort. Experimental modelling and LPV control of a motion system. In *2003 American Control Conference (ACC)*, Denver, USA, 2003.
- M. Tischler and M. Cauffman. Frequency-response method for rotorcraft system identification: Flight applications to BO-105 coupled rotor/fuselage dynamics. *Journal of the American Helicopter Society*, 37(3):3–17, 1992.
- M. Tischler and J. Kaletka. Xv-15 tilt-rotor aircraft dynamics by frequency and time-domain identification techniques. In *AGARD FMP Symposium on Rotorcraft Design and Operations*, AGARD, 1987.
- M. Tischler and R. Remple. *Aircraft And Rotorcraft System Identification: Engineering Methods With Flight-test Examples*. AIAA, 2006.
- M. Tischler and C. Tomashoski. Flight test identification of sh-2g flapped-rotor helicopter flight mechanics models. *Journal of the American Helicopter Society*, 47(1):18–32, 2002.
- F. Tjarnstrom. The use of bootstrap in system identification. Technical Report Report LiTH-ISY-R-2113, Dept. of Electrical Engineering, Linkoping University, 1999.
- F. Tjarnstrom and L. Ljung. Using the bootstrap to estimate the variance in the case of undermodeling. *IEEE Transactions on Automatic Control*, 47(2):395–398, 2002.
- R. Toth. *Modeling and identification of linear parameter-varying systems*, volume 403 of *Lecture Notes in Control and Information Sciences*. Springer, 2010.



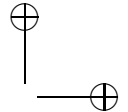
|



- R. Van der Merwe and E. Wan. The unscented kalman filter for nonlinear estimation. In *Symposium on Adaptive Systems for Signal Processing, Communications, and Control*, Lake Louise, Canada, 2000.
- J. Van Doren, P. Van den Hof, J. Hansen, and O. Bosgra. Determining identifiable parameterisations for large-scale physical models in reservoir engineering. In *2008 IFAC World Congress*, Seoul, South Korea, 2008.
- J. van Helvoort, M. Steinbuch, P. Lambrechts, and R. van de Molengraft. Analytical and experimental modelling for gain-scheduling of a double scara robot. In *3rd IFAC Symposium on Mechatronic Systems*, Sydney, Australia, 2004.
- P. Van Overschee and B. De Moor. N4SID: subspace algorithm for the identification of combined deterministic-stochastic system. *Automatica*, 30(1), 1994.
- P. Van Overschee and B. De Moor. Continuous-time frequency domain subspace system identification. *Signal Processing*, 52(2):179–194, 1996.
- P. Van Overschee and B. De Moor. *Subspace identification: theory, implementation, application*. Kluwer Academic Publishers, 1996.
- J. van Wingerden. The asymptotic variance of the pbsidopt algorithm. In *16th IFAC Symposium on System Identification, Brussels, Belgium*, 2012.
- J. van Wingerden and M. Verhaegen. Subspace identification of bilinear and LPV systems for open- and closed-loop data. *Automatica*, 45(2):372–381, 2009.
- A. Varga, A. Hansson, and G. Puyou, editors. *Optimization Based Clearance of Flight Control Laws*. Springer, 2012.
- V. Verdult. *Nonlinear system identification: a state space approach*. PhD thesis, University of Twente, 2002.
- M. Verhaegen. Identification of the deterministic part of MIMO state space models given in innovations form from input-output data. *Automatica*, 30(1):61–74, 1994.
- M. Verhaegen and E. Deprettere. A fast, recursive MIMO state space model identification algorithm. In *30th IEEE Conference on Conference on Decision and Control*, pages 1349–1354, 1991.



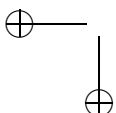
|



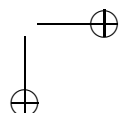
BIBLIOGRAPHY

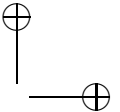
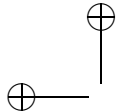
229

- M. Verhaegen and P. Dewilde. Subspace model identification, part 1: output error state space model identification class of algorithms. *International Journal of Control*, 56(5):1187–1210, 1992a.
- M. Verhaegen and P. Dewilde. Subspace model identification, part 2: analysis of the elementary output error state space model identification algorithm. *International Journal of Control*, 56(5):1211–1241, 1992b.
- M. Verhaegen and A. Varga. Some experience with the moesp class of subspace model identification methods in identifying the bo105 helicopter. Technical Report TR R165-94, DLR, 1994.
- M. Verhaegen and V. Verdult. *Filtering and System Identification: A Least Squares Approach*. Cambridge University Press, 2007.
- B. Wahlberg. System identification using Laguerre models. *IEEE Transactions on Automatic Control*, 36(5):551–562, 1991.
- B. Wahlberg. System identification using Kautz models. *IEEE Transactions on Automatic Control*, 39(6):1276–1282, 1994.
-
- B. Wahlberg and P. Mäkilä. On approximation of stable linear dynamical systems using Laguerre and Kautz functions. *Automatica*, 32(5):693–708, 1996.
- N. M. Wereley and S. R. Hall. Frequency response of linear time periodic systems. In *IEEE International Conference on Decision and Control, CDC*, 1990.
- J. Williams, J. Ham, and M. Tischler. Flight test manual - rotorcraft frequency domain flight testing. Technical Report AQTD Project No. 93-14, 1995.
- L. Xie and L. Ljung. Estimate physical parameters by black box modeling. In *Chinese Control Conference, Hangzhou, China*, 2002.
- Y. Yamamoto. A function space approach to sampled-data control systems and tracking problems. *IEEE Transactions on Automatic Control*, 39(4): 703–712, 1994.
- J. Zhou and T. Hagiwara. H_∞ norm computation of continuous-time periodic systems. In *IEEE International Conference on Decision and Control, SICE*, 1990.

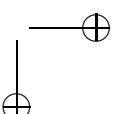
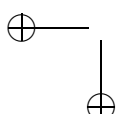
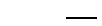


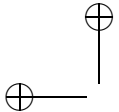
|



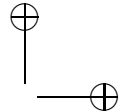


- J. Zhou and T. Hagiwara. H_2 and H_∞ norm computations of linear continuous-time periodic systems via the skew analysis of frequency response operators. *Automatica*, 38(8):1381–1387, 2002a.
- J. Zhou and T. Hagiwara. Existence conditions and properties of the frequency response operators of continuous-time periodic systems. *SIAM Journal on Control and Optimization*, 40(6):1867–1887, 2002b.
- K. Zhou, J. Doyle, and K. Glover. *Robust and optimal control*. Prentice Hall, 1996.





|



PUBLICATIONS

International journals

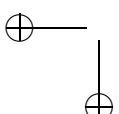
1. M. Bergamasco, F. Della Rossa, L. Piroddi. Active noise control with on-line estimation of non-Gaussian noise characteristics. *Journal of Sound and Vibration*, 331(1):27-40, 2012.
2. M. Bergamasco, M. Lovera. Continuous-time predictor-based subspace identification using Laguerre filters. *IET Control Theory & Applications*, 5(7):856-867, 2011.
3. L. Viganò, M. Bergamasco, M. Lovera, A. Varga. Optimal periodic output feedback control: a continuous-time approach and a case study. *International Journal of Control*, 83(5):897-914, 2010.

Book chapters

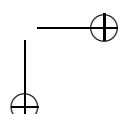
1. M. Bergamasco, M. Lovera. Subspace identification of continuous-time state-space LPV models. In *Linear parameter-varying system identification: New Developments and Trends*, P. Lopes dos Santos, T.P. Azevedo Perdigolos, Novara C., J. A. Ramos, D. E. Rivera editors, Advanced Series in Electrical and Computer Engineering, Volume 14, pages 233 - 262, World Scientific, 2011.

International conferences

1. M. Bergamasco, M. Lovera. Rotorcraft system identification: an integrated time-frequency domain approach. In *2nd CEAS Specialist Conference on Guidance, Navigation & Control*, Delft, Netherlands, 2013.



|



2. M. Bergamasco, M. Lovera. Spacecraft Attitude Control based on Magnetometers and Gyros. In *2nd CEAS Specialist Conference on Guidance, Navigation & Control*, Delft, Netherlands, 2013.
3. M. Bergamasco, M. Lovera. State space model identification: from unstructured to structured models with an \mathcal{H}_∞ approach. In *Joint 2013 SSSC, TDS, FDA Conference*, Grenoble, France, 2013.
4. F. Della Rossa, M. Bergamasco, M. Lovera. Bifurcation analysis of the attitude dynamics for a magnetically controlled spacecraft. In *51th IEEE Conference on Decision and Control*, Maui, U.S., 2012.
5. M. Sguanci, M. Bergamasco, M. Lovera. Continuous-Time Model Identification for Rotorcraft Dynamics. In *16th IFAC Symposium on System Identification*, Brussels, Belgium, 2012.
6. M. Bergamasco, M. Lovera, Y. Ohta. Recursive continuous-time subspace identification using Laguerre filters. In *50th IEEE Conference on Decision and Control*, Orlando, U.S., 2011.
7. M. Bergamasco, M. Lovera. Continuous-time predictor-based subspace identification for helicopter dynamics. In *37th European Rotorcraft Forum*, Italy, 2011.
8. M. Bergamasco, F. Della Rossa, L. Piroddi. Active control of impulsive noise with on-line outlier detection. In *18th IFAC World Congress*, Milano, Italy, 2011.
9. F. Beltramini, M. Bergamasco, M. Lovera. Experiment design for MIMO model identification, with application to rotorcraft dynamics. In *18th IFAC World Congress*, Milano, Italy, 2011.
10. M. Bergamasco, M. Lovera. Continuous-Time Subspace Identification in Closed-Loop Using Laguerre Filters. In *49th IEEE Conference on Decision and Control*, Atlanta, U.S., 2010.
11. M. Bergamasco, L. Piroddi. Active Noise Control of Impulsive Noise Using Online Estimation of an Alpha-Stable Model. In *49th IEEE Conference on Decision and Control*, Atlanta, U.S., 2010.
12. M. Bergamasco, M. Lovera. Continuous-time subspace identification in closed-loop. In *19th International Symposium on Mathematical Theory of Networks and Systems*, Budapest, Hungary, 2010.